



Delft University of Technology
Faculty of Mechanical, Maritime and Materials Engineering

**Fundamental theory and implementation of the
Wang-O'Gara-Tucker model for the modeling of
fiber orientation in fiber filled injection molded
thermoplastics**

A thesis submitted to the
Delft University of Technology
in partial fulfillment of the requirements

for the degree

**MASTER OF SCIENCE
in
MECHANICAL ENGINEERING**

by

ADRIAAN SILLEM

Delft, the Netherlands
March 2010



MSC THESIS MECHANICAL ENGINEERING

”Fundamental theory and implementation of the Wang-O’Gara-Tucker model for the modeling of fiber orientation in fiber filled injection molded thermoplastics”

Adriaan Sillem

Delft University of Technology

Daily supervisor

Prof.dr. J.J.M. Slot

Responsible professor

Prof.dr.ir. D.J. Rixen

Other thesis committee members

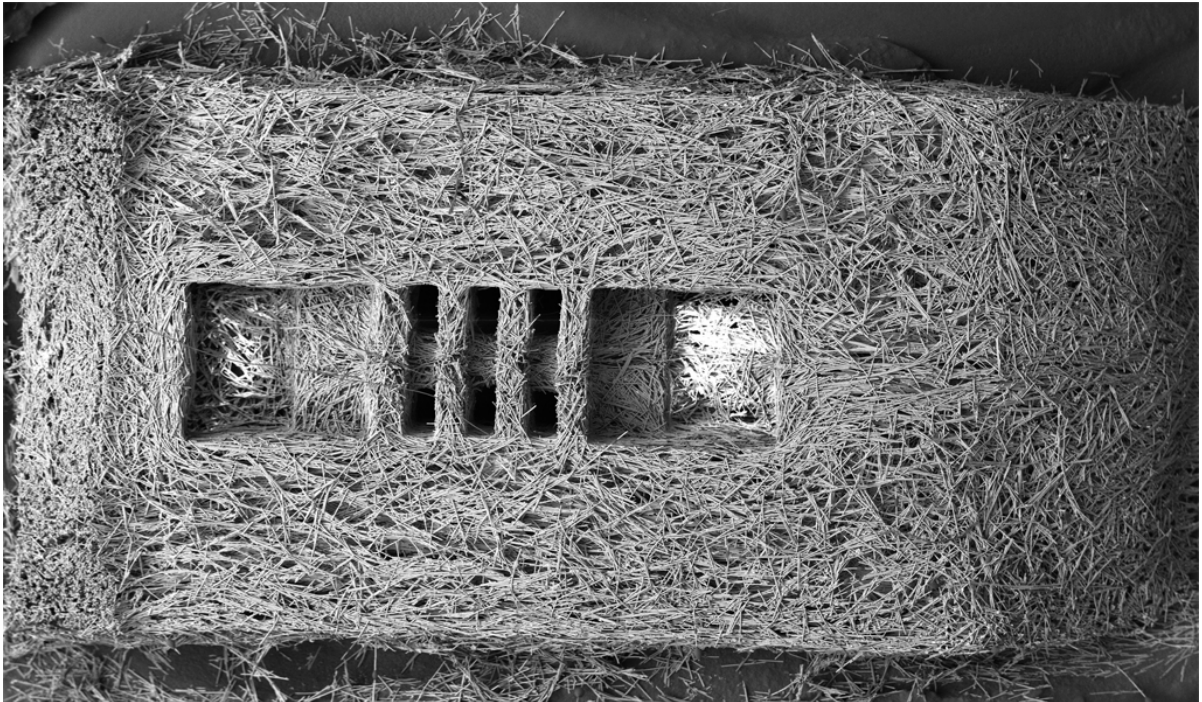
Dr.ir. H. van Melick
Prof.dr.ir. L.J. Sluys
Dr.ir. M.J.B.M. Pourquoi

March 2010

Delft, the Netherlands

Fundamental theory and implementation of the
Wang-O'Gara-Tucker model for the modeling of fiber orientation
in fiber filled injection molded thermoplastics

Adriaan Sillem 1186647



Contents

List of figures	xii
List of tables	xiii
Preface	xv
Project	xv
Outline	xv
Acknowledgements	xvi
I Theory	1
1 Fiber orientation in fiber filled injection molded thermoplastics	3
1.1 Introduction	3
1.2 Injection molding	3
1.3 Fiber filled thermoplastics	4
1.4 Fiber orientation	6
1.5 Past research	6
1.6 Commercial software	7
1.7 Interest	8
1.8 Research method and approach	9
1.9 Contribution	11
2 Notation, conventions and mathematical preliminaries	13
2.1 Introduction	13
2.2 Notation and conventions	13
2.3 Mathematical preliminaries	14
2.3.1 Change of basis	14
2.3.2 Spherical coordinates	15
2.3.3 Projection	17
2.3.4 Constrained differentiation on the surface of the unit sphere	17
2.3.4.1 Definition	17
2.3.4.2 Properties	18
3 Jeffery's equation and the Folgar-Tucker model	23
3.1 Introduction	23
3.2 Jeffery's equation	23
3.2.1 Description in space and assumptions	23
3.2.2 Derivation	24
3.3 Folgar-Tucker model	26
3.3.1 Fiber-fiber interaction	26
3.3.2 Conservation of probability	27
3.3.3 Kinetic theory	28
4 The orientation tensor description	31
4.1 Introduction	31
4.2 Partial information	31
4.3 Definitions and interpretation	32
4.4 Properties	34
4.5 Rate equation for the second order tensor	39
5 Wang-O'Gara-Tucker model	43
5.1 Introduction	43
5.2 Rate equations for the eigenpairs	43
5.2.1 Rate equation for the eigenvalues	43
5.2.2 Rate equation for the eigenvectors	44
5.2.3 Equivalence	49
5.3 Modification and reassembly	49
5.4 Objectivity	50

5.5	Equivalent kinetic theory	52
6	Closure approximations	59
6.1	Introduction	59
6.2	The closure problem	59
6.3	Quadratic closure	59
6.4	Orthotropic closures	60
6.4.1	Orthotropy	60
6.4.2	Reduction of degrees of freedom	60
6.4.3	Domain of the eigenvalues	61
6.4.4	Orthotropic smooth closure	62
6.4.5	Fitted closures	63
7	The Fokker-Planck equation	65
7.1	Introduction	65
7.2	Interpretation	65
7.3	Dimensional analysis	68
7.4	Numerical approach	68
7.4.1	Discretization in space	68
7.4.2	Discretization in time	72
7.4.3	Conditions of the probability density function	73
7.4.3.1	Heads or tails	73
7.4.3.2	Conservation of probability	75
7.4.3.3	Nonnegativity	79
7.4.4	Initial and boundary conditions	79
7.4.5	The modified equation, local truncation error and consistency	80
7.4.6	Stability	84
7.4.6.1	Analytic stability analysis	84
7.4.6.2	Numerical stability analysis	85
8	The RSC tensor form	87
8.1	Introduction	87
8.2	Interpretation	87
8.3	Dimensional analysis	88
8.4	Analytically solvable case	88
8.5	Numerical approach	90
8.5.1	Time discretization	90
8.5.2	Conservation of properties of second order tensor	90
8.5.2.1	Symmetry	90
8.5.2.2	Positive semidefiniteness	91
8.5.2.3	Unit trace	91
8.5.3	Consistency, stability and convergence	92
II	Test models	95
9	Simple shear flow	97
9.1	Introduction	97
9.2	The simple shear flow field	97
9.3	Results Jeffery's equation	99
9.4	Results kinetic theory	107
9.4.1	Relation to Jeffery's equation	107
9.4.2	Adding fiber-fiber interaction	107
9.4.2.1	Probability density	107
9.4.2.2	Second order orientation tensor	119
9.4.3	The RSC extension	131
9.5	Results tensor approximation	134
9.6	Conclusion	143

10 Uniaxial elongational flow	145
10.1 Introduction	145
10.2 The uniaxial elongational flow field	145
10.3 Results Jeffery's equation	146
10.4 Results kinetic theory	150
10.5 Results tensor approximation	150
10.6 Conclusion	159
III Conclusions and recommendations	161
11 Conclusions and recommendations	163
11.1 Introduction	163
11.2 Conclusions	163
11.3 Recommendations	163
IV Appendices, bibliography and nomenclature	165
A Proofs	167
A.1 Introduction	167
A.2 Nonnegative real eigenvalues	167
A.3 Real eigenvectors	167
A.4 Orthonormal eigenvectors	167
A.5 Genuine eigenvectors	168
A.6 Spectral decomposition	168
B Instruction programming codes	169
B.1 Introduction	169
B.2 Example: simple shear flow	169
B.2.1 Preamble	169
B.2.2 Physical and numerical parameters	169
B.2.3 Preliminary calculations	172
B.2.4 Time integration	174
B.2.5 Output	175
B.2.6 Input	180
Bibliography	183
Nomenclature	185

List of Figures

1.1	injection molding schematic.	3
1.2	unfilled thermoplastic granules.	4
1.4	an injection molded phone housing.	4
1.3	an injection molding machine.	5
1.5	diagram of the types of materials used with injection molding. This report treats the red boxes.	5
1.6	fiber orientation made visible by burning away the matrix material.	6
1.7	fiber orientation and warpage analyses in Moldflow [1].	8
1.8	diagram of fiber orientation models.	10
2.1	spherical coordinates for the unit sphere.	16
2.2	projections of \mathbf{u} with respect to \mathbf{e} [8].	17
3.1	a prolate ellipsoid: the short axes are equal, the long axis is unique.	23
3.2	particle immersed in a viscous dominated / Stokes flow.	24
3.3	flux of probability.	27
3.4	angular velocities representing $\dot{\mathbf{p}}$	28
4.1	$p_1 p_1 \sin \theta$	33
4.2	$p_1 p_2 \sin \theta$	33
4.3	$p_1 p_3 \sin \theta$	33
4.4	$p_2 p_2 \sin \theta$	33
4.5	$p_2 p_3 \sin \theta$	33
4.6	$p_3 p_3 \sin \theta$	33
4.7	two dimensional examples of fiber orientation corresponding with second order matrices [20].	35
5.1	map of two points preserving distance and time interval.	51
5.2	change of \mathbf{q} under change of sign of \mathbf{p}	53
6.1	feasible area for the eigenvalues.	61
7.1	meshed surface of the unit sphere.	69
7.2	spherical coordinates.	70
7.3	fluxes for an arbitrary mesh element S_{ij}	70
7.4	boundaries of the domain in question.	79
9.1	simple shear velocity field cones in three dimensional view.	98
9.2	simple shear velocity field cones in x - y view.	98
9.3	$p_2 = \sin(\theta) \sin(\phi)$	99
9.4	$\frac{\sin^2(\theta) \sin(\phi)}{2}$	99
9.5	velocity vectors decomposed along the eigenvectors of \mathbf{D}	100
9.6	stationary point for $\xi = -1, \mathbf{p}_0 = \frac{1}{\sqrt{3}}[1 \ -1 \ 1]^T$	101
9.7	stationary point for $\xi = 1, \mathbf{p}_0 = \frac{1}{\sqrt{3}}[1 \ -1 \ 1]^T$	102
9.8	stationary point for $\xi = 1, \mathbf{p}_0 = [0 \ 0 \ 1]^T$	103
9.9	Jeffery orbit for $r = 25, \mathbf{p}_0 = \frac{1}{\sqrt{3}}[-1 \ -1 \ 1]^T$	105
9.10	Jeffery orbit for $r = 5, \mathbf{p}_0 = \frac{1}{\sqrt{3}}[1 \ 1 \ 1]^T$	106
9.11	development of ψ for the simple shear flow field.	109
9.12	development of ψ for the simple shear flow field.	110
9.13	development of ψ for the simple shear flow field.	111
9.14	deviation of the x_1 axis increases when the diffusion becomes stronger.	112
9.15	location and values of the extrema of the probability density. The maximum is red, the minimum is blue.	113
9.17	logistic function to smoothly build up the shear rate in time.	114
9.16	location and values of the extrema of the probability density for the nonuniform IC (7.23).	115
9.18	location and values of the extrema of the probability density for a time dependent shear rate.	116
9.19	the extrema are less concentrated in space when $\xi \neq 1$	117

9.20	the minima are larger and the maxima are lower when $\xi \neq 1$.	118
9.21	the components of \mathbf{A} and $\dot{\mathbf{A}}$. The blue lines represent the components of \mathbf{A} , the black lines the components of $\dot{\mathbf{A}}$, and the red, green and turquoise lines the LD, FFI and RSC contributions hereof respectively.	120
9.22	initial state of the eigenpairs.	121
9.23	the principal axes almost align with the flow field axes.	122
9.24	diffusion pulls the principal axes away from the flow field axes, to a random orientation state.	123
9.25	making the IC nonuniform changes the balance between convection and diffusion.	125
9.26	building up the shear rate changes the balance between convection and diffusion.	126
9.27	the components of \mathbf{A} and $\dot{\mathbf{A}}$.	127
9.28	diffusion pulls the principal axes away from the flow field axes, to a random orientation state.	128
9.29	the components of \mathbf{A} and $\dot{\mathbf{A}}$.	129
9.30	diffusion pulls the principal axes away from the flow field axes, to a random orientation state.	130
9.31	the extrema are displaced as the strain is reduced by taking $\kappa = 0.1$.	132
9.32	the strain is reduced, prolonging the transient time. The used factors are $\kappa \in \{1, 0.75, 0.5, 0.25, 0.1\}$ in blue, red, green, cyan and purple respectively.	133
9.33	comparison of \mathbf{A} from ψ , in blue, and the QC, OSC and OFC in red, green and black respectively.	136
9.34	comparison of \mathbf{A} from ψ and the QC, OSC and OFC.	137
9.35	comparison of \mathbf{A} from ψ and the QC, OSC and OFC.	138
9.36	comparison of \mathbf{A} from ψ and the QC, OSC and OFC for $(r, C_I) = (5, 0.001)$.	139
9.37	comparison of \mathbf{A} from ψ and the QC, OSC and OFC for $\kappa = 0.75$.	140
9.38	comparison of \mathbf{A} from ψ and the QC, OSC and OFC for $\kappa = 0.75$.	141
9.39	comparison of \mathbf{A} from ψ and the QC, OSC and OFC for $\kappa = 0.1$.	142
10.1	the uniaxial elongational flow field.	145
10.2	the uniaxial elongational flow field, x_1 - x_3 and x_2 - x_3 views.	146
10.3	$\sin^2(\theta) \cos^2(\phi)$.	146
10.4	Jeffery's orbit for uniaxial elongation with $\mathbf{p}_0 = \frac{1}{\sqrt{201}}[1 \ -10 \ 10]^T$.	148
10.5	Jeffery's orbit for uniaxial elongation with $\mathbf{p}_0 = \frac{1}{\sqrt{200}}[0 \ -10 \ 10]^T$.	149
10.6	solution for uniaxial elongation with $(\xi, C_I, \kappa, E) = (1, 0.1, 1, 1)$.	151
10.7	nonuniform IC with $c \in \{\frac{\pi}{8}, \frac{2\pi}{8}, \frac{3\pi}{8}\}$ in red, green and cyan respectively. The results for a uniform IC are depicted in blue.	152
10.8	influence of strain reduction, $\kappa \in \{0.25, 0.5, 0.75, 1\}$.	153
10.9	comparison of KTS and the approximations.	155
10.10	comparison of KTS and the approximations for a larger FFI contribution.	156
10.11	comparison of KTS and the approximations for a larger RSC contribution.	157
10.12	comparison of KTS and the approximations for a larger RSC contribution.	158
B.1	schematic of implementations.	170
B.2	example of the output of the function <code>vis_psi_checks</code> .	178
B.3	example of the output of the function <code>vis_A.4</code> .	179

List of Tables

2.1	Voigt index notation.	15
B.1	tested stable settings.	174
B.2	needed input for program.	181
B.3	needed input for program in the structure <code>plot_and_save</code>	182

Preface

Project

This is the master thesis submitted to the Faculty of Mechanical, Maritime and Materials Engineering of the Delft University of Technology (TUD) in the partial fulfillment of the requirements for the degree of Master of Science in Mechanical Engineering. The graduation is under supervision of the division Engineering Dynamics of the Faculty of Mechanical, Maritime and Materials Engineering and of the division Construction Mechanics of the Faculty of Civil Engineering. It has a duration of six months, rewarded with 45 European credits (EC) when completed successfully.

The graduation was carried out at the DSM branch in Geleen, at the department Performance Materials. DSM, or Royal DSM N.V. in full, is a Dutch multinational company specialized in life sciences and materials sciences. The purpose of the project is to predict the fiber orientation in fiber filled injection molded thermoplastics. The code Matlab, provided by Mathworks, is used for the implementations.

The committee for the examination of this master thesis consists of

prof.dr.ir. L.J. Sluys	TUD, faculty Civil Engineering, division Construction Mechanics,
prof.dr.ir. D.J. Rixen	TUD, faculty Mechanical Engineering, division Engineering Dynamics,
dr.ir. M.J.B.M. Pourquie	TUD, faculty Mechanical Engineering, division Process and Energy,
prof.dr. J.J.M. Slot	DSM, department Performance Materials and
dr.ir. H. van Melick	DSM, department Performance Materials.

Outline

The purpose of this master project is to implement the Wang-O’Gara-Tucker model to simulate the fiber orientation in fiber filled injection molded thermoplastics. A part of the extensive fundamental theory behind this model, and the implementations are treated in Part I of the thesis, the theory part. This part consists of the first eight chapters.

In Chapter 1 an introduction to the thesis is given. Certain preliminaries to understand the scope and purpose of the project are treated. These preliminaries include the process of injection molding, the use of fiber filled thermoplastics, fiber orientation, past research, available commercial software, the interest of DSM in the subject of fiber orientation, the research method and approach and the contribution of this thesis. In Chapter 2 the notation and conventions used throughout this report are treated. As is a selection of the mathematical preliminaries. Chapter 3 starts off with the theory behind Jeffery’s equation, a deterministic model for the fiber orientation of a single ellipsoidal particle in a fully viscous/Stokes flow. This model is extended by Folgar and Tucker with the addition of a fiber-fiber interaction term, using a probability density function. In Chapter 4 an approach using only partial information of the computationally inefficient Folgar-Tucker model is introduced. Chapter 5 treats the model that is the focus of this thesis, the Wang-O’Gara-Tucker model. It slows down the kinetics of the Folgar-Tucker model to adapt the theoretical results to the experimental results. In Chapter 6 the closure problem of the Folgar-Tucker tensor form is explained. Chapter 7 thoroughly treats the Fokker-Planck equation that stems from the Folgar-Tucker probability density form. A numerical scheme is derived to obtain a solution. In Chapter 8 a numerical scheme for solving the tensor form of the Folgar-Tucker model is derived.

Should one not be interested in mathematical details, then proofs can be skipped easily. The idea of the models can be understood even without such details. If one is merely interested in the results of the implementation of the model, then Part I can be skipped entirely. The results are contained in Part II.

Part II uses the implementations of Chapters 7 and 8 to model the fiber orientation for a simple shear flow field in Chapter 9 and for a uniaxial elongational flow in Chapter 10. Results of the probability density are interpreted for different parameter sets. The approximations of the tensor form are compared to the solutions of the probability density, using several closure relations.

Part III concludes the theory and test models with conclusions and recommendations for future research.

Part IV consists of some 'classical' proofs, instructions for the codes that were used to obtain the results in the thesis, the bibliography and the nomenclature. The classical proofs were put in the appendix to make sure that only information specific to the modeling of fiber orientation with the Wang-O'Gara-Tucker model is included in the main parts. With the addition of the instruction of the implementations to the thesis, it is intended to make the thesis offer an integrated approach to the Wang-O'Gara-Tucker model: the theory is presented, two test cases as examples are considered and the usage of the implementations is explained.

Acknowledgements

I wish to thank all of my colleagues at DSM in Geleen. They have made sure that I had an educational environment. Their enthusiasm and stamina seems to be of an infinite order. The gentlemen of the division Performance Materials: Gerard Haagh, Ullrich Heisserer, Wim Zoetelief, Robert Meeks, Lucien Douven, Harold van Melick and Tom Engels. Last but certainly not least, I would like to thank my supervisor Han Slot. His extended knowledge of mathematics and physics, both in the fundamental and applied sense, has made large contributions to my education.

From Delft I wish to thank my two enthusiastic supervisors, Bert Sluys and Daniel Rixen. In addition, I would like to thank Kees Vuik, who I could count on when having questions concerning numerical analysis.

I would like to thank my parents for their financial support and in particular my father for the endless amount of engineering issues we discussed throughout my life. For sure, these discussions have improved my analytical thinking and motivated me for the fields of applied sciences, in particular applied mathematics and mechanical engineering.

Adriaan Sillem
March 2010, Geleen



DSM in Geleen.

Part I
Theory

Chapter 1

Fiber orientation in fiber filled injection molded thermoplastics

1.1 Introduction

In this chapter we give a introductory description of the modeling of fiber orientation in fiber filled injection molded thermoplastics. The process of injection molding is treated. We explain the material properties of fiber filled thermoplastics and why it is important to control the fiber orientation. The interest of DSM in modeling fiber orientation is illuminated. There are already several commercial software packages available on the market for modeling fiber orientation. Their contributions are explained. The various researchers that have contributed to the modeling of fiber orientation are named. We define the problem that will be handled in this report and explain our goals.

1.2 Injection molding

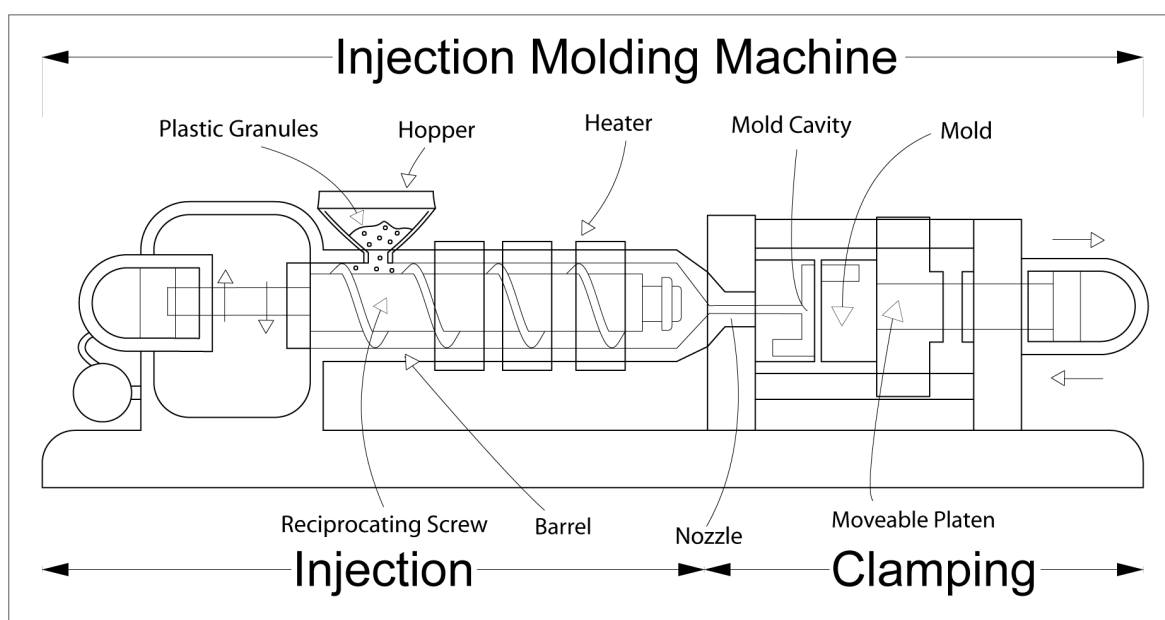


Figure 1.1: injection molding schematic.

Injection molding is the process of injecting a mold with a thermoplastic material, confer Figure 1.1. Thermoplastic granules material is added to the funnel or hopper of the injection molding machine. This granules can be either fiber filled or unfilled. Considering Figure 1.2, one can get an idea of the size of the granules. Sliding down the hopper, the granules comes in an initially closed barrel with a heated screw. The material melts and the barrel fills with melt. When the barrel is full, pressure is maintained and the nozzle is opened so that the mold cavity is injected with the melt. This is called the injection phase. When the injection is complete, the pressure is maintained on the melt by the screw and the packing phase begins. The purpose of the packing phase is to add further material to compensate for shrinkage of material as it cools in the cavity. After some time of packaging, the gate freezes and the cavity is effectively isolated from the pressure applied by the melt in the barrel. This marks the beginning of the cooling phase in which the material continues to cool until the component has sufficient mechanical stiffness to be ejected from the mold. During cooling, the screw starts to rotate and moves back. The rotation assists plastification of the material and a new charge of melt is created in front of the screw. After ejection, the mold closes and the cycle restarts. In summary, injection molding is characterized by the following steps.

1. Mold closing.
2. Injection.



Figure 1.2: unfilled thermoplastic granules.

3. Packing.
4. Cooling.
5. Plastification and returning the screw.
6. Ejection.

In this report, the injection phase is considered. The injected thermoplastic is filled with fibers which will ultimately be frozen in a certain spatial configuration. The purpose is to model certain aspects of these configurations, as explained in Section 1.4.

A substantial part of the production of thermoplastic products is done by an injection molding machine, confer Figure 1.3. Many everyday items are injection molded. Some examples are mobile phone housings, automobile bumpers, television cabinets, compact discs and lunch boxes. A mobile phone housing is depicted in Figure 1.4.

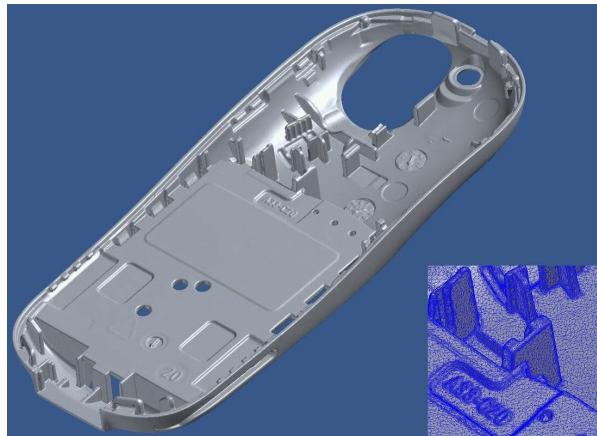


Figure 1.4: an injection molded phone housing.

1.3 Fiber filled thermoplastics

In this report we focus merely on fiber filled thermoplastic materials, confer Figure 1.5. Thermoplastic materials are plastics without crosslinking and thus have a melting point. The used thermoplastic granules are either filled or unfilled. Herewith, it is meant that the material is filled with fibers or not. The fibers can be of various different materials, occurring in various volume or weight fractions and length to diameter ratios. Common values for the volume fraction are 8-30% and for the weight fraction 15-60%. Also the length to diameter ratios in the granules vary. In addition, the fibers break with the injection molding, decreasing the length to diameter ratios. The final product typically contains fibers with lengths of $200-300[\mu\text{m}]$ and $10[\mu\text{m}]$ diameter. This results in typical length to diameter ratios 20-30.



Figure 1.3: an injection molding machine.

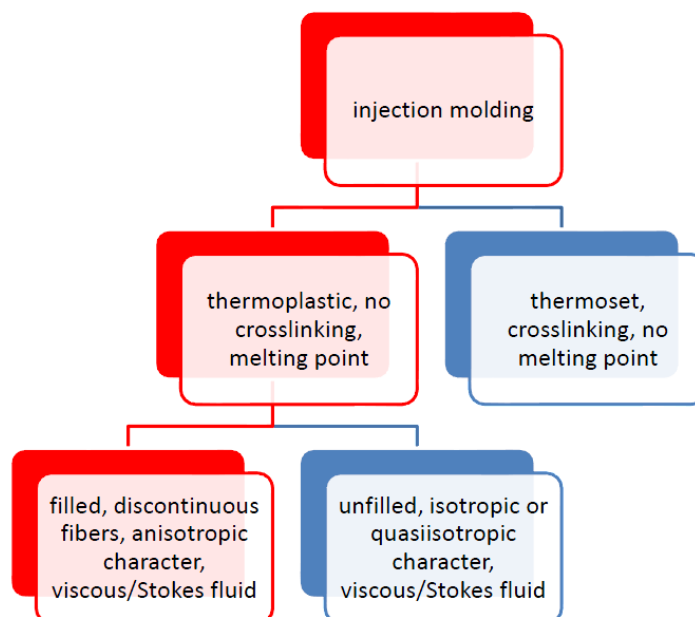


Figure 1.5: diagram of the types of materials used with injection molding. This report treats the red boxes.

1.4 Fiber orientation

In contrast with the isotropic or quasiisotropic character of unfilled plastics, fiber filled plastics have an anisotropic character. Many material properties are inherent to the distribution of the fibers in the final product, confer Figure 1.6. In liquid phase it affects the viscosity. In the solid phase it affects the elastic

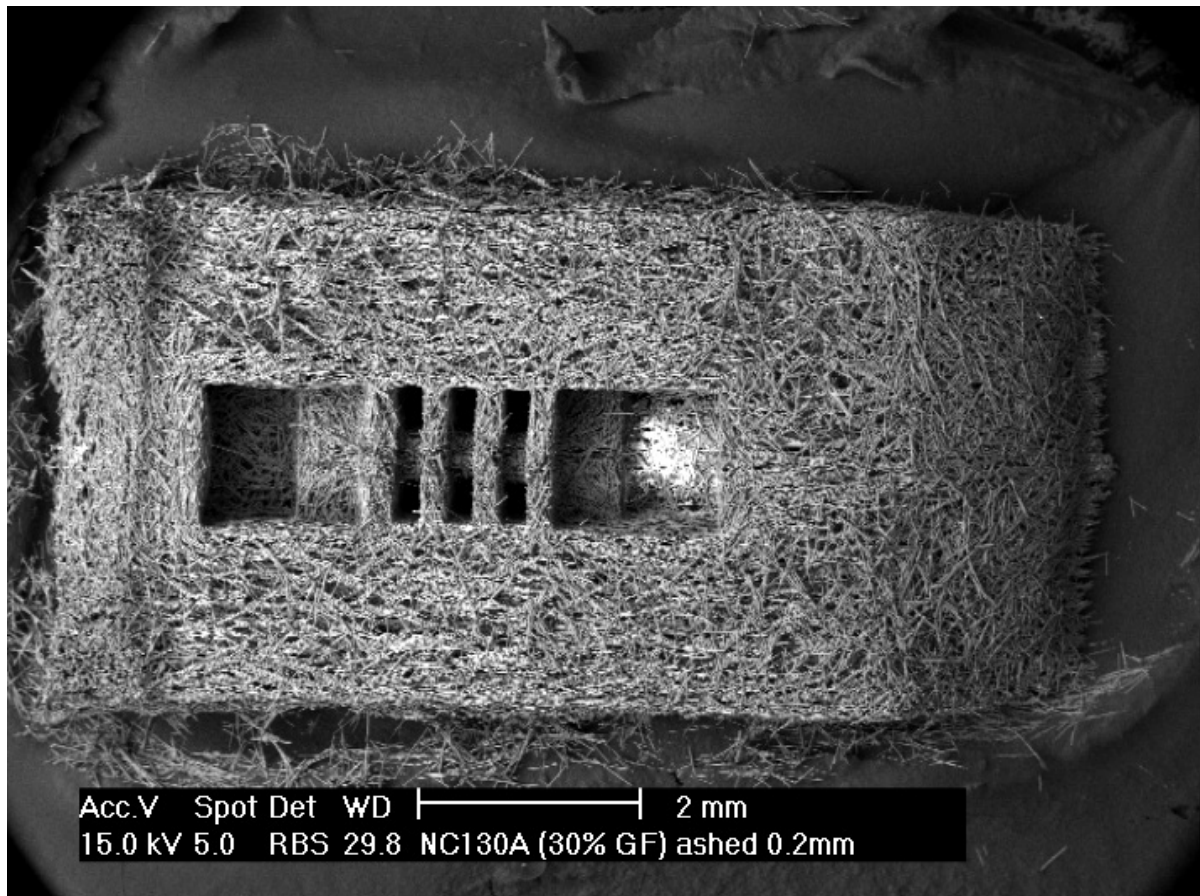


Figure 1.6: fiber orientation made visible by burning away the matrix material.

modulus and thermal expansion. In both the liquid and solid phase it affects the thermal and electrical conductivity [15]. All these properties can vary throughout the spatial dimensions of the thermoplastic part. This complicates the control of the production process. Depending on the distribution of the fibers, the viscosity has a certain distribution which influences the injection phase. It determines the stress distribution in the cooling phase. Before the ejection of the part, the forces of the product and the mold are in balance. In effect, the part has a certain shape, namely that of the mold. Ejecting the part from the mold changes the boundary condition. As a result, the final product may show warpage. The strength properties can be as intended or have local weak spots. The quality of the product is inherent to all the beforementioned properties. It is therefore in the interest of DSM to investigate the factors that determine the distribution of fibers.

The distribution of the fibers in the final product can be divided into two separate distributions. One is the distribution of the centers of mass of the fibers, the other is the orientation with respect to these centers of mass. In this report, the focal point is the distribution of the fiber orientation.

The research on fiber orientation is covered by several disciplines. As the orientation of the solid fibers is highly dependent on the dynamics of the fluid it is immersed in, it is a fluid-structure interaction (FSI) problem. Another relevant discipline is rheology. It is the study of the flow of all materials that 'lie between' two extremes, being an linear elastic solid and a fully viscous fluid.

1.5 Past research

There are several authors that have contributed to the modeling of fiber orientation. The author that stands out the most, is C.L. Tucker III [15, 19, 13, 7, 2, 18, 14]. In 1984, he published an article together

with F. Folgar [7]. In this article, they extended Jeffery's model, which models the fiber orientation of a single ellipsoidal fiber in viscous/Stokes fluid deterministically, with a isotropic fiber-fiber interaction term by the use a probability density function (PDF). This is described in Chapter 3. Due to the computational inefficiency of the 1984 Folgar-Tucker model, research was done to construct a computationally more efficient approach. This resulted in the publication [18] of S.G. Advani and C.L. Tucker III in 1987, wherein the use of tensors to describe fiber orientation was explained. This approach is described in Chapter 4. A phd student of C.L. Tucker III, R. Bay, published his thesis in 1991 [2], giving a comparison of the theory and experiments of injection molding. Due to the closure problem of the 1987 tensor approximation, research was also spent on how to construct an adequate closure approximation. This resulted in the publications [19] of S.G. Advani and C.L. Tucker III in 1989 and [15] by J.S. Cintra and C.L. Tucker III in 1995, constructing an approximation for the fourth order tensor by the use of physical arguments such as fiber alignment and orthotropy. The theory hereof is treated in Chapter 6. More than a decade later, in 2008, the Folgar-Tucker model from 1984 is extended by J. Wang, J.F. O'Gara and C.L. Tucker III. The Folgar-Tucker model displays a too fast transient response, which is solved in [13]. The Wang-O'Gara-Tucker model is treated in Chapter 5. The latest publication [14] by J.H. Phelps and C.L. Tucker III dates from 2009. In this article, the isotropic rotary diffusion is replaced by an anisotropic rotary diffusion.

Besides the publications mentioned above, wheron the emphasize is in this thesis, contributions to the modeling of fiber orientation were made by various other researchers. Some examples are L.G. Leal and E.J. Hinch, who contributed to the construction of fourth order tensor closure approximations. M.C. Altan and B.N. Rao, who made comparisons of theory and experimental results. D.A. Jack and D.E. Smith, who investigated sixth order tensor closure approximations [3]. And A. Redjeb and A. Megally, for research in two way coupling of the velocity field and the fiber orientation.

1.6 Commercial software

There are several commercial software packages available on the market to simulate the process of injection molding. Some examples are

- Moldflow,
- Moldex 3D,
- Sepran,
- Polyflow,
- and REM 3D.

At the moment, DSM uses the software package Moldflow to simulate injection molding processes. The producer of this software is Autodesk, also known for producing AutoCAD. It is the industry standard, in particular for the automotive industry.

Moldflow solves the conservation of mass, momentum, energy and the fiber orientation as a coupled set of equations using FEM. The pressure, velocity and temperature are solved monolithically. A posteriori, the fiber orientation is solved as a function of the velocity field. I.e. the velocity and fiber orientation are one way coupled.

For thin products, a 'two and a half' dimensional approach can be used. For the thicker products, a full three dimensional approach is used. The former approximates the thickness direction with 12-20 integration point and uses triangular shell elements. The pressure is only solved in the midplane, the velocity and temperature are also solved in the thickness direction. The three dimensional approach solves all three types of unknowns in all three dimensions.

The procedure of the modeling is as follows. First, the product is constructed, using either the two and a half or three dimensional approach. Subsequently, the injection locations have to be defined. The materials are chosen from a database. Several aspects of the injection molding can be modeled: the filling, packing and cooling phases, warpage and fiber orientation. Examples of the latter two are depicted in Figure 1.7. The results of the former three seem to be good. The results of the latter two are found to be poor and too uncontrollable. The parameters that can be varied are

- strength of the fiber-fiber interaction,

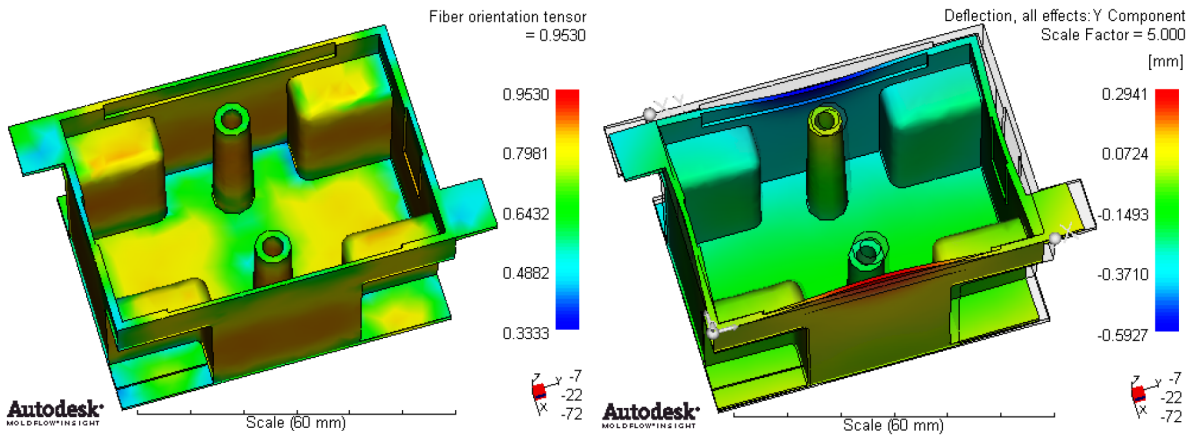


Figure 1.7: fiber orientation and warpage analyses in Moldflow [1].

- injection locations,
- injection velocities,
- mold surface temperature
- and melt temperature.

When the two and a half dimensional approach is used, there is also a thickness parameter that can be varied. Despite the possible variation of the beforementioned parameters, DSM is unable to obtain proper results from the warpage and fiber orientation modules. Investigating the influence of the strength of the fiber-fiber interaction and thickness parameter was in vain. In addition, Autodesk is persistent in appealing to company secrecy when asked for details on the used methods and the Wang-O’Gara-Tucker and Phelps-Tucker models have not been implemented yet.

1.7 Interest

As DSM does not only deliver the thermoplastics, but also the technology for the production, knowledge on the processing of the thermoplastics is of interest. Production must be as cheap and as fast as possible, without loss of quality of the product.

An intrinsic property of injection molding is that the amount of variable process conditions is marginal. The point and velocity of the injection can be varied, but the influence hereof is often insufficient for correcting production problems. Adaption of the mold requires some trial and error and is expensive. Simulations can be performed relatively cheap in the early stages of the part and mold design and offers the ability to evaluate different design options in terms of part, material and mold design. Avoiding problems in the design phase is superior to fixing them in the production phase.

DSM has the commercial tool Moldflow in place to simulate injection molding. A dominating disadvantage of commercial tools is that the implementation of the code is unavailable due to company secrecy. And although there is sometimes theory available on the algorithms used by the code, there are still demanding cases of injection molding where such literature is insufficient for an intensive analysis. It is therefore in the interest of DSM to, besides simulating with commercial tools, study these demanding cases.

An example of a demanding case is where substantial warpage arises. To understand the development of warpage simulation, it is important to appreciate that warpage results from inhomogeneous polymer shrinkage. While all polymers shrink on cooling from the melt to the solid phase, processing causes variation in shrinkage and it is this variation that results in part deformation. One can break the problem into two parts: prediction of isotropic shrinkage and prediction of anisotropic effects. The former is influenced greatly by the pressure and temperature history of the part. Consequently the packing phase is important. Development of anisotropic shrinkage effects is related to structural development of the material as it solidifies. It follows that warpage simulation rests on the ability to model the filling, packing and cooling phases of the injection molding process [16].

In any of the former cases, accurately predicting the fiber configurations in injection molded filled thermoplastics contributes to the quality of the material and the cost savings of the production. Error margins for the design decrease and can thus suffice to more strict demands.

1.8 Research method and approach

The purpose of the project is to gain knowledge on the fiber orientation during the injection phase in a computationally efficient way. The Wang-O’Gara-Tucker model is appropriate for this. The consideration of the latest Phelps-Tucker model is omitted as such an effort would force us to exceed the designated time schedule.

To understand the process of simulating fiber orientation, we will treat a substantial part of the fundamental theory behind the Wang-O’Gara-Tucker model. A schematic of the Wang-O’Gara-Tucker and preceding models is depicted in Figure 1.8. This includes the treatment of Jeffery’s equation for the modeling of a single ellipsoidal particle, immersed in a viscosity dominated or Stokes fluid. A simplified derivation of Jeffery’s equation is given. Subsequently, Jeffery’s equation is extended with a fiber-fiber interaction term by the use of a probability density function. The resulting equation is of a Fokker-Planck form. Herewith, the fiber orientation in concentrated suspensions can be modeled. The resulting model is referred to as the Folgar-Tucker model. This concludes Chapter 3.

Due to the computational inefficiency of solving the probability density of the Folgar-Tucker model, an alternative approach is constructed in Chapter 4. This alternative approach exists of considering the lower order terms of an expansion of the PDF in spherical harmonics, and neglecting the higher order terms. This approach is far more efficient. The lowest order term comes in the form of a second order tensor. Several useful properties of this tensor are deduced. The physical interpretation of the tensor is explained.

In Chapter 5, the Folgar-Tucker tensor form is adapted to obtain longer transient times. Herewith, the phenomenological model has more freedom to be adjusted to the results of experiments. The resulting model is referred to as the Wang-O’Gara-Tucker model, the focal model of the report. An equivalent kinetic theory is deduced.

The Wang-O’Gara-Tucker tensor form is not closed since a fourth order tensor occurs in the rate equation of the second order tensor. This closure problem is solved by approximating the fourth order tensor in terms of the components of the second order tensor, motivated by physical arguments. The class orthotropic closures is treated thoroughly, as in the literature it is often recognized as the best type of closure available. This is done in Chapter 6.

To solve the Fokker-Planck equation of the Wang-O’Gara-Tucker model, an explicit numerical scheme is constructed. It is proven that the scheme conserves the properties inherent to the PDF in question: nonnegativity, conservation of probability and the odd function character. Initial and boundary conditions are given. The consistency and stability of the numerical scheme are considered, to obtain a proof of convergence. This concludes Chapter 7.

For the sake of comparison, also the tensor form of the Wang-O’Gara-Tucker model has to be solved. In accordance, a numerical scheme is constructed, conserving the properties mentioned in Chapter 4. Both the intact and the eigenpair decomposition of the second order tensor are treated. This is done in Chapter 8.

Having treated the theory and implemented the Wang-O’Gara-Tucker model, we can consider flow fields and interpret the results. We limit ourselves to the treatment of homogeneous flow fields, so that the computation time of the kinetic theory remains acceptable. The used flow fields herefore are simple shear and uniaxial elongation flow, considered in Chapters 9 and 10 respectively. The flow fields are analyzed, expectations of the fiber orientation are mentioned. We begin with the simplest case, Jeffery’s equation for a single fiber, add the fiber-fiber interaction term and subsequently treat the full nonlinear Wang-O’Gara-Tucker model. We compare the solution stemming from the kinetic theory and the tensor approximation. In this way, the quality of the used closure approximations can be judged.

In Chapter 11 we draw conclusions and make recommendations. The conclusions are drawn with respect to the numerical schemes used to solve the equations and to the results of the test models. Recommendations are made for future research and improvements.

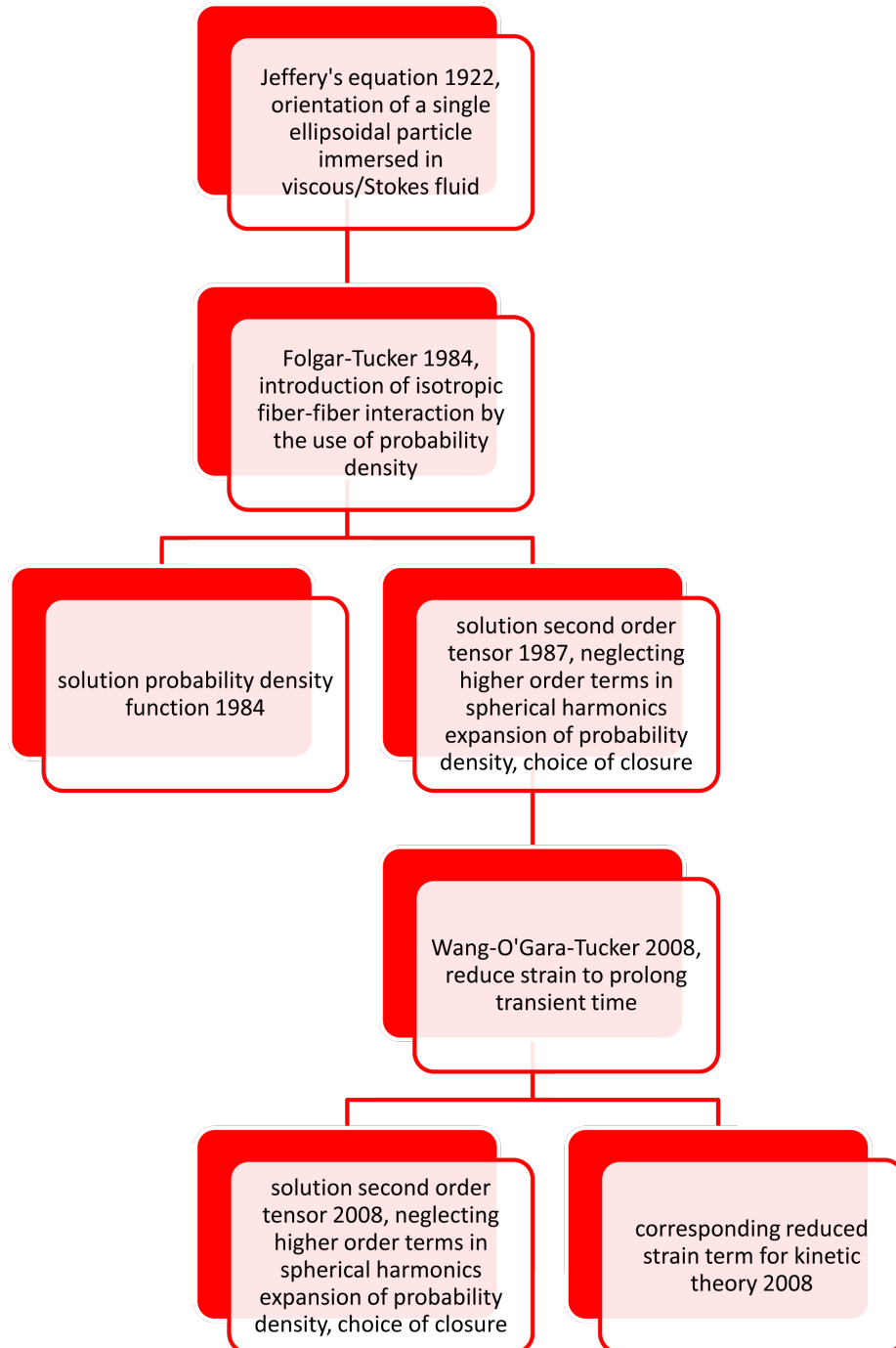


Figure 1.8: diagram of fiber orientation models.

Gaining knowledge on the fiber orientation in homogeneous flow fields is, in particular, enforced by the provision of the implementation of the Wang-O’Gara-Tucker model to DSM personnel. In accordance, Appendix B is dedicated to a thorough user instruction of the implementation in question. In this way, an integrated approach of the Wang-O’Gara-Tucker model is realized: the theory is presented, two test cases are considered as examples and the usage of the implementation is explained.

DSM will gain insight in the modeling of fiber orientation in homogeneous flow field. Different approximations can be compared. DSM will be able to discuss the results of fiber orientation in homogeneous flow fields with the injection molding software industry. The warpage and fiber orientation analyses can be improved. The process of injection molding can then be predicted more accurately. The quality of the products that DSM will offer will be of an even higher order.

1.9 Contribution

The contribution of this thesis exists of the reproduction of literature material, the construction of proofs and derivations, the generation and interpretation of output and the instructions to the implementations of the Wang-O’Gara-Tucker model. With the reproduction of literature material, we maintain our own vision in what is clear. Hopefully, this offers a perspective that is more clear and complete than the perspective that is offered in the literature.

In Chapter 2, we introduce our own notation, repeat some ‘classical’ mathematical preliminaries. We define the constrained gradient and proof some important properties.

Chapter 3 we construct a derivation that results in a particular case of Jeffery’s equation, but is much simpler than the complete proof of the complete model. In this way, the idea is straightforward without a cumbersome argumentation. The introduction of the probability density function to model fiber-fiber interaction, the derivation of its properties and the corresponding kinetic theory is reproduction of literature material. Subsequently, we interpret the kinetic theory.

In Chapter 4 we start with the different argumentations behind the tensor form of the kinetic theory. We show that these different argumentations are actually analogous. We derive the various the properties of the tensor form and repeat some classical proofs. The deduction of the Folgar-Tucker model is a reproduction of literature material.

Chapter 5 starts with the reproduction of the derivations of the rate equations for the eigenpairs of the tensor form. The modification and reassembly of these equations is done conform literature [13]. The notion of objectivity is repeated and the equivalent kinetic theory is reproduced.

In Chapter 6, theory from [15] is reproduced.

Chapters 7 and 8 does not contain any form of reproduction of literature material. We interpret the kinetic theory and tensor form of the Wang-O’Gara-Tucker model. We deduce useful properties, construct numerical schemes and their consistency and stability conditions.

In Chapters 9 and 10 we model the fiber orientation for the simple shear and uniaxial elongation flow fields. Characteristics and expectations of the flow fields are motivated. Results from Jeffery’s equation, the Folgar-Tucker and the Wang-O’Gara-Tucker models are discussed. Comparisons of the exact and approximative tensor forms are made.

In Chapter 11 we draw conclusions and make recommendations with respect to the preceding material.

The contribution of the master project is dominated by the provision of the implementation of the Wang-O’Gara-Tucker model to DSM personnel. To enforce the usage of this implementation, Appendix B is dedicated to giving the reader instructions in the usage of the code.

Chapter 2

Notation, conventions and mathematical preliminaries

2.1 Introduction

Before we discuss the fundamentals of the modeling of the fiber configurations in injection molded filled plastics, we will, for the sake of clarity, explain the notation and conventions used. Also the nontrivial mathematical preliminaries that will occur throughout the report are explained.

2.2 Notation and conventions

Throughout the report, certain notation and conventions will be used. Often, when a notation or convention is used for the first time, we will explain it. The other are explained here.

For scalar quantities we use symbols with a regular thickness. For higher dimensional quantities we use bold notation. First order tensors, or vectors, are denoted in small letters, so $\mathbf{a}, \mathbf{b}, \dots$. Second order tensors are denoted by capital letters in bold, so $\mathbf{A}, \mathbf{B}, \dots$. Third order tensor are denoted caligraphically, capital and bold, so $\mathcal{A}, \mathcal{B}, \dots$. Fourth order tensors are denoted by capital bold letters, $\mathbb{A}, \mathbb{B}, \dots$. We also denote the classes of numbers traditionally with $\mathbb{N}, \mathbb{Z}, \mathbb{Q}, \mathbb{R}, \mathbb{C}$ and probability with \mathbb{P} and thus try to avoid these letters when denoting fourth order tensors. We do not use tensors of orders higher than four. The scalar components of first or higher order tensors are denoted in regular thickness, with the letter, capital or not, corresponding with the tensor. The order of the corresponding tensor can be determined by the number of indices the scalar component of the tensor in question has.

Formally, when a basis is chosen and the components of a tensor are denoted, we use the notation $[\mathbf{a}]_E$, where \mathbf{a} is the tensor and E is the chosen basis. It is however, not often that we switch bases and thus we omit the $[\dots]_E$ notation for the sake of notation. When we want to emphasize a change or choice of basis, we will use the formal notation.

When we speak of eigenvectors, we, traditionally, mean right eigenvectors.

With \cdot we denote a single contraction between two tensors. The last dimension of the tensor to the left of \cdot is contracted with the first dimension of the tensor to the right of the \cdot . For example

$$(\mathbb{A} \cdot \mathbb{B})_{ijklmn} = \sum_p A_{ijkp} B_{plmn}.$$

This operation is also called the dot, inner or scalar product. Analogously, the $:$ operation is a double contraction. It contracts the last dimension of the tensor to the left of the $:$ with the first dimension of tensor on the right of the $:$ and the second to last dimension of the tensor to the right of the $:$ with the second dimension of the tensor to the right of the $:$. For example

$$(\mathbb{A} : \mathbb{B})_{ijkl} = \sum_{m,n} A_{ijmn} B_{nmkl}.$$

When using the summation sign \sum , we denote the index over which is summed, but not the values it takes as these are often trivial and most of the time $\{1, 2, 3\}$. In nontrivial cases, we do denote the values. Components of matrices are denoted between brackets $[\dots]$ and so are dimensions of quantities. In particular, $[\]$ means dimensionless or dimension one. The $:=$ means that we define a quantity. With \dots^T , we denote transposition. We omit the tensor product \otimes in our notation, as its occurrence is always trivial. In certain integrals we use the notation $d^1\mathbf{p}$ or $d^2\mathbf{p}$. Herewith, we emphasize the dimension of the manifold with the superscript and the variable of which the arguments are integrated over.

Throughout the thesis, the symbol δ is used in several ways. When it is denoted in combination with subscripts, it represents the Kronecker delta. I.e.

$$\delta_{ij} = \begin{cases} 1 & \text{if } i = j \\ 0 & \text{if } i \neq j \end{cases} . \quad (2.1)$$

When it is denoted in combination with an argument, it represents the Dirac delta function, i.e.

$$\delta(\mathbf{u}) = \begin{cases} \infty & \text{if } \mathbf{u} = \mathbf{0} \\ 0 & \text{if } \mathbf{u} \neq \mathbf{0} \end{cases} \quad (2.2)$$

such that

$$\int_U \delta(\mathbf{u}) dU = 1.$$

The last type of use of δ is explained in Subsection 2.3.2.

2.3 Mathematical preliminaries

2.3.1 Change of basis

Consider the second order tensor \mathbf{A} and two bases $E_1 = \{\mathbf{e}_1^1, \mathbf{e}_2^1, \mathbf{e}_3^1\}$ and $E_2 = \{\mathbf{e}_1^2, \mathbf{e}_2^2, \mathbf{e}_3^2\}$. The components of \mathbf{A} with respect to basis E_1 are known and the two bases are known. We will determine the components with respect to the basis E_2 . We have

$$\mathbf{A} = \sum_{i,j} A_{ij}^1 \mathbf{e}_i^1 \mathbf{e}_j^1 = \sum_{i,j} A_{ij}^2 \mathbf{e}_i^2 \mathbf{e}_j^2.$$

Component $A_{i'j'}^2$, follows from

$$\begin{aligned} A_{i'j'}^2 &= \sum_{i,j} A_{ij}^2 \delta_{ii'} \delta_{jj'} \\ &= \sum_{i,j} A_{ij}^2 \mathbf{e}_i^2 \mathbf{e}_j^2 \cdot \mathbf{e}_{j'}^2 \cdot \mathbf{e}_{i'}^2 \\ &= \sum_{i,j} A_{ij}^1 \mathbf{e}_i^1 \mathbf{e}_j^1 \cdot \mathbf{e}_{j'}^2 \cdot \mathbf{e}_{i'}^2 \\ &= \sum_{i,j} A_{ij}^1 (\mathbf{e}_i^1 \cdot \mathbf{e}_{i'}^2) (\mathbf{e}_j^1 \cdot \mathbf{e}_{j'}^2) \\ &= \sum_{i,j} A_{ij}^1 (\mathbf{E}_1^T \cdot \mathbf{E}_2)_{ii'} (\mathbf{E}_1^T \cdot \mathbf{E}_2)_{jj'} \\ &= \sum_{i,j} (\mathbf{E}_1^T \cdot \mathbf{E}_2)_{i'i}^T A_{ij}^1 (\mathbf{E}_1^T \cdot \mathbf{E}_2)_{jj'} \\ &= \sum_{i,j} (\mathbf{E}_2^T \cdot \mathbf{E}_1)_{i'i} A_{ij}^1 (\mathbf{E}_1^T \cdot \mathbf{E}_2)_{jj'} \end{aligned}$$

wherewith it follows that the matrices with components of \mathbf{A} with respect to bases E_1 and E_2 are related by

$$\mathbf{A}^2 = \mathbf{E}_2^T \cdot \mathbf{E}_1 \cdot \mathbf{A}^1 \cdot \mathbf{E}_1^T \cdot \mathbf{E}_2.$$

The operations in the latter are optimized in programs such as Matlab. There is no need for the interpretation of loops in this case, which is computationally more efficient.

In a similar way, the components of the fourth order matrices with respect to bases E_1 and E_2 , stemming from a fourth order tensor \mathbb{A} , are related to each other by

$$A_{i'j'k'l'}^2 = \sum_{i,j,k,l} A_{ijkl}^1 (\mathbf{e}_i^1 \cdot \mathbf{e}_{i'}^2) (\mathbf{e}_j^1 \cdot \mathbf{e}_{j'}^2) (\mathbf{e}_k^1 \cdot \mathbf{e}_{k'}^2) (\mathbf{e}_l^1 \cdot \mathbf{e}_{l'}^2) \quad (2.3)$$

which can, in general, not be written in a form involving only matrices and matrix operations. However, if the tensor possesses certain symmetries in the sense of permutations of the indices, it is possible. Motivated, again, by computational efficiency, we will show this here. We consider a fourth order tensor with the symmetries

$$A_{ijkl} = A_{jikl} = A_{ijlk}.$$

Considering the pairs (i, j) and (k, l) that are subjected to swapping, there are for each pair six unique combinations and thus $6 \cdot 6 = 36$ for \mathbb{A} . Using the Voigt index notation conform Table 2.1

Contracted notation	Tensor notation
m or n	ij or kl
1	11
2	22
3	33
4	23 or 32
5	31 or 13
6	12 or 21

Table 2.1: Voigt index notation.

we can write

$$A_{ijkl} = A_{mn},$$

which will be used in a moment.

Introducing

$$\mathbf{E} = \mathbf{E}_1^T \cdot \mathbf{E}_2 = \begin{bmatrix} \mathbf{e}_1^T \cdot \mathbf{e}_1 & \mathbf{e}_1^T \cdot \mathbf{e}_2 & \mathbf{e}_1^T \cdot \mathbf{e}_3 \\ \mathbf{e}_2^T \cdot \mathbf{e}_1 & \mathbf{e}_2^T \cdot \mathbf{e}_2 & \mathbf{e}_2^T \cdot \mathbf{e}_3 \\ \mathbf{e}_3^T \cdot \mathbf{e}_1 & \mathbf{e}_3^T \cdot \mathbf{e}_2 & \mathbf{e}_3^T \cdot \mathbf{e}_3 \end{bmatrix}$$

(2.3) can be written as

$$A_{i'j'k'l'}^2 = \sum_{i,j,k,l} A_{ijkl}^1 E_{ii'} E_{jj'} E_{kk'} E_{ll'}.$$

Introducing a sort of Kronecker delta

$$\delta_{i'j'm'} = \begin{cases} 1 & \text{if regular index pair } (i', j') \text{ corresponds with Voigt index } m' \\ 0 & \text{if regular index pair } (i', j') \text{ does not correspond with Voigt index } m' \end{cases}$$

we can write

$$\begin{aligned} A_{i'j'k'l'}^2 \delta_{i'j'm'} \delta_{k'l'n'} &= \delta_{i'j'm'} \delta_{k'l'n'} \sum_{i,j,k,l} A_{ijkl}^1 E_{ii'} E_{jj'} E_{kk'} E_{ll'} \\ A_{m'n'}^2 &= \delta_{i'j'm'} \delta_{k'l'n'} \sum_{i,j,k,l} A_{ijkl}^1 E_{ii'} E_{jj'} E_{kk'} E_{ll'} \\ A_{m'n'}^2 &= \delta_{i'j'm'} \delta_{k'l'n'} \sum_{m,n} \sum_{i,j,k,l} \delta_{ijm} \delta_{kl n} A_{mn}^1 E_{ii'} E_{jj'} E_{kk'} E_{ll'} \\ A_{m'n'}^2 &= \sum_{m,n} \left[\left(\delta_{i'j'm'} \sum_{i,j} E_{ii'} E_{jj'} \delta_{ijm} \right) A_{mn}^1 \left(\delta_{k'l'n'} \sum_{k,l} E_{kk'} E_{ll'} \delta_{kl n} \right) \right] \\ A_{m'n'}^2 &= \sum_{m,n} \left[\left(\delta_{i'j'm'} \sum_{i,j} (\mathbf{E}^T)_{i'i} \delta_{imj} (\mathbf{E})_{jj'} \right) A_{mn}^1 \left(\delta_{k'l'n'} \sum_{k,l} (\mathbf{E}^T)_{k'k} \delta_{knl} (\mathbf{E})_{ll'} \right) \right] \end{aligned}$$

Say we introduce a third order $3 \times 6 \times 3$ matrix \mathcal{I} with components δ_{imj} , then we can write

$$A_{m'n'}^2 = \sum_{m,n} [(\delta_{i'j'm'} (\mathbf{E}^T \cdot \mathcal{I} \cdot \mathbf{E})_{i'mj'}) A_{mn}^1 (\delta_{k'l'n'} (\mathbf{E}^T \cdot \mathcal{I} \cdot \mathbf{E})_{k'l'n'})].$$

Constructing a 6×6 matrix \mathbf{S} with components $S_{m'm} = \delta_{i'j'm'} (\mathbf{E}^T \cdot \mathcal{I} \cdot \mathbf{E})_{i'mj'}$ we can write

$$A_{m'n'}^2 = \sum_{m,n} S_{m'm} A_{mn}^1 S_{n'n} = \sum_{m,n} (\mathbf{S})_{m'm} A_{mn}^1 (\mathbf{S}^T)_{nn'} \Leftrightarrow \mathbf{A}^2 = \mathbf{S} \cdot \mathbf{A}^1 \cdot \mathbf{S}^T.$$

2.3.2 Spherical coordinates

Besides the 'regular' Cartesian coordinates, also spherical coordinates will be used thoroughly in this report. In particular, the radius is equal to one. The unit vectors representing the radial and tangential components are

$$\mathbf{p} := \begin{bmatrix} \sin(\theta) \cos(\phi) \\ \sin(\theta) \sin(\phi) \\ \cos(\theta) \end{bmatrix}, \quad \mathbf{q} := \begin{bmatrix} \cos(\theta) \cos(\phi) \\ \cos(\theta) \sin(\phi) \\ -\sin(\theta) \end{bmatrix}, \quad \mathbf{s} := \begin{bmatrix} -\sin(\phi) \\ \cos(\phi) \\ 0 \end{bmatrix} \quad (2.4)$$

where $\theta \in [0; \pi]$ is the elevation and $\phi \in [0; 2\pi]$ the azimuth. In accordance with the notation in [2], the vectors \mathbf{p} , \mathbf{q} and \mathbf{s} are also referred to by δ_r , δ_θ and δ_ϕ respectively. The spherical coordinates are depicted in Figure 2.1. For the angles we have the relations

$$\begin{aligned}\theta &= \arctan \frac{\sqrt{p_1^2 + p_2^2}}{p_3} \\ \phi &= \arctan \frac{p_2}{p_1}.\end{aligned}\quad (2.5)$$

The tensor products of the three vectors are also used often throughout the report. They are as follows.

$$\begin{aligned}\mathbf{pp} = \delta_r \delta_r &= \begin{bmatrix} \sin^2(\theta) \cos^2(\phi) & \sin^2(\theta) \sin(\phi) \cos(\phi) & \sin(\theta) \cos(\theta) \cos(\phi) \\ \sin^2(\theta) \sin(\phi) \cos(\phi) & \sin^2(\theta) \sin^2(\phi) & \sin(\theta) \cos(\theta) \sin(\phi) \\ \sin(\theta) \cos(\theta) \cos(\phi) & \sin(\theta) \cos(\theta) \sin(\phi) & \cos^2(\theta) \end{bmatrix} \\ &= \begin{bmatrix} \sin^2(\theta) \cos^2(\phi) & \frac{\sin^2(\theta) \sin(2\phi)}{2} & \frac{\sin(2\theta) \cos(\phi)}{2} \\ \frac{\sin^2(\theta) \sin(2\phi)}{2} & \sin^2(\theta) \sin^2(\phi) & \frac{\sin(2\theta) \sin(\phi)}{2} \\ \frac{\sin(2\theta) \cos(\phi)}{2} & \frac{\sin(2\theta) \sin(\phi)}{2} & \cos^2(\theta) \end{bmatrix}.\end{aligned}\quad (2.6)$$

$$\begin{aligned}\mathbf{pq} = \delta_r \delta_\theta &= \begin{bmatrix} \sin(\theta) \cos(\theta) \cos^2(\phi) & \sin(\theta) \cos(\theta) \sin(\phi) \cos(\phi) & -\sin^2(\theta) \cos(\phi) \\ \sin(\theta) \cos(\theta) \sin(\phi) \cos(\phi) & \sin(\theta) \cos(\theta) \sin^2(\phi) & -\sin^2(\theta) \sin(\phi) \\ \cos^2(\theta) \cos(\phi) & \cos^2(\theta) \sin(\phi) & -\sin(\theta) \cos(\theta) \end{bmatrix} \\ &= \begin{bmatrix} \frac{\sin(2\theta)(\cos(2\phi)+1)}{4} & \frac{\sin(2\theta) \sin(2\phi)}{4} & \frac{(\cos(2\theta)-1) \cos(\phi)}{2} \\ \frac{\sin(2\theta) \sin(2\phi)}{4} & \frac{\sin(2\theta)(1-\cos(2\phi))}{4} & \frac{(\cos(2\theta)-1) \sin(\phi)}{2} \\ \frac{(\cos(2\theta)+1) \cos(\phi)}{2} & \frac{(\cos(2\theta)+1) \sin(\phi)}{2} & -\frac{\sin(2\theta)}{2} \end{bmatrix}.\end{aligned}\quad (2.7)$$

$$\begin{aligned}\mathbf{ps} = \delta_r \delta_\phi &= \begin{bmatrix} -\sin(\theta) \sin(\phi) \cos(\phi) & \sin(\theta) \cos^2(\phi) & 0 \\ -\sin(\theta) \sin^2(\phi) & \sin(\theta) \sin(\phi) \cos(\phi) & 0 \\ -\cos(\theta) \sin(\phi) & \cos(\theta) \cos(\phi) & 0 \end{bmatrix} \\ &= \begin{bmatrix} -\frac{\sin(\theta) \sin(2\phi)}{2} & \frac{\sin(\theta)(\cos(2\phi)+1)}{2} & 0 \\ -\frac{\sin(\theta)(1-\cos(2\phi))}{2} & \frac{\sin(\theta) \sin(2\phi)}{2} & 0 \\ -\cos(\theta) \sin(\phi) & \cos(\theta) \cos(\phi) & 0 \end{bmatrix}.\end{aligned}\quad (2.8)$$

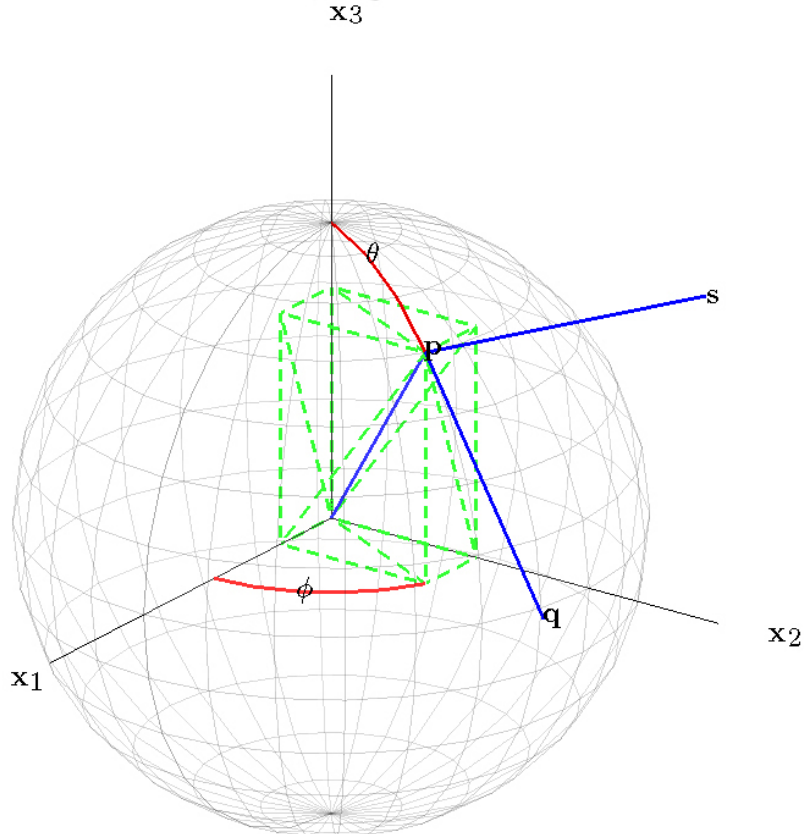


Figure 2.1: spherical coordinates for the unit sphere.

2.3.3 Projection

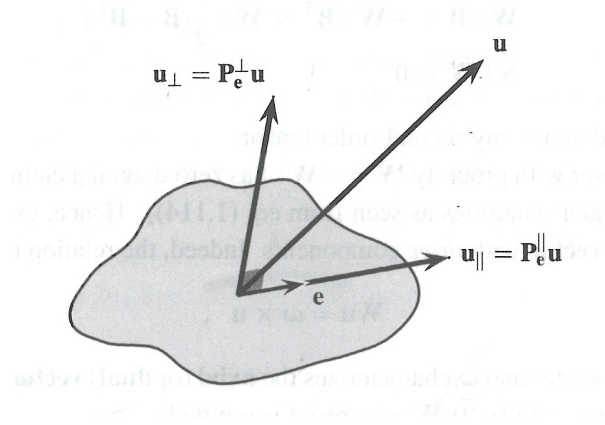


Figure 2.2: projections of \mathbf{u} with respect to \mathbf{e} [8].

Consider any vector \mathbf{u} and a unit vector \mathbf{e} . With reference to Figure 2.2, we write $\mathbf{u} = \mathbf{u}_{\parallel} + \mathbf{u}_{\perp}$, with \mathbf{u}_{\parallel} and \mathbf{u}_{\perp} characterizing the projection of \mathbf{u} onto the line spanned by \mathbf{e} and onto the plane normal to \mathbf{e} , respectively. We deduce that

$$\mathbf{u}_{\parallel} = (\mathbf{u} \cdot \mathbf{e})\mathbf{e} = (\mathbf{e}\mathbf{e}) \cdot \mathbf{u} = \mathbf{P}_{\mathbf{e}}^{\parallel} \mathbf{u}$$

and

$$\mathbf{u}_{\perp} = \mathbf{u} - \mathbf{u}_{\parallel} = \mathbf{u} - (\mathbf{e}\mathbf{e}) \cdot \mathbf{u} = (\mathbf{I} - \mathbf{e}\mathbf{e}) \cdot \mathbf{u} = \mathbf{P}_{\mathbf{e}}^{\perp} \mathbf{u} \quad (2.9)$$

where $\mathbf{P}_{\mathbf{e}}^{\parallel} = \mathbf{e}\mathbf{e}$ and $\mathbf{P}_{\mathbf{e}}^{\perp} = \mathbf{I} - \mathbf{e}\mathbf{e}$ are projection tensors of order two. The projection tensor $\mathbf{P}_{\mathbf{e}}^{\parallel}$ applied to any vector \mathbf{u} maps \mathbf{u} into the direction of \mathbf{e} , while $\mathbf{P}_{\mathbf{e}}^{\perp}$ applied to \mathbf{u} gives the projection of \mathbf{u} onto the plane normal to \mathbf{e} , confer Figure 2.2.

Definition 2.1. A tensor \mathbf{P} is a projection if \mathbf{P} is symmetric and $\mathbf{P}^n = \mathbf{P}$, $n \in \mathbb{Z}^+$.

A projection has the properties

$$\begin{aligned} \mathbf{P}_{\mathbf{e}}^{\parallel} + \mathbf{P}_{\mathbf{e}}^{\perp} &= \mathbf{I} \\ \mathbf{P}_{\mathbf{e}}^{\parallel} \cdot \mathbf{P}_{\mathbf{e}}^{\parallel} &= \mathbf{P}_{\mathbf{e}}^{\parallel} \\ \mathbf{P}_{\mathbf{e}}^{\perp} \cdot \mathbf{P}_{\mathbf{e}}^{\perp} &= \mathbf{P}_{\mathbf{e}}^{\perp} \\ \mathbf{P}_{\mathbf{e}}^{\parallel} \cdot \mathbf{P}_{\mathbf{e}}^{\perp} &= \mathbf{O}. \end{aligned}$$

2.3.4 Constrained differentiation on the surface of the unit sphere

2.3.4.1 Definition

We want to define the gradient of a unit vector $\mathbf{p} \in \mathbb{R}^3$ on the surface S of the unit sphere. As a unit vector is subjected to the constraint

$$\|\mathbf{p}\|_2 = 1 \quad \Leftrightarrow \quad p_1^2 + p_2^2 + p_3^2 = 1, \quad (2.10)$$

the components of the unit vector \mathbf{p} depend on each other. This seemingly small detail changes the gradient of a unit vector on S drastically. The differentiation is also constrained due to (2.10). We denote this 'constrained' gradient by

$$\tilde{\nabla}^{\otimes} = \frac{\tilde{\partial}}{\partial \mathbf{p}}^{\otimes}, \quad \text{or} \quad \tilde{\nabla} = \frac{\tilde{\partial}}{\partial \mathbf{p}}$$

in short, where the \sim emphasizes the constraint. We note that because \mathbf{p} is a unit vector and thus dimensionless by convention, that also the gradient is dimensionless. To define the constrained gradient we first introduce the set of orthonormal vectors as depicted in Figure 2.1

$$\mathbf{p} = \begin{bmatrix} \sin(\theta) \cos(\phi) \\ \sin(\theta) \sin(\phi) \\ \cos(\theta) \end{bmatrix}, \quad \mathbf{q} = \begin{bmatrix} \cos(\theta) \cos(\phi) \\ \cos(\theta) \sin(\phi) \\ -\sin(\theta) \end{bmatrix}, \quad \mathbf{s} = \begin{bmatrix} -\sin(\phi) \\ \cos(\phi) \\ 0 \end{bmatrix}$$

where spherical coordinates are used. Note that (2.4) spans \mathbb{R}^3 and can thus be used as a basis of vectors in \mathbb{R}^3 . The 'regular' gradient with respect to basis (2.4) is defined by

$$\nabla = \mathbf{p} \frac{\partial}{\partial r} + \mathbf{q} \frac{1}{r} \frac{\partial}{\partial \theta} + \mathbf{s} \frac{1}{r \sin \theta} \frac{\partial}{\partial \phi} \quad (2.11)$$

where r is the length of the vector. The target space of $\tilde{\nabla}$ is tangent to its domain space, which is the surface of the unit sphere. The $\tilde{\nabla}$ operator will therefore contain the projection tensor $\mathbf{P}_p^\perp = \mathbf{I} - \mathbf{p}\mathbf{p}$, confer (2.9). Say

$$\begin{aligned} \tilde{\nabla} &= \mathbf{P}_p^\perp \cdot \nabla \\ &= \mathbf{P}_p^\perp \cdot \left(\mathbf{p} \frac{\partial}{\partial r} + \mathbf{q} \frac{1}{r} \frac{\partial}{\partial \theta} + \mathbf{s} \frac{1}{r \sin \theta} \frac{\partial}{\partial \phi} \right) \\ &= \mathbf{q} \frac{1}{r} \frac{\partial}{\partial \theta} + \mathbf{s} \frac{1}{r \sin \theta} \frac{\partial}{\partial \phi}, \end{aligned} \quad (2.12)$$

then the units of left hand side (LHS) and right hand side (RHS) are [1] and $[\frac{1}{m}]$ respectively. This is impossible as the units on both sides should match. We recall that

$$\tilde{\nabla} = \frac{\tilde{\partial}}{\partial \mathbf{p}},$$

and that thus the unit of the LHS of (2.12) is correct. To conclude the definition of $\tilde{\nabla}$, we multiply the RHS of (2.12) by r , which corrects the unit to [1].

Definition 2.2. *The constrained gradient operator on S , denoted by $\tilde{\nabla}$, is defined as*

$$\tilde{\nabla} = r(\mathbf{I} - \mathbf{p}\mathbf{p}) \cdot \nabla = r\mathbf{P}_p^\perp \cdot \nabla = \mathbf{q} \frac{\partial}{\partial \theta} + \mathbf{s} \frac{1}{\sin \theta} \frac{\partial}{\partial \phi}$$

as $r = 1$ for S , and has a target space that is tangential to S .

2.3.4.2 Properties

The constrained gradient operator $\tilde{\nabla}$ as defined in Definition 2.2 results in certain properties which will be used throughout the report. These properties will be treated here.

Property 2.1. *The constrained gradient operator on the first order tensor \mathbf{p} results in*

$$\tilde{\nabla} \mathbf{p} = \mathbf{P}_p^\perp$$

and has components

$$(\tilde{\nabla} \mathbf{p})_{ij} = \delta_{ij} - p_i p_j.$$

Proof. Consider the constrained gradient operator on \mathbf{p}

$$\tilde{\nabla} \mathbf{p} = \mathbf{q} \frac{\partial \mathbf{p}}{\partial \theta} + \mathbf{s} \frac{1}{\sin \theta} \frac{\partial \mathbf{p}}{\partial \phi}.$$

Note that due to (2.4) we have that

$$\frac{\partial \mathbf{p}}{\partial \theta} = \mathbf{q}, \quad \frac{\partial \mathbf{p}}{\partial \phi} = \mathbf{s} \sin \theta.$$

Furthermore, since (2.4) forms an orthonormal basis, the unit second order tensor is by definition

$$\mathbf{p}\mathbf{p} + \mathbf{q}\mathbf{q} + \mathbf{s}\mathbf{s} = \mathbf{I}.$$

Herewith,

$$\mathbf{q} \frac{\partial \mathbf{p}}{\partial \theta} + \mathbf{s} \frac{1}{\sin \theta} \frac{\partial \mathbf{p}}{\partial \phi} = \mathbf{q}\mathbf{q} + \mathbf{s}\mathbf{s} = \mathbf{I} - \mathbf{p}\mathbf{p} = \mathbf{P}_p^\perp.$$

with components

$$(\tilde{\nabla} \mathbf{p})_{ij} = (\mathbf{I} - \mathbf{p}\mathbf{p})_{ij} = \mathbf{I}_{ij} - p_i p_j = \delta_{ij} - p_i p_j.$$

This result can also be written as

$$\frac{\partial p_i}{\partial p_j} = \delta_{ij} - p_i p_j.$$

□

Property 2.2. *The constrained gradient operator on the second order tensor \mathbf{pp} has components*

$$(\tilde{\nabla}(\mathbf{pp}))_{ijk} = \delta_{ij}p_k + \delta_{ik}p_j - 2p_i p_j p_k.$$

Proof. Consider the components of $\tilde{\nabla}(\mathbf{pp})$, using Definition 2.2

$$\begin{aligned} (\tilde{\nabla}(\mathbf{pp}))_{ijk} &= \frac{\tilde{\partial}}{\partial p_i}(p_j p_k) \\ &= \frac{\tilde{\partial} p_j}{\partial p_i} p_k + p_j \frac{\tilde{\partial} p_k}{\partial p_i} \\ &= (\delta_{ji} - p_j p_i) p_k + p_j (\delta_{ki} - p_k p_i) \\ &= \delta_{ij} p_k + \delta_{ik} p_j - 2p_i p_j p_k. \end{aligned}$$

□

Property 2.3. *The constrained Laplacian operator on the second order tensor \mathbf{pp} has the result*

$$\tilde{\nabla} \cdot \tilde{\nabla}(\mathbf{pp}) = 2(\mathbf{I} - 3\mathbf{pp}).$$

Proof. The second order tensor $\tilde{\nabla} \cdot \tilde{\nabla}(\mathbf{pp})$ has components

$$\begin{aligned} (\tilde{\nabla} \cdot \tilde{\nabla}(\mathbf{pp}))_{ij} &= \sum_k \frac{\tilde{\partial}}{\partial p_k} \frac{\tilde{\partial}}{\partial p_k}(p_i p_j) \\ &= \sum_k \frac{\tilde{\partial}}{\partial p_k} (\delta_{ki} p_j + \delta_{kj} p_i - 2p_k p_i p_j) \\ &= \sum_k \left[\delta_{ki} \frac{\tilde{\partial} p_j}{\partial p_k} \right] + \sum_k \left[\delta_{kj} \frac{\tilde{\partial} p_i}{\partial p_k} \right] - 2 \sum_k \frac{\tilde{\partial}}{\partial p_k} (p_k p_i p_j) \\ &= \frac{\tilde{\partial} p_j}{\partial p_i} + \frac{\tilde{\partial} p_i}{\partial p_j} - 2 \sum_k \left[\frac{\tilde{\partial} p_k}{\partial p_k} (p_i p_j) + \frac{\tilde{\partial} p_i}{\partial p_k} p_k p_j + \frac{\tilde{\partial} p_j}{\partial p_k} p_k p_i \right] \\ &= \delta_{ij} - p_i p_j + \delta_{ij} - p_i p_j - 2 \sum_k [(\delta_{kk} - p_k p_k) p_i p_j + (\delta_{ik} - p_i p_k) p_k p_j + (\delta_{jk} - p_j p_k) p_k p_i] \\ &= 2(\delta_{ij} - p_i p_j) - 2(3p_i p_j - p_i p_j + p_i p_j - p_i p_j + p_i p_j - p_j p_i) \\ &= 2(\delta_{ij} - p_i p_j) - 4p_i p_j \\ &= 2(\delta_{ij} - 3p_i p_j) \end{aligned}$$

which results in the tensor form $2(\mathbf{I} - 3\mathbf{pp})$, which concludes the proof. □

Property 2.4. *Consider the two scalar vector fields $A(\mathbf{p})$ and $B(\mathbf{p})$, both functions of \mathbf{p} and π and 2π periodic in θ and ϕ respectively. Then*

$$\int_S B \tilde{\nabla} \cdot \tilde{\nabla} A d^2 \mathbf{p} = \int_S A \tilde{\nabla} \cdot \tilde{\nabla} B d^2 \mathbf{p}.$$

Proof.

$$\begin{aligned} \tilde{\nabla} \cdot \tilde{\nabla} &= \left(\mathbf{q} \frac{\partial}{\partial \theta} + \mathbf{s} \frac{1}{\sin \theta} \frac{\partial}{\partial \phi} \right) \cdot \left(\mathbf{q} \frac{\partial}{\partial \theta} + \mathbf{s} \frac{1}{\sin \theta} \frac{\partial}{\partial \phi} \right) \\ &= \left(\mathbf{q} \frac{\partial}{\partial \theta} \right) \cdot \left(\mathbf{q} \frac{\partial}{\partial \theta} \right) + \left(\mathbf{q} \frac{\partial}{\partial \theta} \right) \cdot \left(\mathbf{s} \frac{1}{\sin \theta} \frac{\partial}{\partial \phi} \right) \\ &\quad + \left(\mathbf{s} \frac{1}{\sin \theta} \frac{\partial}{\partial \phi} \right) \cdot \left(\mathbf{q} \frac{\partial}{\partial \theta} \right) + \left(\mathbf{s} \frac{1}{\sin \theta} \frac{\partial}{\partial \phi} \right) \cdot \left(\mathbf{s} \frac{1}{\sin \theta} \frac{\partial}{\partial \phi} \right) \\ &= \mathbf{q} \cdot \frac{\partial \mathbf{q}}{\partial \theta} \frac{\partial}{\partial \theta} + \frac{\partial^2}{\partial \theta^2} + \mathbf{q} \cdot \frac{\partial \mathbf{s}}{\partial \theta} \frac{1}{\sin \theta} \frac{\partial}{\partial \phi} + \mathbf{s} \cdot \frac{\partial \mathbf{q}}{\partial \phi} \frac{1}{\sin \theta} \frac{\partial}{\partial \theta} + \mathbf{s} \frac{\partial \mathbf{s}}{\partial \phi} \frac{1}{\sin^2 \theta} \frac{\partial}{\partial \phi} + \frac{1}{\sin^2 \theta} \frac{\partial^2}{\partial \phi^2} \end{aligned} \quad (2.13)$$

From (2.4) it follows that

$$\frac{\partial \mathbf{q}}{\partial \theta} = -\mathbf{p}, \quad \frac{\partial \mathbf{q}}{\partial \phi} = \mathbf{s} \cos \theta, \quad \frac{\partial \mathbf{s}}{\partial \theta} = \mathbf{0}, \quad \frac{\partial \mathbf{s}}{\partial \phi} = -\mathbf{p} \sin(\theta) - \mathbf{q} \cos(\theta)$$

wherewith, in combination with orthogonality, (2.13) becomes

$$\begin{aligned}
\tilde{\nabla} \cdot \tilde{\nabla} &= \frac{\partial^2}{\partial \theta^2} + \frac{\cos \theta}{\sin \theta} \frac{\partial}{\partial \theta} + \frac{1}{\sin^2 \theta} \frac{\partial^2}{\partial \phi^2} \\
&= \frac{1}{\sin \theta} \frac{\partial}{\partial \theta} \left(\sin(\theta) \frac{\partial}{\partial \theta} \right) + \frac{1}{\sin^2 \theta} \frac{\partial^2}{\partial \phi^2} \\
&= \frac{1}{\sin \theta} \left(\frac{\partial}{\partial \theta} \left(\sin(\theta) \frac{\partial}{\partial \theta} \right) + \frac{1}{\sin \theta} \frac{\partial^2}{\partial \phi^2} \right). \tag{2.14}
\end{aligned}$$

As a result, we get

$$\begin{aligned}
\int_S B \tilde{\nabla} \cdot \tilde{\nabla} A \, d^2 \mathbf{p} &= \int_{\phi=0}^{2\pi} \int_{\theta=0}^{\pi} B \frac{1}{\sin \theta} \left(\frac{\partial}{\partial \theta} \left(\sin(\theta) \frac{\partial}{\partial \theta} \right) + \frac{1}{\sin \theta} \frac{\partial^2}{\partial \phi^2} \right) A \sin(\theta) d\theta d\phi \\
&= \int_{\phi=0}^{2\pi} \int_{\theta=0}^{\pi} B \left(\frac{\partial}{\partial \theta} \left(\sin(\theta) \frac{\partial A}{\partial \theta} \right) + \frac{1}{\sin \theta} \frac{\partial^2 A}{\partial \phi^2} \right) d\theta d\phi \\
&= \int_{\phi=0}^{2\pi} \int_{\theta=0}^{\pi} B \frac{\partial}{\partial \theta} \left(\sin(\theta) \frac{\partial A}{\partial \theta} \right) d\theta d\phi + \int_{\phi=0}^{2\pi} \int_{\theta=0}^{\pi} \frac{B}{\sin \theta} \frac{\partial^2 A}{\partial \phi^2} d\theta d\phi \\
&= \int_{\phi=0}^{2\pi} \left[\left[B \sin(\theta) \frac{\partial A}{\partial \theta} \right]_{\theta=0}^{\pi} - \int_{\theta=0}^{\pi} \sin(\theta) \frac{\partial A}{\partial \theta} \frac{\partial B}{\partial \theta} d\theta \right] d\phi \\
&\quad + \int_{\theta=0}^{\pi} \frac{1}{\sin \theta} \left[\left[B \frac{\partial A}{\partial \phi} \right]_{\phi=0}^{2\pi} - \int_{\phi=0}^{2\pi} \frac{\partial A}{\partial \phi} \frac{\partial B}{\partial \phi} d\phi \right] d\theta \\
&= - \int_{\phi=0}^{2\pi} \int_{\theta=0}^{\pi} \left[\sin(\theta) \frac{\partial A}{\partial \theta} \frac{\partial B}{\partial \theta} + \frac{1}{\sin \theta} \frac{\partial A}{\partial \phi} \frac{\partial B}{\partial \phi} \right] d\phi d\theta \tag{2.15}
\end{aligned}$$

where we used the periodicity properties of B and integration by parts. Using integration by parts and the periodicity properties of A , we obtain

$$\begin{aligned}
\int_{\theta=0}^{\pi} \sin(\theta) \frac{\partial A}{\partial \theta} \frac{\partial B}{\partial \theta} d\theta &= \left[\sin(\theta) A \frac{\partial B}{\partial \theta} \right]_{\theta=0}^{\pi} - \int_{\theta=0}^{\pi} A \frac{\partial}{\partial \theta} \left(\sin(\theta) \frac{\partial B}{\partial \theta} \right) d\theta \\
&= - \int_{\theta=0}^{\pi} A \frac{\partial}{\partial \theta} \left(\sin(\theta) \frac{\partial B}{\partial \theta} \right) d\theta
\end{aligned}$$

and

$$\begin{aligned}
\int_{\phi=0}^{2\pi} \frac{\partial A}{\partial \phi} \frac{\partial B}{\partial \phi} d\phi &= \left[A \frac{\partial B}{\partial \phi} \right]_{\phi=0}^{2\pi} - \int_{\phi=0}^{2\pi} A \frac{\partial^2 B}{\partial \phi^2} d\phi \\
&= - \int_{\phi=0}^{2\pi} A \frac{\partial^2 B}{\partial \phi^2} d\phi.
\end{aligned}$$

simplifying (2.15) as

$$\begin{aligned}
-\int_{\phi=0}^{2\pi} \int_{\theta=0}^{\pi} \left[\sin(\theta) \frac{\partial A}{\partial \theta} \frac{\partial B}{\partial \theta} d\theta d\phi + \frac{1}{\sin \theta} \frac{\partial A}{\partial \phi} \frac{\partial B}{\partial \phi} \right] d\theta d\phi &= -\int_{\phi=0}^{2\pi} \int_{\theta=0}^{\pi} \sin(\theta) \frac{\partial A}{\partial \theta} \frac{\partial B}{\partial \theta} d\theta d\phi - \int_{\phi=0}^{2\pi} \int_{\theta=0}^{\pi} \frac{1}{\sin \theta} \frac{\partial A}{\partial \phi} \frac{\partial B}{\partial \phi} d\theta d\phi \\
&= -\int_{\phi=0}^{2\pi} \int_{\theta=0}^{\pi} \sin(\theta) \frac{\partial A}{\partial \theta} \frac{\partial B}{\partial \theta} d\theta d\phi - \int_{\theta=0}^{\pi} \int_{\phi=0}^{2\pi} \frac{1}{\sin \theta} \frac{\partial A}{\partial \phi} \frac{\partial B}{\partial \phi} d\phi d\theta \\
&= \int_{\phi=0}^{2\pi} \int_{\theta=0}^{\pi} A \frac{\partial}{\partial \theta} \left(\sin(\theta) \frac{\partial B}{\partial \theta} \right) d\theta d\phi + \int_{\theta=0}^{\pi} \int_{\phi=0}^{2\pi} \frac{1}{\sin \theta} A \frac{\partial^2 B}{\partial \phi^2} d\phi d\theta \\
&= \int_{\phi=0}^{2\pi} \int_{\theta=0}^{\pi} A \frac{1}{\sin \theta} \left[\frac{\partial}{\partial \theta} \left(\sin(\theta) \frac{\partial}{\partial \theta} \right) + \frac{1}{\sin \theta} \frac{\partial^2}{\partial \phi^2} \right] B \sin(\theta) d\theta d\phi \\
&= \int_S A \tilde{\nabla} \cdot \tilde{\nabla} B d^2 \mathbf{p},
\end{aligned}$$

which concludes the proof. □

Chapter 3

Jeffery's equation and the Folgar-Tucker model

3.1 Introduction

In our progression towards the Wang-O'Gara-Tucker model, the preceding attempts to model fiber orientation can not be skipped. The two most important attempts, which are also the fundament of the Wang-O'Gara-Tucker model, were made by G.B. Jeffery in 1922 and, more than half a century later, by F. Folgar and C.L. Tucker in 1984.

We explain the idea's behind Jeffery' equation, including the assumptions and a derivation of the equation in one particular case. The extension of Jeffery's equation, made by F. Folgar and C.L. Tucker III is considered subsequently. This gives rise to partial differential equation (PDE). A derivation is included. This kinetic theory, as it is called, is computationally expensive, which leads us to the next chapter wherein a more computationally attractive alternative is introduced.

3.2 Jeffery's equation

3.2.1 Description in space and assumptions

The modeling of fiber orientation starts with the construction of a quantitative description in space. Self evidently, there are many possibilities in doing so. Considering a flexible fiber as a finite pathline $\in \mathbb{R}^3$, functions describing the set of the infinite amount of points of the line in space can be constructed. Such a description is in our case overly detailed and cumbersome, as making some plausible assumptions simplifies the modeling and gives rise to a spatial description.

In 1922, G.B. Jeffery published an article describing the motion of prolate ellipsoidal particles immersed in a viscosity dominated fluid [9]. Herein, he considers particles with an ellipsoidal shape with two unique axes, confer Figure 3.1. He assumes that the particles do not bend, but are rigid and straight.

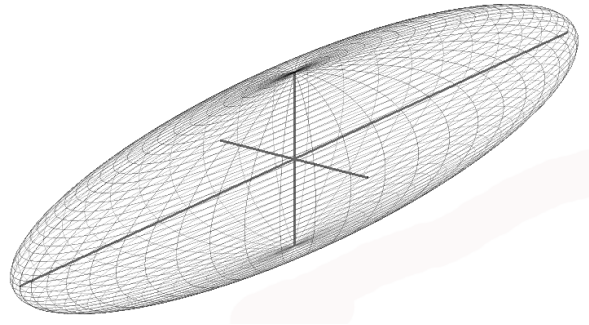


Figure 3.1: a prolate ellipsoid: the short axes are equal, the long axis is unique.

When the long axis is much larger than the short axis of the ellipsoid, $\frac{l}{d} \gg 1$, torque about the long axis is neglected as it is small in comparison with the torque about the short axis. Furthermore, the immersing fluid is assumed to be fully viscous, and so inertial and body forces can be neglected. The velocity field is treated as homogeneous at length scales comparable to the particle size. In other words, the velocity field does not change in space, so

$$\nabla \mathbf{v} = \mathbf{0}.$$

The velocity field can thus be expressed as

$$\mathbf{v} = \mathbf{K} \cdot \mathbf{x} + \mathbf{c} \quad (3.1)$$

with $\mathbf{K} = (\nabla \mathbf{v})^T$ constant in space \mathbf{x} , but not necessarily constant in time t . Furthermore, \mathbf{K} is subjected to the condition $\nabla \cdot \mathbf{v} = 0$ as we assume that the flow is incompressible. As a consequence, we must have that

$$\text{tr}(\mathbf{K}) = \sum_i ((\nabla \mathbf{v})^T)_{ii} = \nabla \cdot \mathbf{v} = 0.$$

Vector \mathbf{c} in (3.1) is a vector that is constant in space, but also not necessarily constant in time.

The beforementioned gives rise to a spatial description. The orientation of the ellipsoid can be described by a unit vector \mathbf{p} with its coordinates with respect to a Cartesian basis on the surface of the unit sphere. The latter space will be used frequently throughout this report, and we thus define

$$S = \{\mathbf{p} \in \mathbb{R}^3 : \|\mathbf{p}\|_2 = 1\},$$

as depicted in Figure 2.1. Note that since \mathbf{p} is a unit vector and thus merely a direction, it is dimensionless. This description is used often in the literature concerning fiber orientation. The unit vector \mathbf{p} can be parametrized using generalized coordinates θ, ϕ with respect to a Cartesian basis. Doing so decreases the number of degrees of freedom (#DOF) [4] and yields

$$\mathbf{p} = \begin{bmatrix} \sin(\theta) \cos(\phi) \\ \sin(\theta) \sin(\phi) \\ \cos(\theta) \end{bmatrix}. \quad (3.2)$$

The path of \mathbf{p} on the surface of the unit sphere is called a Jeffery's orbit.

With the above assumptions, a derivation of Jeffery's equation for a particular case will be made. A complete derivation is cumbersome and redundant as the following derivation suffices in explaining the ideas behind the equation.

3.2.2 Derivation

Consider a massless fiber in a fully viscous fluid with its two end points located at positions \mathbf{r}_1 and \mathbf{r}_2 with respect to a chosen origin O , as depicted in 3.2. We assume free draining between the end

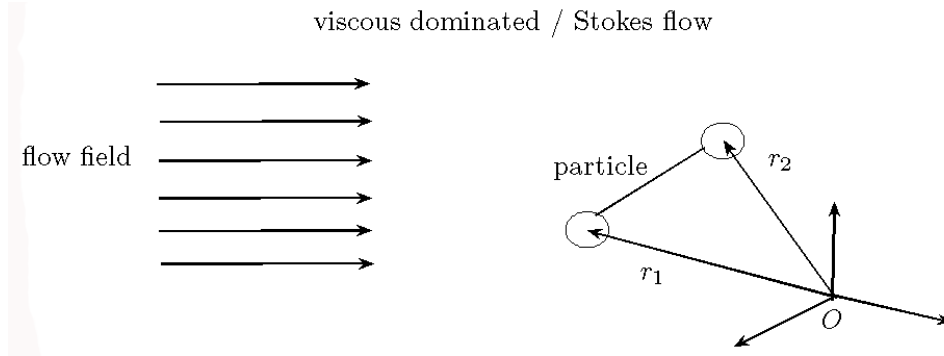


Figure 3.2: particle immersed in a viscous dominated / Stokes flow.

points. This means that the fluid flow between the end points is not subjected to stresses by the fiber. Say $\mathbf{q} = \mathbf{r}_2 - \mathbf{r}_1$. The length $\|\mathbf{q}\|_2$ is fixed as the fiber is considered rigid. Because we consider only homogeneous flows, we can write $\mathbf{v} = \mathbf{K} \cdot \mathbf{x}$ with \mathbf{K} in $[\frac{1}{s}]$. The viscous force on the particles is described by

$$\mathbf{F}_i = -\zeta(\dot{\mathbf{r}}_i - \mathbf{v}_i) = -\zeta(\dot{\mathbf{r}}_i - \mathbf{K} \cdot \mathbf{r}_i), i \in \{1, 2\}$$

where $\zeta = 6\pi\eta a [\frac{kg}{s}]$ is the friction of a sphere with radius $a [m]$ in Stokes flow with viscosity $\eta [\frac{kg}{ms}]$ under no slip conditions. Say we call the internal force in the fiber, enforcing the constraint of the fixed length $\|\mathbf{q}\|_2 = \text{constant}$, by \mathbf{F}_c . Then we must have

$$\begin{aligned} \mathbf{F}_1 + \mathbf{F}_c &= 0 \\ \mathbf{F}_2 - \mathbf{F}_c &= 0. \end{aligned}$$

Subtracting the first equation from the second we obtain

$$\begin{aligned} \mathbf{F}_2 - \mathbf{F}_1 - 2\mathbf{F}_c &= 0 \\ -\zeta((\dot{\mathbf{r}}_2 - \dot{\mathbf{r}}_1) - \mathbf{K} \cdot (\mathbf{r}_2 - \mathbf{r}_1)) - 2\mathbf{F}_c &= 0 \\ -\zeta(\dot{\mathbf{q}} - \mathbf{K} \cdot \mathbf{q}) - 2\mathbf{F}_c &= 0. \end{aligned}$$

Because \mathbf{q} and \mathbf{F}_c have the same direction, namely \mathbf{p} , we can write

$$\mathbf{q} = l\mathbf{p}, \quad \mathbf{F}_c = F_c\mathbf{p}$$

resulting in

$$-\zeta(l\dot{\mathbf{p}} - l\mathbf{K} \cdot \mathbf{p}) - 2F_c \mathbf{p} = 0.$$

Taking the inner product with \mathbf{p} gives, due to $\|\mathbf{p}\|_2 = 1 \Rightarrow \mathbf{p} \cdot \mathbf{p} = 1, \dot{\mathbf{p}} \cdot \mathbf{p} = 0$, that

$$\begin{aligned} \zeta l \mathbf{p} \cdot \mathbf{K} \cdot \mathbf{p} - 2F_c &= 0 \\ F_c &= \frac{\zeta l}{2} \mathbf{p} \cdot \mathbf{K} \cdot \mathbf{p}. \end{aligned}$$

Filling this in in the original subtraction, we get

$$\begin{aligned} -\zeta(l\dot{\mathbf{p}} - l\mathbf{K} \cdot \mathbf{p}) - 2\left(\frac{\zeta l}{2} \mathbf{p} \cdot \mathbf{K} \cdot \mathbf{p}\right) \mathbf{p} &= 0 \\ \dot{\mathbf{p}} - \mathbf{K} \cdot \mathbf{p} + \mathbf{p} \cdot \mathbf{K} \cdot \mathbf{p} \mathbf{p} &= 0 \\ \dot{\mathbf{p}} &= \mathbf{K} \cdot \mathbf{p} - \mathbf{p} \cdot \mathbf{K} \cdot \mathbf{p} \mathbf{p}. \end{aligned}$$

Splitting \mathbf{K} into its symmetric and antisymmetric part

$$\mathbf{D} = \frac{1}{2}(\mathbf{K} + \mathbf{K}^T), \quad \mathbf{W} = \frac{1}{2}(\mathbf{K} - \mathbf{K}^T)$$

respectively, $\mathbf{K} = \mathbf{D} + \mathbf{W}$, we get the ordinary differential equation (ODE)

$$\begin{aligned} \dot{\mathbf{p}} &= (\mathbf{D} + \mathbf{W}) \cdot \mathbf{p} - \mathbf{p} \cdot (\mathbf{D} + \mathbf{W}) \cdot \mathbf{p} \mathbf{p} \\ \dot{\mathbf{p}} &= \mathbf{W} \cdot \mathbf{p} + \mathbf{D} \cdot \mathbf{p} - \mathbf{p} \cdot \mathbf{D} \cdot \mathbf{p} \mathbf{p} \\ \dot{\mathbf{p}} &= \mathbf{W} \cdot \mathbf{p} + \mathbf{D} \cdot \mathbf{p} - \mathbf{D} : \mathbf{p} \mathbf{p} \mathbf{p}, \end{aligned}$$

where we used the property $\mathbf{x} \cdot \mathbf{W} \cdot \mathbf{x} = 0 \forall \mathbf{x}$ for an antisymmetric tensor. The first two terms stem from the difference in velocity of the end points of the fiber. This gives rise to a rotation generated by $\mathbf{W} \cdot \mathbf{p}$ and a strain generated by $\mathbf{D} \cdot \mathbf{p}$. The last term stems from the internal force in the fiber, also generating a strain.

A complete derivation of Jeffery's equation would lead to

$$\dot{\mathbf{p}} = \mathbf{W} \cdot \mathbf{p} + \xi(\mathbf{D} \cdot \mathbf{p} - \mathbf{D} : \mathbf{p} \mathbf{p} \mathbf{p}) \quad (3.3)$$

where

$$\xi = \frac{r_e^2 - 1}{r_e^2 + 1}, \quad r_e = \sqrt{-\frac{\xi + 1}{\xi - 1}}, \quad r_e = \frac{l}{d},$$

with l the length of the long axis of the ellipsoid and d the length of the short axis. Note that

$$\begin{aligned} \lim_{\xi \uparrow 1} r_e &= \infty \\ \lim_{\xi \downarrow -1} r_e &= 0 \end{aligned}$$

so that $-1 < \xi < 1$ is realistic. Describing (3.3) by the use of generalized coordinates we get

$$\begin{aligned} \dot{\theta} &= (\lambda^- \mathbf{K}^T + \lambda^+ \mathbf{K}) : \delta_r \delta_\theta \\ \dot{\phi} \sin \theta &= (\lambda^- \mathbf{K}^T + \lambda^+ \mathbf{K}) : \delta_r \delta_\phi \end{aligned} \quad (3.4)$$

where

$$\lambda^- = \frac{\xi - 1}{2} \quad \lambda^+ = \frac{\xi + 1}{2}$$

and $(\delta_r, \delta_\theta, \delta_\phi) = (\mathbf{p}, \mathbf{q}, \mathbf{s})$ confer [2]. This description is obtained by taking the inner product of (3.3) with δ_θ or δ_ϕ respectively.

With this result, Jeffery determined that center of such a particle translates with the bulk motion of the fluid, and that the particle rotates with a period that depends on its shape. The speed of rotation is not constant. The particle rotates slower when aligned with the flow direction.

The length of the fibers used in injection molding is small in comparison with the variation of the streamlines of the main flow. Jeffery's equation therefore suffices to describe the motion of a single fiber immersed in a viscous fluid. However, even dilute suspensions of filled plastics used with injection molding contain an amount of fibers that calls for the consideration of interaction among the fibers, so called fiber-fiber interaction (FFI). This leads us to the Folgar-Tucker model.

3.3 Folgar-Tucker model

3.3.1 Fiber-fiber interaction

F. Folgar and C.L. Tucker III recognized that Jeffery's equation needed to be extended, as it does not take the effects of high concentrations of fibers into account [7]. The interaction among the fibers influences the orientation of the fibers. Even in dilute suspensions, the interaction is substantial, and so it would not be logical to attempt to describe it deterministically. A stochastic description is more obvious. Folgar and Tucker therefore introduced a probability density function (PDF) $\psi(\mathbf{p}, t)$ as a function of orientation \mathbf{p} and time t , which describes the probability density of the fiber having a certain direction on S . Subsequently, the FFI can be described in terms of ψ . The definition is as follows.

Definition 3.1. *Let P be a continuous random variable with realizations \mathbf{p} in event space S , then $\psi : S \times \mathbb{R} \rightarrow \mathbb{R}$ is defined such that*

$$\mathbb{P}(P \in S', t) = \oint_{S'} \psi(\mathbf{p}, t) d^2 \mathbf{p},$$

under the conditions that

$$\forall \mathbf{p}, t \quad \psi(\mathbf{p}, t) \geq 0 \quad \wedge \quad \forall t \quad \oint_S \psi(\mathbf{p}, t) d^2 \mathbf{p} = 1 \quad \wedge \quad \forall \mathbf{p}, t \quad \psi(\mathbf{p}, t) = \psi(-\mathbf{p}, t).$$

The $\mathbb{P}(P \in S', t)$ denotes the probability of a fiber lying in a direction represented by $S' \subset S$. Such a representation stems from the end point of a fiber being enclosed by the surface element S' .

As S is not a space with a physical interpretation but merely a mathematical notion, we can choose the dimension of the infinitesimal elements $d^2 \mathbf{p}$. For the sake of simplicity, we choose $d^2 \mathbf{p}$ to be dimensionless. Because probability is also dimensionless, also ψ must be dimensionless.

The first two conditions are intrinsic to the definition of a PDF. The third condition stems from the spherical symmetry of \mathbf{p} . It states that, because \mathbf{p} represents a fiber orientation, it is invariant under the 'labeling' of its ends as head or tail. In terms of the generalized coordinates, this is described by

$$\psi(\theta, \phi) = \psi(\pi - \theta, \phi + \pi) \Leftrightarrow \psi(\mathbf{p}, t) = \psi(-\mathbf{p}, t).$$

The term modeling the FFI phenomenologically is

$$-C_I \dot{\gamma} \tilde{\nabla} \ln \psi = -\frac{C_I \dot{\gamma} \tilde{\nabla} \psi}{\psi}. \quad (3.5)$$

The coefficient C_I is called the interaction coefficient, which determines how strong the FFI is present in the flow. It is typically of the order $O(10^{-3}) - O(10^{-1})$. The $\dot{\gamma}$ does not have a unique definition. It depends on which flow field is considered. In case of a simple shear flow field for instance we have

$$\mathbf{v} = \mathbf{K} \cdot \mathbf{x}, \quad \mathbf{K} = \begin{bmatrix} 0 & \dot{\gamma} & 0 \\ 0 & 0 & 0 \\ 0 & 0 & 0 \end{bmatrix} \quad (3.6)$$

so that

$$\mathbf{D} = \frac{1}{2}(\mathbf{K} + \mathbf{K}^T) = \frac{\dot{\gamma}}{2} \begin{bmatrix} 0 & 1 & 0 \\ 1 & 0 & 0 \\ 0 & 0 & 0 \end{bmatrix} \Leftrightarrow \dot{\gamma} = \sqrt{2\mathbf{D} : \mathbf{D}}.$$

The $\dot{\gamma}$ is merely to make the FFI proportional to the deformation rate. When $\dot{\gamma} = 0$, there is no FFI. The $\tilde{\nabla}$ is as defined in Definition 2.2.

The origin of (3.5) stems from a derivation analogous to the derivation of the Fokker-Planck equation. It is similar to the way thermal effects cause a rotary diffusion in molecular theories [2], in particular in kinetic theory. The derivation will not be treated here.

Besides the assumptions made for the derivation of Jeffery's equation, for the derivation of (3.5) it

is additionally assumed that the flow is incompressible. This implies a solenoidal velocity field \mathbf{v} , so that

$$\begin{aligned} 0 = \nabla \cdot \mathbf{v} &= \sum_i \nabla_i v_i = \sum_i K_{ii} = \text{tr}(\mathbf{K}) \\ &= \sum_{i,j} K_{ij} \delta_{ji} = \mathbf{K} : \mathbf{I}. \end{aligned} \quad (3.7)$$

By adding the FFI (3.5) to Jeffery's equation (3.3), we obtain the extended equation

$$\dot{\mathbf{p}} = \mathbf{W} \cdot \mathbf{p} + \xi(\mathbf{D} \cdot \mathbf{p} - \mathbf{D} : \mathbf{p}\mathbf{p}\mathbf{p}) - C_I \dot{\gamma} \tilde{\nabla} \ln \psi. \quad (3.8)$$

As (3.3) is an equation for $\mathbf{p}(t)$ under the condition that the flow field \mathbf{v} is given, so is (3.8), under the additional condition that $\psi(\mathbf{p}(t), t)$ is known. The latter is, however, not the case. The PDF ψ is solved by a PDE, which is treated in the next subsection.

3.3.2 Conservation of probability

The PDE for ψ originates from a conservation law for ψ . It has the same form as the conservation of mass. When an amount of fibers or directions \mathbf{p} 'leave' an area $S_1 \subset S$, they have to 'enter' another area $S_2 \subset S \setminus S_1$, confer Figure 3.3. This can be considered as a convective effect, inducing a change of

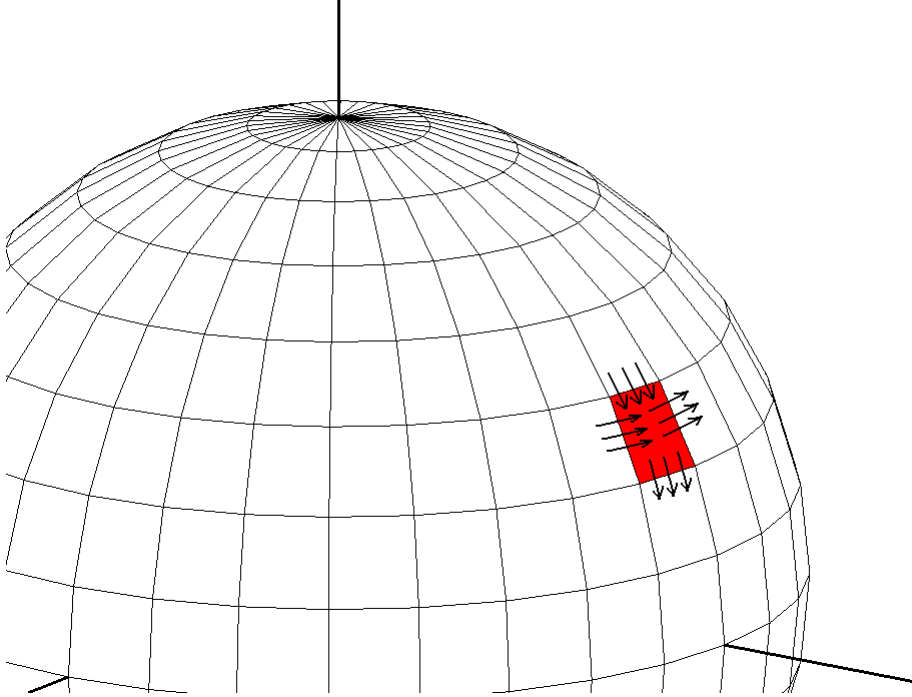


Figure 3.3: flux of probability.

ψ in time t . Considering $S_1 \subset S$, the net amount of fibers that leave the area is denoted as

$$\oint_{\mathbf{p} \in C_1} \psi \mathbf{v}_{\mathbf{p}} \cdot \mathbf{n} d^1 \mathbf{p},$$

where C_1 is the circumference of area S_1 and $\mathbf{v}_{\mathbf{p}}$ the velocity at which the fibers enter and leave S_1 . Note that with the divergence theorem we obtain

$$\oint_{\mathbf{p} \in C_1} \psi \mathbf{v}_{\mathbf{p}} \cdot \mathbf{n} d^1 \mathbf{p} = \int_{\mathbf{p} \in S_1} \tilde{\nabla} \cdot (\psi \mathbf{v}_{\mathbf{p}}) d^2 \mathbf{p}. \quad (3.9)$$

The change of ψ in time induced by the convection is

$$\frac{d}{dt} \int_{\mathbf{p} \in S_1} \psi d^2 \mathbf{p} = \int_{\mathbf{p} \in S_1} \dot{\psi} d^2 \mathbf{p} \quad (3.10)$$

where we used the independence of S_1 and t . Combining (3.9) and (3.10) leads to the equation

$$\int_{\mathbf{p} \in S_1} \dot{\psi} d^2 \mathbf{p} = - \int_{\mathbf{p} \in S_1} \tilde{\nabla} \cdot (\psi \mathbf{v}_{\mathbf{p}}) d^2 \mathbf{p}.$$

Since S_1 is arbitrary, it follows that

$$\dot{\psi} = -\tilde{\nabla} \cdot (\psi \mathbf{v}_{\mathbf{p}}). \quad (3.11)$$

The LHS is independent of the chosen basis and thus so is the RHS. Say we choose the spherical coordinates to write out the RHS. We then have, maintaining the notation used in [2],

$$\begin{aligned} \tilde{\nabla} &= \boldsymbol{\delta}_r \frac{\partial}{\partial r} + \frac{1}{r} \boldsymbol{\delta}_\theta \frac{\partial}{\partial \theta} + \frac{1}{r \sin \theta} \boldsymbol{\delta}_\phi \frac{\partial}{\partial \phi} = \boldsymbol{\delta}_\theta \frac{\partial}{\partial \theta} + \frac{1}{\sin \theta} \boldsymbol{\delta}_\phi \frac{\partial}{\partial \phi} \\ \mathbf{v}_{\mathbf{p}} &= v_r \boldsymbol{\delta}_r + v_\theta \boldsymbol{\delta}_\theta + v_\phi \boldsymbol{\delta}_\phi = \dot{\theta} \boldsymbol{\delta}_\theta + \dot{\phi} \sin(\theta) \boldsymbol{\delta}_\phi. \end{aligned}$$

From the latter and Figure 3.4 it stands out that $\mathbf{v}_{\mathbf{p}} = \dot{\mathbf{p}}$. Substitution in (3.11) gives

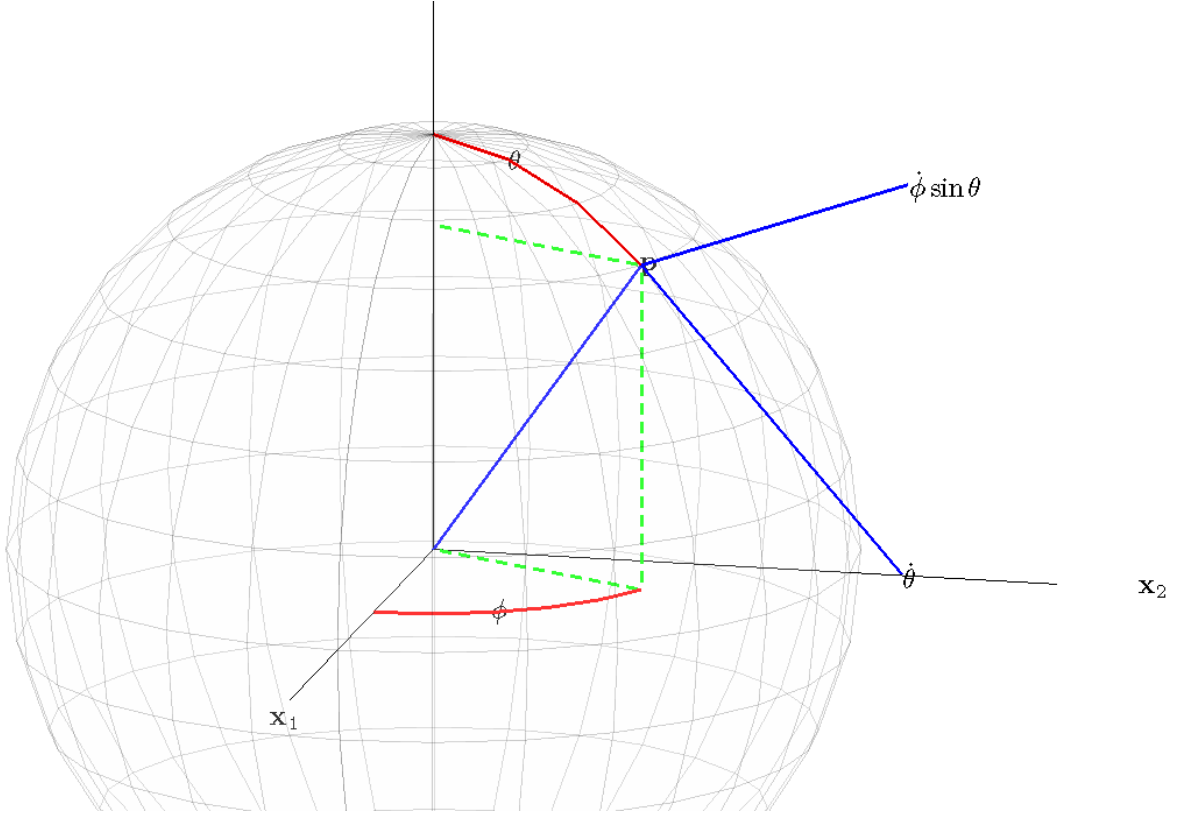


Figure 3.4: angular velocities representing $\dot{\mathbf{p}}$.

$$\dot{\psi} = -\tilde{\nabla} \cdot (\psi \dot{\mathbf{p}}). \quad (3.12)$$

As $\dot{\mathbf{p}}$ is known from (3.8), we can write out (3.12) further to obtain the so called kinetic theory.

3.3.3 Kinetic theory

Kinetic theory is the theory that gases are made up of atoms, all of which are in constant, random motion. The rapidly moving particles constantly collide with each other and with their surroundings. This is often described with the use of Brownian motion. Kinetic theory explains properties of gases on macroscale by microscale effects. As the FFI term has similarities with kinetic theories, one often refers to kinetic theory when considering the differential equation for ψ , which will be derived here.

Recall (3.8)

$$\dot{\mathbf{p}} = \mathbf{W} \cdot \mathbf{p} + \xi(\mathbf{D} \cdot \mathbf{p} - \mathbf{D} : \mathbf{p}\mathbf{p}\mathbf{p}) - C_I \dot{\gamma} \tilde{\nabla} \ln \psi.$$

We again maintain the notation as used in [2], so $(\mathbf{p}, \mathbf{q}, \mathbf{s}) = (\boldsymbol{\delta}_r, \boldsymbol{\delta}_\theta, \boldsymbol{\delta}_\phi)$, $D_r = C_I \dot{\gamma}$, $\lambda = \xi$ and

$$\lambda^- = \frac{\lambda - 1}{2}, \quad \lambda^+ = \frac{\lambda + 1}{2}.$$

We write

$$\begin{aligned}
\dot{\mathbf{p}} &= \frac{1}{2}(\mathbf{K} - \mathbf{K}^T) \cdot \boldsymbol{\delta}_r + \lambda \left(\frac{1}{2}(\mathbf{K} + \mathbf{K}^T) \cdot \boldsymbol{\delta}_r - \frac{1}{2}(\mathbf{K} + \mathbf{K}^T) : \boldsymbol{\delta}_r \boldsymbol{\delta}_r \boldsymbol{\delta}_r \right) - \frac{D_r}{\psi} \left(\boldsymbol{\delta}_\theta \frac{\partial \psi}{\partial \theta} + \boldsymbol{\delta}_\phi \frac{1}{\sin \theta} \frac{\partial \psi}{\partial \phi} \right) \\
&= \frac{\lambda - 1}{2} \mathbf{K}^T \cdot \boldsymbol{\delta}_r + \frac{\lambda + 1}{2} \mathbf{K} \cdot \boldsymbol{\delta}_r - \lambda \frac{\mathbf{K} + \mathbf{K}^T}{2} : \boldsymbol{\delta}_r \boldsymbol{\delta}_r \boldsymbol{\delta}_r - \frac{D_r}{\psi} \left(\boldsymbol{\delta}_\theta \frac{\partial \psi}{\partial \theta} + \boldsymbol{\delta}_\phi \frac{1}{\sin \theta} \frac{\partial \psi}{\partial \phi} \right) \\
&= \lambda^- \mathbf{K}^T \cdot \boldsymbol{\delta}_r + \lambda^+ \mathbf{K} \cdot \boldsymbol{\delta}_r - \lambda \mathbf{K} : \boldsymbol{\delta}_r \boldsymbol{\delta}_r \boldsymbol{\delta}_r - \frac{D_r}{\psi} \left(\boldsymbol{\delta}_\theta \frac{\partial \psi}{\partial \theta} + \boldsymbol{\delta}_\phi \frac{1}{\sin \theta} \frac{\partial \psi}{\partial \phi} \right)
\end{aligned}$$

where we used $\mathbf{K} : \boldsymbol{\delta}_r \boldsymbol{\delta}_r = \mathbf{K}^T : \boldsymbol{\delta}_r \boldsymbol{\delta}_r$ to obtain the last equivalence. Taking the left single contraction with the unit tensor $\boldsymbol{\delta} = \boldsymbol{\delta}_r \boldsymbol{\delta}_r + \boldsymbol{\delta}_\theta \boldsymbol{\delta}_\theta + \boldsymbol{\delta}_\phi \boldsymbol{\delta}_\phi$ we obtain

$$\begin{aligned}
\dot{\mathbf{p}} &= \lambda^- (\mathbf{K}^T : \boldsymbol{\delta}_r \boldsymbol{\delta}_r \boldsymbol{\delta}_r + \mathbf{K}^T : \boldsymbol{\delta}_r \boldsymbol{\delta}_\theta \boldsymbol{\delta}_\theta + \mathbf{K}^T : \boldsymbol{\delta}_r \boldsymbol{\delta}_\phi \boldsymbol{\delta}_\phi) + \lambda^+ (\mathbf{K} : \boldsymbol{\delta}_r \boldsymbol{\delta}_r \boldsymbol{\delta}_r + \mathbf{K} : \boldsymbol{\delta}_r \boldsymbol{\delta}_\theta \boldsymbol{\delta}_\theta + \mathbf{K} : \boldsymbol{\delta}_r \boldsymbol{\delta}_\phi \boldsymbol{\delta}_\phi) \\
&\quad - \lambda \mathbf{K} : \boldsymbol{\delta}_r \boldsymbol{\delta}_r \boldsymbol{\delta}_r - \frac{D_r}{\psi} \left(\boldsymbol{\delta}_\theta \frac{\partial \psi}{\partial \theta} + \boldsymbol{\delta}_\phi \frac{1}{\sin \theta} \frac{\partial \psi}{\partial \phi} \right) \\
&= \lambda^- (\mathbf{K}^T : \boldsymbol{\delta}_r \boldsymbol{\delta}_\theta \boldsymbol{\delta}_\theta + \mathbf{K}^T : \boldsymbol{\delta}_r \boldsymbol{\delta}_\phi \boldsymbol{\delta}_\phi) + \lambda^+ (\mathbf{K} : \boldsymbol{\delta}_r \boldsymbol{\delta}_\theta \boldsymbol{\delta}_\theta + \mathbf{K} : \boldsymbol{\delta}_r \boldsymbol{\delta}_\phi \boldsymbol{\delta}_\phi) - \frac{D_r}{\psi} \left(\boldsymbol{\delta}_\theta \frac{\partial \psi}{\partial \theta} + \boldsymbol{\delta}_\phi \frac{1}{\sin \theta} \frac{\partial \psi}{\partial \phi} \right) \\
&= \left(\lambda^- \mathbf{K}^T : \boldsymbol{\delta}_r \boldsymbol{\delta}_\theta + \lambda^+ \mathbf{K} : \boldsymbol{\delta}_r \boldsymbol{\delta}_\theta - \frac{D_r}{\psi} \frac{\partial \psi}{\partial \theta} \right) \boldsymbol{\delta}_\theta + \left(\lambda^- \mathbf{K}^T : \boldsymbol{\delta}_r \boldsymbol{\delta}_\phi + \lambda^+ \mathbf{K} : \boldsymbol{\delta}_r \boldsymbol{\delta}_\phi - \frac{D_r}{\psi \sin \theta} \frac{\partial \psi}{\partial \phi} \right) \boldsymbol{\delta}_\phi.
\end{aligned} \tag{3.13}$$

Filling the latter in in (3.12)

$$\begin{aligned}
\dot{\psi} &= - \left(\boldsymbol{\delta}_\theta \frac{\partial}{\partial \theta} + \boldsymbol{\delta}_\phi \frac{1}{\sin \theta} \frac{\partial}{\partial \phi} \right) \cdot \left(\psi \left(\left(\lambda^- \mathbf{K}^T : \boldsymbol{\delta}_r \boldsymbol{\delta}_\theta + \lambda^+ \mathbf{K} : \boldsymbol{\delta}_r \boldsymbol{\delta}_\theta - \frac{D_r}{\psi} \frac{\partial \psi}{\partial \theta} \right) \boldsymbol{\delta}_\theta + \right. \right. \\
&\quad \left. \left. \left(\lambda^- \mathbf{K}^T : \boldsymbol{\delta}_r \boldsymbol{\delta}_\phi + \lambda^+ \mathbf{K} : \boldsymbol{\delta}_r \boldsymbol{\delta}_\phi - \frac{D_r}{\psi \sin \theta} \frac{\partial \psi}{\partial \phi} \right) \boldsymbol{\delta}_\phi \right) \right).
\end{aligned}$$

Using $\mathbf{K} : \boldsymbol{\delta}_r \boldsymbol{\delta}_r = \mathbf{K}^T : \boldsymbol{\delta}_r \boldsymbol{\delta}_r$ again, (3.7), the product rule and

$$\begin{aligned}
\frac{\partial \boldsymbol{\delta}_r}{\partial r} &= 0, \quad \frac{\partial \boldsymbol{\delta}_\theta}{\partial r} = 0, \quad \frac{\partial \boldsymbol{\delta}_\phi}{\partial r} = 0, \quad \frac{\partial \boldsymbol{\delta}_r}{\partial \theta} = \boldsymbol{\delta}_\theta, \quad \frac{\partial \boldsymbol{\delta}_\theta}{\partial \theta} = -\boldsymbol{\delta}_r, \quad \frac{\partial \boldsymbol{\delta}_\phi}{\partial \theta} = 0 \\
\frac{\partial \boldsymbol{\delta}_r}{\partial \phi} &= \boldsymbol{\delta}_\phi \sin \theta, \quad \frac{\partial \boldsymbol{\delta}_\theta}{\partial \phi} = \boldsymbol{\delta}_\phi \cos \theta, \quad \frac{\partial \boldsymbol{\delta}_\phi}{\partial \phi} = -\boldsymbol{\delta}_r \sin(\theta) - \boldsymbol{\delta}_\theta \cos(\theta)
\end{aligned}$$

it follows that the kinetic theory is

$$\begin{aligned}
\dot{\psi} &= D_r \frac{\partial^2 \psi}{\partial \theta^2} + \frac{D_r}{\sin^2 \theta} \frac{\partial^2 \psi}{\partial \phi^2} + \frac{\partial \psi}{\partial \theta} \left(D_r \frac{\cos \theta}{\sin \theta} - \lambda^- \mathbf{K}^T : \boldsymbol{\delta}_r \boldsymbol{\delta}_\theta - \lambda^+ \mathbf{K} : \boldsymbol{\delta}_r \boldsymbol{\delta}_\theta \right) \\
&\quad + \frac{1}{\sin \theta} \frac{\partial \psi}{\partial \phi} \left(-\lambda^- \mathbf{K}^T : \boldsymbol{\delta}_r \boldsymbol{\delta}_\phi - \lambda^+ \mathbf{K} : \boldsymbol{\delta}_r \boldsymbol{\delta}_\phi \right) + \psi (3\lambda \mathbf{K} : \boldsymbol{\delta}_r \boldsymbol{\delta}_r) \\
&= D_r \frac{\partial^2 \psi}{\partial \theta^2} + \frac{D_r}{\sin^2 \theta} \frac{\partial^2 \psi}{\partial \phi^2} + \frac{\partial \psi}{\partial \theta} \left(D_r \frac{\cos \theta}{\sin \theta} - \lambda^- \mathbf{K}^T : \boldsymbol{\delta}_r \boldsymbol{\delta}_\theta - \lambda^+ \mathbf{K} : \boldsymbol{\delta}_r \boldsymbol{\delta}_\theta \right) \\
&\quad + \frac{1}{\sin \theta} \frac{\partial \psi}{\partial \phi} \left(-\lambda^- \mathbf{K}^T : \boldsymbol{\delta}_r \boldsymbol{\delta}_\phi - \lambda^+ \mathbf{K} : \boldsymbol{\delta}_r \boldsymbol{\delta}_\phi \right) + \psi (3\lambda \mathbf{D} : \boldsymbol{\delta}_r \boldsymbol{\delta}_r)
\end{aligned} \tag{3.14}$$

where in the last step we used $\mathbf{W} : \boldsymbol{\delta}_r \boldsymbol{\delta}_r = 0$ due to the antisymmetry of \mathbf{W} .

As $\theta \in [0, \pi]$, the PDE has two singularities, namely at $\theta \in \{0, \pi\}$. At these two coordinates there is a division by $\sin 0 = \sin \pi = 0$. Letting $\theta \downarrow 0$ or $\theta \uparrow \pi$ we have

$$\dot{\psi} \rightarrow \frac{D_r}{\sin^2 \theta} \frac{\partial^2 \psi}{\partial \phi^2}$$

which is a one dimensional instationary diffusion equation. Herewith, ψ can be solved with the method of separation of variables. As these are just two points of S , such a solution is not interesting. We will omit the derivation. This observation is however, important for the stability criteria, treated in Subsection 7.4.6.

Equation (3.14) is a PDE, linear in ψ . The domain space is the unit sphere S . At each location on S , described by the generalized coordinates θ and ϕ , the basis vectors $\boldsymbol{\delta}_r$, $\boldsymbol{\delta}_\theta$ and $\boldsymbol{\delta}_\phi$ are known. The

probability density can thus be calculated. Its value represents the probability of fibers having their long axis in this particular direction. Unfortunately, the available asymptotic and exact solutions of (3.14) do not provide all the information that is required [2]. Numerical methods provide an alternative, in particular in case of instationarity. Nonetheless, the available asymptotic and exact solutions can be useful to verify the adequacy of the numerical methods used to solve (3.14).

The finite difference method (FDM) looks appropriate for the treatment of (3.14) on structured grid, but for the sake of the conservation of $\oint_S \psi d^2\mathbf{p} = 1$ we use the finite volume method (FVM). A thorough description of the approach can be found in Chapter 7.

In practical applications of injection molding, the flow field is clearly not homogeneous. A probability density ψ as a function of the generalized coordinates θ and ϕ for the unit sphere and time t is insufficient in such cases. A proper approach would exist of a PDF that is also a function of space \mathbf{x} . In case of a one way coupling between the velocity field and the fiber orientation on a finite grid, the velocity field is calculated and a posteriori the fiber orientation per mesh element, both per element. The PDF values of the elements influence each other by convection. Hence, the partial time derivative as used in (3.14) is substituted with a material or total derivative. In case of a two way coupling, the velocity field and fiber orientation are calculated per time step and per element. This can be done with either weak or strong coupling [11].

Calculating ψ from (3.14) involves a high computational cost when used for practical applications. For example, an injection molding would require 5000 nodes, using 500 locations on the midplane with 10 nodes through the thickness at each location. Describing $\psi(\theta, \phi)$ requires at least 10 increments for θ and 40 for ϕ , giving a total of 400 DOFs per node. That totals $5000 \cdot 400 = 2 \cdot 10^6$ DOFs to describe the orientation in a single molding. As such calculations take an unacceptably long time, research was done to construct a computationally more attractive approach. An alternative description was constructed, as described in the next chapter.

Chapter 4

The orientation tensor description

4.1 Introduction

Having derived the kinetic theory to model the fiber orientation is an elegant result. Nonetheless, obtaining solutions numerically for practical cases is unattractively expensive and the known asymptotic and analytic solutions do not represent the cases that we are interested in. An alternative, computationally less expensive description would be attractive. S.G. Advani and C.L. Tucker III managed to formulate such a description in 1987 [18]. This description implies the use of the so called orientation tensors. The motivation and interpretation are explained, as are the important properties of the orientation tensors. The rate equation for the second order tensor is derived.

4.2 Partial information

The idea behind the kinetic theory is to obtain information about the fiber orientation. This information is contained in ψ . But perhaps a description containing less information than ψ , that is less computationally expensive, contains sufficient information on the fiber orientation. To this end, we consider a certain series expansion of ψ .

In [6], E.T. Onat and F.A. Leckie show that the PDF can be expanded as

$$\psi(\mathbf{p}, t) = f_0 V_0 + \sum_{i,j} [f_{ij}(\mathbf{p}) V_{ij}(t)] + \sum_{i,j,k,l} [f_{ijkl}(\mathbf{p}) V_{ijkl}(t)] + \dots \quad (4.1)$$

where

$$\begin{aligned} f_0 &= 1 \\ f_{ij} &= p_i p_j - \frac{1}{3} \delta_{ij} \\ f_{ijkl} &= p_i p_j p_k p_l \\ &\quad - \frac{1}{7} (p_i p_j \delta_{kl} + p_i p_k \delta_{jl} + p_i p_l \delta_{jk} + p_k p_l \delta_{ij} + p_j p_l \delta_{ik} + p_j p_k \delta_{il}) \\ &\quad + \frac{1}{35} (\delta_{ij} \delta_{kl} + \delta_{ik} \delta_{jl} + \delta_{il} \delta_{jk}) \\ &\quad \vdots \end{aligned}$$

are the traceless basis functions and

$$V_{ij\dots}(t) = \frac{1}{4\pi} \frac{1}{N!} \prod_{x=0}^N (2x+1) \oint_S \psi(\mathbf{p}, t) f_{ij\dots} d^2 \mathbf{p}$$

are the corresponding Fourier coefficients, with N representing the number of subindices of the Fourier coefficient in question. The basis functions do not change in time and thus only need to be calculated $\forall \mathbf{p} \in S$. When solving the PDF numerically, this increases the efficiency as the basis functions only need to be calculated once in space and not per time step. The Fourier coefficients vary with time and need to be calculated every time step. By neglecting the higher order terms in (4.1) we approximate the ψ and increase the computational efficiency of numerical solving methods even further.

It can be seen that the integrals

$$\oint_S \psi(\mathbf{p}, t) f_{ij\dots} d^2 \mathbf{p}$$

in the Fourier coefficients are the components of the deviatoric versions of the tensors

$$1 = \oint_S \psi(\mathbf{p}, t) d^2 \mathbf{p}, \quad \mathbf{A}(t) = \oint_S \psi(\mathbf{p}, t) \mathbf{p} \mathbf{p} d^2 \mathbf{p}, \quad \mathbb{A}(t) = \oint_S \psi(\mathbf{p}, t) \mathbf{p} \mathbf{p} \mathbf{p} \mathbf{p} d^2 \mathbf{p}, \quad \dots$$

From the latter it stands out that the tensors of odd order are not present. This is because they are equal to zero due to ψ being an even function on S by Definition 3.1. It follows that by calculating \mathbb{A}

and \mathbb{A} , we can approximate ψ . The tensors thus contain a substantial amount of information on the fiber orientation. In addition, the tensors \mathbf{A} and \mathbb{A} turn out to possess several useful properties, which leads us into the next section.

The expansion (4.1) turns out to be identical to the expansion of ψ in spherical harmonics [3]. Spherical harmonics are orthogonal basis functions for the unit sphere S . They are of importance in the analysis of the linear Fokker-Planck equation (3.14) [12]. Integrating the analysis of the spherical harmonics in this thesis would certainly be a substantial contribution. Nonetheless, such an analysis is omitted as it is beyond the time schedule set for this thesis.

4.3 Definitions and interpretation

We introduce the following two definitions.

Definition 4.1. *The second order moment tensor is defined as*

$$\mathbf{A}(t) = \oint_S \psi(\mathbf{p}, t) \mathbf{p} \mathbf{p} d^2 \mathbf{p}.$$

Definition 4.2. *Analogously, the fourth order moment tensor is defined as*

$$\mathbb{A}(t) = \oint_S \psi(\mathbf{p}, t) \mathbf{p} \mathbf{p} \mathbf{p} \mathbf{p} d^2 \mathbf{p}.$$

Tensors \mathbf{A} and \mathbb{A} contain information about the orientation of the fibers. For this reason they are also often in the literature referred to as the orientation tensors.

The tensors \mathbf{A} and \mathbb{A} can be seen as a sum of ψ times the weights $\mathbf{p} \mathbf{p} \sin \theta$ and $\mathbf{p} \mathbf{p} \mathbf{p} \mathbf{p} \sin \theta$ respectively, where all the three quantities vary in space. Depending on the position on the sphere, the probability density is represented with a certain 'strength' in \mathbf{A} and \mathbb{A} . To get an idea of this strength in the case of \mathbf{A} , we consider

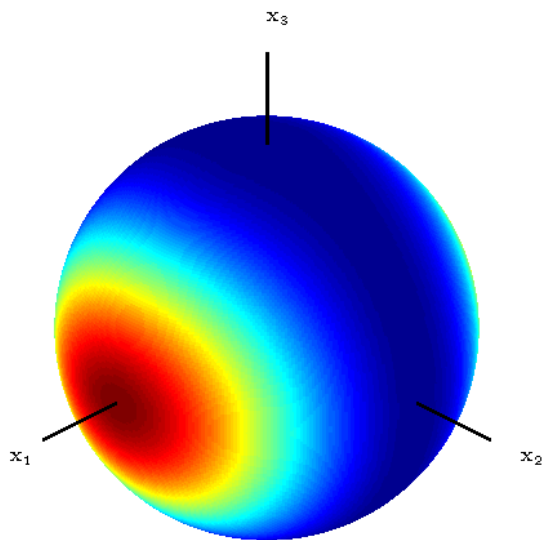
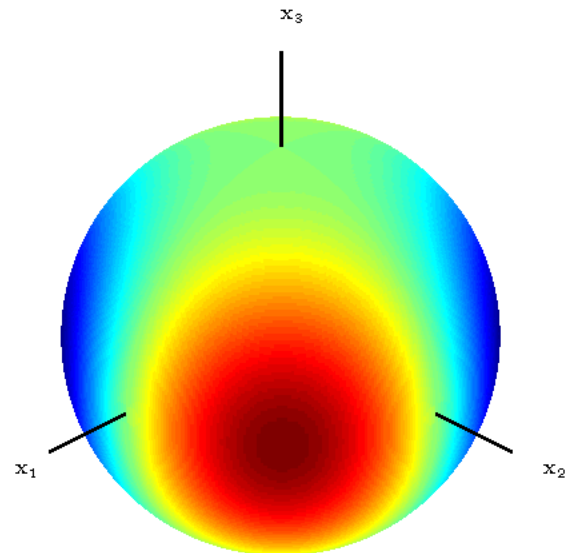
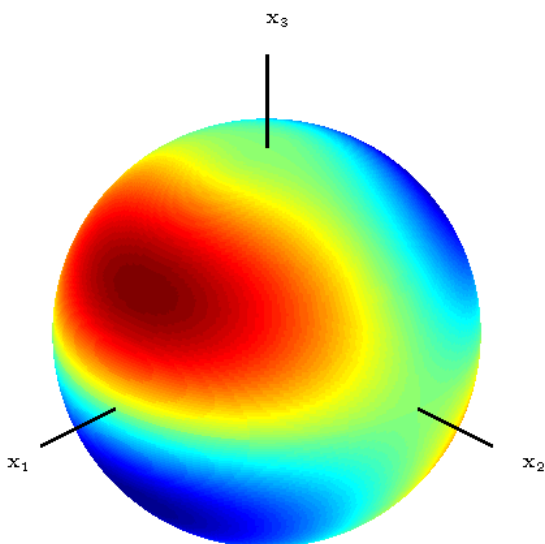
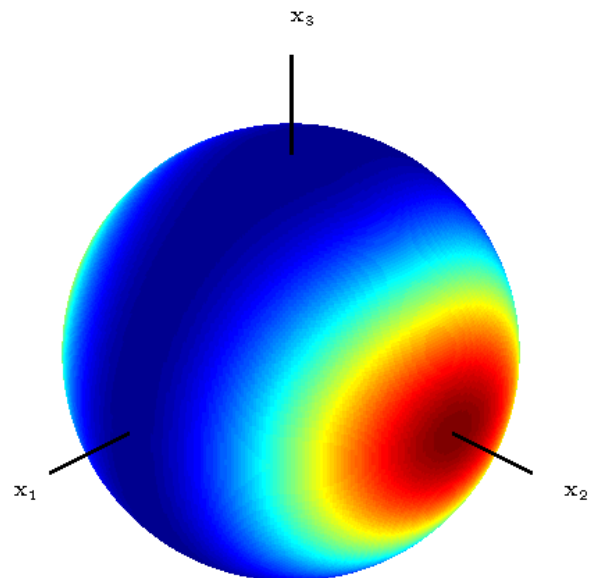
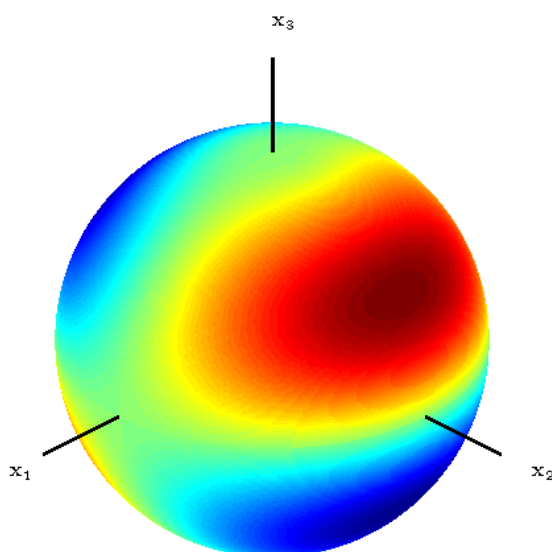
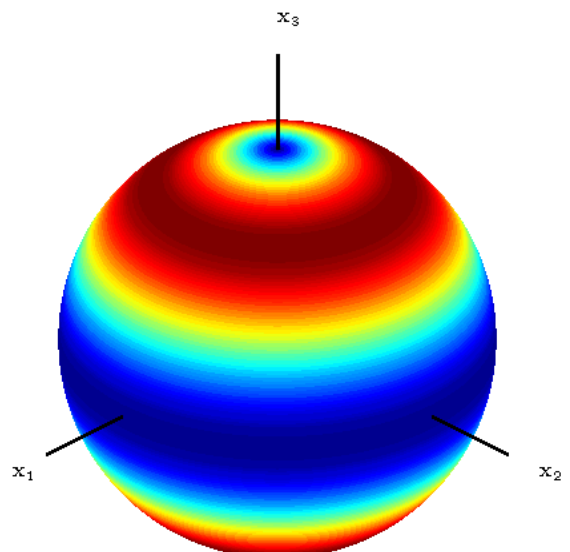
$$\begin{aligned} \mathbf{p} \mathbf{p} \sin \theta &= \begin{bmatrix} \sin^2(\theta) \cos^2(\phi) & \frac{\sin^2(\theta) \sin(2\phi)}{2} & \frac{\sin(2\theta) \cos(\phi)}{2} \\ \frac{\sin^2(\theta) \sin(2\phi)}{2} & \sin^2(\theta) \sin^2(\phi) & \frac{\sin(2\theta) \sin(\phi)}{2} \\ \frac{\sin(2\theta) \cos(\phi)}{2} & \frac{\sin(2\theta) \sin(\phi)}{2} & \cos^2(\theta) \end{bmatrix} \sin \theta \\ &= \begin{bmatrix} \sin^3(\theta) \cos^2(\phi) & \frac{\sin^3(\theta) \sin(2\phi)}{2} & (1 - \cos^2(\theta)) \cos(\theta) \cos(\phi) \\ \frac{\sin^3(\theta) \sin(2\phi)}{2} & \sin^3(\theta) \sin^2(\phi) & (1 - \cos^2(\theta)) \cos(\theta) \sin(\phi) \\ (1 - \cos^2(\theta)) \cos(\theta) \cos(\phi) & (1 - \cos^2(\theta)) \cos(\theta) \sin(\phi) & \sin(\theta) \cos^2(\theta) \end{bmatrix}. \end{aligned} \quad (4.2)$$

It follows that the diagonal components have strictly nonnegative contributions, as $\psi \geq 0$ and $p_i p_i \sin \theta \geq 0$. The components are depicted in Figures 4.1-4.6 to indicate where the PDF is represented stronger or weaker, per component of \mathbf{A} . The strength of $\mathbf{p} \mathbf{p} \mathbf{p} \mathbf{p} \sin \theta$ follows in an analogous way.

An alternative way to obtain the physical interpretation of \mathbf{A} is to consider its eigenpairs. Say we consider \mathbf{A} with respect to its eigenvectors or principal axes, then $[\mathbf{A}]_{pb}$ is a diagonal matrix with its eigenvalues on the diagonal. From the beforementioned, we recall that for all time t

$$\begin{aligned} A_{11}(t) &= \int_{\phi=0}^{2\pi} \int_{\theta=0}^{\pi} \psi(\theta, \phi, t) \sin^3(\theta) \cos^2(\phi) d\theta d\phi = \lambda_1(t) \\ A_{22}(t) &= \int_{\phi=0}^{2\pi} \int_{\theta=0}^{\pi} \psi(\theta, \phi, t) \sin^3(\theta) \sin^2(\phi) d\theta d\phi = \lambda_2(t) \\ A_{33}(t) &= \int_{\phi=0}^{2\pi} \int_{\theta=0}^{\pi} \psi(\theta, \phi, t) \sin(\theta) \cos^2(\theta) d\theta d\phi = \lambda_3(t), \end{aligned}$$

which are all $\in [0, 1]$. Recalling Figures 4.1, 4.4 and 4.6, the A_{11} , A_{22} and A_{33} represent the PDF stronger or weaker depending on the location on the sphere S . Due to the locations of the extrema of the diagonal components of $\mathbf{p} \mathbf{p} \sin \theta$, the eigenvalues of $[\mathbf{A}]_{pb}$ are measures for the 'strength' of the fiber orientation in the direction of the corresponding eigenvector. Some examples will be clarifying.

Figure 4.1: $p_1 p_1 \sin \theta$.Figure 4.2: $p_1 p_2 \sin \theta$.Figure 4.3: $p_1 p_3 \sin \theta$.Figure 4.4: $p_2 p_2 \sin \theta$.Figure 4.5: $p_2 p_3 \sin \theta$.Figure 4.6: $p_3 p_3 \sin \theta$.

1. If the $\lambda_i = 1$, then all the fibers lie in the \mathbf{e}_i direction. I.e., the length axes of the fibers are aligned with the \mathbf{e}_i direction.
2. If $\lambda_i = \lambda_j = \frac{1}{2}$, the fibers have, in an average sense, equal components in the \mathbf{e}_i and \mathbf{e}_j direction. As $\sum_i \lambda_i = 1$, the last direction has zero strength and thus the fibers lie in the $i - j$ plane. This set of eigenpairs includes random orientation in the $i - j$ plane.
3. If $\lambda_1 = \lambda_2 = \lambda_3 = \frac{1}{3}$, the fibers have, in an average sense, equal components in all three directions. This set of eigenpairs includes random orientation in \mathbb{R}^3 .

More examples are depicted in Figure 4.7. If the off diagonal components of \mathbf{A} are nonzero, then the principal axes do not coincide with the axes of the chosen basis.

While drawing conclusions from \mathbf{A} one should keep the nonunique relation between ψ and \mathbf{A} in mind. Namely, the PDF ψ can change in a sense of its moments other than the second, without \mathbf{A} changing. This implies the possibility of more distributions $\{\psi_1, \psi_2, \dots\}$ corresponding to the same orientation tensor state \mathbf{A} .

4.4 Properties

It turns out that the orientation tensors have some useful properties. These properties will be used throughout the report and are thus explained here.

Property 4.1. *For the orientation tensors \mathbf{A} and \mathbb{A} we have*

$$\forall i, j \quad (\mathbf{A})_{ij} : \mathbb{R} \rightarrow \left[-\frac{1}{2}; 1\right] \quad \wedge \quad \forall i, j, k, l \quad (\mathbb{A})_{ijkl} : \mathbb{R} \rightarrow \left[-\frac{1}{8}; 1\right].$$

Proof. The elements of the second order orientation tensor are defined by

$$A_{ij} := (\mathbf{A})_{ij} = \left(\oint_S \psi \mathbf{p} \mathbf{p} \, d^2 \mathbf{p} \right)_{ij} = \oint_S \psi p_i p_j \, d^2 \mathbf{p}.$$

As $p_i \leq 1, \forall i$ and $\int_S \psi \, d^2 \mathbf{p} = 1$ it follows that

$$\oint_S \psi p_i p_j \, d^2 \mathbf{p} \leq \oint_S \psi \, d^2 \mathbf{p} = 1$$

with equality occurring when $p_i p_j = 1$ in combination with $\psi = \delta(\mathbf{p} - \mathbf{u})$ and \mathbf{u} such that $u_i u_j = 1$. The δ is as defined in Section 2.2. Similarly, $p_i p_j p_k p_l$ is maximal if $p_i p_j p_k p_l = 1$ so that

$$A_{ijkl} := (\mathbb{A})_{ijkl} = \left(\int_S \psi \mathbf{p} \mathbf{p} \mathbf{p} \mathbf{p} \, d^2 \mathbf{p} \right)_{ijkl} = \int_S \psi p_i p_j p_k p_l \, d^2 \mathbf{p} \leq \oint_S \psi \, d^2 \mathbf{p} = 1$$

with equality occurring when $p_i p_j p_k p_l = 1$ in combination with $\psi = \delta(\mathbf{p} - \mathbf{u})$ and \mathbf{u} such that $u_i u_j u_k u_l = 1$.

The minimum of A_{ij} is achieved by minimizing the product $p_i p_j$. It is clear that $i \neq j$ at the minimum because the square of a real scalar is nonnegative. Taking $p_k = 0, k \neq i, k \neq j$ gives us the most 'space' to minimize the product. Due to the unit length of \mathbf{p} we have $p_i^2 + p_j^2 = 1$ which represents the unit disk. The minimum of the product is found by taking $p_i = -p_j, p_i = \pm \frac{1}{2} \sqrt{2}$, which gives $p_i p_j = -\frac{1}{2}$. It follows that

$$\forall i, j \quad -\frac{1}{2} \leq A_{ij} \leq 1.$$

By minimizing $p_i p_j p_k p_l$ we will find the minimum of A_{ijkl} . The minimum of $p_i p_j p_k p_l$ is found by using Lagrange multipliers. Define

$$L(\mathbf{p}, \lambda) = p_1^2 p_2 p_3 + \lambda(p_1^2 + p_2^2 + p_3^2 - 1).$$

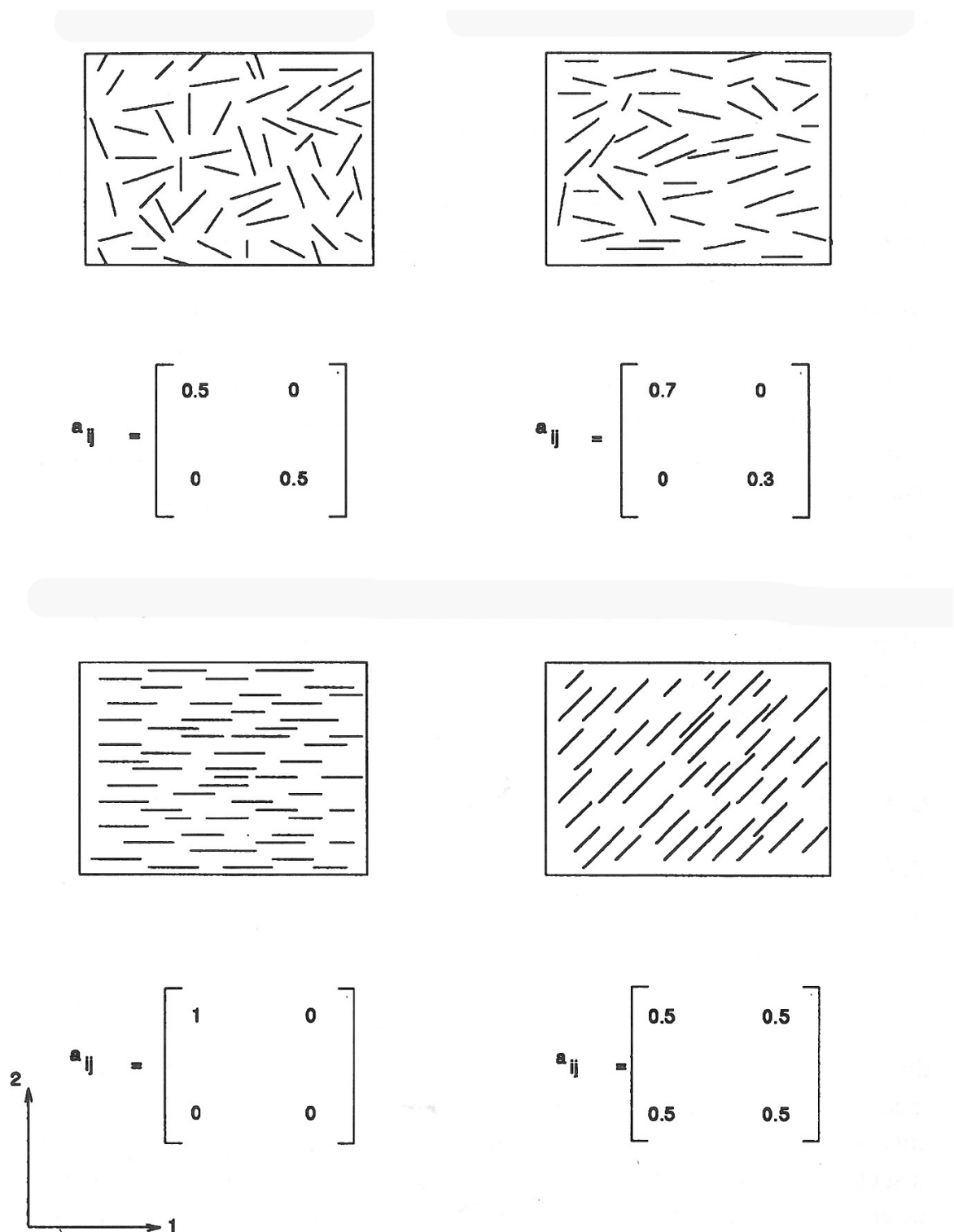


Figure 4.7: two dimensional examples of fiber orientation corresponding with second order matrices [20].

Investigating the latter is sufficient as one of the indices i, j, k and l will occur twice, resulting in the square, and due to the invariance of $p_i p_j p_k p_l$ under permutation. Then

$$\begin{aligned} \frac{\partial L}{\partial p_1} = 0 &\Leftrightarrow 2p_1 p_2 p_3 + 2\lambda p_1 = 0 \\ &\Leftrightarrow p_1(2p_2 p_3 + 2\lambda) = 0 \\ &\Leftrightarrow p_1 = 0 \quad \vee \quad p_2 p_3 = -\lambda \\ \frac{\partial L}{\partial p_2} = 0 &\Leftrightarrow p_1^2 p_3 + 2\lambda p_2 = 0 \\ \frac{\partial L}{\partial p_3} = 0 &\Leftrightarrow p_1^2 p_2 + 2\lambda p_3 = 0 \\ \frac{\partial L}{\partial \lambda} = 0 &\Leftrightarrow p_1^2 + p_2^2 + p_3^2 = 1. \end{aligned}$$

The case $p_1 = 0$ results in a value of zero for $p_1^2 p_2 p_3$. The case $p_2 p_3 = -\lambda$ gives

$$\begin{aligned} p_1^2 p_3 + 2\lambda p_2 = 0 &\Leftrightarrow p_1^2 p_3 - 2p_2^2 p_3 = 0 \\ &\Leftrightarrow p_3(p_1^2 - 2p_2^2) = 0 \\ &\Leftrightarrow p_3 = 0 \quad \vee \quad p_1 = \pm\sqrt{2p_2^2} \\ p_1^2 p_2 + 2\lambda p_3 = 0 &\Leftrightarrow p_1^2 p_2 - 2p_2 p_3^2 = 0 \\ &\Leftrightarrow p_2(p_1^2 - 2p_3^2) = 0 \\ &\Leftrightarrow p_2 = 0 \quad \vee \quad p_1 = \pm\sqrt{2p_3^2}. \end{aligned}$$

The cases $p_2 = 0$ and $p_3 = 0$ give the value zero to $p_1^2 p_2 p_3$, which was already achieved. The case $p_1 = \pm\sqrt{2p_2^2}$ results in

$$\begin{aligned} p_1^2 p_2 + 2\lambda p_3 = 0 &\Leftrightarrow 2p_2^3 - 2p_2 p_3^2 = 0 \\ &\Leftrightarrow 2p_2(p_2^2 - p_3^2) = 0 \\ &\Leftrightarrow p_2 = 0 \quad \vee \quad p_2 = \pm p_3. \end{aligned}$$

The normalization condition gives $p_2 = \pm\frac{1}{2}$ and so $p_3 = \pm\frac{1}{2}, p_1 = \pm\frac{1}{\sqrt{2}}$ resulting in $p_1^2 p_2 p_3 = \frac{1}{8}$. In effect,

$$\forall i, j, k, l \quad -\frac{1}{8} \leq A_{ijkl} \leq 1.$$

with the equality for the lower bound when $p_i p_j p_k p_l = \frac{1}{8}$ in combination with $\psi = \delta(\mathbf{p} - \mathbf{q})$ and \mathbf{q} such that $q_i q_j q_k q_l = \frac{1}{8}$.

Note that in a similar way, an alternative argument for the lower bound of A_{ij} can be constructed. \square

An important property of \mathbf{A} is that it is a symmetric positive definite tensor.

Property 4.2. *The second order orientation tensor \mathbf{A} is symmetric positive semidefinite (SPSD) by definition.*

Proof. We start with proving the symmetry of \mathbf{A}

$$\mathbf{A}^T = \left(\int_S \psi \mathbf{p} \mathbf{p} d^2 \mathbf{p} \right)^T = \int_S (\psi \mathbf{p} \mathbf{p})^T d^2 \mathbf{p} = \int_S \psi \mathbf{p} \mathbf{p} d^2 \mathbf{p} = \mathbf{A}$$

where we used the invariance of scalars under transposition and $(\mathbf{uv})^T = \mathbf{vu}$.

Positive definiteness follows from

$$\begin{aligned} \mathbf{x} \cdot \mathbf{A} \cdot \mathbf{x} &= \mathbf{x} \cdot \int_S \psi \mathbf{p} \mathbf{p} d^2 \mathbf{p} \cdot \mathbf{x} \\ &= \int_S \psi \mathbf{x} \cdot \mathbf{p} \mathbf{p} \cdot \mathbf{x} d^2 \mathbf{p} \\ &= \int_S \underbrace{\psi}_{\geq 0 \forall \mathbf{p} \in S} \underbrace{(\mathbf{x} \cdot \mathbf{p})^2}_{\geq 0 \forall \mathbf{p} \in S, \mathbf{x} \in \mathbb{R}^3 \setminus \{\mathbf{0}\}} d^2 \mathbf{p} \\ &\geq 0. \end{aligned}$$

□

Note that as $\mathbf{A} \in \mathbb{R}^{3 \times 3}$ and $\mathbf{A} = \mathbf{A}^T$, \mathbf{A} is also Hermitian, which we denote by $\mathbf{A} = \mathbf{A}^*$.

The fact that tensor \mathbf{A} is SPSD, has some useful implications which are used later on in this report.

Property 4.3. *Tensor \mathbf{A} only has nonnegative eigenvalues $\in \mathbb{R}$.*

Proof. See Section A.2. □

Property 4.4. *The eigenvectors of \mathbf{A} are real, $\forall i \mathbf{e}_i \in \mathbb{R}^3$.*

Proof. See Section A.3. □

Property 4.5. *Unit eigenvectors of \mathbf{A} corresponding to different eigenvalues are orthonormal.*

Proof. See Section A.4. □

Property 4.6. *Eigenvectors of tensor \mathbf{A} are never generalized, only genuine.*

Proof. See Section A.5. □

It is concluded that \mathbf{A} does not have a Jordan canonical form. All the eigenvectors of \mathbf{A} are genuine. As $\mathbf{A} \in \mathbb{R}^{3 \times 3}$, the three genuine eigenvectors have to span $\mathbb{R}^{3 \times 3}$ and thus the equality of two or three eigenvectors is excluded.

Property 4.7. *There exists a spectral decomposition for \mathbf{A} .*

Proof. See Section A.6. □

Note that at some time t , equality of two or three of the eigenvalues may occur. Say we consider the case that equality of two eigenvalues, say $\lambda_1 = \lambda_2 = \lambda, \lambda_3 \neq \lambda$, occurs, then we have

$$\begin{aligned}
 \mathbf{A} &= \sum_i \lambda_i \mathbf{e}_i \mathbf{e}_i \\
 &= \lambda(\mathbf{e}_1 \mathbf{e}_1 + \mathbf{e}_2 \mathbf{e}_2) + \lambda_3 \mathbf{e}_3 \mathbf{e}_3 \\
 &= \lambda(\mathbf{I} - \mathbf{e}_3 \mathbf{e}_3) + \lambda_3 \mathbf{e}_3 \mathbf{e}_3 \\
 &= \lambda \mathbf{P}_{\mathbf{e}_3}^\perp + \lambda_3 \mathbf{P}_{\mathbf{e}_3}^\parallel.
 \end{aligned} \tag{4.3}$$

It follows from (4.3)₂ that \mathbf{e}_1 and \mathbf{e}_2 are not determined uniquely, but element of $E_{ob} |_{\mathbf{e}_3}$ with

$$E_{ob} = \{E : \mathbf{e}_i \cdot \mathbf{e}_j = \delta_{ij}\} \tag{4.4}$$

where the subscript *ob* stands for orthonormal basis. In other words, \mathbf{e}_1 and \mathbf{e}_2 can be chosen arbitrarily in the plane perpendicular to \mathbf{e}_3 , provided that they are orthonormal.

When we consider the case that three of the eigenvalues are equal to λ , we have

$$\begin{aligned}
 \mathbf{A} &= \sum_i \lambda_i \mathbf{e}_i \mathbf{e}_i \\
 &= \lambda \sum_i \mathbf{e}_i \mathbf{e}_i \\
 &= \lambda \mathbf{I}
 \end{aligned} \tag{4.5}$$

where $E \in E_{ob}$. In other words, all three eigenvectors can be chosen arbitrarily, under the condition that they are mutually orthogonal and normalized to length one.

Property 4.8. *We have*

$$\sum_i \lambda_i = 1 \quad \wedge \quad 0 \leq \lambda_i \leq 1 \quad \forall i$$

Proof. Using Definition 4.1 and Property 4.7 we have

$$\int_S \psi \mathbf{p} \mathbf{p} d^2 \mathbf{p} = \sum_i \lambda_i \mathbf{e}_i \mathbf{e}_i.$$

Taking the trace on both sides gives

$$\begin{aligned} \operatorname{tr} \left(\int_S \psi \mathbf{p} \mathbf{p} d^2 \mathbf{p} \right) &= \operatorname{tr} \left(\sum_i \lambda_i \mathbf{e}_i \mathbf{e}_i \right) \\ \int_S \psi \operatorname{tr}(\mathbf{p} \mathbf{p}) d^2 \mathbf{p} &= \sum_i \lambda_i \operatorname{tr}(\mathbf{e}_i \mathbf{e}_i) \\ \int_S \psi \mathbf{p} \cdot \mathbf{p} d^2 \mathbf{p} &= \sum_i \lambda_i \mathbf{e}_i \cdot \mathbf{e}_i \\ \int_S \psi d^2 \mathbf{p} &= \sum_i \lambda_i \\ 1 &= \sum_i \lambda_i. \end{aligned}$$

Since Property 4.2 states that $\lambda_i \geq 0 \forall i$ it immediately follows that

$$0 \leq \lambda_i \leq 1 \forall i.$$

□

Property 4.9. For an even function $\psi(-\mathbf{p}, t) = \psi(\mathbf{p}, t)$ the second order tensor can be rewritten as

$$\mathbf{A}(t) = 2 \int_{S^{up}} \psi(\mathbf{p}, t) \mathbf{p} \mathbf{p} d^2 \mathbf{p}$$

where S^{up} is the surface of the upper hemisphere.

Proof. Say we consider the components of \mathbf{A} in combination with generalized coordinates,

$$A_{ij}(t) = \int_{\phi=0}^{2\pi} \int_{\theta=0}^{\pi} \psi(\theta, \phi, t) p_i(\theta, \phi) p_j(\theta, \phi) \sin(\theta) d\theta d\phi,$$

with $p_i(\theta, \phi, t) = p_i(\pi - \theta, \phi + \pi, t)$. We recall (4.2) and note that the substitution $\theta := \pi - \theta, \phi = \phi + \pi$ gives the same result. We can thus write

$$\begin{aligned} A_{ij}(t) &= \int_{\phi=0}^{2\pi} \int_{\theta=0}^{\pi} \psi p_i p_j \sin(\theta) d\theta d\phi \\ &= \int_{\phi=0}^{2\pi} \int_{\theta=0}^{\frac{\pi}{2}} \psi p_i p_j \sin(\theta) d\theta d\phi + \int_{\phi=0}^{2\pi} \int_{\theta=\frac{\pi}{2}}^{\pi} \psi p_i p_j \sin(\theta) d\theta d\phi \\ &= \int_{\phi=0}^{2\pi} \int_{\theta=0}^{\frac{\pi}{2}} \psi p_i p_j \sin(\theta) d\theta d\phi + \int_{\phi=-\pi}^{\pi} \int_{\theta=\frac{\pi}{2}}^0 \psi p_i p_j \sin(\theta) \cdot -d\theta d\phi \\ &= \int_{\phi=0}^{2\pi} \int_{\theta=0}^{\frac{\pi}{2}} \psi p_i p_j \sin(\theta) d\theta d\phi + \int_{\phi=-\pi}^{\pi} \int_{\theta=0}^{\frac{\pi}{2}} \psi p_i p_j \sin(\theta) d\theta d\phi \\ &= 2 \int_{\phi=0}^{2\pi} \int_{\theta=0}^{\frac{\pi}{2}} \psi p_i p_j \sin(\theta) d\theta d\phi \\ &= 2 \int_{S^{up}} \psi p_i p_j d^2 \mathbf{p} \end{aligned}$$

As scalars are independent of the chosen basis we have

$$\mathbf{A}(t) = 2 \oint_{S^{u_p}} \psi(\mathbf{p}, t) \mathbf{p} \mathbf{p} d^2 \mathbf{p}.$$

□

From (4.2) we see that the diagonal components of \mathbf{A} are always nonnegative.

The fourth order tensor \mathbb{A} also has certain symmetric properties.

Property 4.10. *The fourth order tensor \mathbb{A} has $4! = 24$ indicial symmetries and 15 independent components.*

Proof. We recall that the components of \mathbb{A} are defined as

$$A_{ijkl} := \int_S \psi p_i p_j p_k p_l d^2 \mathbf{p}.$$

Due to commutivity of scalars, we can permute the four indices as we want, resulting in $4! = 24$ permutation symmetries.

To determine the number of independent components we assume that we choose the indices such that $i \leq j \leq k \leq l$. This does not result in a loss of generality, as the indices can be permuted in any of the 24 ways. As $i, j, k, l \in \{1, 2, 3\}$, we introduce two separators | to indicate where in the sequence i, j, k, l the number increases by one or two. Herewith, the total number of 'positions' becomes $4 + 2 = 6$, where the two separators can be chosen in $\binom{6}{2} = 15$ ways. Ergo, the number of independent components of \mathbb{A} is 15. □

To clarify the latter we give some examples. The sequence 1111 is represented by 0000|. The first four positions, all equal to zero, represent the number of ones. The next position is a separator. If after this separator we have positions with zeros, they will represent the number of occurrences of two. However, there are not any zero positions after the first separator. Instead, there is another separator implying the 'jump' to three. Again, there are no zeros after this separator and thus the sequence has ended. The sequence 1123 is represented by 00|0|0, and so on. It stands out that the number of possible sequences is determined by in how many ways the two separators can be chosen in the six positions. Indeed, if we know the positions of the separators, we know the original sequence. Therefore, the total amount of possibilities is $\binom{6}{2} = 15$.

4.5 Rate equation for the second order tensor

Although we have defined \mathbf{A} in Definition 4.1, there is still no equation available wherefrom \mathbf{A} should be solved. Such an equation is derived by combining Definitions 4.1 and 4.2 with (3.8) and (3.12), as proven in the following theorem.

Theorem 4.1. *The system*

$$\begin{aligned} \dot{\mathbf{p}} &= \mathbf{W} \cdot \mathbf{p} + \xi(\mathbf{D} \cdot \mathbf{p} - \mathbf{D} : \mathbf{p} \mathbf{p} \mathbf{p}) - C_I \dot{\gamma} \tilde{\nabla} \ln \psi \\ \dot{\psi} &= -\tilde{\nabla} \cdot (\dot{\mathbf{p}} \psi) \end{aligned}$$

implies the relation

$$\dot{\mathbf{A}} = \mathbf{W} \cdot \mathbf{A} - \mathbf{A} \cdot \mathbf{W} + \xi(\mathbf{D} \cdot \mathbf{A} + \mathbf{A} \cdot \mathbf{D} - 2\mathbb{A} : \mathbf{D}) + 2C_I \dot{\gamma} (\mathbf{I} - 3\mathbf{A}).$$

Proof. From Definition 4.1, it follows that

$$\dot{\mathbf{A}} = \frac{d}{dt} \int_S \psi \mathbf{p} \mathbf{p} d^2 \mathbf{p}.$$

Because the integration domain S is independent of t , the derivative and integral can be interchanged

$$\dot{\mathbf{A}} = \int_S \frac{\partial}{\partial t} [\psi \mathbf{p} \mathbf{p}] d^2 \mathbf{p}.$$

Since \mathbf{p} is in this case the integration variable and thus independent of t we obtain

$$\dot{\mathbf{A}} = \int_S \frac{\partial \psi}{\partial t} \mathbf{p} \mathbf{p} d^2 \mathbf{p}.$$

Using the conservation equation for ψ (3.12), the latter becomes

$$\dot{\mathbf{A}} = - \int_S \tilde{\nabla} \cdot (\dot{\mathbf{p}} \psi) \mathbf{p} \mathbf{p} d^2 \mathbf{p}.$$

We proceed by introducing a splitting of (3.8)

$$\dot{\mathbf{p}} = \underbrace{\mathbf{W} \cdot \mathbf{p} + \xi(\mathbf{D} \cdot \mathbf{p} - \mathbf{D} : \mathbf{p} \mathbf{p} \mathbf{p})}_{:= \dot{\mathbf{p}}_J} - \underbrace{C_I \dot{\gamma} \tilde{\nabla} \ln \psi}_{:= \dot{\mathbf{p}}_{FT}}$$

so that

$$\dot{\mathbf{A}} = - \int_S \tilde{\nabla} \cdot ((\dot{\mathbf{p}}_J + \dot{\mathbf{p}}_{FT}) \psi) \mathbf{p} \mathbf{p} d^2 \mathbf{p} = - \int_S \tilde{\nabla} \cdot (\dot{\mathbf{p}}_J \psi) \mathbf{p} \mathbf{p} d^2 \mathbf{p} - \int_S \tilde{\nabla} \cdot (\dot{\mathbf{p}}_{FT} \psi) \mathbf{p} \mathbf{p} d^2 \mathbf{p}.$$

The indices J and FT stand for Jeffery and Folgar-Tucker respectively. We consider the 'Jeffery' term

$$- \int_S \tilde{\nabla} \cdot (\dot{\mathbf{p}}_J \psi) \mathbf{p} \mathbf{p} d^2 \mathbf{p}.$$

Omitting the index J for the sake of notation, $\tilde{\nabla} \cdot (\dot{\mathbf{p}} \psi \mathbf{p} \mathbf{p})$ has components

$$\begin{aligned} (\tilde{\nabla} \cdot (\dot{\mathbf{p}} \psi \mathbf{p} \mathbf{p}))_{ij} &= \sum_k \frac{\tilde{\partial}}{\partial p_k} (\dot{p}_k \psi p_i p_j) \\ &= \sum_k \left[\frac{\tilde{\partial}}{\partial p_k} (\dot{p}_k \psi) p_i p_j + \dot{p}_k \psi \frac{\tilde{\partial}}{\partial p_k} (p_i p_j) \right] \\ &= \sum_k \left[\frac{\tilde{\partial}}{\partial p_k} (\dot{p}_k \psi) p_i p_j \right] + \sum_k \left[\dot{p}_k \psi \frac{\tilde{\partial}}{\partial p_k} (p_i p_j) \right] \end{aligned}$$

from which it follows that

$$\tilde{\nabla} \cdot (\dot{\mathbf{p}} \psi \mathbf{p} \mathbf{p}) = \tilde{\nabla} \cdot (\dot{\mathbf{p}} \psi) \mathbf{p} \mathbf{p} + \dot{\mathbf{p}} \psi \cdot \tilde{\nabla} \mathbf{p} \mathbf{p}.$$

Herewith, the Jeffery term becomes

$$\begin{aligned} - \int_S \tilde{\nabla} \cdot (\dot{\mathbf{p}} \psi) \mathbf{p} \mathbf{p} d^2 \mathbf{p} &= - \int_S \left[\tilde{\nabla} \cdot (\dot{\mathbf{p}} \psi \mathbf{p} \mathbf{p}) - \dot{\mathbf{p}} \psi \cdot \tilde{\nabla} \mathbf{p} \mathbf{p} \right] d^2 \mathbf{p} \\ &= \int_S \dot{\mathbf{p}} \psi \cdot \tilde{\nabla} \mathbf{p} \mathbf{p} d^2 \mathbf{p} \end{aligned}$$

where we used the closedness of S in the latter step to make the integral of the first term on the RHS vanish. A proof hereof uses a variant of the divergence theorem and spherical coordinates for \mathbf{p} . A formal proof is rather cumbersome and will be omitted. To proceed, we recall Property 2.2 which gives

$$\begin{aligned} \left(\int_S \dot{\mathbf{p}} \psi \cdot \tilde{\nabla} \mathbf{p} \mathbf{p} d^2 \mathbf{p} \right)_{ij} &= \int_S \psi \sum_k \left[\dot{p}_k \frac{\tilde{\partial}}{\partial p_k} (p_i p_j) \right] d^2 \mathbf{p} \\ &= \int_S \psi \sum_k [\dot{p}_k (\delta_{ki} p_j + \delta_{kj} p_i - 2 p_i p_j p_k)] d^2 \mathbf{p} \\ &= \int_S \psi \sum_k [\dot{p}_k \delta_{ki} p_j + \dot{p}_k \delta_{kj} p_i - \dot{p}_k 2 p_i p_j p_k] d^2 \mathbf{p} \\ &= \int_S \psi \left[\dot{p}_i p_j + \dot{p}_j p_i - 2 p_i p_j \sum_k \dot{p}_k p_k \right] d^2 \mathbf{p} \end{aligned}$$

Because \mathbf{p} is a unit vector, we have

$$\sum_k p_k^2 = 1 \Rightarrow \left(\sum_k p_k^2 \right) = (\dot{1}) \Leftrightarrow \sum_k 2p_k \dot{p}_k = 0 \Leftrightarrow \sum_k p_k \dot{p}_k = 0$$

and thus the last term vanishes, leaving

$$\int_S \psi [\dot{p}_i p_j + \dot{p}_j p_i] d^2 \mathbf{p}.$$

Using the Jeffery term $\dot{\mathbf{p}}_J$ in component form, we find

$$\begin{aligned} \int_S \psi [\dot{p}_i p_j + \dot{p}_j p_i] d^2 \mathbf{p} &= \int_S \psi \left[\left(\sum_k [W_{ik} p_k] + \xi \left(\sum_k [W_{ik} p_k] - \sum_{k,l} [D_{kl} p_l p_k p_i] \right) \right) p_j \right. \\ &\quad \left. + \left(\sum_k [W_{jk} p_k] + \xi \left(\sum_k [D_{jk} p_k] - \sum_{k,l} [D_{kl} p_l p_k p_j] \right) \right) p_i \right] d^2 \mathbf{p} \\ &= \sum_k \left[W_{ik} \int_S \psi p_k p_j d^2 \mathbf{p} \right] + \xi \sum_k \left[D_{ik} \int_S \psi p_k p_j d^2 \mathbf{p} \right] - \xi \sum_{k,l} D_{kl} \left[\int_S \psi p_l p_k p_i p_j d^2 \mathbf{p} \right] \\ &\quad + \sum_k \left[W_{jk} \int_S \psi p_k p_i d^2 \mathbf{p} \right] + \xi \sum_k \left[D_{jk} \int_S \psi p_k p_i d^2 \mathbf{p} \right] - \xi \sum_{k,l} D_{kl} \left[\int_S \psi p_l p_k p_j p_i d^2 \mathbf{p} \right] \\ &= \sum_k \left[W_{ik} \int_S \psi p_k p_j d^2 \mathbf{p} \right] + \xi \sum_k \left[D_{ik} \int_S \psi p_k p_j d^2 \mathbf{p} \right] - \xi \sum_{k,l} D_{kl} \left[\int_S \psi p_l p_k p_i p_j d^2 \mathbf{p} \right] \\ &\quad - \sum_k \left[\int_S \psi p_k p_i d^2 \mathbf{p} W_{kj} \right] + \xi \sum_k \left[\int_S \psi p_k p_i d^2 \mathbf{p} D_{kj} \right] - \xi \sum_{k,l} D_{kl} \left[\int_S \psi p_l p_k p_i p_j d^2 \mathbf{p} \right] \end{aligned}$$

where in the last step the symmetry of \mathbf{D} , the antisymmetry of \mathbf{W} and commutivity of scalars were used. This gives rise to the tensor form

$$\mathbf{W} \cdot \mathbf{A} - \mathbf{A} \cdot \mathbf{W} + \xi (\mathbf{D} \cdot \mathbf{A} + \mathbf{A} \cdot \mathbf{D} - 2\mathbf{A} : \mathbf{D}) \quad (4.6)$$

which concludes the Jeffery term.

For the 'Folgar-Tucker' term, we have

$$\begin{aligned} - \int_S \tilde{\nabla} \cdot (\dot{\mathbf{p}}_{FT} \psi) \mathbf{p} \mathbf{p} d^2 \mathbf{p} &= - \int_S \tilde{\nabla} \cdot ((-C_I \dot{\gamma} \tilde{\nabla} \ln(\psi)) \psi) \\ &= C_I \dot{\gamma} \int_S (\tilde{\nabla} \cdot \tilde{\nabla} \ln \psi) \psi \mathbf{p} \mathbf{p} d^2 \mathbf{p}. \end{aligned}$$

The factor $\tilde{\nabla} \ln \psi$ has components

$$(\tilde{\nabla} \ln \psi)_i = \frac{\tilde{\partial}}{\partial p_i} \ln \psi = \frac{1}{\psi} \frac{\tilde{\partial} \psi}{\partial p_i}$$

and thus

$$\tilde{\nabla} \ln \psi = \frac{1}{\psi} \tilde{\nabla} \psi.$$

Using the latter and Properties 2.4 and 2.3, the Folgar-Tucker term is

$$\begin{aligned}
C_{I\dot{\gamma}} \int_S (\tilde{\nabla} \cdot (\psi \tilde{\nabla} \ln \psi)) \mathbf{p}\mathbf{p} \, d^2\mathbf{p} &= C_{I\dot{\gamma}} \int_S (\tilde{\nabla} \cdot \tilde{\nabla} \psi) \mathbf{p}\mathbf{p} \, d^2\mathbf{p} \\
&= C_{I\dot{\gamma}} \int_S \psi (\tilde{\nabla} \cdot \tilde{\nabla} \mathbf{p}\mathbf{p}) \, d^2\mathbf{p} \\
&= C_{I\dot{\gamma}} \int_S \psi (2(\mathbf{I} - 3\mathbf{p}\mathbf{p})) \, d^2\mathbf{p} \\
&= 2C_{I\dot{\gamma}} \left(\int_S \psi \, d^2\mathbf{p} \cdot \mathbf{I} - 3 \int_S \psi \mathbf{p}\mathbf{p} \, d^2\mathbf{p} \right) \\
&= 2C_{I\dot{\gamma}} (\mathbf{I} - 3\mathbf{A})
\end{aligned} \tag{4.7}$$

Adding the Jeffery and Folgar-Tucker terms (4.6) and (4.7), we obtain the rate equation for \mathbf{A}

$$\dot{\mathbf{A}} = \mathbf{W} \cdot \mathbf{A} - \mathbf{A} \cdot \mathbf{W} + \xi(\mathbf{D} \cdot \mathbf{A} + \mathbf{A} \cdot \mathbf{D} - 2\mathbb{A} : \mathbf{D}) + 2C_{I\dot{\gamma}}(\mathbf{I} - 3\mathbf{A}) \tag{4.8}$$

which concludes the proof. \square

Note that for practical injection molding processes, we have that ψ is a function of the space \mathbf{x} and thus \mathbf{A} is a function of \mathbf{x} . The implication has been proven, but the \mathbb{A} makes finding a solution impossible. Deriving a rate equation for \mathbb{A} would lead to the introduction of a sixth order tensor. Deriving a rate equation for the sixth order tensor would lead to the introduction of a eight order tensor, and so on. Such a strategy is cumbersome and futile. This closure problem can be solved by approximating \mathbb{A} as a function of \mathbf{A} . In the literature, several of these closure approximations are available. In particular, orthotropic closure approximations stand out [15]. The Wang-O'Gara-Tucker model does not imply a closure approximation and thus this issue will not be discussed here, but in Chapter 6.

Chapter 5

Wang-O'Gara-Tucker model

5.1 Introduction

Although (4.8) has been widely used in academia and industries, it displays an orientational relaxation rate that is too fast. Steady state situations are reached too quickly in comparison with experiments. J. Wang, J.F. O'Gara and C.L. Tucker III have attempted to correct this rate of kinetics, which was published in 2008 in [13]. Their model is derived, its objectivity is proven and the equivalent kinetic theory is constructed.

5.2 Rate equations for the eigenpairs

A straightforward way to slow the dynamics down is demonstrated by the strain reduction factor (SRF) model [13]. The RHS of (4.8) is multiplied with a strain reduction factor $\kappa < 1$, resulting in

$$\dot{\mathbf{A}} = \kappa (\mathbf{W} \cdot \mathbf{A} - \mathbf{A} \cdot \mathbf{W} + \xi(\mathbf{D} \cdot \mathbf{A} + \mathbf{A} \cdot \mathbf{D} - 2\mathbb{A} : \mathbf{D}) - 2C_I \dot{\gamma}(\mathbf{I} - 3\mathbf{A})).$$

The argument of using the former is that the fibers are concentrated into clusters that experience less strain than the bulk. It, however, does not obey the condition of objectivity for time derivatives [8]

$$\dot{\mathbf{A}}^+ = \dot{\mathbf{Q}}\mathbf{A}\mathbf{Q}^T + \mathbf{Q}\dot{\mathbf{A}}\mathbf{Q}^T + \mathbf{Q}\mathbf{A}(\dot{\mathbf{Q}}^T)$$

and can thus give different answers in different coordinate systems. Note that the $+$ refers to an observer O^+ different from O , in the sense of the Euclidean transformation

$$\mathbf{x}^+ = \mathbf{c}(t) + \mathbf{Q}(t) \cdot \mathbf{x}, \quad t^+ = t - \alpha$$

where

$$\mathbf{c}(t) = \mathbf{x}_0^+ - \mathbf{Q}(t) \cdot \mathbf{x}_0, \quad \alpha = t_0^+ - t_0.$$

The $\mathbf{Q}(t)$ represents a rotation, the $\mathbf{c}(t)$ a translation. This variance under change of basis originates from the multiplication of \mathbf{W} with κ , which introduces a variance under rigid body rotation. The SRF model does not suffice. The notion of objectivity is treated more thoroughly in Section 5.4.

The strategy used in [13] to resolve the issue of the orientational relaxation rate is decomposing the equation for $\dot{\mathbf{A}}$ into rate equations for the eigenpairs of \mathbf{A} , modifying the equation for the eigenvalues and reassembling the equations for the eigenpairs to obtain an equation for $\dot{\mathbf{A}}$ again.

5.2.1 Rate equation for the eigenvalues

Theorem 5.1. *The rate equation (4.8) for the second order tensor \mathbf{A} implies the rate equation*

$$\dot{\lambda}_j = 2\xi(\lambda_j \mathbf{D} : \mathbf{e}_j \mathbf{e}_j - \mathbf{e}_j \mathbf{e}_j : \mathbb{A} : \mathbf{D}) + 2C_I \dot{\gamma}(1 - 3\lambda_j)$$

for the eigenvalues of \mathbf{A} .

Proof. We start with the derivation of the rate equation for the eigenvalues. For this, we recall Property 4.7

$$\mathbf{A} = \sum_i \lambda_i \mathbf{e}_i \mathbf{e}_i$$

and substitute it in in (4.8). For the LHS we get

$$\dot{\mathbf{A}} = \left(\sum_i \lambda_i \mathbf{e}_i \mathbf{e}_i \right) = \sum_i \dot{\lambda}_i \mathbf{e}_i \mathbf{e}_i + \lambda_i \dot{\mathbf{e}}_i \mathbf{e}_i + \lambda_i \mathbf{e}_i \dot{\mathbf{e}}_i.$$

For the RHS, substitution is trivial. The equation with the spectral expansion used is

$$\begin{aligned} \sum_i \dot{\lambda}_i \mathbf{e}_i \mathbf{e}_i + \lambda_i \dot{\mathbf{e}}_i \mathbf{e}_i + \lambda_i \mathbf{e}_i \dot{\mathbf{e}}_i &= \sum_i [\lambda_i \mathbf{W} \cdot \mathbf{e}_i \mathbf{e}_i - \lambda_i \mathbf{e}_i \mathbf{e}_i \cdot \mathbf{W} + \xi(\lambda_i \mathbf{D} \cdot \mathbf{e}_i \mathbf{e}_i + \lambda_i \mathbf{e}_i \mathbf{e}_i \cdot \mathbf{D}) \\ &\quad + 2C_I \dot{\gamma}(1 - 3\lambda_i) \mathbf{e}_i \mathbf{e}_i] - 2\xi \mathbb{A} : \mathbf{D}. \end{aligned} \quad (5.1)$$

To obtain separate equations for the rates of change of the eigenvalues, we apply $\mathbf{e}_j \cdot (\dots) \cdot \mathbf{e}_j$ on both sides of the latter equation. Moreover, we use the properties $\mathbf{e}_i \cdot \mathbf{e}_j = \delta_{ij}$ and $\mathbf{e}_j \cdot \dot{\mathbf{e}}_j = 0$, where the latter follows from orthonormality

$$\mathbf{e}_j \cdot \mathbf{e}_j = 1 \quad \Rightarrow \quad (\mathbf{e}_j \cdot \dot{\mathbf{e}}_j) = 0 \quad \Leftrightarrow \quad \dot{\mathbf{e}}_j \cdot \mathbf{e}_j + \mathbf{e}_j \cdot \dot{\mathbf{e}}_j = 0 \quad \Leftrightarrow \quad \Leftrightarrow \quad \mathbf{e}_j \cdot \dot{\mathbf{e}}_j = 0.$$

We obtain for the LHS

$$\begin{aligned} \mathbf{e}_j \cdot \left(\sum_i \dot{\lambda}_i \mathbf{e}_i \mathbf{e}_i + \lambda_i \dot{\mathbf{e}}_i \mathbf{e}_i + \lambda_i \mathbf{e}_i \dot{\mathbf{e}}_i \right) \cdot \mathbf{e}_j &= \sum_i \left[\dot{\lambda}_i \mathbf{e}_j \cdot \mathbf{e}_i \mathbf{e}_i \cdot \mathbf{e}_j + \lambda_i \mathbf{e}_j \cdot \dot{\mathbf{e}}_i \mathbf{e}_i \cdot \mathbf{e}_j + \lambda_i \mathbf{e}_j \cdot \mathbf{e}_i \dot{\mathbf{e}}_i \cdot \mathbf{e}_j \right] \\ &= \sum_i \left[\dot{\lambda}_i \delta_{ij} \delta_{ij} + \lambda_i \mathbf{e}_j \cdot \dot{\mathbf{e}}_i \delta_{ij} + \lambda_i \delta_{ij} \dot{\mathbf{e}}_i \cdot \mathbf{e}_j \right] \\ &= \dot{\lambda}_j + \lambda_j \mathbf{e}_j \cdot \dot{\mathbf{e}}_j + \lambda_j \dot{\mathbf{e}}_j \cdot \mathbf{e}_j \\ &= \dot{\lambda}_j. \end{aligned}$$

For the RHS, we get

$$\begin{aligned} \mathbf{e}_j \cdot \left(\sum_i [\lambda_i \mathbf{W} \cdot \mathbf{e}_i \mathbf{e}_i - \lambda_i \mathbf{e}_i \mathbf{e}_i \cdot \mathbf{W} \right. & \quad \left. \sum_i [\lambda_i \mathbf{e}_j \cdot \mathbf{W} \cdot \mathbf{e}_i \mathbf{e}_i \cdot \mathbf{e}_j - \lambda_i \mathbf{e}_j \cdot \mathbf{e}_i \mathbf{e}_i \cdot \mathbf{W} \cdot \mathbf{e}_j \right. \\ & \left. + \xi(\lambda_i \mathbf{D} \cdot \mathbf{e}_i \mathbf{e}_i + \lambda_i \mathbf{e}_i \mathbf{e}_i \cdot \mathbf{D}) \right) = \left. + \xi(\lambda_i \mathbf{e}_j \cdot \mathbf{D} \cdot \mathbf{e}_i \mathbf{e}_i \cdot \mathbf{e}_j + \lambda_i \mathbf{e}_j \cdot \mathbf{e}_i \mathbf{e}_i \cdot \mathbf{D} \cdot \mathbf{e}_j) \right. \\ & \left. + 2C_I \dot{\gamma}(1 - 3\lambda_i) \mathbf{e}_i \mathbf{e}_i \right] - 2\xi \mathbb{A} : \mathbf{D} \cdot \mathbf{e}_j \quad \left. + 2C_I \dot{\gamma}(1 - 3\lambda_i) \mathbf{e}_j \cdot \mathbf{e}_i \mathbf{e}_i \cdot \mathbf{e}_j \right] - 2\xi \mathbf{e}_j \cdot \mathbb{A} : \mathbf{D} \cdot \mathbf{e}_j \end{aligned}$$

which simplifies to

$$\begin{aligned} \sum_i [\delta_{ij} (\lambda_i \mathbf{e}_j \cdot \mathbf{W} \cdot \mathbf{e}_i - \lambda_i \mathbf{e}_i \cdot \mathbf{W} \cdot \mathbf{e}_j + \xi(\lambda_i \mathbf{e}_j \cdot \mathbf{D} \cdot \mathbf{e}_i + \lambda_i \mathbf{e}_i \cdot \mathbf{D} \cdot \mathbf{e}_j) + 2C_I \dot{\gamma}(1 - 3\lambda_i))] - 2\xi \mathbf{e}_j \cdot \mathbb{A} : \mathbf{D} \cdot \mathbf{e}_j = \\ \lambda_j \mathbf{e}_j \cdot \mathbf{W} \cdot \mathbf{e}_j - \lambda_j \mathbf{e}_j \cdot \mathbf{W} \cdot \mathbf{e}_j + \xi(\lambda_j \mathbf{e}_j \cdot \mathbf{D} \cdot \mathbf{e}_j + \lambda_j \mathbf{e}_j \cdot \mathbf{D} \cdot \mathbf{e}_j) + 2C_I \dot{\gamma}(1 - 3\lambda_j) - 2\xi \mathbf{e}_j \cdot \mathbb{A} : \mathbf{D} \cdot \mathbf{e}_j = \\ 2\xi \lambda_j \mathbf{e}_j \cdot \mathbf{D} \cdot \mathbf{e}_j + 2C_I \dot{\gamma}(1 - 3\lambda_j) - 2\xi \mathbf{e}_j \cdot \mathbb{A} : \mathbf{D} \cdot \mathbf{e}_j. \end{aligned}$$

Note that

$$\mathbf{e}_j \cdot \mathbf{D} \cdot \mathbf{e}_j = \mathbf{D} : \mathbf{e}_j \mathbf{e}_j \quad \wedge \quad \mathbf{e}_j \cdot \mathbb{A} : \mathbf{D} \cdot \mathbf{e}_j = \mathbf{e}_j \mathbf{e}_j : \mathbb{A} : \mathbf{D}$$

which concludes the derivation of both the left and RHS to get

$$\begin{aligned} \dot{\lambda}_j &= 2\xi \lambda_j \mathbf{D} : \mathbf{e}_j \mathbf{e}_j + 2C_I \dot{\gamma}(1 - 3\lambda_j) - 2\xi \mathbf{e}_j \mathbf{e}_j : \mathbb{A} : \mathbf{D} \\ &= 2\xi (\lambda_j \mathbf{D} : \mathbf{e}_j \mathbf{e}_j - \mathbf{e}_j \mathbf{e}_j : \mathbb{A} : \mathbf{D}) + 2C_I \dot{\gamma}(1 - 3\lambda_j). \end{aligned} \tag{5.2}$$

□

5.2.2 Rate equation for the eigenvectors

Theorem 5.2. *The rate equation (4.8) for the second order tensor \mathbf{A} implies the rate equation*

$$\begin{aligned} \dot{\mathbf{e}}_i &= \mathbf{W} \cdot \mathbf{e}_i + \xi \frac{\lambda_2 + \lambda_1 - 4\bar{A}_{1212}}{\lambda_2 - \lambda_1} (\mathbf{D} : \mathbf{e}_1 \mathbf{e}_2) (\delta_{2i} \mathbf{e}_1 - \delta_{1i} \mathbf{e}_2) \\ &+ \xi \frac{\lambda_3 + \lambda_2 - 4\bar{A}_{2323}}{\lambda_3 - \lambda_2} (\mathbf{D} : \mathbf{e}_2 \mathbf{e}_3) (\delta_{3i} \mathbf{e}_2 - \delta_{2i} \mathbf{e}_3) \\ &+ \xi \frac{\lambda_1 + \lambda_3 - 4\bar{A}_{3131}}{\lambda_1 - \lambda_3} (\mathbf{D} : \mathbf{e}_3 \mathbf{e}_1) (\delta_{1i} \mathbf{e}_3 - \delta_{3i} \mathbf{e}_1) \end{aligned}$$

for the eigenvectors of \mathbf{A} .

Proof. Recall (5.1)

$$\begin{aligned} \sum_i \dot{\lambda}_i \mathbf{e}_i \mathbf{e}_i + \lambda_i (\dot{\mathbf{e}}_i \mathbf{e}_i + \mathbf{e}_i \dot{\mathbf{e}}_i) &= \sum_i [\lambda_i \mathbf{W} \cdot \mathbf{e}_i \mathbf{e}_i - \lambda_i \mathbf{e}_i \mathbf{e}_i \cdot \mathbf{W} + \xi(\lambda_i \mathbf{D} \cdot \mathbf{e}_i \mathbf{e}_i + \lambda_i \mathbf{e}_i \mathbf{e}_i \cdot \mathbf{D}) \\ &+ 2C_I \dot{\gamma}(1 - 3\lambda_i) \mathbf{e}_i \mathbf{e}_i] - 2\xi \mathbb{A} : \mathbf{D}. \end{aligned}$$

We reorder the equation as

$$\begin{aligned} \sum_i \lambda_i (\dot{\mathbf{e}}_i \mathbf{e}_i + \mathbf{e}_i \dot{\mathbf{e}}_i) &= \sum_i [\lambda_i \mathbf{W} \cdot \mathbf{e}_i \mathbf{e}_i - \lambda_i \mathbf{e}_i \mathbf{e}_i \cdot \mathbf{W} + \xi(\lambda_i \mathbf{D} \cdot \mathbf{e}_i \mathbf{e}_i + \lambda_i \mathbf{e}_i \mathbf{e}_i \cdot \mathbf{D}) \\ &+ 2C_I \dot{\gamma}(1 - 3\lambda_i) \mathbf{e}_i \mathbf{e}_i] - 2\xi \mathbb{A} : \mathbf{D} - \sum_i \dot{\lambda}_i \mathbf{e}_i \mathbf{e}_i. \end{aligned} \tag{5.3}$$

The term $\mathbf{e}\mathbf{e} \cdot \mathbf{W}$ has components

$$\sum_j e_i e_j W_j \Leftrightarrow e_i \sum_j W_j e_j$$

and can thus be written as $\mathbf{e}(\mathbf{W} \cdot \mathbf{e}) = \mathbf{e}\mathbf{W} \cdot \mathbf{e}$. Moreover, with the use of (5.2), we can write

$$\begin{aligned} \sum_i \dot{\lambda}_i \mathbf{e}_i \mathbf{e}_i &= \sum_i (2\xi (\lambda_i \mathbf{D} : \mathbf{e}_i \mathbf{e}_i - \mathbf{e}_i \mathbf{e}_i : \mathbb{A} : \mathbf{D}) + 2C_I \dot{\gamma} (1 - 3\lambda_i)) \mathbf{e}_i \mathbf{e}_i \\ &= \sum_i [2\xi \lambda_i \mathbf{D} : \mathbf{e}_i \mathbf{e}_i \mathbf{e}_i \mathbf{e}_i] - \sum_i [2\xi \mathbf{e}_i \mathbf{e}_i : \mathbb{A} : \mathbf{D} \mathbf{e}_i \mathbf{e}_i] + \sum_i [2C_I \dot{\gamma} (1 - 3\lambda_i) \mathbf{e}_i \mathbf{e}_i]. \end{aligned}$$

Substitution in (5.3) results in the cancellation of the interaction terms and

$$\begin{aligned} \sum_i \lambda_i (\dot{\mathbf{e}}_i \mathbf{e}_i + \mathbf{e}_i \dot{\mathbf{e}}_i) &= \sum_i [\lambda_i (\mathbf{W} \cdot \mathbf{e}_i \mathbf{e}_i - \mathbf{e}_i \mathbf{W} \cdot \mathbf{e}_i) + \lambda_i \xi (\mathbf{D} \cdot \mathbf{e}_i \mathbf{e}_i + \mathbf{e}_i \mathbf{e}_i \cdot \mathbf{D} - 2\mathbf{D} : \mathbf{e}_i \mathbf{e}_i \mathbf{e}_i \mathbf{e}_i)] \\ &\quad - 2\xi \left(\mathbb{A} : \mathbf{D} - \sum_i \mathbf{e}_i \mathbf{e}_i : \mathbb{A} : \mathbf{D} \mathbf{e}_i \mathbf{e}_i \right). \end{aligned} \quad (5.4)$$

The last term can be simplified by writing

$$\mathbb{A} : \mathbf{D} = \sum_{i,j,k,l} \bar{A}_{ijkl} \bar{D}_{kl} \mathbf{e}_i \mathbf{e}_j.$$

where we use the notation $([A]_E)_{ab\dots} = \bar{A}_{ab\dots}$ to emphasize that the components are taken with respect to basis E . Also

$$\mathbb{A} = \sum_{j,k,l,m} \bar{A}_{jklm} \mathbf{e}_j \mathbf{e}_k \mathbf{e}_l \mathbf{e}_m \Rightarrow \mathbf{e}_i \mathbf{e}_i : \mathbb{A} = \mathbf{e}_i \mathbf{e}_i : \sum_{j,k,l,m} \bar{A}_{jklm} \mathbf{e}_j \mathbf{e}_k \mathbf{e}_l \mathbf{e}_m = \sum_{j,k,l,m} \bar{A}_{jklm} \mathbf{e}_i \mathbf{e}_i : \mathbf{e}_j \mathbf{e}_k \mathbf{e}_l \mathbf{e}_m.$$

Note that

$$\mathbf{e}_i \mathbf{e}_i : \mathbf{e}_j \mathbf{e}_k = \sum_{n,p} (\mathbf{e}_i)_n (\mathbf{e}_i)_p (\mathbf{e}_j)_n (\mathbf{e}_k)_p = \sum_n (\mathbf{e}_i)_n (\mathbf{e}_j)_n \sum_p (\mathbf{e}_i)_p (\mathbf{e}_k)_p = (\mathbf{e}_i \cdot \mathbf{e}_j) (\mathbf{e}_i \cdot \mathbf{e}_k) = \delta_{ij} \delta_{ik}$$

so that

$$\sum_{j,k,l,m} \bar{A}_{jklm} \mathbf{e}_i \mathbf{e}_i : \mathbf{e}_j \mathbf{e}_k \mathbf{e}_l \mathbf{e}_m = \sum_{l,m} \bar{A}_{iilm} \mathbf{e}_l \mathbf{e}_m.$$

Writing

$$\mathbf{D} = \sum_{j,k} \bar{D}_{jk} \mathbf{e}_j \mathbf{e}_k$$

and taking the left double contraction with $\mathbf{e}_i \mathbf{e}_i : \mathbb{A}$ gives

$$\begin{aligned} \mathbf{e}_i \mathbf{e}_i : \mathbb{A} : \mathbf{D} &= \left(\sum_{l,m} \bar{A}_{iilm} \mathbf{e}_l \mathbf{e}_m \right) : \sum_{j,k} \bar{D}_{jk} \mathbf{e}_j \mathbf{e}_k \\ &= \sum_{j,k,l,m} \bar{A}_{iilm} \bar{D}_{jk} \mathbf{e}_l \mathbf{e}_m : \mathbf{e}_j \mathbf{e}_k \\ &= \sum_{j,k,l,m} \bar{A}_{iilm} \bar{D}_{jk} \delta_{jl} \delta_{km} \\ &= \sum_{j,k} \bar{A}_{iijk} \bar{D}_{jk}. \end{aligned}$$

Because we can choose the indices arbitrarily, we rewrite the latter as

$$\sum_{k,l} \bar{A}_{iikl} \bar{D}_{kl}$$

for the sake of clarity in the addition

$$\begin{aligned} \mathbb{A} : \mathbf{D} - \sum_i \mathbf{e}_i \mathbf{e}_i : \mathbb{A} : \mathbf{D} \mathbf{e}_i \mathbf{e}_i &= \sum_{i,j,k,l} [\bar{A}_{ijkl} \bar{D}_{kl} \mathbf{e}_i \mathbf{e}_j] - \sum_{i,k,l} [\bar{A}_{iikl} \bar{D}_{kl} \mathbf{e}_i \mathbf{e}_i] \\ &= \sum_i \left(\sum_j \sum_{k,l} [\bar{A}_{ijkl} \bar{D}_{kl} \mathbf{e}_i \mathbf{e}_j] - \sum_{k,l} [\bar{A}_{iikl} \bar{D}_{kl} \mathbf{e}_i \mathbf{e}_i] \right). \end{aligned}$$

From the latter it is clear that the terms with $i = j$ are cancelled. The terms with

$$(i, j) \in \{(1, 2), (1, 3), (2, 1), (2, 3), (3, 1), (3, 2)\}$$

remain. Furthermore, $A_{ijkl} = A_{jikl}$ so the remaining terms are

$$\sum_{k,l} [\bar{A}_{12kl} \bar{D}_{kl} (\mathbf{e}_1 \mathbf{e}_2 + \mathbf{e}_2 \mathbf{e}_1)] + \sum_{k,l} [\bar{A}_{23kl} \bar{D}_{kl} (\mathbf{e}_2 \mathbf{e}_3 + \mathbf{e}_3 \mathbf{e}_2)] + \sum_{k,l} [\bar{A}_{31kl} \bar{D}_{kl} (\mathbf{e}_3 \mathbf{e}_1 + \mathbf{e}_1 \mathbf{e}_3)].$$

If the fourth order orientation tensor is replaced by an orthotropic closure, as explained in Chapter 6, then all components of $\bar{\mathbb{A}}$ are zero except for $\bar{A}_{1212}, \bar{A}_{2323}, \bar{A}_{3131}$ and their symmetric counterparts. This leaves us with

$$\begin{aligned} \mathbb{A} : \mathbf{D} - \sum_i \mathbf{e}_i \mathbf{e}_i : \mathbb{A} : \mathbf{D} \mathbf{e}_i \mathbf{e}_i &= 2 (\bar{A}_{1212} \bar{D}_{12} (\mathbf{e}_1 \mathbf{e}_2 + \mathbf{e}_2 \mathbf{e}_1) + \bar{A}_{2323} \bar{D}_{23} (\mathbf{e}_2 \mathbf{e}_3 + \mathbf{e}_3 \mathbf{e}_2) \\ &\quad + \bar{A}_{3131} \bar{D}_{31} (\mathbf{e}_3 \mathbf{e}_1 + \mathbf{e}_1 \mathbf{e}_3)). \end{aligned} \quad (5.5)$$

In constructing the rate equation for the eigenvectors, we continue with the assumption that a solution of the form

$$\dot{\mathbf{e}}_i = \mathbf{W}_n \cdot \mathbf{e}_i \quad (5.6)$$

exists, where \mathbf{W}_n is unknown. Furthermore, we assume skew or anti symmetry $\mathbf{W}_n = -\mathbf{W}_n^T$. A skew symmetric tensor in an ODE generates a proper orthogonal tensor in the solution, which guarantees that \mathbf{e}_i has a constant length and that all \mathbf{e}_i s remain orthonormal. Again, we use the components with respect to the principal axes of \mathbf{A} and denote them with overbars. We take

$$\mathbf{W}_n = \begin{bmatrix} 0 & \bar{W}_{n12} & -\bar{W}_{n31} \\ -\bar{W}_{n12} & 0 & \bar{W}_{n23} \\ \bar{W}_{n31} & -\bar{W}_{n23} & 0 \end{bmatrix}$$

and a similar expression for \mathbf{W} , without the ns . Note that

$$\begin{aligned} \mathbf{W}_n \cdot \mathbf{e}_1 &= -\bar{W}_{n12} \mathbf{e}_2 + \bar{W}_{n31} \mathbf{e}_3 \\ \mathbf{W}_n \cdot \mathbf{e}_2 &= -\bar{W}_{n23} \mathbf{e}_3 + \bar{W}_{n12} \mathbf{e}_1 \\ \mathbf{W}_n \cdot \mathbf{e}_3 &= -\bar{W}_{n31} \mathbf{e}_1 + \bar{W}_{n23} \mathbf{e}_2 \end{aligned} \quad (5.7)$$

and $\mathbf{e}_l \cdot \mathbf{W}_n \cdot \mathbf{e}_m = (\bar{W}_n)_{lm}$. With the latter, we will find the components of \mathbf{W}_n if possible and construct a solution of the form (5.6).

We substitute (5.5), (5.6), (5.7) and

$$\mathbf{D} = \sum_{j,k} \bar{D}_{jk} \mathbf{e}_j \mathbf{e}_k$$

in (5.4) and take $\mathbf{e}_l \cdot (\dots) \cdot \mathbf{e}_m$ to obtain expressions for $(\bar{W}_n)_{lm}$. For the LHS we get

$$\begin{aligned} \mathbf{e}_l \cdot \left(\sum_i \lambda_i (\dot{\mathbf{e}}_i \mathbf{e}_i + \mathbf{e}_i \dot{\mathbf{e}}_i) \right) \cdot \mathbf{e}_m &= \sum_i \lambda_i (\mathbf{e}_l \cdot (\mathbf{W}_n \cdot \mathbf{e}_i) \mathbf{e}_i \cdot \mathbf{e}_m + \mathbf{e}_l \cdot \mathbf{e}_i (\mathbf{W}_n \cdot \mathbf{e}_i) \cdot \mathbf{e}_m) \\ &= \sum_i [\lambda_i \mathbf{e}_l \cdot (\mathbf{W}_n \cdot \mathbf{e}_i) \mathbf{e}_i \cdot \mathbf{e}_m] + \sum_i [\lambda_i \mathbf{e}_l \cdot \mathbf{e}_i (\mathbf{W}_n \cdot \mathbf{e}_i) \cdot \mathbf{e}_m] \\ &= \sum_i [\lambda_i \mathbf{e}_l \cdot (\mathbf{W}_n \cdot \mathbf{e}_i) \delta_{im}] + \sum_i [\lambda_i \delta_{il} (\mathbf{W}_n \cdot \mathbf{e}_i) \cdot \mathbf{e}_m] \\ &= \lambda_m \mathbf{e}_l \cdot (\mathbf{W}_n \cdot \mathbf{e}_m) + \lambda_l (\mathbf{W}_n \cdot \mathbf{e}_l) \cdot \mathbf{e}_m \end{aligned}$$

where the factors $\mathbf{W}_n \cdot \mathbf{e}_m$ and $\mathbf{W}_n \cdot \mathbf{e}_l$ follow from (5.7). The RHS is rather large and we thus treat the terms separately.

$$\begin{aligned}
\mathbf{e}_l \cdot \left(\sum_i [\lambda_i (\mathbf{W} \cdot \mathbf{e}_i) \mathbf{e}_i] \right) \cdot \mathbf{e}_m &= \sum_i [\lambda_i \mathbf{e}_l \cdot (\mathbf{W} \cdot \mathbf{e}_i) \mathbf{e}_i \cdot \mathbf{e}_m] \\
&= \sum_i [\lambda_i \mathbf{e}_l \cdot (\mathbf{W} \cdot \mathbf{e}_i) \delta_{im}] \\
&= \lambda_m \mathbf{e}_l \cdot (\mathbf{W} \cdot \mathbf{e}_m) \\
\mathbf{e}_l \cdot \left(\sum_i [\lambda_i \mathbf{e}_i (\mathbf{W} \cdot \mathbf{e}_i)] \right) \cdot \mathbf{e}_m &= \sum_i [\lambda_i \mathbf{e}_l \cdot \mathbf{e}_i (\mathbf{W} \cdot \mathbf{e}_i) \cdot \mathbf{e}_m] \\
&= \sum_i [\lambda_i \delta_{il} (\mathbf{W} \cdot \mathbf{e}_i) \cdot \mathbf{e}_m] \\
&= \lambda_l (\mathbf{W} \cdot \mathbf{e}_l) \cdot \mathbf{e}_m \\
\mathbf{e}_l \cdot \left(\sum_i \lambda_i \left(\sum_{j,k} \bar{D}_{jk} \mathbf{e}_j \mathbf{e}_k \right) \cdot \mathbf{e}_i \mathbf{e}_i \right) \cdot \mathbf{e}_m &= \sum_{i,j,k} [\lambda_i \bar{D}_{jk} \mathbf{e}_l \cdot (\mathbf{e}_j \mathbf{e}_k \cdot \mathbf{e}_i \mathbf{e}_i) \cdot \mathbf{e}_m] \\
&= \sum_{i,j,k} [\lambda_i \bar{D}_{jk} \delta_{ik} \delta_{jl} \delta_{im}] \\
&= \lambda_m \bar{D}_{lm} \\
\mathbf{e}_l \cdot \left(\sum_i \lambda_i \mathbf{e}_i \mathbf{e}_i \cdot \left(\sum_{j,k} \bar{D}_{jk} \mathbf{e}_j \mathbf{e}_k \right) \right) \cdot \mathbf{e}_m &= \sum_{i,j,k} [\lambda_i \bar{D}_{jk} \mathbf{e}_l \cdot (\mathbf{e}_i \mathbf{e}_i \cdot \mathbf{e}_j \mathbf{e}_k) \cdot \mathbf{e}_m] \\
&= \sum_{i,j,k} [\lambda_i \bar{D}_{jk} \delta_{ij} \delta_{il} \delta_{km}] \\
&= \lambda_l \bar{D}_{lm} \\
\mathbf{e}_l \cdot \left(\sum_i \lambda_i \left(\sum_{j,k} \bar{D}_{jk} \mathbf{e}_j \mathbf{e}_k \right) : \mathbf{e}_i \mathbf{e}_i \mathbf{e}_i \mathbf{e}_i \right) \cdot \mathbf{e}_m &= \sum_{i,j,k} [\lambda_i \bar{D}_{jk} \mathbf{e}_l \cdot (\mathbf{e}_j \mathbf{e}_k : \mathbf{e}_i \mathbf{e}_i \mathbf{e}_i \mathbf{e}_i) \cdot \mathbf{e}_m] \\
&= \sum_{i,j,k} [\lambda_i \bar{D}_{jk} \delta_{ij} \delta_{ik} \delta_{il} \delta_{im}] \\
&= \lambda_l \bar{D}_{ll} \delta_{lm} \\
&= \lambda_m \bar{D}_{mm} \delta_{lm}
\end{aligned}$$

In the last term of (5.4), the kernels

$$\mathbf{e}_1 \mathbf{e}_2 + \mathbf{e}_2 \mathbf{e}_1, \mathbf{e}_2 \mathbf{e}_3 + \mathbf{e}_3 \mathbf{e}_2, \mathbf{e}_3 \mathbf{e}_1 + \mathbf{e}_1 \mathbf{e}_3$$

merely change to

$$\delta_{1l} \delta_{2m} + \delta_{2l} \delta_{1m}, \delta_{2l} \delta_{3m} + \delta_{3l} \delta_{2m}, \delta_{3l} \delta_{1m} + \delta_{1l} \delta_{3m}.$$

Herewith, the final result is

$$\begin{aligned}
\lambda_m \mathbf{e}_l \cdot (\mathbf{W}_n \cdot \mathbf{e}_m) + \lambda_l (\mathbf{W}_n \cdot \mathbf{e}_l) \cdot \mathbf{e}_m &= \lambda_m \mathbf{e}_l \cdot (\mathbf{W} \cdot \mathbf{e}_m) + \lambda_l (\mathbf{W} \cdot \mathbf{e}_l) \cdot \mathbf{e}_m + \xi \lambda_m \bar{D}_{lm} + \xi \lambda_l \bar{D}_{lm} \\
&\quad - 2\xi \lambda_m \bar{D}_{mm} \delta_{lm} - 4\xi (\bar{A}_{1212} \bar{D}_{12} (\delta_{1l} \delta_{2m} + \delta_{2l} \delta_{1m}) \\
&\quad + \bar{A}_{2323} \bar{D}_{23} (\delta_{2l} \delta_{3m} + \delta_{3l} \delta_{2m}) + \bar{A}_{3131} \bar{D}_{31} (\delta_{3l} \delta_{1m} + \delta_{1l} \delta_{3m}))
\end{aligned} \tag{5.8}$$

which, in combination with (5.7), gives us the elements of \mathbf{W}_n . We construct \mathbf{W}_n via its expansion

$$\begin{aligned}
\mathbf{W}_n &= \sum_{i,j} (\bar{W}_n)_{ij} \mathbf{e}_i \mathbf{e}_j \\
&= \bar{W}_{n12} (\mathbf{e}_1 \mathbf{e}_2 - \mathbf{e}_2 \mathbf{e}_1) + \bar{W}_{n23} (\mathbf{e}_2 \mathbf{e}_3 - \mathbf{e}_3 \mathbf{e}_2) + \bar{W}_{n31} (\mathbf{e}_3 \mathbf{e}_1 - \mathbf{e}_1 \mathbf{e}_3)
\end{aligned} \tag{5.9}$$

where we used the the skew symmetry of \mathbf{W}_n , implying zero diagonal terms and the three independent elements $\bar{W}_{n12}, \bar{W}_{n23}, \bar{W}_{n31}$. We find the latter by taking $(l, m) \in \{(1, 2), (2, 3), (3, 1)\}$ in (5.8).

$$\begin{aligned}
\lambda_2 \mathbf{e}_1 \cdot (\mathbf{W}_n \cdot \mathbf{e}_2) + \lambda_1 (\mathbf{W}_n \cdot \mathbf{e}_1) \cdot \mathbf{e}_2 &= \lambda_2 \mathbf{e}_1 \cdot (\mathbf{W} \cdot \mathbf{e}_2) + \lambda_1 (\mathbf{W} \cdot \mathbf{e}_1) \cdot \mathbf{e}_2 + \xi \lambda_2 \bar{D}_{12} + \xi \lambda_1 \bar{D}_{12} \\
&\quad - 2\xi \lambda_2 \bar{D}_{22} \delta_{12} - 4\xi (\bar{A}_{1212} \bar{D}_{12} (\delta_{11} \delta_{22} + \delta_{21} \delta_{12}) \\
&\quad + \bar{A}_{2323} \bar{D}_{23} (\delta_{21} \delta_{32} + \delta_{31} \delta_{22}) + \bar{A}_{3131} \bar{D}_{31} (\delta_{31} \delta_{12} + \delta_{11} \delta_{32})) \\
\lambda_2 \bar{W}_{n12} - \lambda_1 \bar{W}_{n12} &= \lambda_2 \bar{W}_{12} - \lambda_1 \bar{W}_{12} + \xi \lambda_2 \bar{D}_{12} + \xi \lambda_1 \bar{D}_{12} - 4\xi \bar{A}_{1212} \bar{D}_{12} \\
(\lambda_2 - \lambda_1) \bar{W}_{n12} &= (\lambda_2 - \lambda_1) \bar{W}_{12} + \xi (\lambda_2 + \lambda_1 - 4\bar{A}_{1212}) \bar{D}_{12} \\
\bar{W}_{n12} &= \bar{W}_{12} + \xi \frac{\lambda_2 + \lambda_1 - 4\bar{A}_{1212}}{\lambda_2 - \lambda_1} \bar{D}_{12}
\end{aligned}$$

$$\begin{aligned}
\lambda_3 \mathbf{e}_2 \cdot (\mathbf{W}_n \cdot \mathbf{e}_3) + \lambda_2 (\mathbf{W}_n \cdot \mathbf{e}_2) \cdot \mathbf{e}_3 &= \lambda_3 \mathbf{e}_2 \cdot (\mathbf{W} \cdot \mathbf{e}_3) + \lambda_2 (\mathbf{W} \cdot \mathbf{e}_2) \cdot \mathbf{e}_3 + \xi \lambda_3 \bar{D}_{23} + \xi \lambda_2 \bar{D}_{23} \\
&\quad - 2\xi \lambda_3 \bar{D}_{33} \delta_{23} - 4\xi (\bar{A}_{1212} \bar{D}_{12} (\delta_{12} \delta_{23} + \delta_{22} \delta_{13}) \\
&\quad + \bar{A}_{2323} \bar{D}_{23} (\delta_{22} \delta_{33} + \delta_{32} \delta_{23}) + \bar{A}_{3131} \bar{D}_{31} (\delta_{32} \delta_{13} + \delta_{12} \delta_{33})) \\
\lambda_3 \bar{W}_{n23} - \lambda_2 \bar{W}_{n23} &= \lambda_3 \bar{W}_{23} - \lambda_2 \bar{W}_{23} + \xi \lambda_3 \bar{D}_{23} + \xi \lambda_2 \bar{D}_{23} \\
&\quad - 4\xi \bar{A}_{2323} \bar{D}_{23} \\
(\lambda_3 - \lambda_2) \bar{W}_{n23} &= (\lambda_3 - \lambda_2) \bar{W}_{23} + \xi (\lambda_3 + \lambda_2 - 4\bar{A}_{2323}) \bar{D}_{23} \\
\bar{W}_{n23} &= \bar{W}_{23} + \xi \frac{\lambda_3 + \lambda_2 - 4\bar{A}_{2323}}{\lambda_3 - \lambda_2} \bar{D}_{23}
\end{aligned}$$

$$\begin{aligned}
\lambda_1 \mathbf{e}_3 \cdot (\mathbf{W}_n \cdot \mathbf{e}_1) + \lambda_3 (\mathbf{W}_n \cdot \mathbf{e}_3) \cdot \mathbf{e}_1 &= \lambda_3 \mathbf{e}_3 \cdot (\mathbf{W} \cdot \mathbf{e}_1) + \lambda_3 (\mathbf{W} \cdot \mathbf{e}_3) \cdot \mathbf{e}_1 + \xi \lambda_1 \bar{D}_{31} + \xi \lambda_3 \bar{D}_{31} \\
&\quad - 2\xi \lambda_1 \bar{D}_{11} \delta_{31} - 4\xi (\bar{A}_{1212} \bar{D}_{12} (\delta_{13} \delta_{21} + \delta_{23} \delta_{11}) \\
&\quad + \bar{A}_{2323} \bar{D}_{23} (\delta_{23} \delta_{31} + \delta_{33} \delta_{21}) + \bar{A}_{3131} \bar{D}_{31} (\delta_{33} \delta_{11} + \delta_{13} \delta_{31})) \\
\lambda_1 \bar{W}_{n31} - \lambda_3 \bar{W}_{n31} &= \lambda_3 \bar{W}_{31} - \lambda_3 \bar{W}_{31} + \xi \lambda_1 \bar{D}_{31} + \xi \lambda_3 \bar{D}_{31} - 4\xi \bar{A}_{3131} \bar{D}_{31} \\
(\lambda_1 - \lambda_3) \bar{W}_{n31} &= (\lambda_1 - \lambda_3) \bar{W}_{31} + \xi (\lambda_1 + \lambda_3 - 4\bar{A}_{3131}) \bar{D}_{31} \\
\bar{W}_{n31} &= \bar{W}_{31} + \xi \frac{\lambda_1 + \lambda_3 - 4\bar{A}_{3131}}{\lambda_1 - \lambda_3} \bar{D}_{31}
\end{aligned}$$

Herewith, (5.9) becomes

$$\begin{aligned}
\mathbf{W}_n &= \left(\bar{W}_{12} + \xi \frac{\lambda_2 + \lambda_1 - 4\bar{A}_{1212}}{\lambda_2 - \lambda_1} \bar{D}_{12} \right) (\mathbf{e}_1 \mathbf{e}_2 - \mathbf{e}_2 \mathbf{e}_1) \\
&\quad + \left(\bar{W}_{n23} + \xi \frac{\lambda_3 + \lambda_2 - 4\bar{A}_{2323}}{\lambda_3 - \lambda_2} \bar{D}_{23} \right) (\mathbf{e}_2 \mathbf{e}_3 - \mathbf{e}_3 \mathbf{e}_2) \\
&\quad + \left(\bar{W}_{n31} + \xi \frac{\lambda_1 + \lambda_3 - 4\bar{A}_{3131}}{\lambda_1 - \lambda_3} \bar{D}_{31} \right) (\mathbf{e}_3 \mathbf{e}_1 - \mathbf{e}_1 \mathbf{e}_3).
\end{aligned}$$

Using an expansion similar to (5.9) for \mathbf{W} and

$$\begin{aligned}
\mathbf{D} : \mathbf{e}_i \mathbf{e}_j &= \left(\sum_{k,l} \bar{D}_{kl} \mathbf{e}_k \mathbf{e}_l \right) : \mathbf{e}_i \mathbf{e}_j \\
&= \sum_{k,l} \bar{D}_{kl} \delta_{ik} \delta_{jl} \\
&= \bar{D}_{ij}
\end{aligned}$$

we get

$$\begin{aligned}
\mathbf{W}_n &= \mathbf{W} + \xi \frac{\lambda_2 + \lambda_1 - 4\bar{A}_{1212}}{\lambda_2 - \lambda_1} (\mathbf{D} : \mathbf{e}_1 \mathbf{e}_2) (\mathbf{e}_1 \mathbf{e}_2 - \mathbf{e}_2 \mathbf{e}_1) \\
&\quad + \xi \frac{\lambda_3 + \lambda_2 - 4\bar{A}_{2323}}{\lambda_3 - \lambda_2} (\mathbf{D} : \mathbf{e}_2 \mathbf{e}_3) (\mathbf{e}_2 \mathbf{e}_3 - \mathbf{e}_3 \mathbf{e}_2) \\
&\quad + \xi \frac{\lambda_1 + \lambda_3 - 4\bar{A}_{3131}}{\lambda_1 - \lambda_3} (\mathbf{D} : \mathbf{e}_3 \mathbf{e}_1) (\mathbf{e}_3 \mathbf{e}_1 - \mathbf{e}_1 \mathbf{e}_3)
\end{aligned}$$

which leads to the rate equation for the eigenvectors (5.6), denoted as

$$\begin{aligned}
\dot{\mathbf{e}}_i &= \mathbf{W}_n \cdot \mathbf{e}_i \\
&= \left(\mathbf{W} + \xi \frac{\lambda_2 + \lambda_1 - 4\bar{A}_{1212}}{\lambda_2 - \lambda_1} (\mathbf{D} : \mathbf{e}_1 \mathbf{e}_2) (\mathbf{e}_1 \mathbf{e}_2 - \mathbf{e}_2 \mathbf{e}_1) \right. \\
&\quad + \xi \frac{\lambda_3 + \lambda_2 - 4\bar{A}_{2323}}{\lambda_3 - \lambda_2} (\mathbf{D} : \mathbf{e}_2 \mathbf{e}_3) (\mathbf{e}_2 \mathbf{e}_3 - \mathbf{e}_3 \mathbf{e}_2) \\
&\quad \left. + \xi \frac{\lambda_1 + \lambda_3 - 4\bar{A}_{3131}}{\lambda_1 - \lambda_3} (\mathbf{D} : \mathbf{e}_3 \mathbf{e}_1) (\mathbf{e}_3 \mathbf{e}_1 - \mathbf{e}_1 \mathbf{e}_3) \right) \cdot \mathbf{e}_i \\
&= \mathbf{W} \cdot \mathbf{e}_i + \xi \frac{\lambda_2 + \lambda_1 - 4\bar{A}_{1212}}{\lambda_2 - \lambda_1} (\mathbf{D} : \mathbf{e}_1 \mathbf{e}_2) (\delta_{2i} \mathbf{e}_1 - \delta_{1i} \mathbf{e}_2) \\
&\quad + \xi \frac{\lambda_3 + \lambda_2 - 4\bar{A}_{2323}}{\lambda_3 - \lambda_2} (\mathbf{D} : \mathbf{e}_2 \mathbf{e}_3) (\delta_{3i} \mathbf{e}_2 - \delta_{2i} \mathbf{e}_3) \\
&\quad + \xi \frac{\lambda_1 + \lambda_3 - 4\bar{A}_{3131}}{\lambda_1 - \lambda_3} (\mathbf{D} : \mathbf{e}_3 \mathbf{e}_1) (\delta_{1i} \mathbf{e}_3 - \delta_{3i} \mathbf{e}_1). \tag{5.10}
\end{aligned}$$

□

Note that for any choice i , always one of the last three terms will vanish.

5.2.3 Equivalence

The system (5.2), (5.10)

$$\begin{aligned}
\dot{\lambda}_i &= 2\xi (\lambda_i \mathbf{D} : \mathbf{e}_i \mathbf{e}_i - \mathbf{e}_i \mathbf{e}_i : \mathbb{A} : \mathbf{D}) + 2C_I \dot{\gamma} (1 - 3\lambda_i) \\
\dot{\mathbf{e}}_i &= \mathbf{W} \cdot \mathbf{e}_i + \xi \frac{\lambda_2 + \lambda_1 - 4\bar{A}_{1212}}{\lambda_2 - \lambda_1} (\mathbf{D} : \mathbf{e}_1 \mathbf{e}_2) (\delta_{2i} \mathbf{e}_1 - \delta_{1i} \mathbf{e}_2) \\
&\quad + \xi \frac{\lambda_3 + \lambda_2 - 4\bar{A}_{2323}}{\lambda_3 - \lambda_2} (\mathbf{D} : \mathbf{e}_2 \mathbf{e}_3) (\delta_{3i} \mathbf{e}_2 - \delta_{2i} \mathbf{e}_3) \\
&\quad + \xi \frac{\lambda_1 + \lambda_3 - 4\bar{A}_{3131}}{\lambda_1 - \lambda_3} (\mathbf{D} : \mathbf{e}_3 \mathbf{e}_1) (\delta_{1i} \mathbf{e}_3 - \delta_{3i} \mathbf{e}_1)
\end{aligned}$$

is equivalent to (4.8)

$$\dot{\mathbf{A}} = \mathbf{W} \cdot \mathbf{A} - \mathbf{A} \cdot \mathbf{W} + \xi (\mathbf{D} \cdot \mathbf{A} + \mathbf{A} \cdot \mathbf{D} - 2\mathbb{A} : \mathbf{D}) + 2C_I \dot{\gamma} (\mathbf{I} - 3\mathbf{A}).$$

The eigenvectors affect the rates of change of the eigenvalues, as they appear in the first two terms of $\dot{\lambda}_i$. Similarly, the eigenvalues affect the rates of change of the eigenvectors. The fourth order tensor \mathbb{A} affects both the eigenvalues and the eigenvectors. In contrast, the rotary diffusion term appears only in the eigenvalue equation, because this term is isotropic.

5.3 Modification and reassembly

In this section we conclude the Wang-O'Gara-Tucker model. The concept is to modify the growth rates of the eigenvalues of the orientation tensor by an empirical factor $0 < \kappa \leq 1$, but to leave the rate expressions for the eigenvectors unchanged. The new model is called the reduced strain closure (RSC) model, for reasons that will become apparent. In cases where both the standard and RSC model are considered, superscripts RSC and std are used for clarity.

The essence of the RSC model is

$$\dot{\lambda}_i^{\text{RSC}} = \kappa \dot{\lambda}_i^{\text{std}} \quad \wedge \quad \dot{\mathbf{e}}_i^{\text{RSC}} = \dot{\mathbf{e}}_i^{\text{std}}.$$

Indeed, the growth rates of the eigenvalues are multiplied with a factor $\kappa < 1$ and the eigenvectors remain unchanged. Note that $\dot{\lambda}_i^{\text{RSC}} = 0 \Leftrightarrow \dot{\lambda}_i^{\text{std}} = 0$ so that the steady state values for the eigenvalues, in case there are any, remain the same. It follows that the steady state values of the eigenvectors, which depend on the steady state values of the eigenvalues, also remain the same.

To obtain a rate equation for tensor \mathbf{A} , we write

$$\dot{\mathbf{A}}^{\text{RSC}} = \sum_i \dot{\lambda}_i^{\text{RSC}} \mathbf{e}_i^{\text{RSC}} \mathbf{e}_i^{\text{RSC}} = \sum_i \kappa \dot{\lambda}_i^{\text{std}} \mathbf{e}_i^{\text{std}} \mathbf{e}_i^{\text{std}} = \dot{\mathbf{A}}^{\text{std}} - (1 - \kappa) \sum_i \dot{\lambda}_i^{\text{std}} \mathbf{e}_i^{\text{std}} \mathbf{e}_i^{\text{std}}. \tag{5.11}$$

The last term can be rewritten using (5.2)

$$\begin{aligned}\sum_i \dot{\lambda}_i \mathbf{e}_i \mathbf{e}_i &= \sum_i (2\xi (\lambda_i \mathbf{D} : \mathbf{e}_i \mathbf{e}_i - \mathbf{e}_i \mathbf{e}_i : \mathbb{A} : \mathbf{D}) + 2C_I \dot{\gamma} (1 - 3\lambda_i)) \mathbf{e}_i \mathbf{e}_i \\ &= 2\xi \sum_i [\lambda_i \mathbf{D} : \mathbf{e}_i \mathbf{e}_i \mathbf{e}_i \mathbf{e}_i - \mathbf{e}_i \mathbf{e}_i : \mathbb{A} : \mathbf{D} \mathbf{e}_i \mathbf{e}_i] + 2C_I \dot{\gamma} \sum_i [\mathbf{e}_i \mathbf{e}_i - 3\lambda_i \mathbf{e}_i \mathbf{e}_i].\end{aligned}$$

Introducing, for the sake of notation,

$$\mathbb{L} = \sum_i \lambda_i \mathbf{e}_i \mathbf{e}_i \mathbf{e}_i \mathbf{e}_i \quad \wedge \quad \mathbb{M} = \sum_i \mathbf{e}_i \mathbf{e}_i \mathbf{e}_i \mathbf{e}_i$$

and recalling

$$\mathbf{I} = \sum_i \mathbf{e}_i \mathbf{e}_i$$

we can write

$$\sum_i \dot{\lambda}_i \mathbf{e}_i \mathbf{e}_i = 2\xi (\mathbb{L} - \mathbb{M} : \mathbb{A}) : \mathbf{D} + 2C_I \dot{\gamma} (\mathbf{I} - 3\mathbf{A}). \quad (5.12)$$

Combining (5.11), (5.12) and (4.8) gives

$$\begin{aligned}\dot{\mathbf{A}}^{\text{RSC}} &= \mathbf{W} \cdot \mathbf{A} - \mathbf{A} \cdot \mathbf{W} + \xi (\mathbf{D} \cdot \mathbf{A} + \mathbf{A} \cdot \mathbf{D} - 2\mathbb{A} : \mathbf{D}) + 2C_I \dot{\gamma} (\mathbf{I} - 3\mathbf{A}) \\ &\quad - (1 - \kappa) (2\xi (\mathbb{L} - \mathbb{M} : \mathbb{A}) : \mathbf{D} + 2C_I \dot{\gamma} (\mathbf{I} - 3\mathbf{A})) \\ &= \mathbf{W} \cdot \mathbf{A} - \mathbf{A} \cdot \mathbf{W} + \xi \{ \mathbf{D} \cdot \mathbf{A} + \mathbf{A} \cdot \mathbf{D} - 2[\mathbb{A} + (1 - \kappa)(\mathbb{L} - \mathbb{M} : \mathbb{A})] : \mathbf{D} \} + 2\kappa C_I \dot{\gamma} (\mathbf{I} - 3\mathbf{A})\end{aligned} \quad (5.13)$$

Equation (5.13) is the primary result of [13]. Comparing (4.8) with (5.13) we see two differences. We see that the diffusion term is multiplied with a scalar factor $\kappa < 1$. Herewith, the amount of rotary diffusion decreases, making the inclination to a random orientation state smaller. The other difference is that the closure term \mathbb{A} is replaced with

$$\mathbb{A} + (1 - \kappa)(\mathbb{L} - \mathbb{M} : \mathbb{A}).$$

Herein, the κ serves as a decrease of the elements of \mathbb{A} , inducing a decrease in the effect of the strain term

$$(\mathbb{A} + (1 - \kappa)(\mathbb{L} - \mathbb{M} : \mathbb{A})) : \mathbf{D}$$

on the orientation. Herein lies the origin of the name RSC for the model.

When using a closure approximation for \mathbb{A} , it depends on \mathbf{A} and is thus calculated for every time step and will display slow kinetics that match those of \mathbf{A} .

5.4 Objectivity

Now that we have formulated the RSC model, it is important to check if it is objective. To formulate objectivity, or invariance under change of basis, or frame indifferent, we recall some notions [8].

The description of a physical process is related directly to the choice of an observer, which we denote by O . An arbitrarily chosen observer in three dimensional Euclidean space and in time is equipped to measure

1. relative positions of points in space, with a ruler, and
2. instants of time, with a clock.

An event is noticed by an observer in terms of position, place \mathbf{x} , and time t .

Consider two arbitrary events in the Euclidean space characterized by the pairs (\mathbf{x}_0, t_0) and (\mathbf{x}, t) . We assume that (\mathbf{x}_0, t_0) is 'frozen' as long as the event (\mathbf{x}, t) occurs. An observer records that the pair of points in space is separated by the distance $|\mathbf{x} - \mathbf{x}_0|$, and that the time interval, or lapse, between the events under observation is $t - t_0$. In the following we let the pairs (\mathbf{x}_0, t_0) and (\mathbf{x}, t) map to (\mathbf{x}_0^+, t_0^+) and (\mathbf{x}^+, t^+) so that both the distance $|\mathbf{x} - \mathbf{x}_0|$ and $t - t_0$ are preserved, confer Figure 5.1. A spatial mapping

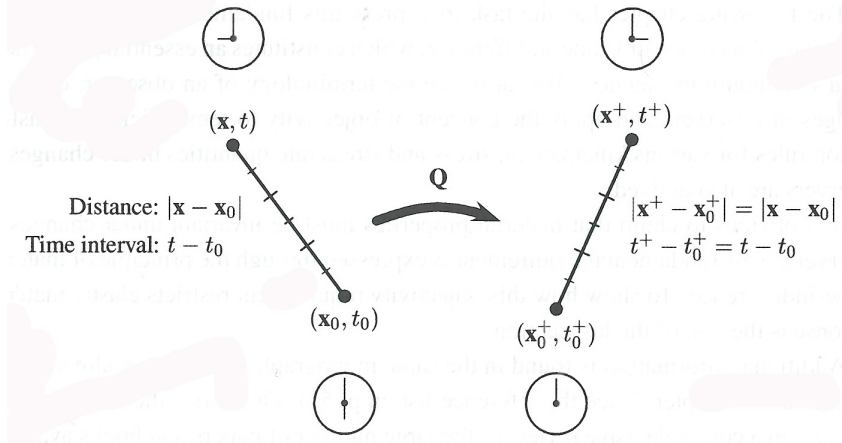


Figure 5.1: map of two points preserving distance and time interval.

that satisfies the requirements above may be represented by the time dependent transformation

$$\mathbf{x}^+ - \mathbf{x}_0^+ = \mathbf{Q}(t) \cdot (\mathbf{x} - \mathbf{x}_0) \quad (5.14)$$

where \mathbf{Q} a proper orthogonal tensor, so $\mathbf{Q}^{-1} = \mathbf{Q}^T$ and $\det(\mathbf{Q}) = 1$. For our convenience, we rewrite (5.14) as

$$\mathbf{x}^+ = \mathbf{c}(t) + \mathbf{Q}(t) \cdot \mathbf{x}, \quad t^+ = t - \alpha \quad (5.15)$$

where

$$\mathbf{c}(t) = \mathbf{x}_0^+ - \mathbf{Q}(t) \cdot \mathbf{x}_0, \quad \alpha = t_0^+ - t_0.$$

Relation (5.15) is often referred to as an Euclidean transformation and it denotes the most general time dependent change of observer from O to O^+ .

In order to describe a physical process in the three dimensional Euclidean space and on the real time axis we assign to each of the observers O and O^+ , a rectangular Cartesian coordinate system, characterized by the bases $\{\mathbf{e}_i\}$ and $\{\mathbf{e}_i^+\}$ respectively. Hence, any points \mathbf{x} and \mathbf{x}^+ may be represented by the position vectors $\mathbf{x} = \sum_i x_i \mathbf{e}_i$ and $\mathbf{x}^+ = \sum_i x_i^+ \mathbf{e}_i^+$. The shift in time scale between the observers remain $t^+ = t + \alpha$. Furthermore, we identify $\mathbf{Q}(t)$ as the relative rotation of the reference frames of the observers, so $\mathbf{e}_i^+ = \mathbf{Q}(t) \cdot \mathbf{e}_i$.

The condition for objectivity for a vector is constructed as follows. Consider two arbitrary points of a continuum body identified by their position vectors \mathbf{x} and \mathbf{y} at time t . The events (\mathbf{x}, t) and (\mathbf{y}, t) are recorded by an observer O with the reference frame $\{\mathbf{e}_i\}$. A second observer O^+ with the reference frame $\{\mathbf{e}_i^+\}$ records the same events at the associated points \mathbf{x}^+ and \mathbf{y}^+ at time t^+ . Then for the vectors $\mathbf{u} = \mathbf{x} - \mathbf{y}$ and $\mathbf{u}^+ = \mathbf{x}^+ - \mathbf{y}^+$ we have the relation

$$\mathbf{u}^+ = \mathbf{x}^+ - \mathbf{y}^+ = (\mathbf{c}(t) + \mathbf{Q}(t) \cdot \mathbf{x}) - (\mathbf{c}(t) + \mathbf{Q}(t) \cdot \mathbf{y}) = \mathbf{Q}(t) \cdot \mathbf{u}.$$

A vector is thus objective is we have

$$\mathbf{u}^+ = \mathbf{Q}(t) \cdot \mathbf{u}. \quad (5.16)$$

For higher order tensors constructed as dyads, the condition extends to

$$(\mathbf{u}_1 \mathbf{u}_2 \dots \mathbf{u}_n)^+ = (\mathbf{Q} \cdot \mathbf{u}_1)(\mathbf{Q} \cdot \mathbf{u}_2) \dots (\mathbf{Q} \cdot \mathbf{u}_n). \quad (5.17)$$

In particular, for a second order tensor $\mathbf{A} = \mathbf{u}_1 \mathbf{u}_2$ we have

$$\mathbf{A}^+ = (\mathbf{u}_1 \mathbf{u}_2)^+ = (\mathbf{Q} \cdot \mathbf{u}_1)(\mathbf{Q} \cdot \mathbf{u}_2) = (\mathbf{Q} \cdot \mathbf{u}_1)(\mathbf{u}_2 \cdot \mathbf{Q}^T) = \mathbf{Q} \cdot \mathbf{A} \cdot \mathbf{Q}^T. \quad (5.18)$$

Using the chain rule, it follows that for a time derivative to be objective we must have

$$\dot{\mathbf{A}}^+ = \overline{\dot{\mathbf{Q}} \cdot \mathbf{A} \cdot \mathbf{Q}^T} = \dot{\mathbf{Q}} \cdot \mathbf{A} \cdot \mathbf{Q}^T + \mathbf{Q} \cdot \dot{\mathbf{A}} \cdot \mathbf{Q}^T + \mathbf{Q} \cdot \mathbf{A} \cdot \overline{\dot{\mathbf{Q}}^T} \quad (5.19)$$

where we used the bar to emphasize whereof the time derivative is taken. This is the condition that must hold for (5.13) to be objective.

Theorem 5.3. *The RSC equation (5.13) is objective.*

Proof. When we move the vorticity terms on the RHS of (5.13) to the LHS, the LHS becomes

$$\overset{\circ}{\mathbf{A}} := \dot{\mathbf{A}}^{\text{RSC}} - \mathbf{W} \cdot \mathbf{A} + \mathbf{A} \cdot \mathbf{W}. \quad (5.20)$$

The latter is known as the Jaumann derivative, or Jaumann-Zaremba rate or co-rotational rate. A rather trivial, but cumbersome proof exists that (5.20) is objective [8]. We will omit such a proof. It remains to prove the objectivity of the remaining terms on the RHS of (5.13)

$$\xi \{ \mathbf{D} \cdot \mathbf{A} + \mathbf{A} \cdot \mathbf{D} - 2[\mathbb{A} + (1 - \kappa)(\mathbb{L} - \mathbb{M} : \mathbb{A})] : \mathbf{D} \} + 2\kappa C_I \dot{\gamma}(\mathbf{I} - 3\mathbf{A}).$$

With the existence of a spectral decomposition of \mathbf{A} proven in Property 4.7, the proof of the objectivity of the tensors \mathbf{A} and \mathbf{D} is rather simple. We can write \mathbf{A} as

$$\mathbf{A} = \sum_i \lambda_i \mathbf{e}_i \mathbf{e}_i.$$

Considering tensor \mathbf{A} from two different observers O and O^+ we have

$$\begin{aligned} \mathbf{A}^+(t^+) &= \sum_i \lambda_i^+(t^+) \mathbf{e}_i^+(t^+) \mathbf{e}_i^+(t^+) \\ &= \sum_i \lambda_i(t) \mathbf{Q}(t) \cdot \mathbf{e}_i(t) \mathbf{Q}(t) \cdot \mathbf{e}_i(t) \\ &= \sum_i \lambda_i(t) \mathbf{Q}(t) \cdot \mathbf{e}_i(t) \mathbf{e}_i(t) \cdot \mathbf{Q}(t) \\ &= \mathbf{Q}(t) \cdot \left(\sum_i \lambda_i(t) \mathbf{e}_i(t) \mathbf{e}_i(t) \right) \cdot \mathbf{Q}(t) \\ &= \mathbf{Q}(t) \cdot \mathbf{A}(t) \cdot \mathbf{Q}(t). \end{aligned}$$

Note that as \mathbf{D} and \mathbf{I} are also symmetric, thus also have a spectral decomposition and are objective.

From the property $\mathbf{Q}^T = \mathbf{Q}^{-1}$ it follows that

$$(\mathbf{D} \cdot \mathbf{A})^+ = \mathbf{D}^+ \cdot \mathbf{A}^+ = \mathbf{Q} \cdot \mathbf{D} \cdot \mathbf{Q}^T \cdot \mathbf{Q} \cdot \mathbf{A} \cdot \mathbf{Q}^T = \mathbf{Q} \cdot \mathbf{D} \cdot \mathbf{Q}^{-1} \cdot \mathbf{Q} \cdot \mathbf{A} \cdot \mathbf{Q}^T = \mathbf{Q} \cdot \mathbf{D} \cdot \mathbf{A} \cdot \mathbf{Q}^T$$

so that the product $\mathbf{D} \cdot \mathbf{A}$ is objective. The proof of the objectivity of $\mathbf{A} \cdot \mathbf{D}$ is similar.

For $\mathbb{A} : \mathbf{D}$ we have

$$\begin{aligned} \mathbb{A}^+ : \mathbf{D}^+ &= \sum_{i,j,k,l} A_{ijkl}^+ \mathbf{f}_i^+ \mathbf{f}_j^+ \mathbf{f}_k^+ \mathbf{f}_l^+ : \sum_{m,n} D_{mn}^+ \mathbf{f}_m^+ \mathbf{f}_n^+ \\ &= \sum_{i,j,k,l} A_{ijkl}^+ D_{lk}^+ \mathbf{f}_i^+ \mathbf{f}_j^+ \\ &= \sum_{i,j,k,l} A_{ijkl} D_{lk} \mathbf{Q} \cdot \mathbf{f}_i \mathbf{Q} \cdot \mathbf{f}_j \\ &= \sum_{i,j,k,l} A_{ijkl} D_{lk} \mathbf{Q} \cdot \mathbf{f}_i \mathbf{f}_j \cdot \mathbf{Q}^T \\ &= \mathbf{Q} \cdot \mathbb{A} : \mathbf{D} \cdot \mathbf{Q}^T. \end{aligned}$$

The former does not only hold for \mathbb{A} double contracted with \mathbf{D} , but for any fourth order tensor double contracted with \mathbf{D} . Thus also for $(\mathbb{L} - \mathbb{M} : \mathbb{A}) : \mathbf{D}$. This concludes the proof. \square

5.5 Equivalent kinetic theory

The RSC model (5.13) is developed at the level of the moment tensor equation. In contrast, most other models are initially developed at the level of kinetic theory. Kinetic theories contain explicit expressions for the fiber motion and provide a Fokker-Planck equation that can be solved for ψ . These solutions are much more expensive to compute than solutions to the moment tensor equation, so moment tensor equations are typically used in the process modeling. However, moment tensor equations always require a closure approximation, while kinetic theories do not. Thus, kinetic theory equations provide important

information for the formation and testing of closure approximations.

It is interesting to ask if there is a kinetic theory that corresponds to the RSC model (5.13). Finding such an extended kinetic theory would give more insight in how the kinetics are slowed down. It appears that the new RSC terms can not be reproduced by an additional term for fiber orientation $\dot{\mathbf{p}}$, nor by an additional rotary diffusion term [13]. Adding an additional flux density \mathbf{q} does the job, as proved in Theorem 5.4. This flux is added to the fluxes due to Jeffery motion and rotary diffusion, so the continuity equation (3.12) is modified to read

$$\dot{\psi} = -\tilde{\nabla} \cdot (\psi \dot{\mathbf{p}} + \mathbf{q}). \quad (5.21)$$

where, again, the \sim emphasizes the presence of the constraint $\|\mathbf{p}\|_2 = 1$.

Because \mathbf{q} is a 'flux of probability' on the unit sphere, three requirements have to be met.

1. The flux vector is always tangent to the surface of the unit sphere, since this is the direction in which fibers 'enter' and 'leave' a infinitesimal surface dS on the unit sphere. Thus, we must have

$$\mathbf{q} \cdot \mathbf{p} = 0.$$

2. If the sign of \mathbf{p} changes, then the sign of \mathbf{q} changes according to

$$\mathbf{q}|_{-\mathbf{p}} = -\mathbf{q}|_{\mathbf{p}}.$$

One can think of this as a vector \mathbf{p} with a vector \mathbf{q} attached to its end on the unit sphere, making a 180° rotation in the plane containing \mathbf{p} , so that both vectors get opposite directions, confer Figure 5.2.

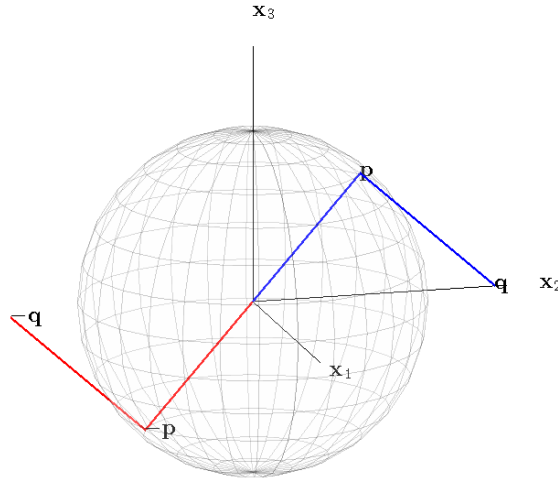


Figure 5.2: change of \mathbf{q} under change of sign of \mathbf{p} .

3. Eigenvectors are determined up to a constant. Normalized eigenvectors or unit eigenvectors are thus determined up to their sign. The flux vector should be invariant under the change of this particular sign, so

$$\mathbf{q}|_{-\mathbf{e}_i} = \mathbf{q}|_{\mathbf{e}_i} \quad \forall i, \mathbf{p}.$$

These three constraints for \mathbf{q} restrict the space from which \mathbf{q} can be chosen. Nevertheless, the flux vector \mathbf{q} is certainly not determined uniquely. A suitable form is

$$\mathbf{q} = \sum_i \beta_i (\mathbf{e}_i \cdot \mathbf{p}) (\mathbf{e}_i - (\mathbf{e}_i \cdot \mathbf{p}) \mathbf{p}), \quad (5.22)$$

where the scalar coefficients β_i are yet to be determined. Note that (5.22) suffices to the three constraints. The proof the latter is trivial. Flux vector \mathbf{q} is, in this case, chosen such that it 'draws' fibers toward, or 'pushes' them away from, the eigenvectors \mathbf{e}_i of \mathbf{A} . This is done with 'strength'

$$\beta_i \mathbf{e}_i \cdot \mathbf{p} = \beta_i \|\mathbf{e}_i\|_2 \|\mathbf{p}\|_2 \cos \theta = \beta_i \cos \theta$$

in the direction

$$\mathbf{e}_i - (\mathbf{e}_i \cdot \mathbf{p})\mathbf{p}$$

which points from vector $(\mathbf{e}_i \cdot \mathbf{p})\mathbf{p}$ to \mathbf{e}_i . Here, θ is the angle between vectors \mathbf{e}_i and \mathbf{p} .

In the following theorem, the coefficients β_i and equivalent kinetic theory are derived.

Theorem 5.4. *The kinetic theory*

$$\begin{aligned} \dot{\psi} &= -\tilde{\nabla} \cdot (\psi \dot{\mathbf{p}} + \mathbf{q}) \\ \dot{\mathbf{p}} &= \mathbf{W} \cdot \mathbf{p} + \xi(\mathbf{D} \cdot \mathbf{p} - \mathbf{D} : \mathbf{p}\mathbf{p}\mathbf{p}) - C_I \dot{\gamma} \tilde{\nabla} \ln \psi \\ \mathbf{q} &= \sum_i \beta_i (\mathbf{e}_i \mathbf{e}_i \cdot \mathbf{p} - \mathbf{e}_i \mathbf{e}_i : \mathbf{p}\mathbf{p}\mathbf{p}) \\ \beta_i &= -\frac{5(1-\kappa)}{4\pi} [\xi(\lambda_i \mathbf{D} : \mathbf{e}_i \mathbf{e}_i - \mathbf{e}_i \mathbf{e}_i : \mathbb{A} : \mathbf{D}) + C_I \dot{\gamma} (1 - 3\lambda_i)] \end{aligned} \quad (5.23)$$

implies the relation

$$\dot{\mathbf{A}}^{RSC} = \mathbf{W} \cdot \mathbf{A} - \mathbf{A} \cdot \mathbf{W} + \xi \{ \mathbf{D} \cdot \mathbf{A} + \mathbf{A} \cdot \mathbf{D} - 2[\mathbb{A} + (1-\kappa)(\mathbb{L} - \mathbb{M} : \mathbb{A})] : \mathbf{D} \} + 2\kappa C_I \dot{\gamma} (\mathbf{I} - 3\mathbf{A}).$$

Proof. We consider (5.21) and take the right tensor product with \mathbf{p} twice and integrate it over the unit sphere

$$\int_S \dot{\psi} \mathbf{p}\mathbf{p} d^2 \mathbf{p} = \int_S -\tilde{\nabla} \cdot (\psi \dot{\mathbf{p}} + \mathbf{q}) \mathbf{p}\mathbf{p} d^2 \mathbf{p}$$

The LHS and first term on the RHS have already been proven to be equivalent with the Folgar-Tucker tensor model (4.8) in Section 4.5. This leaves us to consider only the term containing \mathbf{q} on the RHS.

Because we have (5.11), it follows that

$$\int_S -(\tilde{\nabla} \cdot \mathbf{q}) \mathbf{p}\mathbf{p} d^2 \mathbf{p} = -(1-\kappa) \sum_i \lambda_i^{\text{std}} \mathbf{e}_i^{\text{std}} \mathbf{e}_i^{\text{std}}. \quad (5.24)$$

The LHS can be rewritten as follows. Consider the components

$$\begin{aligned} (\tilde{\nabla} \cdot (\mathbf{q}\mathbf{p}\mathbf{p}))_{ij} &= \sum_k \frac{\tilde{\partial}}{\partial p_k} (q_k p_i p_j) \\ &= \sum_k \left[\frac{\tilde{\partial}}{\partial p_k} (q_k) p_i p_j \right] + \sum_k \left[q_k \frac{\tilde{\partial}}{\partial p_k} (p_i p_j) \right] \\ &= \sum_k \left[\frac{\tilde{\partial}}{\partial p_k} (q_k) p_i p_j \right] + \sum_k [q_k (\delta_{jk} p_i + \delta_{ik} p_j - 2p_i p_j p_k)] \\ &= \sum_k \left[\frac{\tilde{\partial}}{\partial p_k} (q_k) p_i p_j \right] + q_j p_i + q_i p_j - 2p_i p_j \sum_k q_k p_k \\ &= \sum_k \left[\frac{\tilde{\partial}}{\partial p_k} (q_k) p_i p_j \right] + q_j p_i + q_i p_j \end{aligned}$$

where we used, in order, the product rule, Property 2.1 and $\mathbf{q} \cdot \mathbf{p} = 0$. This results in

$$\begin{aligned} \tilde{\nabla} \cdot (\mathbf{q}\mathbf{p}\mathbf{p}) &= \tilde{\nabla} \cdot (\mathbf{q}) \mathbf{p}\mathbf{p} + \mathbf{p}\mathbf{q} + \mathbf{q}\mathbf{p} \\ -\tilde{\nabla} \cdot (\mathbf{q}) \mathbf{p}\mathbf{p} &= -\tilde{\nabla} \cdot (\mathbf{q}\mathbf{p}\mathbf{p}) + \mathbf{q}\mathbf{p} + \mathbf{p}\mathbf{q} \\ \int_S -\tilde{\nabla} \cdot (\mathbf{q}) \mathbf{p}\mathbf{p} d^2 \mathbf{p} &= -\int_S \tilde{\nabla} \cdot (\mathbf{q}\mathbf{p}\mathbf{p}) d^2 \mathbf{p} + \int_S (\mathbf{q}\mathbf{p} + \mathbf{p}\mathbf{q}) d^2 \mathbf{p} \\ -(1-\kappa) \sum_i \lambda_i^{\text{std}} \mathbf{e}_i^{\text{std}} \mathbf{e}_i^{\text{std}} &= \int_S (\mathbf{q}\mathbf{p} + \mathbf{p}\mathbf{q}) d^2 \mathbf{p}. \end{aligned}$$

In the third step we used the closedness of S .

Filling in (5.22) in the RHS of the latter integral gives

$$\int_S \left[\left(\sum_i \beta_i (\mathbf{e}_i \mathbf{e}_i \cdot \mathbf{p} - \mathbf{e}_i \mathbf{e}_i : \mathbf{p} \mathbf{p} \mathbf{p}) \right) \mathbf{p} + \mathbf{p} \left(\sum_i \beta_i (\mathbf{e}_i \mathbf{e}_i \cdot \mathbf{p} - \mathbf{e}_i \mathbf{e}_i : \mathbf{p} \mathbf{p} \mathbf{p}) \right) \right] d^2 \mathbf{p} = \sum_i \beta_i \int_S [\mathbf{e}_i \mathbf{e}_i \cdot \mathbf{p} \mathbf{p} - \mathbf{e}_i \mathbf{e}_i : \mathbf{p} \mathbf{p} \mathbf{p} \mathbf{p} + \mathbf{p} \mathbf{e}_i \mathbf{e}_i \cdot \mathbf{p} - \mathbf{p} \mathbf{e}_i \mathbf{e}_i : \mathbf{p} \mathbf{p} \mathbf{p}] d^2 \mathbf{p}.$$

Note that

$$\mathbf{p} \mathbf{e}_i \mathbf{e}_i \cdot \mathbf{p} = \mathbf{p} \mathbf{e}_i (\mathbf{e}_i \cdot \mathbf{p}) = \mathbf{p} (\mathbf{e}_i \cdot \mathbf{p}) \mathbf{e}_i = \mathbf{p} (\mathbf{p} \cdot \mathbf{e}_i) \mathbf{e}_i = \mathbf{p} \mathbf{p} \cdot \mathbf{e}_i \mathbf{e}_i$$

and

$$\mathbf{p} \mathbf{e}_i \mathbf{e}_i : \mathbf{p} \mathbf{p} \mathbf{p} = \mathbf{p} (\mathbf{e}_i \mathbf{e}_i : \mathbf{p} \mathbf{p}) \mathbf{p} = (\mathbf{e}_i \mathbf{e}_i : \mathbf{p} \mathbf{p}) \mathbf{p} \mathbf{p} = \mathbf{e}_i \mathbf{e}_i : \mathbf{p} \mathbf{p} \mathbf{p} \mathbf{p}$$

so that the integral becomes

$$\sum_i \beta_i \int_S [\mathbf{e}_i \mathbf{e}_i \cdot \mathbf{p} \mathbf{p} + \mathbf{p} \mathbf{p} \cdot \mathbf{e}_i \mathbf{e}_i - 2 \mathbf{e}_i \mathbf{e}_i : \mathbf{p} \mathbf{p} \mathbf{p} \mathbf{p}] d^2 \mathbf{p}. \quad (5.25)$$

The eigenvectors \mathbf{e}_i are independent of S . Herewith, the eigenvectors can be taken out of the integrals and we get the integrals

$$\int_S \mathbf{p} \mathbf{p} d^2 \mathbf{p} \quad \wedge \quad \int_S \mathbf{p} \mathbf{p} \mathbf{p} \mathbf{p} d^2 \mathbf{p}.$$

Using generalized coordinates, the former is calculated to take the value $\frac{4\pi}{3} \mathbf{I}$. The latter integral is harder to solve. We note that

$$\sum_i \mathbf{e}_i \mathbf{e}_i : \int_S \mathbf{p} \mathbf{p} \mathbf{p} \mathbf{p} d^2 \mathbf{p} = \int_S \sum_i (\mathbf{e}_i \cdot \mathbf{p})^2 \mathbf{p} \mathbf{p} d^2 \mathbf{p} = \int_S \mathbf{p} \mathbf{p} d^2 \mathbf{p} = \frac{4\pi}{3} \mathbf{I}.$$

Say we assume that the components have a part dependent of \mathbf{e}_i and a part independent of \mathbf{e}_i

$$\mathbf{e}_i \mathbf{e}_i : \int_S \mathbf{p} \mathbf{p} \mathbf{p} \mathbf{p} d^2 \mathbf{p} = \alpha \mathbf{I} + \beta \mathbf{e}_i \mathbf{e}_i. \quad (5.26)$$

Thus, to solve the fourth order integral, we need two equations for the two unknowns α and β . The first equation is found by recalling the sum over i

$$\begin{aligned} \sum_i [\alpha \mathbf{I} + \beta \mathbf{e}_i \mathbf{e}_i] &= \sum_i \mathbf{e}_i \mathbf{e}_i : \int_S \mathbf{p} \mathbf{p} \mathbf{p} \mathbf{p} d^2 \mathbf{p} \\ \sum_i [\alpha \mathbf{I} + \beta \mathbf{e}_i \mathbf{e}_i] &= \frac{4\pi}{3} \mathbf{I} \\ 3\alpha \mathbf{I} + \beta \sum_i \mathbf{e}_i \mathbf{e}_i &= \frac{4\pi}{3} \mathbf{I} \\ (3\alpha + \beta) \mathbf{I} &= \frac{4\pi}{3} \mathbf{I} \\ 3\alpha + \beta &= \frac{4\pi}{3}. \end{aligned}$$

The second equation stems from taking the left or right double contraction with $\mathbf{e}_i \mathbf{e}_i$,

$$\begin{aligned} \mathbf{e}_i \mathbf{e}_i : \left(\mathbf{e}_i \mathbf{e}_i : \int_S \mathbf{p} \mathbf{p} \mathbf{p} \mathbf{p} d^2 \mathbf{p} \right) &= \mathbf{e}_i \mathbf{e}_i : (\alpha \mathbf{I} + \beta \mathbf{e}_i \mathbf{e}_i) \\ \int_S \mathbf{e}_i \mathbf{e}_i : (\mathbf{e}_i \mathbf{e}_i : \mathbf{p} \mathbf{p} \mathbf{p} \mathbf{p}) d^2 \mathbf{p} &= \alpha \mathbf{e}_i \mathbf{e}_i : \mathbf{I} + \beta \mathbf{e}_i \mathbf{e}_i : \mathbf{e}_i \mathbf{e}_i \\ \int_S (\mathbf{e}_i \cdot \mathbf{p})^4 d^2 \mathbf{p} &= \alpha \mathbf{e}_i \mathbf{e}_i : \left(\sum_j \mathbf{e}_j \mathbf{e}_j \right) + \beta \\ \int_S p_i^4 d^2 \mathbf{p} &= \alpha + \beta \quad \forall i \\ \int_{\phi=0}^{2\pi} \int_{\theta=0}^{\pi} \cos^4(\theta) \sin \theta d\theta d\phi &= \alpha + \beta \\ 2\pi \left[-\frac{1}{5} \cos^5 \theta \right]_{\theta=0}^{\pi} &= \alpha + \beta \\ \frac{4\pi}{5} &= \alpha + \beta. \end{aligned}$$

where we chose $p_i = p_3 = \cos \theta$ and recall the Jacobian for spherical coordinates $J = \sin \theta$. This results in

$$(\alpha, \beta) = \left(\frac{4\pi}{15}, \frac{8\pi}{15} \right).$$

Apparently assumption (5.26) was sufficient to determine the unique integral

$$\mathbf{e}_i \mathbf{e}_i : \int_S \mathbf{p} \mathbf{p} \mathbf{p} \mathbf{p} d^2 \mathbf{p} = \frac{4\pi}{15} \mathbf{I} + \frac{8\pi}{15} \mathbf{e}_i \mathbf{e}_i$$

making (5.25)

$$\sum_i \beta_i \mathbf{e}_i \mathbf{e}_i \cdot \frac{4\pi}{3} \mathbf{I} + \frac{4\pi}{3} \mathbf{I} \cdot \mathbf{e}_i \mathbf{e}_i - 2 \left(\frac{4\pi}{15} \mathbf{I} + \frac{8\pi}{15} \mathbf{e}_i \mathbf{e}_i \right).$$

Noting that

$$\mathbf{e}_i \mathbf{e}_i \cdot \mathbf{I} = \mathbf{e}_i \mathbf{e}_i \cdot \sum_j \mathbf{e}_j \mathbf{e}_j = \mathbf{e}_i \sum_j \delta_{ij} \mathbf{e}_j = \mathbf{e}_i \mathbf{e}_i \quad \wedge \quad \mathbf{I} \cdot \mathbf{e}_i \mathbf{e}_i = \left(\sum_j \mathbf{e}_j \mathbf{e}_j \right) \cdot \mathbf{e}_i \mathbf{e}_i = \sum_j \mathbf{e}_j \delta_{ij} \mathbf{e}_i = \mathbf{e}_i \mathbf{e}_i$$

we get

$$\sum_i \beta_i \frac{8\pi}{15} (3\mathbf{e}_i \mathbf{e}_i - \mathbf{I}).$$

Getting back to (5.24), we get

$$\begin{aligned} \sum_i \beta_i \frac{8\pi}{15} (3\mathbf{e}_i \mathbf{e}_i - \mathbf{I}) &= -(1 - \kappa) \sum_i \dot{\lambda}_i^{\text{std}} \mathbf{e}_i \mathbf{e}_i \\ \sum_i \left(\frac{8\pi}{5} \beta_i + (1 - \kappa) \dot{\lambda}_i^{\text{std}} \right) \mathbf{e}_i \mathbf{e}_i - \frac{8\pi}{15} \beta_i \mathbf{I} &= \mathbf{O} \\ \left(\sum_i \left(\frac{8\pi}{5} \beta_i + (1 - \kappa) \dot{\lambda}_i^{\text{std}} \right) \mathbf{e}_i \mathbf{e}_i - \frac{8\pi}{15} \beta_i \mathbf{I} \right) : \mathbf{e}_j \mathbf{e}_j &= \mathbf{O} \\ \frac{8\pi}{5} \beta_j + (1 - \kappa) \dot{\lambda}_j^{\text{std}} - \frac{8\pi}{15} \sum_i \beta_i \sum_k \mathbf{e}_k \mathbf{e}_k : \mathbf{e}_j \mathbf{e}_j &= \mathbf{O} \\ \frac{8\pi}{5} \beta_j + (1 - \kappa) \dot{\lambda}_j^{\text{std}} - \frac{8\pi}{15} \sum_i \beta_i &= \mathbf{O} \end{aligned}$$

leading to

$$\beta_j = \frac{5}{8\pi} (\kappa - 1) \dot{\lambda}_j^{\text{std}} + \frac{1}{15} \sum_i \beta_i \tag{5.27}$$

Summing over j we get

$$\begin{aligned}
\sum_j \beta_j &= \frac{5}{8\pi}(\kappa - 1) \sum_j \dot{\lambda}_j^{\text{std}} + \frac{3}{15} \sum_i \beta_i \\
\left(1 - \frac{3}{15}\right) \sum_j \beta_j &= \frac{5}{8\pi}(\kappa - 1) \sum_j \dot{\lambda}_j^{\text{std}} \\
\sum_j \beta_j &= \frac{25}{32\pi}(\kappa - 1) \left(\sum_j \dot{\lambda}_j^{\text{std}} \right) \\
\sum_j \beta_j &= 0
\end{aligned}$$

where we used Property 4.8 for the sum of eigenvalues of \mathbf{A} . Equation (5.27) becomes

$$\begin{aligned}
\beta_j &= \frac{5}{8\pi}(\kappa - 1) \dot{\lambda}_j^{\text{std}} + \frac{1}{15} \sum_i \beta_i \\
&= \frac{5}{8\pi}(\kappa - 1) \dot{\lambda}_j^{\text{std}} \\
&= \frac{5}{8\pi}(\kappa - 1) [2\xi(\lambda_j \mathbf{D} : \mathbf{e}_j \mathbf{e}_j - \mathbf{e}_j \mathbf{e}_j : \mathbb{A} : \mathbf{D}) + 2C_I \dot{\gamma}(1 - 3\lambda_j)] \\
&= -\frac{5(1 - \kappa)}{4\pi} [\xi(\lambda_j \mathbf{D} : \mathbf{e}_j \mathbf{e}_j - \mathbf{e}_j \mathbf{e}_j : \mathbb{A} : \mathbf{D}) + C_I \dot{\gamma}(1 - 3\lambda_j)] \tag{5.28}
\end{aligned}$$

which concludes the proof of the equivalence of the kinetic theory and moment tensor form. \square

Interpreting this physically, each β_i denotes the rate at which fibers are attracted to, or repelled from, the corresponding eigenvector \mathbf{e}_i . The $\lambda_i \mathbf{D} : \mathbf{e}_i \mathbf{e}_i$ term on the RHS of (5.28) shows that fibers are being repelled from eigenvectors along which the stretching rate $\mathbf{D} : \mathbf{e}_i \mathbf{e}_i$ is positive, and attracted to eigenvectors along which the stretching rate is negative. This slows the growth rates of the eigenvalues by partially counteracting the Jefferey term, which rotates fibers towards directions of positive stretching. One can regard this as the main kinetic effect of the RSC model, with the $\mathbb{A} : \mathbf{D}$ term serving to preserve $\text{tr}(\mathbf{A}) = 1$. The effect of the rotary diffusion term is also partially counteracted, by the term containing C_I .

Chapter 6

Closure approximations

6.1 Introduction

At this point, attempting to solve the derived RSC model is futile. The cause hereof is the fact that the RSC model is, at least not yet, closed. The fourth order tensor \mathbb{A} is the origin of this closure problem. In this chapter, this closure problem is considered and solved by the use of so-called closure approximations or closure in short. The main focus lies on the, in the literature dominating, orthotropic closure approximations. The fundamentals behind the closures are discussed.

6.2 The closure problem

To solve the rate equation for \mathbf{A} (5.13)

$$\dot{\mathbf{A}} = \mathbf{W} \cdot \mathbf{A} - \mathbf{A} \cdot \mathbf{W} + \xi \{ \mathbf{D} \cdot \mathbf{A} + \mathbf{A} \cdot \mathbf{D} - 2[\mathbb{A} + (1 - \kappa)(\mathbb{L} - \mathbb{M} : \mathbb{A})] : \mathbf{D} \} + 2\kappa C_I \dot{\gamma} (\mathbf{I} - 3\mathbf{A})$$

we first need to determine \mathbb{A} as defined by Definition 4.2

$$\mathbb{A} = \int_S \psi \mathbf{p} \mathbf{p} \mathbf{p} \mathbf{p} d^2 \mathbf{p}.$$

Deriving a rate equation for \mathbb{A} in an attempt to solve \mathbb{A} would lead to the introduction of a sixth order tensor. Deriving a rate equation for the sixth order tensor would lead to the introduction of an eight order tensor. This sequence goes to infinity and thus, the equation can not be closed by such an approach. This is called the closure problem.

The sequence of orientation tensors essentially represents the coefficients in a series expansion of ψ in terms of Legendre polynomials [15, 10]. Thus \mathbf{A} and \mathbb{A} contain only partial information about ψ . An attempt to reconstruct the missing information comes in the form of a closure approximation, or closure in short. In our case, we make an attempt to reconstruct the missing information with \mathbf{A} . In other words, we approximate \mathbb{A} in terms of \mathbf{A} .

A variety of forms has been proposed to approximate \mathbb{A} in terms of \mathbf{A} . The majority works well only for specific flows but not for all flows. Exceptions are the class of orthotropic and natural closures. Our focus will be on the former.

6.3 Quadratic closure

For the sake of simplicity, we start with the treatment of the quadratic closure (QC). It was introduced by E.J. Hinch and L.G. Leal in 1976. It is formulated as

$$\mathbb{A} = \mathbf{A} \mathbf{A}. \tag{6.1}$$

No physical or mathematical arguments have been used in its construction. Nonetheless, it results in an approximation of \mathbf{A} that is able to follow the tendency of the real \mathbf{A} . In addition, we have for an alternative observer O^+

$$\begin{aligned} \mathbf{A}^+ \mathbf{A}^+ &= \left(\sum_i \lambda_i^+ \mathbf{e}_i^+ \mathbf{e}_i^+ \right) \left(\sum_j \lambda_j^+ \mathbf{e}_j^+ \mathbf{e}_j^+ \right) \\ &= \sum_{i,j} \lambda_i^+ \lambda_j^+ \mathbf{e}_i^+ \mathbf{e}_i^+ \mathbf{e}_j^+ \mathbf{e}_j^+ \\ &= \sum_{i,j} \lambda_i \lambda_j \mathbf{Q} \cdot \mathbf{e}_i \mathbf{Q} \cdot \mathbf{e}_i \mathbf{Q} \cdot \mathbf{e}_j \mathbf{Q} \cdot \mathbf{e}_j, \end{aligned}$$

which, because of the distributive property of the tensor product, can be written in the form (5.17) and is thus objective.

The quadratic closure is easy to implement, computed efficiently and thus provides a good check for programs.

6.4 Orthotropic closures

6.4.1 Orthotropy

With approximating \mathbb{A} in terms of \mathbf{A} , we are looking for a relation

$$\exists \mathbb{F} : \mathbb{A} = \mathbb{F}(\mathbf{A}).$$

A valid closure should be objective, which requires \mathbb{F} to take all of its directional information from \mathbf{A} . To explain the name orthotropic closure we introduce the definition of orthotropy.

Definition 6.1. *Orthotropy is a geometric property specifying the state of having three orthogonal symmetry axes or alternately three orthogonal planes of symmetry.*

Recalling Property 4.5, tensor \mathbf{A} has three orthogonal eigenvectors. As it is required that \mathbb{F} takes all of its directional information from \mathbf{A} , \mathbb{F} must have the same principal axes as \mathbf{A} . The principal axes are in this case orthogonal and thus \mathbb{F} has three orthogonal symmetry axes. Hence the name orthotropic closure.

6.4.2 Reduction of degrees of freedom

For determining \mathbb{F} , we are interested in how many degrees of freedom (DOF) we have to describe. Tensor $\mathbb{A} \in \mathbb{R}^{3 \times 3 \times 3 \times 3}$ and thus has $3^4 = 81$ DOFs. Recalling Definition 4.2, the components of \mathbb{A} are

$$A_{ijkl} = \int_S \psi p_i p_j p_k p_l d^2 \mathbf{p}.$$

Due to the commutivity of scalars, \mathbb{A} has $4! = 24$ symmetries. The sequence $ijkl$ can thus be ordered in twentyfour ways. These symmetries reduce the #DOF. Say we first consider the two symmetries

$$A_{ijkl} = A_{jikl} = A_{ijlk}.$$

Considering the pairs (i, j) and (k, l) that are subjected to swapping, there are for each pair six unique combinations and thus $6 \cdot 6 = 36$ for \mathbb{A} . Using the Voigt index notation conform Table 2.1 we replace

$$A_{ijkl} = \mathbf{A}_{mn}.$$

When we denote \mathbb{A} with respect to the principal axes, many elements are equal to zero

$$\bar{\mathbf{A}} = \begin{bmatrix} \bar{\mathbf{A}}_{11} & \bar{\mathbf{A}}_{12} & \bar{\mathbf{A}}_{13} & 0 & 0 & 0 \\ \bar{\mathbf{A}}_{21} & \bar{\mathbf{A}}_{22} & \bar{\mathbf{A}}_{23} & 0 & 0 & 0 \\ \bar{\mathbf{A}}_{31} & \bar{\mathbf{A}}_{32} & \bar{\mathbf{A}}_{33} & 0 & 0 & 0 \\ 0 & 0 & 0 & \bar{\mathbf{A}}_{44} & 0 & 0 \\ 0 & 0 & 0 & 0 & \bar{\mathbf{A}}_{55} & 0 \\ 0 & 0 & 0 & 0 & 0 & \bar{\mathbf{A}}_{66} \end{bmatrix} \quad (6.2)$$

where the $\bar{}$ emphasizes the principal basis. This leaves us with twelve DOFs. Recalling the symmetry $A_{ijkl} = A_{klij}$ it follows that $\mathbf{A}_{mn} = \mathbf{A}_{nm}$ which gives the upper triangular part of (6.2) including the diagonal and thus nine DOFs. The symmetries

$$A_{ijkl} = A_{kjil} = A_{ljki} = A_{ikjl} = A_{ilkj}$$

give us

$$\mathbf{A}_{12} = \mathbf{A}_{66} \quad \wedge \quad \mathbf{A}_{23} = \mathbf{A}_{44} \quad \wedge \quad \mathbf{A}_{13} = \mathbf{A}_{55}$$

reducing the #DOF to six. Furthermore

$$\sum_k A_{ijkk} = \sum_k \int_S \psi p_i p_j p_k p_k d^2 \mathbf{p} = \int_S \psi p_i p_j \sum_k p_k^2 d^2 \mathbf{p} = \int_S \psi p_i p_j d^2 \mathbf{p} = A_{ij}$$

so

$$\sum_k A_{11kk} = A_{1111} + A_{1122} + A_{1133} = A_{11} + A_{12} + A_{13} = A_{11} + \mathbf{A}_{66} + \mathbf{A}_{55} = A_{11}$$

$$\sum_k A_{22kk} = A_{2211} + A_{2222} + A_{2233} = A_{21} + A_{22} + A_{23} = \mathbf{A}_{66} + A_{22} + \mathbf{A}_{44} = A_{22}$$

$$\sum_k A_{33kk} = A_{3311} + A_{3322} + A_{3333} = A_{31} + A_{32} + A_{33} = \mathbf{A}_{55} + \mathbf{A}_{44} + \mathbf{A}_{33} = A_{33}$$

reducing the #DOF to three. In the principal axes form (6.2) this leaves us with

$$\begin{aligned}\bar{A}_{11} &= \bar{F}_{11}(\mathbf{A}) \\ \bar{A}_{22} &= \bar{F}_{22}(\mathbf{A}) \\ \bar{A}_{33} &= \bar{F}_{33}(\mathbf{A})\end{aligned}$$

and thus three functions F_{ii} to construct, to approximate \mathbb{A} as good as possible. Tensor \mathbf{A} is completely determined by its eigenpairs $(\lambda_i, \mathbf{e}_i)$. Due to Property 4.8, we have a dependence between the eigenvalues and thus knowing two of them is sufficient to determine all the eigenvalues. Say we choose λ_1 and λ_2 for this. Furthermore, the F_{ii} are already in the principal axes form. With these arguments, we can state

$$\begin{aligned}\bar{A}_{11} &= \bar{F}_{11}(\lambda_1, \lambda_2) \\ \bar{A}_{22} &= \bar{F}_{22}(\lambda_1, \lambda_2) \\ \bar{A}_{33} &= \bar{F}_{33}(\lambda_1, \lambda_2)\end{aligned}\tag{6.3}$$

or

$$\bar{\mathbf{F}}(\lambda_1, \lambda_2) \equiv \begin{bmatrix} \bar{A}_{11} \\ \bar{A}_{22} \\ \bar{A}_{33} \end{bmatrix}$$

in short.

6.4.3 Domain of the eigenvalues

Recalling Property 4.8 we have

$$\sum_i \lambda_i = 1.$$

Say we choose the numbering of the eigenvalues such that

$$\lambda_1 \geq \lambda_2 \geq \lambda_3.\tag{6.4}$$

Since this numbering (6.4) is arbitrary, it does not imply a loss of generality. We construct a domain for λ_1 and λ_2 , confer Figure 6.1. The green region represents (6.4). The corners and edges of this region

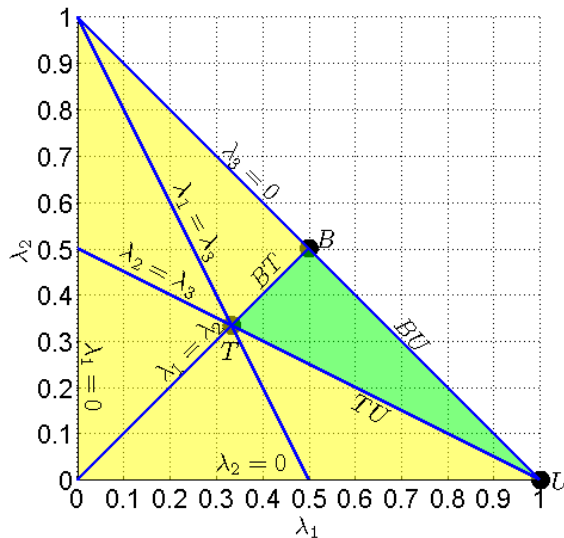


Figure 6.1: feasible area for the eigenvalues.

have significant physical meaning. The point labeled U corresponds to uniaxial orientation, where all fibers are aligned in a single direction, parallel to \mathbf{e}_1 . Point B contains all biaxial orientation states, where fibers are evenly divided between to perpendicular axes, in this case \mathbf{e}_1 and \mathbf{e}_2 . Random-in-plane orientation, with fibers evenly distributed in the $\mathbf{e}_1 - \mathbf{e}_2$ plane, also falls on point B . Point T corresponds to triaxial orientation, with fibers equally divided among all three coordinate axes. Isotropic, or random-in-space, orientation also falls on point T . In addition, the edge BU contains all planar orientation states, where $\lambda_3 = 0$ and all the fibers lie in the $\mathbf{e}_1 - \mathbf{e}_2$ plane. The edges TU and TB

contain all of the transversely isotropic states, where the orientation is cylindrically symmetric about a single axis. Along TU , the axis of symmetry is \mathbf{e}_1 and the dominant orientation is parallel to that axis, while along TB the symmetry axis is \mathbf{e}_3 and the dominant orientation is normal to the axis.

6.4.4 Orthotropic smooth closure

One way to form an orthotropic closure is to choose specific values for the three functions (6.3) at fixed points in Figure 6.1 and interpolate between them for all the remaining points of the domain. One simple choice is to fix values at the corner points U, B and T and use linear interpolation over the interior of the shaded triangle. This particular case will be explained below.

We consider point U defined by $(\lambda_1, \lambda_2, \lambda_3) = (1, 0, 0)$ which represents the state of uniaxial orientation, where all fibers are aligned in a single direction, namely parallel to \mathbf{e}_1 . Using spherical coordinates with unit radius, direction \mathbf{e}_1 corresponds with $(\theta, \phi) = (\frac{\pi}{2}, 0)$ which gives rise to the PDF

$$\psi_U(\theta, \phi) = \delta(\theta - \frac{\pi}{2})\delta(\phi)$$

where δ is the Dirac delta function. Note that the integral of ψ_U over the surface of the unit sphere S is equal to one. It follows that

$$\begin{aligned} \bar{A}_{11} &= \bar{A}_{1111} \\ &= \int_S \psi p_1^4 d^2 \mathbf{p} \\ &= \int_{\phi=0}^{2\pi} \int_{\theta=0}^{\pi} \delta(\theta - \frac{\pi}{2})\delta(\phi) (\sin(\theta) \cos(\phi))^4 \sin(\theta) d\theta d\phi \\ &= \int_{\phi=0}^{2\pi} \int_{\theta=0}^{\pi} \delta(\theta - \frac{\pi}{2})\delta(\phi) \sin^5(\theta) \cos^4(\phi) d\theta d\phi \\ &= \sin^5(\frac{\pi}{2}) \cos^4(0) \\ &= 1, \end{aligned}$$

$$\begin{aligned} \bar{A}_{22} &= \bar{A}_{2222} \\ &= \int_S \psi p_2^4 d^2 \mathbf{p} \\ &= \int_{\phi=0}^{2\pi} \int_{\theta=0}^{\pi} \delta(\theta - \frac{\pi}{2})\delta(\phi) (\sin(\theta) \sin(\phi))^4 \sin(\theta) d\theta d\phi \\ &= \int_{\phi=0}^{2\pi} \int_{\theta=0}^{\pi} \delta(\theta - \frac{\pi}{2})\delta(\phi) \sin^5(\theta) \sin^4(\phi) d\theta d\phi \\ &= \sin^5(\frac{\pi}{2}) \sin^4(0) \\ &= 0, \end{aligned}$$

$$\begin{aligned} \bar{A}_{33} &= \bar{A}_{3333} \\ &= \int_S \psi p_3^4 d^2 \mathbf{p} \\ &= \int_{\phi=0}^{2\pi} \int_{\theta=0}^{\pi} \delta(\theta - \frac{\pi}{2})\delta(\phi) \cos^4(\theta) \sin(\theta) d\theta d\phi \\ &= \cos^4(\frac{\pi}{2}) \sin(\frac{\pi}{2}) \\ &= 0, \end{aligned}$$

or

$$\begin{bmatrix} \bar{A}_{11} \\ \bar{A}_{22} \\ \bar{A}_{33} \end{bmatrix} = \begin{bmatrix} 1 \\ 0 \\ 0 \end{bmatrix} \equiv \bar{\mathbf{F}}_U$$

in short. Note that the latter gives the only possible fourth order tensor at point U , due to the uniqueness of the state. In contrast, there are many possible sets of $(\bar{A}_{11}, \bar{A}_{22}, \bar{A}_{33})$ for points B and T , as they certainly do not imply unique states.

We consider point B defined by $(\lambda_1, \lambda_2, \lambda_3) = (\frac{1}{2}, \frac{1}{2}, 0)$ which represents all biaxial orientation states, where fibers are evenly divided between to perpendicular axes, in this case \mathbf{e}_1 and \mathbf{e}_2 . Random-in-plane orientation, with fibers evenly distributed in the $\mathbf{e}_1 - \mathbf{e}_2$ plane, also falls on point B . The latter corresponds with the PDF

$$\psi_B(\theta, \phi) = \frac{1}{2\pi} \delta(\theta - \frac{\pi}{2}).$$

The latter implies, in a similar manner as for point U , that

$$\begin{bmatrix} \bar{A}_{11} \\ \bar{A}_{22} \\ \bar{A}_{33} \end{bmatrix} = \begin{bmatrix} \frac{3}{8} \\ \frac{3}{8} \\ 0 \end{bmatrix} \equiv \bar{\mathbf{F}}_B.$$

We consider point T defined by $(\lambda_1, \lambda_2, \lambda_3) = (\frac{1}{3}, \frac{1}{3}, \frac{1}{3})$ which represents triaxial orientation, with fibers equally divided among all three coordinate axes. Isotropic, or random-in-space, orientation also falls on point T . The latter implies

$$\psi_T(\theta, \phi) = \frac{1}{4\pi}$$

giving rise to

$$\begin{bmatrix} \bar{A}_{11} \\ \bar{A}_{22} \\ \bar{A}_{33} \end{bmatrix} = \begin{bmatrix} \frac{1}{5} \\ \frac{1}{5} \\ \frac{1}{5} \end{bmatrix} \equiv \bar{\mathbf{F}}_T.$$

Using linear interpolation, we can define $\bar{\mathbf{F}}$ on the rest of the domain. Say

$$\bar{\mathbf{F}}(\lambda_1, \lambda_2) = \bar{\mathbf{F}}_0 + \lambda_1 \bar{\mathbf{F}}_1 + \lambda_2 \bar{\mathbf{F}}_2$$

with

$$\begin{aligned} \bar{\mathbf{F}}|_U &= \bar{\mathbf{F}}_0 + \bar{\mathbf{F}}_1 = \bar{\mathbf{F}}_U \\ \bar{\mathbf{F}}|_B &= \bar{\mathbf{F}}_0 + \frac{1}{2} \bar{\mathbf{F}}_1 + \frac{1}{2} \bar{\mathbf{F}}_2 = \bar{\mathbf{F}}_B \\ \bar{\mathbf{F}}|_T &= \bar{\mathbf{F}}_0 + \frac{1}{3} \bar{\mathbf{F}}_1 + \frac{1}{3} \bar{\mathbf{F}}_2 = \bar{\mathbf{F}}_T. \end{aligned}$$

These nine equations for nine unknowns determine

$$\bar{\mathbf{F}}(\lambda_1, \lambda_2) = (-2\bar{\mathbf{F}}_B + 3\bar{\mathbf{F}}_T) + \lambda_1(\bar{\mathbf{F}}_U + 2\bar{\mathbf{F}}_B - 3\bar{\mathbf{F}}_T) + \lambda_2(-\bar{\mathbf{F}}_U + 4\bar{\mathbf{F}}_B - 3\bar{\mathbf{F}}_T) \quad (6.5)$$

as a common form, and explicitly

$$\bar{\mathbf{F}}(\lambda_1, \lambda_2) = \begin{bmatrix} -0.15 + 1.15\lambda_1 - 0.1\lambda_2 \\ -0.15 + 0.15\lambda_1 + 0.9\lambda_2 \\ 0.6 - 0.6\lambda_1 - 0.6\lambda_2 \end{bmatrix} \quad (6.6)$$

which is called the orthotropic smooth closure (OSC).

6.4.5 Fitted closures

As mentioned before, the orientation tensors are essentially the coefficients in a series expansion of ψ in terms of Legendre polynomials, so \mathbf{A} contains only partial information about ψ . Any closure is an attempt to reconstruct the higher order information [15, 10]. In this reconstruction the fiber orientation problem presents the opportunity to calculate ψ for specific flow histories. It would be prohibitively expensive to calculate ψ for every point in an injection molded part, but it is certainly possible to calculate ψ for a single material point in a few well defined flow fields. The fourth order components calculated this way can be used to form a closure in the same manner that the values U, B and T were used in the previous section. This is the basis of the orthotropic fitted closures (OFC). In this approach the closure is chosen to match the fourth order tensor values that are generated by the dynamics of fiber orientation. In effect, the closure is 'tuned' to a particular fiber orientation model.

The procedure for setting up an orthotropic fitted closure is as follows.

1. Analyze the flow field. What kind of effects are the fibers expected to be subjected to? Shear, elongation, compression? In what ratio's? Is there a dominating effect?
2. Choose homogeneous flow fields that suit the expected effects.
3. Choose a parameter set.
4. Find the solution of (5.23) for each of the chosen homogeneous flow fields, preferably for the chosen parameter set.
5. Choose an interpolation function. It depends how many points of the 'exact' solution of \mathbb{A} you need to calculate to obtain the coefficients in the interpolation function.
6. Choose a set of points in the green domain of Figure 6.1 where the exact \mathbb{A} should be calculated. These points will determine the coefficients in the chosen interpolation function.
7. Calculate the values of the corresponding fourth order tensor \mathbb{A} at the chosen points.
8. Determine the coefficients of the interpolation function, such that the difference between the exact solution and the approximation is minimal in some norm.

This concludes the construction of an orthotropic fitted closure. The QC, OSC and OFC will be used in Part II to compare the approximations with the exact solutions.

Chapter 7

The Fokker-Planck equation

7.1 Introduction

As mentioned before, the analysis of the equation for the PDF was somewhat postponed so that the final form can be analyzed thoroughly in coincidence with the construction of solution strategy. In Section 7.2 we interpret the system of equations. We check if the system conserves the intrinsic properties of the PDF. In Section 7.3 we make the system dimensionless to gain more information on the character of the system. Subsequently, we construct a numerical scheme to solve the system in Section 7.4. We discretize in both space and time and check if the properties of the PDF are conserved by the scheme. Initial and boundary conditions are formulated to close the system. We do a modified equation analysis to obtain the local truncation error (LTE) and its character. Stability analysis completes the conditions for convergence of the numerical solution to the exact solution.

7.2 Interpretation

We recall the system of equations (5.23)

$$\begin{aligned}\dot{\psi} &= -\tilde{\nabla} \cdot (\psi \dot{\mathbf{p}} + \mathbf{q}) \\ \dot{\mathbf{p}} &= \mathbf{W} \cdot \mathbf{p} + \xi(\mathbf{D} \cdot \mathbf{p} - \mathbf{D} : \mathbf{p}\mathbf{p}\mathbf{p}) - C_I \dot{\gamma} \tilde{\nabla} \ln \psi \\ \mathbf{q} &= \sum_l \beta_l (\mathbf{e}_l \mathbf{e}_l \cdot \mathbf{p} - \mathbf{e}_l \mathbf{e}_l : \mathbf{p}\mathbf{p}\mathbf{p}) \\ \beta_l &= -\frac{5(1-\kappa)}{4\pi} [\xi(\lambda_l \mathbf{D} : \mathbf{e}_l \mathbf{e}_l - \mathbf{e}_l \mathbf{e}_l : \mathbb{A} : \mathbf{D}) + C_I \dot{\gamma} (1 - 3\lambda_l)]\end{aligned}\quad (7.1)$$

and Definition 3.1. System (7.1) solves the PDF ψ , which 'lives' on the surface of the unit sphere, also denoted with S , and takes values in $\{\mathbb{R}^+ \cup 0\}$. In notation, $\psi : S \times \mathbb{R} \rightarrow \mathbb{R}^+ \cup 0$. By definition, the PDF has to suffice to certain conditions, as mentioned in Definition 3.1. We recall

$$\forall \mathbf{p}, t \quad \psi(\mathbf{p}, t) \geq 0 \quad \wedge \quad \forall t \quad \oint_S \psi(\mathbf{p}, t) d^2 \mathbf{p} = 1 \quad \wedge \quad \forall \mathbf{p}, t \quad \psi(\mathbf{p}, t) = \psi(-\mathbf{p}, t). \quad (7.2)$$

The condition

$$\forall \mathbf{p}, t \quad \psi(\mathbf{p}, t) = \psi(-\mathbf{p}, t)$$

stems from the fact that it does not matter for the probability density which end of a fiber is the head and which is the tail. The condition should be a property inherent to (7.1).

Property 7.1. *The system (7.1) satisfies*

$$\forall \mathbf{p}, t \quad \psi(\mathbf{p}, t) = \psi(-\mathbf{p}, t). \quad (7.3)$$

Proof. We recall

$$\tilde{\nabla} = \frac{\partial}{\partial \mathbf{p}}$$

so that

$$\mathbf{p} := -\mathbf{p} \quad \Rightarrow \quad \tilde{\nabla} := -\tilde{\nabla}.$$

Herewith,

$$\begin{aligned}\dot{\psi}(-\mathbf{p}, t) &= \mathbf{W} \cdot -\mathbf{p} + \xi(\mathbf{D} \cdot -\mathbf{p} - \mathbf{D} : (-\mathbf{p})(-\mathbf{p})(-\mathbf{p})) - C_I \dot{\gamma} \cdot -\tilde{\nabla} \ln \psi(-\mathbf{p}, t) \\ &= -(\mathbf{W} \cdot \mathbf{p} + \xi(\mathbf{D} \cdot \mathbf{p} - \mathbf{D} : \mathbf{p}\mathbf{p}\mathbf{p}) - C_I \dot{\gamma} \tilde{\nabla} \ln \psi(-\mathbf{p}, t))\end{aligned}$$

so that

$$\begin{aligned}\frac{d}{dt} \psi(-\mathbf{p}, t) &= -(-\tilde{\nabla}) \cdot (\psi(-\mathbf{p}, t) \dot{\mathbf{p}}(-\mathbf{p}, t) + \mathbf{q}(-\mathbf{p}, t)) \\ \frac{d}{dt} \psi(-\mathbf{p}, t) &= \tilde{\nabla} \cdot \left(\psi(-\mathbf{p}, t) \cdot \left(-(\mathbf{W} \cdot \mathbf{p} + \xi(\mathbf{D} \cdot \mathbf{p} - \mathbf{D} : \mathbf{p}\mathbf{p}\mathbf{p}) - C_I \dot{\gamma} \tilde{\nabla} \ln \psi(-\mathbf{p}, t)) \right) (\mathbf{p}) - \mathbf{q}(\mathbf{p}) \right) \\ \dot{\psi} &= -\tilde{\nabla} \cdot (\psi \dot{\mathbf{p}} + \mathbf{q})\end{aligned}$$

where in the last line we merely suppressed the arguments to emphasize that the PDE remains the same. We conclude that (7.1)₁ indeed satisfies (7.3) and is thus invariant under the labeling of the ends. \square

Property 7.2. *The system (7.1) satisfies*

$$\oint_S \psi(\mathbf{p}, t) d^2 \mathbf{p} = 1 \quad (7.4)$$

provided that ψ_0 is such that

$$\oint_S \psi_0 d^2 \mathbf{p} = 1.$$

Proof. Condition (7.4) holds by Definition 3.1. Integrating (7.1)₁ over its complete domain gives

$$\begin{aligned} \oint_S \dot{\psi} d^2 \mathbf{p} &= \oint_S -\tilde{\nabla} \cdot (\psi \dot{\mathbf{p}} + \mathbf{q}) d^2 \mathbf{p} \\ \frac{d}{dt} \oint_S \psi d^2 \mathbf{p} &= 0 \end{aligned}$$

where the latter follows immediately from the closedness of S . Hence, the quantity $\oint_S \psi d^2 \mathbf{p}$ does not change with time. If the initial density ψ_0 is such that $\oint_S \psi_0 d^2 \mathbf{p} = 1$, it remains at one. \square

Note that Property 7.2 is equivalent with

$$\forall t \quad \mathbb{P}(P \in S, t) = 1,$$

which simply states that a fiber must have a direction at any time t . If a fiber is not probable to have direction represented by $S' \subset S$, it is probable to have a direction represented by the complement $(S')^c = S \setminus S'$ and taking all possible directions into account sums up to a probability equal to one.

The condition

$$\psi \geq 0 \quad (7.5)$$

stems from the notion of probability in the sense that probability is defined to be $\in [0; 1]$ and thus nonnegative, so

$$\forall S', t \quad \mathbb{P}(P \in S', t) \geq 0.$$

A proof of the inference of (7.5) to (7.1) in the general sense is cumbersome and will be omitted. In the particular case that $D_r = 0, \kappa = 1$, the proof is manageable.

Property 7.3. *The solution of (7.1) with $D_r = 0, \kappa = 1$ is nonnegative, provided that $\psi_0 \geq 0$ everywhere.*

Proof. Consider

$$\begin{aligned} \dot{\psi} &= -\tilde{\nabla} \cdot (\psi \dot{\mathbf{p}}_J) \\ \dot{\mathbf{p}}_J &= \mathbf{W} \cdot \mathbf{p} + \xi(\mathbf{D} \cdot \mathbf{p} - \mathbf{D} : \mathbf{p}\mathbf{p}\mathbf{p}) \end{aligned}$$

and write

$$\begin{aligned} \dot{\psi} &= -\tilde{\nabla} \cdot (\psi \dot{\mathbf{p}}_J) \\ &= -\dot{\mathbf{p}}_J \tilde{\nabla} \psi - \psi \tilde{\nabla} \cdot \dot{\mathbf{p}}_J \\ &= -\dot{\mathbf{p}}_J \nabla \psi + \psi \xi \mathbf{D} : \mathbf{p}\mathbf{p}. \end{aligned}$$

In the last term on the RHS we, recalling Subsection 3.2.2, recognize $\mathbf{D} : \mathbf{p}\mathbf{p} = \mathbf{K} : \mathbf{p}\mathbf{p} = \frac{2}{\zeta_l} F_c$, a measure for the internal stress of the fiber. If the flow field depends on time t , then so does this term.

Say we consider \mathbf{p} along an observer moving in time, or characteristic, then $\mathbf{p} = \mathbf{p}(\mathbf{p}_0, t)$ so that all quantities dependent of \mathbf{p} become dependent of \mathbf{p}_0 and t . The PDE can be rewritten as

$$\frac{d\psi}{dt} = \frac{\partial \psi}{\partial t} + \frac{\partial \psi}{\partial \mathbf{p}} \cdot \frac{\partial \mathbf{p}}{\partial t} = \frac{\partial \psi}{\partial t} + \nabla(\psi) \cdot \dot{\mathbf{p}}_J = \xi \mathbf{D} : \mathbf{p}\mathbf{p}\psi$$

so that

$$\psi(\mathbf{p}(t), t) = \psi(\mathbf{p}_0, t_0) e^{\xi \int_{t'=t_0}^t \mathbf{D}(t') dt' : \mathbf{p}(t) \mathbf{p}(t)}$$

if \mathbf{D} depends on time. If this is not the case, the latter simplifies to

$$\psi(\mathbf{p}(t), t) = \psi(\mathbf{p}_0, t_0) e^{\xi \mathbf{D} : \mathbf{p}(t) \mathbf{p}(t) (t-t_0)}.$$

As it is given that $\psi_0 \geq 0$ everywhere and an exponential is never negative, the solution ψ is nonnegative for all choices \mathbf{p}_0, t . In notation,

$$\forall \mathbf{p}_0, t \quad \psi(\mathbf{p}_0, t) \geq 0$$

which concludes the proof. \square

If $\mathbf{q} = \mathbf{0}$, (7.1)₁

$$\dot{\psi} = -\tilde{\nabla} \cdot (\psi \dot{\mathbf{p}} + \mathbf{q})$$

is a three dimensional Fokker-Planck equation, which is very similar to an advection-diffusion equation. A Fokker-Planck equation has the form

$$\frac{\partial f}{\partial t} = \sum_{i=1}^N \left[\frac{\partial}{\partial x_i} \left(d_i^1(x_1, x_2, \dots, x_N) + \sum_{j=1}^N \frac{\partial}{\partial x_j} D_{ij}^2(x_1, x_2, \dots, x_N) \right) \right] (f) \quad (7.6)$$

where \mathbf{d}^1 is called the drift vector and \mathbf{D}^2 the diffusion tensor. The latter results from the presence of stochastic force, which is different from the advection-diffusion equation. The other difference is that the (7.6) form contains mixed derivatives, whereas the advection-diffusion equation does not.

Integration over $S' \subset S$ and using the divergence theorem makes the occurrence of convection induced by a flux out of S' even more clear:

$$\frac{d}{dt} \int_{S'} \psi d^2 \mathbf{p} = \int_{S'} \dot{\psi} d^2 \mathbf{p} = - \int_{S'} \tilde{\nabla} \cdot (\psi \dot{\mathbf{p}} + \mathbf{q}) d^2 \mathbf{p} = - \int_{C'} (\psi \dot{\mathbf{p}} + \mathbf{q}) \cdot \mathbf{n} d^1 \mathbf{p}. \quad (7.7)$$

Note that this form was originally the concept wherefrom (7.1)₁ was derived in Subsection 3.3.2.

The change of the variable ψ in time at a position $\mathbf{p} \in S$ depends on what the initial state of ψ at this position was and how the convection of ψ has behaved there, after the initial state. The rate of convection is determined by $\dot{\mathbf{p}}$ and $\frac{\mathbf{q}}{\psi}$. Considering the simplified case that $C_I = 0 \wedge \kappa = 1$, hence no FFI or additional rotation counteraction, the convection is determined by

$$\dot{\mathbf{p}} = \mathbf{W} \cdot \mathbf{p} + \xi (\mathbf{D} \cdot \mathbf{p} - \mathbf{D} : \mathbf{p} \mathbf{p} \mathbf{p})$$

and thus only by the rotation induced by the lift and drag (LD) of the flow field \mathbf{v} on the fibers. Alternatively, one could say by the change of the velocity field in space, $\nabla \mathbf{v}$. Adding the FFI term

$$-C_I \dot{\gamma} \tilde{\nabla} \ln \psi = -\frac{C_I \dot{\gamma}}{\psi} \tilde{\nabla} \psi,$$

when $C_I \neq 0$, to $\dot{\mathbf{p}}$ makes the convection of ψ dependent on ψ itself. Considering an orientation \mathbf{p} , the local convection will be large if ψ is small, $\psi(\mathbf{p}, t) < 1$, and its surroundings take larger values, i.e. $\tilde{\nabla} \psi(\mathbf{p}, t) > 0$. The local convection will be small if ψ takes large values, $\psi(\mathbf{p}, t) > 1$, and its surroundings take smaller values, so $\tilde{\nabla} \psi(\mathbf{p}, t) < 0$. Note that the sign of the FFI is the opposite of the convection stemming from the flow field. Therefore, these two types of convection counteract each other. By writing

$$\begin{aligned} \dot{\psi} &= -\tilde{\nabla} \cdot (\psi \dot{\mathbf{p}} + \mathbf{q}) \\ &= -\tilde{\nabla} \cdot \left(\psi (\mathbf{W} \cdot \mathbf{p} + \xi (\mathbf{D} \cdot \mathbf{p} - \mathbf{D} : \mathbf{p} \mathbf{p} \mathbf{p})) - C_I \dot{\gamma} \tilde{\nabla} \psi + \mathbf{q} \right) \end{aligned}$$

one can alternatively consider the $-C_I \dot{\gamma} \tilde{\nabla} \psi$ term as convection of $\tilde{\nabla} \psi$ or diffusion of ψ instead of convection of ψ .

Interpreting the convection of (7.1)₃ in combination with (7.1)₄ when $\kappa \neq 1$ was already done in Section 5.5. In addition, we recall that it merely stems from decreasing the eigenvalues of

$$\mathbf{A} = \int_S \psi \mathbf{p} \mathbf{p} d^2 \mathbf{p}$$

to slow down the kinetics, as derived in Sections 5.3 and 5.5. Therefore, this term also counteracts the LD induced rotation.

7.3 Dimensional analysis

For the dimensional analysis of (7.1)₁ we first consider (7.1)₂

$$\dot{\mathbf{p}} = \mathbf{W} \cdot \mathbf{p} + \xi(\bar{\mathbf{D}} \cdot \mathbf{p} - \bar{\mathbf{D}} : \mathbf{p}\mathbf{p}\mathbf{p}) - C_I \dot{\gamma} \tilde{\nabla} \ln \psi. \quad (7.8)$$

The dimensions of $\dot{\mathbf{p}}, \mathbf{W}, \mathbf{D}, \dot{\gamma}$ are $[\frac{1}{s}]$. The rest of the dimensions is [1]. The dimension $[\frac{1}{s}]$ in the beforementioned variables and parameters all stem from the strain and shear rates E and G respectively. These rates determine the 'strength' of \mathbf{K} and it is thus interesting to scale the equation to this strength. However, this strength, represented by $\dot{\gamma}$, is not uniquely determined, as mentioned in Subsection 3.3.1. Alternatively, we describe the strength of \mathbf{K} with the sum of the absolute values of the elements of \mathbf{K} :

$$m = \sum_{i,j} |\kappa_{ij}| \quad (7.9)$$

in $[\frac{1}{s}]$. Introducing

$$\dot{\bar{\mathbf{p}}} = \frac{\partial \mathbf{p}}{\partial (tm)} = \frac{1}{m} \frac{\partial \mathbf{p}}{\partial t} = \frac{\dot{\mathbf{p}}}{m}, \quad \bar{\mathbf{W}} = \frac{\mathbf{W}}{m}, \quad \bar{\mathbf{D}} = \frac{\mathbf{D}}{m}, \quad \dot{\bar{\gamma}} = \frac{\dot{\gamma}}{m},$$

equation (7.8) divided by m becomes

$$\dot{\bar{\mathbf{p}}} = \bar{\mathbf{W}} \cdot \mathbf{p} + \xi(\bar{\mathbf{D}} \cdot \mathbf{p} - \bar{\mathbf{D}} : \mathbf{p}\mathbf{p}\mathbf{p}) - C_I \dot{\bar{\gamma}} \tilde{\nabla} \ln \psi. \quad (7.10)$$

The scaling also forces (7.1)₁ to be scaled with m . Introducing

$$\bar{\dot{\psi}} = \frac{\partial \psi}{\partial (tm)} = \frac{1}{m} \frac{\partial \psi}{\partial t} = \frac{\dot{\psi}}{m}, \quad \bar{\mathbf{q}} = \frac{\mathbf{q}}{m}$$

we obtain

$$\bar{\dot{\psi}} = -\tilde{\nabla} \cdot (\psi \dot{\bar{\mathbf{p}}} + \bar{\mathbf{q}}). \quad (7.11)$$

For the sake of notation, we shall omit the bars in the rest of the report.

7.4 Numerical approach

7.4.1 Discretization in space

The Fokker-Planck equation for ψ (7.1)₁ is

$$\dot{\psi} = -\tilde{\nabla} \cdot (\psi \dot{\mathbf{p}} + \mathbf{q}) \quad (7.12)$$

or with $\dot{\mathbf{p}}$ written out and $\kappa = 1$ (3.14)

$$\begin{aligned} \dot{\psi} = & D_r \frac{\partial^2 \psi}{\partial \theta^2} + \frac{D_r}{\sin^2 \theta} \frac{\partial^2 \psi}{\partial \phi^2} + \frac{\partial \psi}{\partial \theta} \left(D_r \frac{\cos \theta}{\sin \theta} - \lambda^- \mathbf{K}^T : \boldsymbol{\delta}_r \boldsymbol{\delta}_\theta - \lambda^+ \mathbf{K} : \boldsymbol{\delta}_r \boldsymbol{\delta}_\theta \right) \\ & + \frac{1}{\sin \theta} \frac{\partial \psi}{\partial \phi} (-\lambda^- \mathbf{K}^T : \boldsymbol{\delta}_r \boldsymbol{\delta}_\phi - \lambda^+ \mathbf{K} : \boldsymbol{\delta}_r \boldsymbol{\delta}_\phi) + \psi (3\lambda \mathbf{K} : \boldsymbol{\delta}_r \boldsymbol{\delta}_r). \end{aligned} \quad (7.13)$$

The latter is a PDE linear in ψ , where ψ is a function of the three variables θ, ϕ and t . The additional flux

$$\mathbf{q} = \sum_l \beta_l (\mathbf{e}_l \mathbf{e}_l \cdot \mathbf{p} - \mathbf{e}_l \mathbf{e}_l : \mathbf{p}\mathbf{p}\mathbf{p}) \quad (7.14)$$

$$\beta_l = -\frac{5(1-\kappa)}{4\pi} [\xi(\lambda_l \mathbf{D} : \mathbf{e}_l \mathbf{e}_l - \mathbf{e}_l \mathbf{e}_l : \mathbb{A} : \mathbf{D}) + C_I \dot{\gamma} (1 - 3\lambda_l)] \quad (7.15)$$

however, makes the PDE more difficult. It is a function of ψ in the sense that $(\lambda_l, \mathbf{e}_l)$ are the eigenpairs of

$$\mathbf{A} = \int_S \psi \mathbf{p}\mathbf{p}\mathbf{p} d^2 \mathbf{p}$$

and that it contains the fourth order tensor

$$\mathbb{A} = \int_S \psi \mathbf{p}\mathbf{p}\mathbf{p}\mathbf{p} d^2 \mathbf{p}.$$

The eigenvalues λ_l can be expressed explicitly and nonlinearly in terms of \mathbf{A} , which in turn can be expressed in terms of ψ . This is also possible for the eigenvectors [5]. Doing so is rather cumbersome. The nonlinearities ask for an explicit time integration or methods like Newton-Raphson. To prevent the cumbersome calculations of Jacobian matrices, we maintain explicit time integration to solve the nonlinearity.

Although (7.13) seems suitable for FDM in the structured space S , writing (7.12) again as (7.7)

$$\frac{d}{dt} \int_{S'} \psi d^2 \mathbf{p} = - \int_{C'} (\psi \dot{\mathbf{p}} + \mathbf{q}) \cdot \mathbf{n} d^1 \mathbf{p} \quad (7.16)$$

calls for the FVM¹ for S . Say we mesh S as depicted in Figure 7.1 and consider one element

$$S_{ij} = [\theta_{i-\frac{1}{2}}; \theta_{i+\frac{1}{2}}] \times [\phi_{j-\frac{1}{2}}; \phi_{j+\frac{1}{2}}]$$

with closed boundary C_{ij} in spherical coordinates confer Figures 7.2 and 7.3. We can then approximate

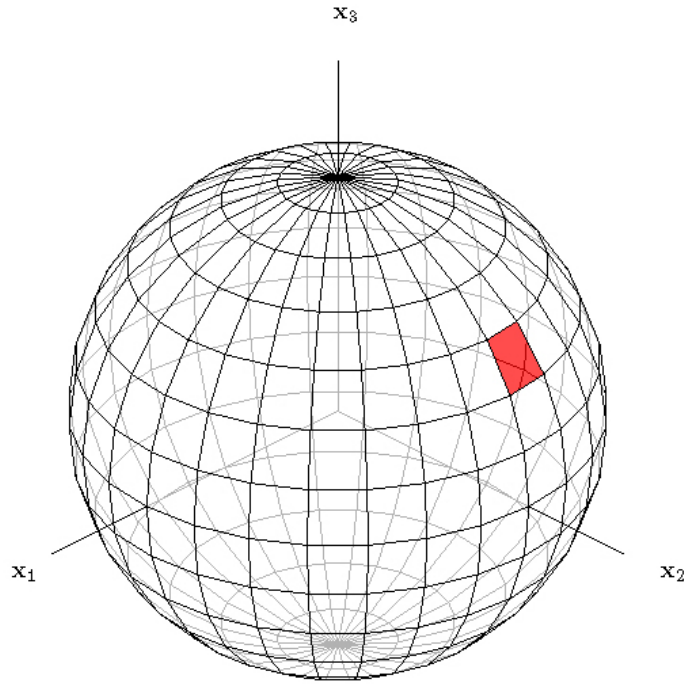


Figure 7.1: meshed surface of the unit sphere.

(7.16) using the FVM. Let us consider the LHS

$$\frac{d}{dt} \int_{S_{ij}} \psi d^2 \mathbf{p}.$$

If we take S_{ij} small, we can assume that ψ is constant for across S_{ij} and so

$$\frac{d}{dt} \int_{S_{ij}} \psi d^2 \mathbf{p} \approx \frac{d}{dt} \left(\psi_{i,j} \int_{S_{ij}} d^2 \mathbf{p} \right) = \frac{d\psi_{i,j}}{dt} \int_{S_{ij}} d^2 \mathbf{p} = \psi_{i,j} \int_{\phi=\phi_{j-\frac{1}{2}}}^{\phi_{j+\frac{1}{2}}} \int_{\theta=\theta_{i-\frac{1}{2}}}^{\theta_{i+\frac{1}{2}}} \sin(\theta) d\theta d\phi = \psi_{i,j} \Delta\phi \cdot (\cos(\theta_{i-\frac{1}{2}}) - \cos(\theta_{i+\frac{1}{2}})),$$

where the subindices i, j refer to the partitioned elements S_{ij} with cell centers θ_i, ϕ_j . In addition, $\Delta\phi = \phi_{j+\frac{1}{2}} - \phi_{j-\frac{1}{2}}$. In short, we denote

$$\frac{d}{dt} \int_{S_{ij}} \psi d^2 \mathbf{p} \approx \dot{\psi}_{i,j} |S_{ij}|,$$

¹As we are actually dealing with surface elements, the name finite volume method can be somewhat confusing. It is illuminating to know that this name merely stems from the approach of considering the average value of a quantity over a cell, be it a line, surface, volume of higher dimensional cell element.

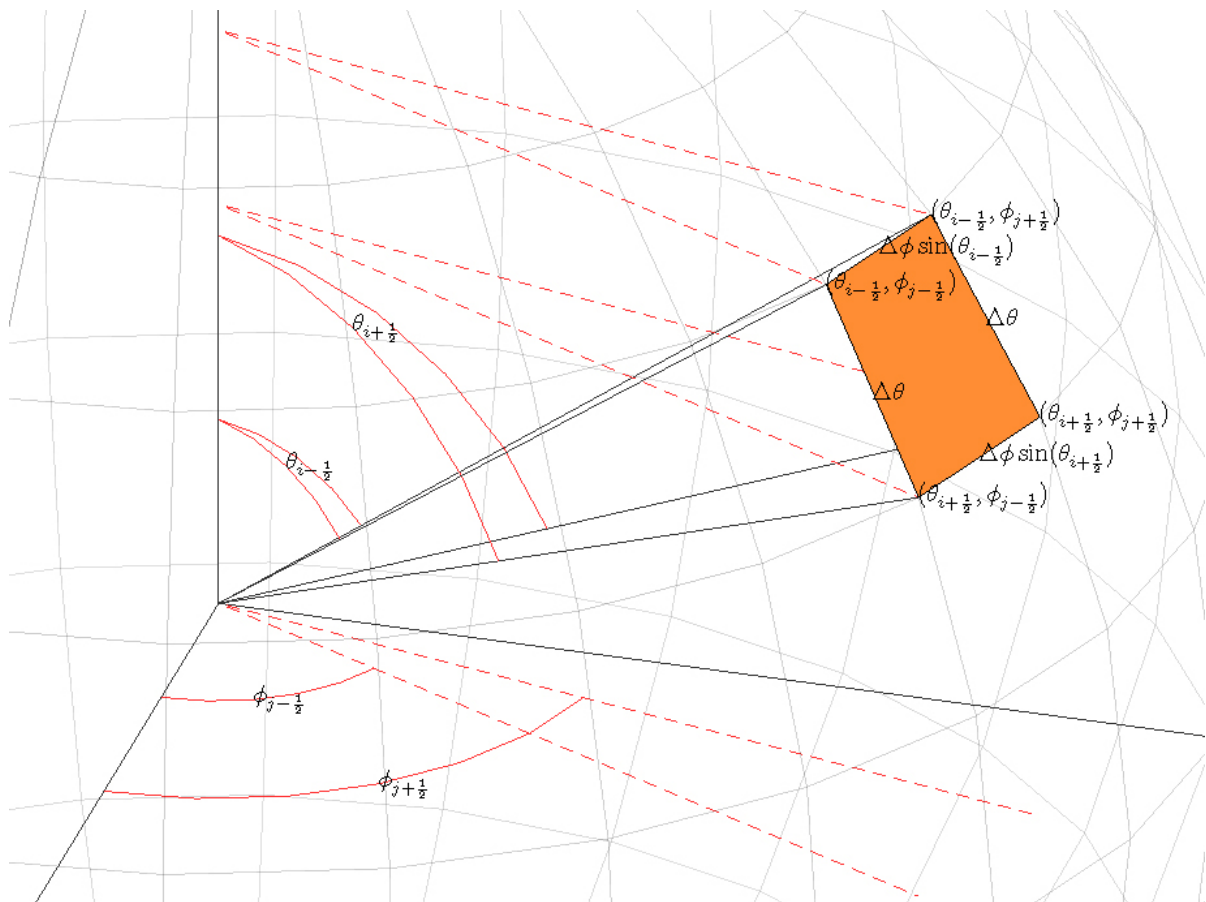
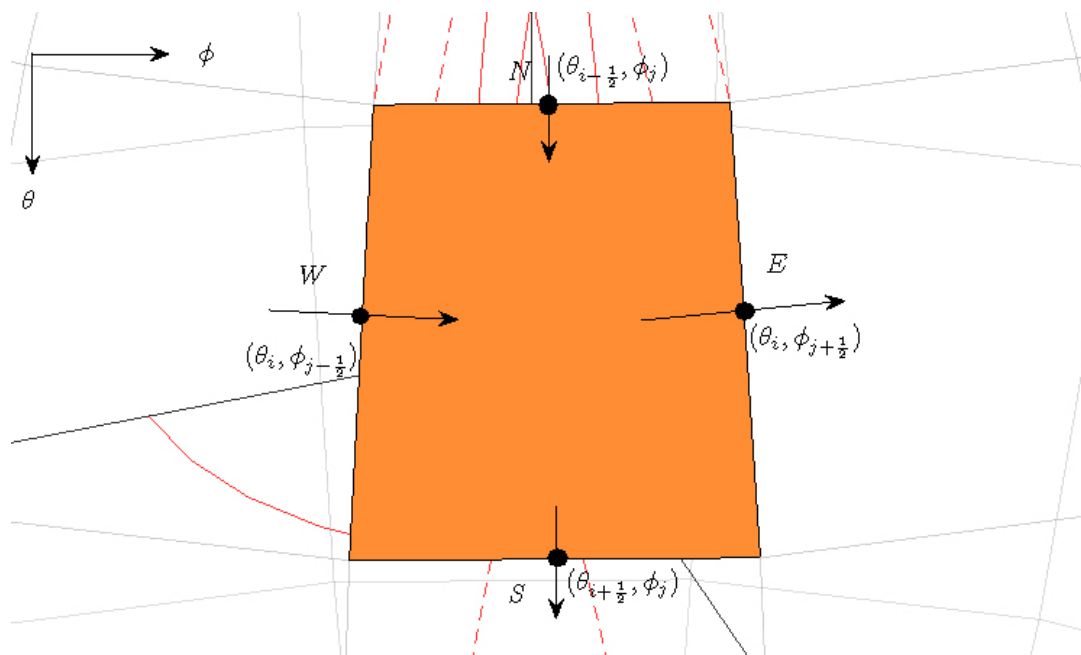


Figure 7.2: spherical coordinates.

Figure 7.3: fluxes for an arbitrary mesh element S_{ij} .

where we denote the size of the mesh element S_i with $|S_i|$, giving

$$\begin{aligned}
|S_i| &= \Delta\phi \cdot (\cos(\theta_{i-\frac{1}{2}}) - \cos(\theta_{i+\frac{1}{2}})) \\
&= \Delta\phi \left(\sum_{q=0}^{\infty} \left[\left(\frac{-\Delta\theta}{2} \right)^q \frac{1}{q!} \left(\frac{d^q}{d\theta^q} \cos \theta \right)_i \right] - \sum_{q=0}^{\infty} \left[\left(\frac{\Delta\theta}{2} \right)^q \frac{1}{q!} \left(\frac{d^q}{d\theta^q} \cos \theta \right)_i \right] \right) \\
&= \Delta\phi \cdot -2 \sum_{q \in \{1,3,\dots\}} \left[\left(\frac{\Delta\theta}{2} \right)^q \frac{1}{q!} \left(\frac{d^q}{d\theta^q} \cos \theta \right)_i \right] \\
&= -2\Delta\phi \sum_{q \in \{1,3,\dots\}} \left[\left(\frac{\Delta\theta}{2} \right)^q \frac{1}{q!} (\mathbf{1}_{q \in \{3,7,\dots\}} - \mathbf{1}_{q \in \{1,5,\dots\}}) \sin \theta_i \right] \\
&= \Delta\phi \Delta\theta \sin(\theta_i) + O(\Delta\phi(\Delta\theta)^3).
\end{aligned}$$

For reasons that will become apparent in Subsection 7.4.5, we will omit the higher order terms and take

$$|S_i| = \Delta\phi \Delta\theta \sin \theta_i.$$

Note that we omit the subindex j as $|S_i|$ is independent of it. In accordance, we also write $|C_{ij}| = |C_i|$.

Let us consider the RHS

$$- \int_{C_{ij}} (\psi \dot{\mathbf{p}} + \mathbf{q}) \cdot \mathbf{n} d^1 \mathbf{p}.$$

Considering a finite element as depicted in Figure 7.3 we can write

$$\int_{C_{ij}} (\psi \dot{\mathbf{p}} + \mathbf{q}) \cdot \mathbf{n} d^1 \mathbf{p} = \int_{C_{ij}^N} (\psi \dot{\mathbf{p}} + \mathbf{q}) \cdot \mathbf{n} d^1 \mathbf{p} + \int_{C_{ij}^W} (\psi \dot{\mathbf{p}} + \mathbf{q}) \cdot \mathbf{n} d^1 \mathbf{p} + \int_{C_{ij}^S} (\psi \dot{\mathbf{p}} + \mathbf{q}) \cdot \mathbf{n} d^1 \mathbf{p} + \int_{C_{ij}^E} (\psi \dot{\mathbf{p}} + \mathbf{q}) \cdot \mathbf{n} d^1 \mathbf{p}. \quad (7.17)$$

Element S_{ij} was taken small, which implies that the edges C_{ij}^N , C_{ij}^W , C_{ij}^S and C_{ij}^E are also small. The integrand can be assumed constant over the edges we can thus approximate the north flux f_{ij}^N corresponding with cell S_{ij} as

$$f_{ij}^N := \int_{C_{ij}^N} (\psi \dot{\mathbf{p}} + \mathbf{q}) \cdot \mathbf{n} d^1 \mathbf{p} = ((\psi \dot{\mathbf{p}} + \mathbf{q}) \cdot \mathbf{n})_{ij}^N \int_{C_{ij}^N} d^1 \mathbf{p} = ((\psi \dot{\mathbf{p}} + \mathbf{q}) \cdot \mathbf{n})_{ij}^N |C_{ij}^N|.$$

We choose the midpoint of the north side to represent the flux, so $N = (\theta_{i-\frac{1}{2}}, \phi_j)$. At this point, $\mathbf{n}^N = (-\delta_\theta)_{i-\frac{1}{2},j}$. The north flux becomes

$$f_{ij}^N = -(\psi \dot{\mathbf{p}} \cdot \delta_\theta + \mathbf{q} \cdot \delta_\theta)_{i-\frac{1}{2},j} \Delta\phi \cdot \sin \theta_{i-\frac{1}{2}}.$$

Recalling (3.13), we get

$$\dot{\mathbf{p}} \cdot \delta_\theta = \lambda^- \mathbf{K}^T : \delta_r \delta_\theta + \lambda^+ \mathbf{K} : \delta_r \delta_\theta - \frac{D_r}{\psi} \frac{\partial \psi}{\partial \theta}.$$

Recalling (7.14) and recalling that $\mathbf{p} = \delta_r$, we get

$$\mathbf{q} \cdot \delta_\theta = \sum_l \beta_l (\mathbf{e}_l \cdot \delta_r) (\mathbf{e}_l \cdot \delta_\theta).$$

Eventually, the north flux becomes

$$f_{ij}^N = - \left(\psi (\lambda^- \mathbf{K}^T : \delta_r \delta_\theta + \lambda^+ \mathbf{K} : \delta_r \delta_\theta) - D_r \frac{\partial \psi}{\partial \theta} + \sum_l \beta_l (\mathbf{e}_l \cdot \delta_r) (\mathbf{e}_l \cdot \delta_\theta) \right)_{i-\frac{1}{2},j} \Delta\phi \cdot \sin \theta_{i-\frac{1}{2}}.$$

Note that the flux is still not uniquely determined, as we did not state how we will approximate $\psi_{i-\frac{1}{2},j}$ and $\left(\frac{\partial \psi}{\partial \theta} \right)_{i-\frac{1}{2},j}$. This is a key issue in the conservation of probability and will be discussed after determining the rest of the fluxes and the time integration method.

The south flux differs from the north flux in the sense that the midpoint of the south side of cell S_{ij} is $S = (\theta_{i+\frac{1}{2}}, \phi_j)$, resulting in $\mathbf{n}^S = \boldsymbol{\delta}_\theta$ instead of $-\boldsymbol{\delta}_\theta$. The south flux is thus

$$f_{ij}^S := \left(\psi (\lambda^- \mathbf{K}^T : \boldsymbol{\delta}_r \boldsymbol{\delta}_\theta + \lambda^+ \mathbf{K} : \boldsymbol{\delta}_r \boldsymbol{\delta}_\theta) - D_r \frac{\partial \psi}{\partial \theta} + \sum_l \beta_l (\mathbf{e}_l \cdot \boldsymbol{\delta}_r) (\mathbf{e}_l \cdot \boldsymbol{\delta}_\theta) \right)_{i+\frac{1}{2}, j} \Delta \phi \cdot \sin \theta_{i+\frac{1}{2}}.$$

The west and east fluxes differ slightly. The normals at the west and east sides are $\mathbf{n}^W = -\boldsymbol{\delta}_\phi$ and $\mathbf{n}^E = \boldsymbol{\delta}_\phi$ respectively. The midpoints on these sides are represented by $W = (\theta_i, \phi_{j-\frac{1}{2}})$ and $E = (\theta_i, \phi_{j+\frac{1}{2}})$. The contributions from $\dot{\mathbf{p}}$ and \mathbf{q} are

$$\dot{\mathbf{p}} \cdot \boldsymbol{\delta}_\phi = \lambda^- \mathbf{K}^T : \boldsymbol{\delta}_r \boldsymbol{\delta}_\phi + \lambda^+ \mathbf{K} : \boldsymbol{\delta}_r \boldsymbol{\delta}_\phi - \frac{D_r}{\psi \sin \theta} \frac{\partial \psi}{\partial \theta}.$$

and

$$\mathbf{q} \cdot \boldsymbol{\delta}_\phi = \sum_l \beta_l (\mathbf{e}_l \cdot \boldsymbol{\delta}_r) (\mathbf{e}_l \cdot \boldsymbol{\delta}_\phi).$$

respectively. Hence, the fluxes are determined by

$$f_{ij}^W := - \left(\psi (\lambda^- \mathbf{K}^T : \boldsymbol{\delta}_r \boldsymbol{\delta}_\phi + \lambda^+ \mathbf{K} : \boldsymbol{\delta}_r \boldsymbol{\delta}_\phi) - \frac{D_r}{\sin \theta} \frac{\partial \psi}{\partial \theta} + \sum_l \beta_l (\mathbf{e}_l \cdot \boldsymbol{\delta}_r) (\mathbf{e}_l \cdot \boldsymbol{\delta}_\phi) \right)_{i, j-\frac{1}{2}} \Delta \theta$$

and

$$f_{ij}^E := \left(\psi (\lambda^- \mathbf{K}^T : \boldsymbol{\delta}_r \boldsymbol{\delta}_\phi + \lambda^+ \mathbf{K} : \boldsymbol{\delta}_r \boldsymbol{\delta}_\phi) - \frac{D_r}{\sin \theta} \frac{\partial \psi}{\partial \theta} + \sum_l \beta_l (\mathbf{e}_l \cdot \boldsymbol{\delta}_r) (\mathbf{e}_l \cdot \boldsymbol{\delta}_\phi) \right)_{i, j+\frac{1}{2}} \Delta \theta.$$

Thusfar, the approximation looks like

$$\begin{aligned} \dot{\psi}_{i,j} |S_i| &= -(f^N + f^W + f^S + f^E)_{ij} \\ &= \left(\psi (\lambda^- \mathbf{K}^T : \boldsymbol{\delta}_r \boldsymbol{\delta}_\theta + \lambda^+ \mathbf{K} : \boldsymbol{\delta}_r \boldsymbol{\delta}_\theta) - D_r \frac{\partial \psi}{\partial \theta} + \sum_l \beta_l (\mathbf{e}_l \cdot \boldsymbol{\delta}_r) (\mathbf{e}_l \cdot \boldsymbol{\delta}_\theta) \right)_{i-\frac{1}{2}, j} \Delta \phi \cdot \sin \theta_{i-\frac{1}{2}} \\ &\quad + \left(\psi (\lambda^- \mathbf{K}^T : \boldsymbol{\delta}_r \boldsymbol{\delta}_\phi + \lambda^+ \mathbf{K} : \boldsymbol{\delta}_r \boldsymbol{\delta}_\phi) - \frac{D_r}{\sin \theta} \frac{\partial \psi}{\partial \theta} + \sum_l \beta_l (\mathbf{e}_l \cdot \boldsymbol{\delta}_r) (\mathbf{e}_l \cdot \boldsymbol{\delta}_\phi) \right)_{i, j-\frac{1}{2}} \Delta \theta \\ &\quad - \left(\psi (\lambda^- \mathbf{K}^T : \boldsymbol{\delta}_r \boldsymbol{\delta}_\theta + \lambda^+ \mathbf{K} : \boldsymbol{\delta}_r \boldsymbol{\delta}_\theta) - D_r \frac{\partial \psi}{\partial \theta} + \sum_l \beta_l (\mathbf{e}_l \cdot \boldsymbol{\delta}_r) (\mathbf{e}_l \cdot \boldsymbol{\delta}_\theta) \right)_{i+\frac{1}{2}, j} \Delta \phi \cdot \sin \theta_{i+\frac{1}{2}} \\ &\quad - \left(\psi (\lambda^- \mathbf{K}^T : \boldsymbol{\delta}_r \boldsymbol{\delta}_\phi + \lambda^+ \mathbf{K} : \boldsymbol{\delta}_r \boldsymbol{\delta}_\phi) - \frac{D_r}{\sin \theta} \frac{\partial \psi}{\partial \theta} + \sum_l \beta_l (\mathbf{e}_l \cdot \boldsymbol{\delta}_r) (\mathbf{e}_l \cdot \boldsymbol{\delta}_\phi) \right)_{i, j+\frac{1}{2}} \Delta \theta. \end{aligned} \quad (7.18)$$

7.4.2 Discretization in time

Conform [2], we use Euler forward to approximate the time derivative:

$$\psi_{i,j}^{k+1} = \psi_{i,j}^k + \int_{t'=t_k}^{t_{k+1}} \dot{\psi}_{i,j}(t') dt' \approx \psi_{i,j}^k + \Delta t \dot{\psi}_{i,j}^k \Leftrightarrow \dot{\psi}_{i,j}^k \approx \frac{\psi_{i,j}^{k+1} - \psi_{i,j}^k}{\Delta t}. \quad (7.19)$$

The numerical scheme is now

$$\psi_{i,j}^{k+1} = \psi_{i,j}^k - \frac{\Delta t}{|S_i|} (f^N + f^W + f^S + f^E)^k. \quad (7.20)$$

This immediately gets rid of the nonlinearities and the need to express the eigenpairs of \mathbf{A} explicitly. Although the scheme is extremely simple, explicit time integration is infamous for its need of small time steps. In [15], the authors speak of a time step of 10^{-5} . In comparison with more stable time integration methods, it is thus more important for the calculations made for space discretization to be fast.

The following quantities all have to be determined at each midpoint of the sides of the cells, and at each time step.

1. Probability density ψ .
2. Derivatives $\frac{\partial\psi}{\partial\theta}$ and $\frac{\partial\psi}{\partial\phi}$.
3. Eigenpairs λ_l, e_l of \mathbf{A} .
4. Fourth order tensor \mathbb{A} .
5. Double contractions to calculate β_l .

Concerning (7.20), we have to assure that the conditions as mentioned in Definition 3.1 and Section 7.2 are satisfied.

7.4.3 Conditions of the probability density function

7.4.3.1 Heads or tails

Let us check if the conditions of the PDF ψ are satisfied by the numerical scheme (7.20), maintaining the same order as in Section 7.2. The first condition is (7.3)

$$\forall \mathbf{p}, t \quad \psi(\mathbf{p}, t) = \psi(-\mathbf{p}, t),$$

which in spherical coordinates results in

$$\forall \theta, \phi, t \quad \psi(\theta, \phi, t) = \psi(\pi - \theta, \phi + \pi, t).$$

In the discrete case, this condition 'translates' to an alternative expression.

Say we partition the θ domain $[0; \pi]$ and ϕ domain $[0; 2\pi]$ in n_θ and n_ϕ parts respectively. Furthermore, let us denote $\psi = (\psi_{i,j}^k)$ with $i \in \{1, 2, \dots, n_\theta\}, j \in \{1, 2, \dots, n_\phi\}$. Then the condition is represented by

$$\begin{aligned} \psi_{i,j}^{k+1} &= \psi(\theta_i, \phi_j, t_{k+1}) \\ &= \psi(\pi - \theta_i, \phi_j + \pi, t_{k+1}) \\ &= \psi(\theta_{n_\theta - i}, \phi_j + \phi_{\frac{n_\phi}{2}}, t_{k+1}) \\ &= \psi(\theta_{n_\theta - i}, \phi_{j + \frac{n_\phi}{2}}, t_{k+1}) \\ &= \psi_{n_\theta - i, j + \frac{n_\phi}{2}}^{k+1} \end{aligned} \tag{7.21}$$

given that $\psi_{i,j}^0 = \psi_{n_\theta - i, j + \frac{n_\phi}{2}}^0$. Notice that (7.20) already fails to satisfy the condition if n_ϕ is odd because it does not give an integer when divided by two. The partition number n_ϕ is obliged to be even, which we assume from hereon.

Property 7.4. *The scheme (7.20) conserves the discrete analogue (7.21) of (7.3).*

Proof. We prove the satisfaction of this condition by induction. It is given that

$$\psi_{i,j}^0 = \psi_{n_\theta - i, j + \frac{n_\phi}{2}}^0.$$

The LHS propagates to $\psi_{i,j}^1$, so also the RHS has to. The RHS becomes

$$\begin{aligned} \psi_{n_\theta - i, j + \frac{n_\phi}{2}}^1 &= \psi_{n_\theta - i, j + \frac{n_\phi}{2}}^0 - \frac{\Delta t}{|S_{n_\theta - i}|} (f^N + f^W + f^S + f^E)_{n_\theta - i, j + \frac{n_\phi}{2}}^0 \\ &= \psi_{i,j}^0 - \frac{\Delta t}{|S_{n_\theta - i}|} (f^N + f^W + f^S + f^E)_{n_\theta - i, j + \frac{n_\phi}{2}}^0. \end{aligned}$$

We have

$$\begin{aligned} |S_{n_\theta - i}| &= \Delta\phi\Delta\theta \sin \theta_{n_\theta - i} \\ &= \Delta\phi\Delta\theta \sin(\theta_{n_\theta} - \theta_i) \\ &= \Delta\phi\Delta\theta \sin(\pi - \theta_i) \\ &= \Delta\phi\Delta\theta \sin(\theta_i) \\ &= |S_i|. \end{aligned}$$

For the north fluxes we get

$$f_{n_\theta-i, j+\frac{n_\phi}{2}}^N = \left(\psi (\lambda^- \mathbf{K}^T : \boldsymbol{\delta}_r \boldsymbol{\delta}_\theta + \lambda^+ \mathbf{K} : \boldsymbol{\delta}_r \boldsymbol{\delta}_\theta) - D_r \frac{\partial \psi}{\partial \theta} + \sum_l \beta_l (\mathbf{e}_l \cdot \boldsymbol{\delta}_r) (\mathbf{e}_l \cdot \boldsymbol{\delta}_\theta) \right) \frac{\Delta \phi \cdot \sin \theta_{n_\theta-i-\frac{1}{2}}}{n_\theta-i-\frac{1}{2}, j+\frac{n_\phi}{2}}.$$

We can not fully determine $f_{n_\theta-i, j+\frac{n_\phi}{2}}^N$, as the approximations of ψ and $\frac{\partial \psi}{\partial \theta}$ have not yet been determined. Recalling (2.4), it follows that

$$(\boldsymbol{\delta}_r)_{n_\theta-i-\frac{1}{2}, j+\frac{n_\phi}{2}} = -(\boldsymbol{\delta}_r)_{i+\frac{1}{2}, j}, \quad (\boldsymbol{\delta}_\theta)_{n_\theta-i-\frac{1}{2}, j+\frac{n_\phi}{2}} = (\boldsymbol{\delta}_\theta)_{i+\frac{1}{2}, j}$$

The sinus becomes

$$\sin \theta_{n_\theta-i-\frac{1}{2}} = \sin \theta_{n_\theta-(i+\frac{1}{2})} = \sin \theta_{i+\frac{1}{2}}.$$

For the south fluxes we get analogously

$$(\boldsymbol{\delta}_r)_{n_\theta-i+\frac{1}{2}, j+\frac{n_\phi}{2}} = -(\boldsymbol{\delta}_r)_{i-\frac{1}{2}, j}, \quad (\boldsymbol{\delta}_\theta)_{n_\theta-i+\frac{1}{2}, j+\frac{n_\phi}{2}} = (\boldsymbol{\delta}_\theta)_{i-\frac{1}{2}, j}, \quad \sin \theta_{n_\theta-i+\frac{1}{2}} = \sin \theta_{i-\frac{1}{2}}.$$

For the west and east fluxes we obtain

$$(\boldsymbol{\delta}_r)_{n_\theta-i, j+\frac{n_\phi}{2}-\frac{1}{2}} = -(\boldsymbol{\delta}_r)_{i, j-\frac{1}{2}}, \quad (\boldsymbol{\delta}_\phi)_{n_\theta-i, j+\frac{n_\phi}{2}-\frac{1}{2}} = -(\boldsymbol{\delta}_\phi)_{i, j-\frac{1}{2}}, \quad \sin \theta_{n_\theta-i} = \sin \theta_i.$$

and

$$(\boldsymbol{\delta}_r)_{n_\theta-i, j+\frac{n_\phi}{2}+\frac{1}{2}} = -(\boldsymbol{\delta}_r)_{i, j+\frac{1}{2}}, \quad (\boldsymbol{\delta}_\phi)_{n_\theta-i, j+\frac{n_\phi}{2}+\frac{1}{2}} = -(\boldsymbol{\delta}_\phi)_{i, j+\frac{1}{2}}, \quad \sin \theta_{n_\theta-i} = \sin \theta_i.$$

respectively. Filling these observations in in (7.18) we conclude that (7.21) is satisfied and

$$\psi_{n_\theta-i, j+\frac{n_\phi}{2}}^1 = \psi_{i, j}^0 - \frac{\Delta t}{|S_i|} (f^N + f^W + f^S + f^E)_{i, j}^0 = \psi_{i, j}^1.$$

if for the north fluxes we have

$$\psi_{n_\theta-i-\frac{1}{2}, j+\frac{n_\phi}{2}} = \psi_{i+\frac{1}{2}, j}, \quad \left(\frac{\partial \psi}{\partial \theta} \right)_{n_\theta-i-\frac{1}{2}, j+\frac{n_\phi}{2}} = - \left(\frac{\partial \psi}{\partial \theta} \right)_{i+\frac{1}{2}, j},$$

for the south fluxes

$$\psi_{n_\theta-i+\frac{1}{2}, j+\frac{n_\phi}{2}} = \psi_{i-\frac{1}{2}, j}, \quad \left(\frac{\partial \psi}{\partial \theta} \right)_{n_\theta-i+\frac{1}{2}, j+\frac{n_\phi}{2}} = - \left(\frac{\partial \psi}{\partial \theta} \right)_{i-\frac{1}{2}, j},$$

for the west fluxes

$$\psi_{n_\theta-i, j+\frac{n_\phi}{2}-\frac{1}{2}} = \psi_{i, j-\frac{1}{2}}, \quad \left(\frac{\partial \psi}{\partial \phi} \right)_{n_\theta-i, j+\frac{n_\phi}{2}-\frac{1}{2}} = \left(\frac{\partial \psi}{\partial \phi} \right)_{i, j-\frac{1}{2}},$$

and the east fluxes

$$\psi_{n_\theta-i, j+\frac{n_\phi}{2}+\frac{1}{2}} = \psi_{i, j+\frac{1}{2}}, \quad \left(\frac{\partial \psi}{\partial \phi} \right)_{n_\theta-i, j+\frac{n_\phi}{2}+\frac{1}{2}} = \left(\frac{\partial \psi}{\partial \phi} \right)_{i, j+\frac{1}{2}}.$$

Looking carefully at the indices on the RHSs, we conclude that by considering $(\theta_{n_\theta-i}, \phi_{j+\frac{n_\phi}{2}})$ instead of (θ_i, ϕ_j) , the north and south fluxes are interchanged and the west and east fluxes remain the same. The analytic analogue (7.17) results in the same interchange and conservations.

Now having obtained criteria on how to choose the ψ and its derivatives in space at the sides of the cells, it is logical to approximate these quantities by using their two closest cell values in the direction in question. This means

$$\psi_{i-\frac{1}{2}, j} = \frac{\psi_{i, j} + \psi_{i-1, j}}{2}, \quad \left(\frac{\partial \psi}{\partial \theta} \right)_{i-\frac{1}{2}, j} = \frac{\psi_{i, j} - \psi_{i-1, j}}{\Delta \theta}$$

for the north sides,

$$\psi_{i+\frac{1}{2}, j} = \frac{\psi_{i+1, j} + \psi_{i, j}}{2}, \quad \left(\frac{\partial \psi}{\partial \theta} \right)_{i+\frac{1}{2}, j} = \frac{\psi_{i+1, j} - \psi_{i, j}}{\Delta \theta}$$

for the south sides,

$$\psi_{i,j-\frac{1}{2}} = \frac{\psi_{i,j} + \psi_{i,j-1}}{2}, \quad \left(\frac{\partial \psi}{\partial \phi} \right)_{i,j-\frac{1}{2}} = \frac{\psi_{i,j} - \psi_{i,j-1}}{\Delta \phi}$$

for the west sides and last

$$\psi_{i,j+\frac{1}{2}} = \frac{\psi_{i,j+1} + \psi_{i,j}}{2}, \quad \left(\frac{\partial \psi}{\partial \phi} \right)_{i,j+\frac{1}{2}} = \frac{\psi_{i,j+1} - \psi_{i,j}}{\Delta \phi}$$

for the east sides. These approximations suffice to the beforementioned conditions and we thus have

$$\psi_{n_\theta-i,j+\frac{n_\phi}{2}}^1 = \psi_{i,j}^1.$$

To complete the proof of induction, we assume that

$$\psi_{n_\theta-i,j+\frac{n_\phi}{2}}^k = \psi_{i,j}^k$$

and must prove that the relation also holds for the subsequent time step. We have

$$\begin{aligned} \psi_{n_\theta-i,j+\frac{n_\phi}{2}}^{k+1} &= \psi_{n_\theta-i,j+\frac{n_\phi}{2}}^k - \frac{\Delta t}{|S_{n_\theta-i}|} (f^N + f^W + f^S + f^E)^k_{n_\theta-i,j+\frac{n_\phi}{2}} \\ &= \psi_{i,j}^k - \frac{\Delta t}{|S_i|} (f^N + f^W + f^S + f^E)^k_{n_\theta-i,j+\frac{n_\phi}{2}}. \end{aligned}$$

As the basis of the surface of the unit sphere S is Eulerian, the procedure to obtain

$$(f^N + f^W + f^S + f^E)^k_{n_\theta-i,j+\frac{n_\phi}{2}} = (f^N + f^W + f^S + f^E)^k_{i,j}$$

is exactly the same as for time zero. We conclude

$$\psi_{n_\theta-i,j+\frac{n_\phi}{2}}^{k+1} = \psi_{i,j}^{k+1},$$

and thus (7.20) satisfies (7.21) for all time and space. \square

Perhaps the proof of the satisfaction of the condition is somewhat cumbersome, but it is definitely worth it. Since we now know that

$$\forall \mathbf{p}, t \quad \psi(-\mathbf{p}, t) = \psi(\mathbf{p}, t),$$

only half of S is interesting, as the other half is just a copy. Herewith, the $\#DOF$ is reduced by a factor two. This results in a vast decrease in calculation time. That is, if (7.20) suffices to the rest of the conditions.

7.4.3.2 Conservation of probability

The conservation of probability is represented by

$$\forall t \quad \oint_S \psi(\mathbf{p}, t) d^2 \mathbf{p} = 1.$$

Its discrete analogue is

$$\forall k \quad 2 \sum_{i,j} \psi_{i,j}^k |S_i| = 1. \quad (7.22)$$

The factor two originates from the fact that we only consider half of S . This implies that from now on $\theta \in [0; \frac{\pi}{2}]$, $\theta_{n_\theta} = \frac{\pi}{2}$. A proof hereof will again be by inductive form. We assume

$$2 \sum_{i,j} \psi_{i,j}^0 |S_i| = 1$$

and must first prove that

$$2 \sum_{i,j} \psi_{i,j}^1 |S_i| = 1.$$

Property 7.5. *The scheme (7.20) conserves probability in the discrete sense (7.22).*

Proof. It follows that

$$\begin{aligned}
2 \sum_{i,j} \psi_{i,j}^1 |S_i| &= 2 \sum_{i,j} \left[\left(\psi_{i,j}^0 - \frac{\Delta t}{|S_i|} (f^N + f^W + f^S + f^E)_{i,j}^0 \right) |S_i| \right] \\
&= 2 \sum_{i,j} [\psi_{i,j}^0 |S_i|] - 2\Delta t \sum_{i,j} (f^N + f^W + f^S + f^E)_{i,j}^0 \\
&= 1 - 2\Delta t \sum_{i,j} (f^N + f^W + f^S + f^E)_{i,j}^0
\end{aligned}$$

and so proving that

$$\sum_{i,j} (f^N + f^W + f^S + f^E)_{i,j}^0 = 0$$

is sufficient. The latter states that the sum of the fluxes must vanish at time zero.

We consider

$$\sum_{i,j} (f^N + f^S)_{i,j}^0$$

with

$$f_{i,j}^N = - \left(\frac{\psi_{i,j} + \psi_{i-1,j}}{2} (\lambda^- \mathbf{K}^T + \lambda^+ \mathbf{K}) : (\boldsymbol{\delta}_r \boldsymbol{\delta}_\theta)_{i-\frac{1}{2},j} - D_r \frac{\psi_{i,j} - \psi_{i-1,j}}{\Delta \theta} + \left(\sum_l \beta_l (\mathbf{e}_l \cdot \boldsymbol{\delta}_r) (\mathbf{e}_l \cdot \boldsymbol{\delta}_\theta) \right)_{i-\frac{1}{2},j} \right) \Delta \phi \cdot \sin \theta_{i-\frac{1}{2}}$$

and

$$f_{i,j}^S = \left(\frac{\psi_{i+1,j} + \psi_{i,j}}{2} (\lambda^- \mathbf{K}^T + \lambda^+ \mathbf{K}) : (\boldsymbol{\delta}_r \boldsymbol{\delta}_\theta)_{i+\frac{1}{2},j} - D_r \frac{\psi_{i+1,j} - \psi_{i,j}}{\Delta \theta} + \left(\sum_l \beta_l (\mathbf{e}_l \cdot \boldsymbol{\delta}_r) (\mathbf{e}_l \cdot \boldsymbol{\delta}_\theta) \right)_{i+\frac{1}{2},j} \right) \Delta \phi \cdot \sin \theta_{i+\frac{1}{2}}.$$

We notice that f^N and f^S only differ in the first index and in their sign. Therefore

$$\begin{aligned}
\sum_{i,j} (f^N + f^S)_{i,j}^0 &= \sum_j \left[\sum_{i=1}^{n_\theta} [f_{i,j}^N] + \sum_{i=1}^{n_\theta} [f_{i,j}^S] \right] \\
&= \sum_j \left[\sum_{i=1}^{n_\theta} [f_{i,j}^N] + \sum_{i-1=1}^{n_\theta} [f_{i-1,j}^S] \right] \\
&= \sum_j \left[\sum_{i=1}^{n_\theta} [f_{i,j}^N] - \sum_{i=2}^{n_\theta+1} [f_{i,j}^N] \right] \\
&= \sum_j [f_{1,j}^N - f_{n_\theta+1,j}^N]
\end{aligned}$$

For $i = 1$ we get

$$\forall j \quad \sin \theta_{i-\frac{1}{2}} = \sin \theta_{\frac{1}{2}} = \sin 0 = 0$$

and thus only

$$\sum_j [f_{n_\theta+1,j}^N]$$

remains. Considering $f_{n_\theta+1,j}^N$, we obtain

$$\left(\frac{\psi_{i,j} + \psi_{i-1,j}}{2} \right)_{n_\theta+1,j} = \frac{\psi_{n_\theta+1,j} + \psi_{n_\theta,j}}{2} = \frac{\psi_{n_\theta,j+\frac{n_\phi}{2}} + \psi_{n_\theta,j}}{2}$$

and for the basis vectors

$$(\boldsymbol{\delta}_r)_{n_\theta+\frac{1}{2},j} = \begin{bmatrix} \sin(\theta_{n_\theta+\frac{1}{2}}) \cos(\phi_j) \\ \sin(\theta_{n_\theta+\frac{1}{2}}) \sin(\phi_j) \\ \cos(\theta_{n_\theta+\frac{1}{2}}) \end{bmatrix} = \begin{bmatrix} \sin(\frac{\pi}{2}) \cos(\phi_j) \\ \sin(\frac{\pi}{2}) \sin(\phi_j) \\ \cos(\frac{\pi}{2}) \end{bmatrix} = \begin{bmatrix} \cos(\phi_j) \\ \sin(\phi_j) \\ 0 \end{bmatrix}$$

and

$$(\delta_\theta)_{n_\theta+\frac{1}{2},j} = \begin{bmatrix} \cos(\theta_{n_\theta+\frac{1}{2}}) \cos(\phi_j) \\ \cos(\theta_{n_\theta+\frac{1}{2}}) \sin(\phi_j) \\ -\sin(\theta_{n_\theta+\frac{1}{2}}) \end{bmatrix} = \begin{bmatrix} \cos(\frac{\pi}{2}) \cos(\phi_j) \\ \cos(\frac{\pi}{2}) \sin(\phi_j) \\ -\sin(\frac{\pi}{2}) \end{bmatrix} = \begin{bmatrix} 0 \\ 0 \\ -1 \end{bmatrix}$$

so that

$$(\delta_r \delta_\theta)_{n_\theta+\frac{1}{2},j} = -(\delta_r \delta_\theta)_{n_\theta+\frac{1}{2},j+\frac{n_\phi}{2}}.$$

Say we call the right factor in the first term $u_{n_\theta+\frac{1}{2},j}$. We then have

$$u_{n_\theta+\frac{1}{2},j} = -u_{n_\theta+\frac{1}{2},j+\frac{n_\phi}{2}}$$

and the first term becomes

$$\begin{aligned} \sum_j \frac{\psi_{n_\theta,j+\frac{n_\phi}{2}} + \psi_{n_\theta,j}}{2} u_{n_\theta+\frac{1}{2},j} &= \frac{1}{2} \sum_j [\psi_{n_\theta,j+\frac{n_\phi}{2}} u_{n_\theta+\frac{1}{2},j} + \psi_{n_\theta,j} u_{n_\theta+\frac{1}{2},j}] \\ &= \frac{1}{2} \sum_j [-\psi_{n_\theta,j+\frac{n_\phi}{2}} u_{n_\theta+\frac{1}{2},j+\frac{n_\phi}{2}} + \psi_{n_\theta,j} u_{n_\theta+\frac{1}{2},j}] \\ &= \frac{1}{2} \left(-\sum_{j=1}^{n_\phi} [\psi_{n_\theta,j+\frac{n_\phi}{2}} u_{n_\theta+\frac{1}{2},j+\frac{n_\phi}{2}}] + \sum_{j=1}^{n_\phi} [\psi_{n_\theta,j} u_{n_\theta+\frac{1}{2},j}] \right) \\ &= \frac{1}{2} \left(-\sum_{j-\frac{n_\phi}{2}=1}^{n_\phi} [\psi_{n_\theta,j} u_{n_\theta+\frac{1}{2},j}] + \sum_{j=1}^{n_\phi} [\psi_{n_\theta,j} u_{n_\theta+\frac{1}{2},j}] \right) \\ &= \frac{1}{2} \left(-\sum_{j=1+\frac{n_\phi}{2}}^{n_\phi+\frac{n_\phi}{2}} [\psi_{n_\theta,j} u_{n_\theta+\frac{1}{2},j}] + \sum_{j=1}^{n_\phi} [\psi_{n_\theta,j} u_{n_\theta+\frac{1}{2},j}] \right) \\ &= \frac{1}{2} \left(-\sum_{j=1}^{n_\phi} [\psi_{n_\theta,j} u_{n_\theta+\frac{1}{2},j}] + \sum_{j=1}^{n_\phi} [\psi_{n_\theta,j} u_{n_\theta+\frac{1}{2},j}] \right) \\ &= 0, \end{aligned}$$

where we used the periodicity of ψ , $\sin \phi$ and $\cos \phi$ in ϕ with a period of 2π and thus also periodicity in j with a period of n_ϕ . Note that again it is obliged that n_ϕ is even to result in an integer when divided by two.

For the term

$$-D_r \frac{\psi_{i,j} - \psi_{i-1,j}}{\Delta\theta} \Delta\phi \cdot \sin \theta_{i-\frac{1}{2}}$$

we get

$$\begin{aligned} \frac{-D_r \Delta\phi \cdot \sin(\theta_{n_\theta+\frac{1}{2}})}{\Delta\theta} \sum_j [\psi_{n_\theta+1,j} - \psi_{n_\theta,j}] &= \frac{-D_r \Delta\phi \cdot \sin(\theta_{n_\theta+\frac{1}{2}})}{\Delta\theta} \sum_j [\psi_{n_\theta,j+\frac{n_\phi}{2}} - \psi_{n_\theta,j}] \\ &= \frac{-D_r \Delta\phi \cdot \sin(\theta_{n_\theta+\frac{1}{2}})}{\Delta\theta} \left(\sum_{j=1}^{n_\phi} [\psi_{n_\theta,j+\frac{n_\phi}{2}}] - \sum_{j=1}^{n_\phi} [\psi_{n_\theta,j}] \right) \\ &= \frac{-D_r \Delta\phi \cdot \sin(\theta_{n_\theta+\frac{1}{2}})}{\Delta\theta} \left(\sum_{j-\frac{n_\phi}{2}=1}^{n_\phi} [\psi_{n_\theta,j+\frac{n_\phi}{2}}] - \sum_{j=1}^{n_\phi} [\psi_{n_\theta,j}] \right) \\ &= \frac{-D_r \Delta\phi \cdot \sin(\theta_{n_\theta+\frac{1}{2}})}{\Delta\theta} \left(\sum_{j=1+\frac{n_\phi}{2}}^{n_\phi+\frac{n_\phi}{2}} [\psi_{n_\theta,j}] - \sum_{j=1}^{n_\phi} [\psi_{n_\theta,j}] \right) \\ &= 0 \end{aligned}$$

where we used periodicity in j with period n_ϕ in the last step.

The last term of the north fluxes are represented by

$$\left(\sum_l \beta_l (\mathbf{e}_l \cdot \delta_r) (\mathbf{e}_l \cdot \delta_\theta) \right)_{i-\frac{1}{2},j} \Delta\phi \cdot \sin \theta_{i-\frac{1}{2}}.$$

We thus get

$$\begin{aligned}
\sum_j \left[\left(\sum_l \beta_l (\mathbf{e}_l \cdot \boldsymbol{\delta}_r) (\mathbf{e}_l \cdot \boldsymbol{\delta}_\theta) \right)_{n_\phi + \frac{1}{2}, j} \Delta\phi \cdot \sin \theta_{n_\phi + \frac{1}{2}} \right] &= \sum_l \left[\beta_l (\mathbf{e}_l \cdot (\boldsymbol{\delta}_\theta)_{n_\phi + \frac{1}{2}, j}) \left(\mathbf{e}_l \cdot \sum_j (\boldsymbol{\delta}_r)_{n_\phi + \frac{1}{2}, j} \right) \right] \Delta\phi \\
&= \sum_l \left[\beta_l (\mathbf{e}_l \cdot (\boldsymbol{\delta}_\theta)_{n_\phi + \frac{1}{2}, j}) \left(\mathbf{e}_l \cdot \sum_j \begin{bmatrix} \cos \phi_j \\ \sin \phi_j \\ 0 \end{bmatrix} \right) \right] \Delta\phi \\
&= \sum_l \left[\beta_l (\mathbf{e}_l \cdot (\boldsymbol{\delta}_\theta)_{n_\phi + \frac{1}{2}, j}) \left(\mathbf{e}_l \cdot \sum_j \begin{bmatrix} 0 \\ 0 \\ 0 \end{bmatrix} \right) \right] \Delta\phi \\
&= 0.
\end{aligned}$$

We conclude that

$$\sum_{i,j} (f^N + f^S)_{i,j}^0 = 0,$$

which leaves us to prove that

$$\sum_{i,j} (f^W + f^E)_{i,j}^0 = 0$$

to prove that the sum of the fluxes is zero at time zero. We recall

$$f_{ij}^W = - \left(\frac{\psi_{i,j} + \psi_{i,j-1}}{2} (\lambda^- \mathbf{K}^T + \lambda^+ \mathbf{K}) : (\boldsymbol{\delta}_r \boldsymbol{\delta}_\phi)_{i,j-\frac{1}{2}} - \frac{D_r}{\sin \theta_i} \frac{\psi_{i,j} - \psi_{i,j-1}}{\Delta\phi} + \left(\sum_l \beta_l (\mathbf{e}_l \cdot \boldsymbol{\delta}_r) (\mathbf{e}_l \cdot \boldsymbol{\delta}_\phi) \right)_{i,j-\frac{1}{2}} \right) \Delta\theta$$

and

$$f_{ij}^E = \left(\frac{\psi_{i,j+1} + \psi_{i,j}}{2} (\lambda^- \mathbf{K}^T + \lambda^+ \mathbf{K}) : (\boldsymbol{\delta}_r \boldsymbol{\delta}_\phi)_{i,j-\frac{1}{2}} - \frac{D_r}{\sin \theta_i} \frac{\psi_{i,j+1} - \psi_{i,j}}{\Delta\phi} + \left(\sum_l \beta_l (\mathbf{e}_l \cdot \boldsymbol{\delta}_r) (\mathbf{e}_l \cdot \boldsymbol{\delta}_\phi) \right)_{i,j+\frac{1}{2}} \right) \Delta\theta.$$

Similar as in the case of the north and south fluxes we have

$$\begin{aligned}
\sum_{i,j} (f^W + f^E)_{i,j} &= \sum_{i,j} [f_{i,j}^W] + \sum_{i,j} [f_{i,j}^E] \\
&= \sum_i \left[\sum_{j=1}^{n_\phi} [f_{i,j}^W] + \sum_{j=1}^{n_\phi} [f_{i,j}^E] \right] \\
&= \sum_i \left[\sum_{j=1}^{n_\phi} [f_{i,j}^W] + \sum_{j-1=1}^{n_\phi} [f_{i,j-1}^E] \right] \\
&= \sum_i \left[\sum_{j=1}^{n_\phi} [f_{i,j}^W] - \sum_{j=2}^{n_\phi+1} [f_{i,j}^W] \right] \\
&= \sum_i [f_{i,1}^W - f_{n_\phi+1,1}^W]
\end{aligned}$$

We notice that

$$\psi_{i,0} = \psi_{i,n_\phi}, \quad \psi_{i,n_\phi+1} = \psi_{i,1}, \quad (\boldsymbol{\delta}_r)_{i,\frac{1}{2}} = (\boldsymbol{\delta}_r)_{i,n_\phi+\frac{1}{2}}, \quad (\boldsymbol{\delta}_\phi)_{i,\frac{1}{2}} = (\boldsymbol{\delta}_\phi)_{i,n_\phi+\frac{1}{2}}$$

wherewith

$$f_{i,1}^W = f_{n_\phi+1,1}^W \Rightarrow \sum_i [f_{i,1}^W - f_{n_\phi+1,1}^W] = 0$$

and thus the sum of the fluxes at time zero is indeed zero. As the beformentioned procedure is independent of time, it immediately follows that

$$\forall k \quad \sum_{i,j} (f^N + f^W + f^S + f^E)_{i,j}^k = 0$$

and so

$$2 \sum_{i,j} \psi_{i,j}^{k+1} |S_i| = 2 \sum_{i,j} [\psi_{i,j}^k |S_i|] - 2\Delta t \sum_{i,j} (f^N + f^W + f^S + f^E)_{i,j}^k = 1$$

given that

$$2 \sum_{i,j} [\psi_{i,j}^k |S_i|] = 1,$$

which concludes our induction proof. The only condition that remains to be satisfied is the nonnegativity of ψ . \square

7.4.3.3 Nonnegativity

Constructing a proof that the solutions of (7.20) are nonnegative is rather cumbersome. Such a proof will be omitted. In the particular case that $D_r = 0$, as also treated analytically in Section 7.2, such a proof is constructed by proving the convergence of the numerical solution to the analytic solution. Convergence of (7.20) is in this case proven by consistency, stability and the fundamental theorem of numerical methods for differential equations. These issues are treated thoroughly in Subsections 7.4.5 and 7.4.6.

For now, we assume that the nonnegativity is conserved and thus (7.20) suffices to all the conditions as long as n_ϕ is even. However, to solve the scheme uniquely we still need initial and boundary conditions.

7.4.4 Initial and boundary conditions

To solve

$$\psi_{i,j}^{k+1} = \psi_{i,j}^k - \frac{\Delta t}{|S_i|} (f^N + f^W + f^S + f^E)_{i,j}^k$$

uniquely we need an IC ψ^0 and BCs for f_{ij}^N when $i = 1$, for f_{ij}^S when $i = n_\theta$, for f_{ij}^W when $j = 1$ and for f_{ij}^E when $j = n_\phi$. The boundaries are depicted in Figure 7.4.

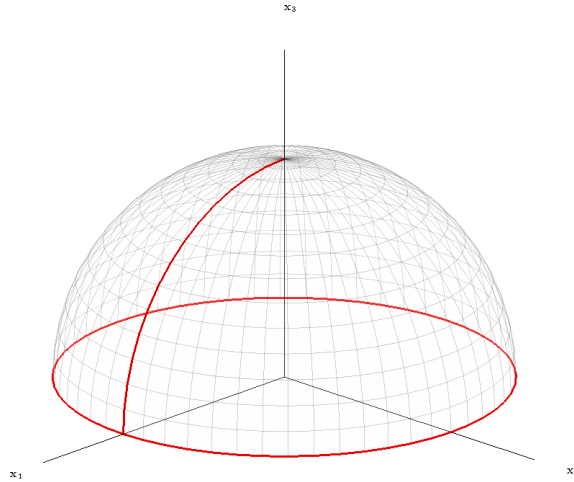


Figure 7.4: boundaries of the domain in question.

In practical situations of injection molding, one can assume that the fibers are initially more or less randomly distributed in the flow. This means that the probability density is the same for each direction, which implies that $\psi = \text{constant}$. We obtain

$$\int_S \psi d^2 \mathbf{p} = \psi \int_S d^2 \mathbf{p} = \psi 4\pi = 1$$

which implies that $\psi = \frac{1}{4\pi}$. Dividing S into finite elements, the discrete analogue is (7.22)

$$\forall k \quad 2 \sum_{i,j} \psi_{i,j}^k |S_i| = 1.$$

As in the continuous case, we must have that $\mathbb{P}(P \in S_{ij}, t)$ is proportional to the size of S_{ij} , so

$$\forall k \quad \mathbb{P}(P \in S_{ij}, t_k) = \psi_{i,j}^k |S_i| \propto |S_i|.$$

This is already the case, so that taking $\psi_{i,j}^0$ constant yields

$$2 \sum_{i,j} \psi_{i,j}^0 |S_i| = 1 \quad \Leftrightarrow \quad \psi_{i,j}^0 \cdot 2 \sum_{i,j} |S_i| = 1 \quad \Leftrightarrow \quad \psi_{i,j}^0 = \frac{1}{4\pi},$$

wherewith we have obtained the uniform initial condition.

To study the effect of the initial condition on the progression of the probability density in both space and time, it is also interesting to consider alternative, nonuniform ICs. To this end we construct an IC of the form

$$\psi_{i,j}^0 = a \cdot (\sin(\theta_i - b))^{2d} (\cos(\phi_j - c))^{2e} + f, \quad a > 0, \quad b \in \left[0, \frac{\pi}{2}\right], \quad c \in [0, 2\pi), \quad d, e \in \mathbb{Z}^+, \quad f \geq 0. \quad (7.23)$$

Note that the constants a , b , c , d , e and f are certainly not unbounded. We must still have that (7.22) holds. This IC sets a lower bound f , an upper bound $f + a$, minima at $\theta = b$, $\phi \in \{\frac{\pi}{2} + c, \frac{3\pi}{2} + c\}$ and the maxima at $\theta = \frac{\pi}{2} + b$ and $\phi \in \{c, \pi + c\}$.

For the boundary conditions we consider the fluxes

$$f_{i,j}^N = - \left(\frac{\psi_{i,j} + \psi_{i-1,j}}{2} (\lambda^- \mathbf{K}^T + \lambda^+ \mathbf{K}) : (\boldsymbol{\delta}_r \boldsymbol{\delta}_\theta)_{i-\frac{1}{2},j} - D_r \frac{\psi_{i,j} - \psi_{i-1,j}}{\Delta\theta} + \left(\sum_l \beta_l (\mathbf{e}_l \cdot \boldsymbol{\delta}_r) (\mathbf{e}_l \cdot \boldsymbol{\delta}_\theta) \right)_{i-\frac{1}{2},j} \right) \Delta\phi \sin \theta_{i-\frac{1}{2}} \quad (7.24)$$

$$f_{i,j}^S = \left(\frac{\psi_{i+1,j} + \psi_{i,j}}{2} (\lambda^- \mathbf{K}^T + \lambda^+ \mathbf{K}) : (\boldsymbol{\delta}_r \boldsymbol{\delta}_\theta)_{i+\frac{1}{2},j} - D_r \frac{\psi_{i+1,j} - \psi_{i,j}}{\Delta\theta} + \left(\sum_l \beta_l (\mathbf{e}_l \cdot \boldsymbol{\delta}_r) (\mathbf{e}_l \cdot \boldsymbol{\delta}_\theta) \right)_{i+\frac{1}{2},j} \right) \Delta\phi \sin \theta_{i+\frac{1}{2}} \quad (7.25)$$

$$f_{i,j}^W = - \left(\frac{\psi_{i,j} + \psi_{i,j-1}}{2} (\lambda^- \mathbf{K}^T + \lambda^+ \mathbf{K}) : (\boldsymbol{\delta}_r \boldsymbol{\delta}_\phi)_{i,j-\frac{1}{2}} - \frac{D_r}{\sin \theta_i} \frac{\psi_{i,j} - \psi_{i,j-1}}{\Delta\phi} + \left(\sum_l \beta_l (\mathbf{e}_l \cdot \boldsymbol{\delta}_r) (\mathbf{e}_l \cdot \boldsymbol{\delta}_\phi) \right)_{i,j-\frac{1}{2}} \right) \Delta\theta \quad (7.26)$$

$$f_{i,j}^E = \left(\frac{\psi_{i,j+1} + \psi_{i,j}}{2} (\lambda^- \mathbf{K}^T + \lambda^+ \mathbf{K}) : (\boldsymbol{\delta}_r \boldsymbol{\delta}_\phi)_{i,j+\frac{1}{2}} - \frac{D_r}{\sin \theta_i} \frac{\psi_{i,j+1} - \psi_{i,j}}{\Delta\phi} + \left(\sum_l \beta_l (\mathbf{e}_l \cdot \boldsymbol{\delta}_r) (\mathbf{e}_l \cdot \boldsymbol{\delta}_\phi) \right)_{i,j+\frac{1}{2}} \right) \Delta\theta \quad (7.27)$$

At the boundary $i = 1$ we have that the north fluxes (7.24) contains the factor $\sin \theta_{1-\frac{1}{2}} = \sin \theta_{\frac{1}{2}} = \sin 0 = 0$ and therefore $f_{1,j}^N = 0$.

At the boundary $i = n_\theta$ the south fluxes (7.25) uses

$$\sin \theta_{n_\theta+\frac{1}{2}} = \sin \frac{\pi}{2} = 1, \quad \psi_{n_\theta+1,j} = \psi_{n_\theta,j+\frac{n_\phi}{2}}.$$

These are element of the interior domain and thus we have obtained the BC for the south fluxes at the south boundary.

The BCs for the west and east fluxes (7.26) and (7.27) respectively, follow from periodicity in j

$$\psi_{i,0}^k = \psi_{i,n_\phi}^k, \quad \psi_{i,n_\phi+1}^k = \psi_{i,1}^k.$$

Herewith, a unique solution of (7.20) can be calculated.

7.4.5 The modified equation, local truncation error and consistency

It remains to prove the convergence of the numerical solution to the analytic solution. According to the fundamental theorem of numerical methods for differential equations, it suffices to prove consistency and stability of (7.20).

Theorem 7.1. *The fundamental theorem of numerical methods for differential equations states*

$$\text{consistency} + \text{stability} \Leftrightarrow \text{convergence}.$$

The proof of this theorem differs per context and will be omitted. The proof for the test equation can be found in [21]. The theorem's reference also differs per context. For linear PDEs it is referred to as the Lax equivalence theorem and for ODEs it is referred to as Dahlquist's equivalence theorem [17].

It thus remains to prove the consistency and stability of (7.20). We will begin with proving consistency for the linear case $\kappa = 1$. A proof of consistency for the case $\kappa \neq 1$ is omitted as its construction is rather cumbersome. Stability will be proven in Subsection 7.4.6.

By doing the modified equation analysis [17] we recover the local truncation error (LTE) and can determine if the numerical scheme (7.20) is consistent with the exact form (7.1). In addition, the modified equation reveals information on how the numerical solution will behave, as we will show.

Property 7.6. *The numerical scheme (7.20) is consistent with (3.14) of the orders one and two for t and θ, ϕ respectively. The LTE is $O(\Delta t) + O((\Delta\theta)^2) + O((\Delta\phi)^2)$.*

Proof. Recall (7.20)

$$\psi_{i,j}^{k+1} = \psi_{i,j}^k - \frac{\Delta t}{|S_i|} (f^W + f^N + f^S + f^E)_{ij}^k \quad (7.28)$$

with the fluxes according to (7.26), (7.24), (7.25) and (7.27). The modified equation is the equation is satisfied exactly by the solution constructed by (7.28). To this end, we widely use Taylor expansions, starting with

$$\psi_{i,j}^{k+1} = \sum_{p=0}^{\infty} \frac{(\Delta t)^p}{p!} \left(\frac{\partial^p \psi}{\partial t^p} \right)_{i,j}^k.$$

We can now write

$$\begin{aligned} \sum_{p=0}^{\infty} \frac{(\Delta t)^p}{p!} \left(\frac{\partial^p \psi}{\partial t^p} \right)_{i,j}^k &= \psi_{i,j}^k - \frac{\Delta t}{|S_i|} (f^W + f^N + f^S + f^E)_{ij}^k \\ -|S_i| \sum_{p=1}^{\infty} \frac{(\Delta t)^{p-1}}{p!} \left(\frac{\partial^p \psi}{\partial t^p} \right)_{i,j}^k &= (f^W + f^N + f^S + f^E)_{ij}^k \end{aligned} \quad (7.29)$$

For the sake of notation, we introduce

$$\begin{aligned} a_{i,j\pm\frac{1}{2}} &:= \frac{(\lambda^- \mathbf{K}^T + \lambda^+ \mathbf{K}) : (\boldsymbol{\delta}_r \boldsymbol{\delta}_\phi)_{i,j\pm\frac{1}{2}} \Delta\theta}{2} \\ b_i &:= \frac{D_r \Delta\theta}{\Delta\phi \sin \theta_i} \\ c_{i,j\pm\frac{1}{2}} &:= \frac{(\lambda^- \mathbf{K}^T + \lambda^+ \mathbf{K}) : (\boldsymbol{\delta}_r \boldsymbol{\delta}_\theta)_{i\pm\frac{1}{2},j} \Delta\phi \sin \theta_{i\pm\frac{1}{2}}}{2} \\ d_{i\pm\frac{1}{2}} &:= \frac{D_r \Delta\phi \sin \theta_{i\pm\frac{1}{2}}}{\Delta\theta}. \end{aligned}$$

Note that these coefficients already contain either $\Delta\theta$, $\Delta\phi$ or both, which will be important in a moment for determining the order of accuracy. With this notation and Taylor expansions around (θ_i, ϕ_j) we can

now write the addition of the fluxes as

$$\begin{aligned}
(f^W + f^N + f^S + f^E)_{ij}^k &= -a_{i,j-\frac{1}{2}}(\psi_{i,j} + \psi_{i,j-1}) + b_i(\psi_{i,j} - \psi_{i,j-1}) \\
&\quad -c_{i-\frac{1}{2},j}(\psi_{i,j} + \psi_{i-1,j}) + d_{i-\frac{1}{2},j}(\psi_{i,j} - \psi_{i-1,j}) \\
&\quad +c_{i+\frac{1}{2},j}(\psi_{i+1,j} + \psi_{i,j}) - d_{i+\frac{1}{2},j}(\psi_{i+1,j} - \psi_{i,j}) \\
&\quad +a_{i,j+\frac{1}{2}}(\psi_{i,j+1} + \psi_{i,j}) - b_i(\psi_{i,j+1} - \psi_{i,j}) \\
&= -a_{i,j-\frac{1}{2}} \left(2\psi_{i,j} + \sum_{p=1}^{\infty} \left[\frac{(-\Delta\phi)^p}{p!} \left(\frac{\partial^p \psi}{\partial \phi^p} \right)_{i,j} \right] \right) - b_i \left(\sum_{p=1}^{\infty} \left[\frac{(-\Delta\phi)^p}{p!} \left(\frac{\partial^p \psi}{\partial \phi^p} \right)_{i,j} \right] \right) \\
&\quad -c_{i-\frac{1}{2},j} \left(2\psi_{i,j} + \sum_{p=1}^{\infty} \left[\frac{(-\Delta\theta)^p}{p!} \left(\frac{\partial^p \psi}{\partial \theta^p} \right)_{i,j} \right] \right) - d_{i-\frac{1}{2},j} \left(\sum_{p=1}^{\infty} \left[\frac{(-\Delta\theta)^p}{p!} \left(\frac{\partial^p \psi}{\partial \theta^p} \right)_{i,j} \right] \right) \\
&\quad +c_{i+\frac{1}{2},j} \left(\sum_{p=1}^{\infty} \left[\frac{(\Delta\theta)^p}{p!} \left(\frac{\partial^p \psi}{\partial \theta^p} \right)_{i,j} \right] + 2\psi_{i,j} \right) - d_{i+\frac{1}{2},j} \left(\sum_{p=1}^{\infty} \left[\frac{(\Delta\theta)^p}{p!} \left(\frac{\partial^p \psi}{\partial \theta^p} \right)_{i,j} \right] \right) \\
&\quad +a_{i,j+\frac{1}{2}} \left(\sum_{p=1}^{\infty} \left[\frac{(\Delta\phi)^p}{p!} \left(\frac{\partial^p \psi}{\partial \phi^p} \right)_{i,j} \right] + 2\psi_{i,j} \right) - b_i \left(\sum_{p=1}^{\infty} \left[\frac{(\Delta\phi)^p}{p!} \left(\frac{\partial^p \psi}{\partial \phi^p} \right)_{i,j} \right] \right).
\end{aligned}$$

For the sake of comparison with (7.1) or more preferably (3.14), we will consider the coefficients per derivative of ψ . Let us start with the original, the zeroth derivative. The coefficient hereof is

$$\begin{aligned}
2(a_{i,j+\frac{1}{2}} - a_{i,j-\frac{1}{2}} + c_{i+\frac{1}{2},j} - c_{i-\frac{1}{2},j}) &= 2 \left(2 \sum_{q \in \{1,3,\dots\}} \left[\frac{(\Delta\phi)^q}{2} \frac{1}{q!} \left(\frac{\partial^q a}{\partial \phi^q} \right)_{i,j} \right] + 2 \sum_{q \in \{1,3,\dots\}} \left[\frac{(\Delta\theta)^q}{2} \frac{1}{q!} \left(\frac{\partial^q c}{\partial \theta^q} \right)_{i,j} \right] \right) \\
&= 2 \left(\Delta\phi \frac{\partial a}{\partial \phi} + \Delta\theta \frac{\partial c}{\partial \theta} \right)_{i,j} + O(\Delta\theta(\Delta\phi)^3) + O((\Delta\theta)^3 \Delta\phi) \\
&= 2 \left(-\frac{3\Delta\theta\Delta\phi \sin(\theta) \mathbf{K} : \boldsymbol{\delta}_r \boldsymbol{\delta}_r}{2} \right)_{i,j} + O(\Delta\theta(\Delta\phi)^3) + O((\Delta\theta)^3 \Delta\phi) \\
&= -|S_i| 3\mathbf{K} : (\boldsymbol{\delta}_r \boldsymbol{\delta}_r)_{i,j} + O(\Delta\theta(\Delta\phi)^3) + O((\Delta\theta)^3 \Delta\phi)
\end{aligned}$$

which is the coefficient for ψ in (3.14) multiplied by $-|S_i|$, which stems from the LHS of (7.29). It stands out that although the conservation of psi has already been proven for (7.28), there is still an error

$$\frac{O(\Delta\theta(\Delta\phi)^3) + O((\Delta\theta)^3 \Delta\phi)}{-|S_i|} = O((\Delta\phi)^2) + O((\Delta\theta)^2)$$

in the coefficient for $\psi_{i,j}^k$. This is still possible because the error is in the local sense, and the conservation of probability is in the global sense. Constructing the modified equation has now determined that (7.28) contains a source or sink error for ψ . Locally, there is a source or sink for the probability density of order $O((\Delta\phi)^2) + O((\Delta\theta)^2)$, which vanishes in the global sense.

We proceed with considering the derivatives in the θ direction. We have

$$\sum_{p=1}^{\infty} \left(-c_{i-\frac{1}{2},j}(-1)^p - d_{i-\frac{1}{2},j}(-1)^p + c_{i+\frac{1}{2},j} - d_{i+\frac{1}{2},j} \right) \frac{(\Delta\theta)^p}{p!} \left(\frac{\partial^p \psi}{\partial \theta^p} \right)_{i,j}.$$

For $p = 1$ we thus have

$$\begin{aligned}
c_{i-\frac{1}{2},j} + d_{i-\frac{1}{2},j} + c_{i+\frac{1}{2},j} - d_{i+\frac{1}{2},j} &= \left(2 \sum_{q \in \{0,2,\dots\}} \left[\left(\frac{\Delta\theta}{2} \right)^q \frac{1}{q!} \frac{\partial^q c}{\partial \theta^q} \right] - 2 \sum_{q \in \{1,3,\dots\}} \left[\left(\frac{\Delta\theta}{2} \right)^q \frac{1}{q!} \frac{\partial^q d}{\partial \theta^q} \right] \right)_{i,j} \\
&= \left(2c - \Delta\theta \frac{\partial d}{\partial \theta} \right)_{i,j} + O((\Delta\theta)^2 \Delta\phi) + O((\Delta\theta)^2 \Delta\phi) \\
&= (\lambda^- \mathbf{K}^T + \lambda^+ \mathbf{K}) : (\boldsymbol{\delta}_r \boldsymbol{\delta}_\theta)_{i,j} \Delta\phi \sin(\theta_i) - D_r \Delta\phi \cos \theta_i + O((\Delta\theta)^2 \Delta\phi).
\end{aligned}$$

Multiplying with $\frac{\Delta\theta}{-|S_i|} = \frac{-1}{\Delta\phi \sin \theta_i}$ we obtain

$$-(\lambda^- \mathbf{K}^T + \lambda^+ \mathbf{K}) : (\boldsymbol{\delta}_r \boldsymbol{\delta}_\theta)_{i,j} + D_r \frac{\cos \theta_i}{\sin \theta_i} + O((\Delta\theta)^2)$$

which resembles the coefficient in (3.14). We conclude that there is also an error of order $O((\Delta\theta)^2)$ with convective behavior in the θ direction.

Taking $p = 2$ results in

$$\begin{aligned} (-c_{i-\frac{1}{2},j} - d_{i-\frac{1}{2}} + c_{i+\frac{1}{2},j} - d_{i+\frac{1}{2}}) \frac{(\Delta\theta)^2}{2} &= \left(2 \sum_{q \in \{1,3,\dots\}} \left[\frac{(\Delta\theta)^{q+2}}{2^{q+1}} \frac{1}{q!} \frac{\partial^q c}{\partial \theta^q} \right] - 2 \sum_{q \in \{0,2,\dots\}} \left[\frac{(\Delta\theta)^{q+2}}{2^{q+1}} \frac{1}{q!} \frac{\partial^q d}{\partial \theta^q} \right] \right)_{i,j} \\ &= (-(\Delta\theta)^2 d)_{i,j} + O((\Delta\theta)^3 \Delta\phi) + O((\Delta\theta)^3 \Delta\phi) \\ &= -D_r \Delta\theta \Delta\phi \sin \theta_i + O((\Delta\theta)^3 \Delta\phi). \end{aligned}$$

Division by $-|S_i|$ gives

$$D_r + O((\Delta\theta)^2).$$

A diffusion error of $O((\Delta\theta)^2)$ is made.

Say we consider the derivatives in the ϕ direction. We have

$$\sum_{p=1}^{\infty} \left(-a_{i,j-\frac{1}{2}} (-1)^p - b_i (-1)^p + a_{i,j+\frac{1}{2}} - b_i \right) \frac{(\Delta\phi)^p}{p!} \left(\frac{\partial^p \psi}{\partial \phi^p} \right)_{i,j}.$$

Say we take $p = 1$, then

$$\begin{aligned} (a_{i,j-\frac{1}{2}} + b_i + a_{i,j+\frac{1}{2}} - b_i) \Delta\phi &= \left(2 \sum_{q \in \{0,2,\dots\}} \left[\left(\frac{\Delta\phi}{2} \right)^q \frac{1}{q!} \frac{\partial^q a}{\partial \phi^q} \right] \right)_{i,j} \Delta\phi \\ &= 2\Delta\phi a_{i,j} + O(\Delta\theta(\Delta\phi)^3) \\ &= \Delta\theta \Delta\phi (\lambda^- \mathbf{K}^T + \lambda^+ \mathbf{K}) : (\boldsymbol{\delta}_r \boldsymbol{\delta}_\theta)_{i,j} + O(\Delta\theta(\Delta\phi)^3). \end{aligned}$$

Division by $-|S_i|$ gives

$$-\frac{(\lambda^- \mathbf{K}^T + \lambda^+ \mathbf{K}) : (\boldsymbol{\delta}_r \boldsymbol{\delta}_\theta)_{i,j}}{\sin \theta_i} + O((\Delta\phi)^2).$$

It can be concluded that there is a convective error of order $O((\Delta\phi)^2)$.

Finally, we consider $p = 2$ and obtain the coefficient

$$\begin{aligned} (-a_{i,j-\frac{1}{2}} - b_i + a_{i,j+\frac{1}{2}} - b_i) \frac{(\Delta\phi)^2}{2} &= \left(2 \sum_{q \in \{1,3,\dots\}} \left[\left(\frac{\Delta\phi}{2} \right)^q \frac{1}{q!} \frac{\partial^q a}{\partial \phi^q} \right] - 2b_i \right)_{i,j} \frac{(\Delta\phi)^2}{2} \\ &= \left(\sum_{q \in \{1,3,\dots\}} \left[\frac{(\Delta\phi)^{q+2}}{2^q} \frac{1}{q!} \frac{\partial^q a}{\partial \phi^q} \right] - \frac{D_r \Delta\theta \Delta\phi}{\sin \theta} \right)_{i,j} \\ &= -\frac{D_r \Delta\theta \Delta\phi}{\sin \theta_i} + O(\Delta\theta(\Delta\phi)^3). \end{aligned}$$

Division by $-|S_i|$ gives

$$\frac{D_r}{\sin^2 \theta_i} + O((\Delta\phi)^2)$$

resulting in a $O((\Delta\phi)^2)$ diffusive error in the ϕ direction. \square

It can be concluded that the LTE is $O(\Delta t) + O((\Delta\theta)^2) + O((\Delta\phi)^2)$ and that (7.28) is consistent with (3.14) of the orders one and two for t and θ, ϕ respectively. The modified equation analysis shows that the scheme induces errors of four different types, namely acceleration, production or vanishing, convection and diffusion. This can help us explain the behavior of the numerical solutions that will be considered in Part II.

To prove the convergence of the numerical solution to the analytic solution, we need stability besides the now proved consistency. The stability is considered in the following subsection.

7.4.6 Stability

7.4.6.1 Analytic stability analysis

To complete the proof of convergence of (7.28) we have to proof the stability. We will construct such a proof for the linear case $\kappa = 1$ in combination with diffusion, so $D_r \neq 0$. A proof for the stability of the nonlinear case $\kappa \neq 1$ will be omitted. Empirical results of the scheme seem to confirm that the stability demands of the nonlinear case are weaker than the for the linear case. This is justifiable as the additional RSC term slows the process down, decreasing the gradients of ψ in time. In general, smaller gradients allow larger time steps. In other words, the stability demands are weakened.

In Subsection 9.4.1 and Section 10.4, examples of flow fields are given wherefore it is impossible to obtain a solution on a finite grid as ψ is diverges to infinity. It is thus impossible to prove stability of the numerical scheme with $D_r = 0$ for all flow fields. The case $D_r = 0$ is therefore not considered.

Both Von Neumann and Gershgorin stability analyses were used. The latter proves to give the most results without too much effort, in contrast with the, in this case, cumbersome Von Neumann stability analysis. Indeed, the Von Neumann analysis is omitted.

For the sake of clarity, we recall Gershgorin's circle theorem.

Theorem 7.2. *Say we consider $\mathbf{C} \in \mathbb{C}^{n \times n}$ with unknown eigenpairs $(\lambda_l, \mathbf{e}_l), l \in \{1, 2, \dots, n\}$. We then have that*

$$\forall l \quad \exists k \quad : \quad |\lambda_l - C_{kk}| \leq \sum_{j \neq k, j=1}^n |C_{kj}|. \quad (7.30)$$

Proof. For the eigenpairs we have

$$\forall l \quad \lambda_l \mathbf{e}_l = \mathbf{C} \cdot \mathbf{e}_l \quad \Leftrightarrow \quad \forall i, l \quad \lambda_l (\mathbf{e}_l)_i = \sum_{j=1}^n C_{ij} (\mathbf{e}_l)_j. \quad (7.31)$$

We know that

$$\forall l \quad \exists k \quad : \quad |(\mathbf{e}_l)_k| \geq |(\mathbf{e}_l)_i|, \quad (\mathbf{e}_l)_k \neq 0$$

otherwise $\mathbf{e}_l = \mathbf{0}$ which is not allowed for an eigenvector. Taking $i = k$, it follows from (7.31) that

$$\forall l \quad \lambda_l - C_{kk} = \sum_{j \neq k, j=1}^n C_{kj} \frac{(\mathbf{e}_l)_j}{(\mathbf{e}_l)_k}.$$

Taking the absolute value on both sides and applying the triangle inequality on the RHS we obtain (7.30) □

Gershgorin's circle theorem states that every eigenvalue $\lambda_l \in \sigma(\mathbf{C})$ is contained in at least one Gershgorin disc with its center at C_{kk} and a radius

$$R_k := \sum_{j \neq k, j=1}^n C_{kj}$$

in the complex plane. For stability, we need that $\forall l \quad |\lambda_l| \leq 1$ for the eigenvalues of the system matrix \mathbf{C} . If in addition $C_{kk} \in \mathbb{R}$, only the real line matters and (7.30) reduces to

$$C_{kk} - R_k \geq -1 \quad \wedge \quad C_{kk} + R_k \leq 1. \quad (7.32)$$

Property 7.7. *The scheme (7.28) is stable under the condition*

$$\frac{\Delta t}{(\Delta \theta)^2 (\Delta \phi)^2} \leq \frac{1}{8D_r} \quad (7.33)$$

when $D_r = O((\Delta \theta)^m), m < 2$.

Proof. When considering the case that $D_r \neq 0, D_r = O((\Delta \theta)^m), m < 2$, the stability criterium is dominated by the singularity of the analytical equation for ψ as mentioned in Subsection 3.3.3. Considering

the top 'ring' of cells wherefore $(\theta_i, \phi_j) = (\frac{\Delta\theta}{2}, \phi_j)$, the terms with a sine in the denominator dominate the equation. Herewith, the scheme reduces to

$$\begin{aligned}\psi_{i,j}^{k+1} &= \psi_{i,j}^k - \frac{\Delta t}{\Delta\theta\Delta\phi \sin \frac{\Delta\theta}{2}} \left(\frac{D_r}{\sin \frac{\Delta\theta}{2}} \frac{\psi_{i,j}^k - \psi_{i,j-1}^k}{\Delta\phi} \Delta\theta - \frac{D_r}{\sin \frac{\Delta\theta}{2}} \frac{\psi_{i,j+1}^k - \psi_{i,j}^k}{\Delta\phi} \Delta\theta \right) \\ &\approx \psi_{i,j}^k + \frac{4D_r\Delta t}{(\Delta\theta)^2} \frac{\psi_{i,j+1}^k - 2\psi_{i,j}^k + \psi_{i,j-1}^k}{(\Delta\phi)^2}\end{aligned}$$

where we used $\sin \frac{\Delta\theta}{2} \approx \frac{\Delta\theta}{2}$. Using Gershgorin's circle theorem with $C_{kk} \in \mathbb{R}$ we get the inequalities

$$1 - \frac{8D_r\Delta t}{(\Delta\theta)^2(\Delta\phi)^2} + \left| \frac{8D_r\Delta t}{(\Delta\theta)^2(\Delta\phi)^2} \right| \leq 1$$

$$1 \leq 1$$

and

$$1 - \frac{8D_r\Delta t}{(\Delta\theta)^2(\Delta\phi)^2} - \left| \frac{8D_r\Delta t}{(\Delta\theta)^2(\Delta\phi)^2} \right| \geq -1$$

$$\frac{\Delta t}{(\Delta\theta)^2(\Delta\phi)^2} \leq \frac{1}{8D_r}.$$

The former is always satisfied so the latter is the stability condition in question. \square

It can be seen from (7.33) that increasing D_r makes the stability criterium more strict. As the space steps are both raised to the power two, it is easier to make a compromise by increasing the space steps than it is by decreasing the time step. However, a fine grid is also preferred as the LTE should not be too large.

If $D_r = O((\Delta\theta)^m)$, $m \geq 2$, also other terms of R_k become significant. The reason hereof is that

$$\frac{D_r}{\Delta\theta \sin \theta_i} = \frac{O((\Delta\theta)^m)}{O((\Delta\theta)^2)} = O((\Delta\theta)^{m-2}), \quad m - 2 \geq 0$$

if $\theta_i = \frac{\Delta\theta}{2}$. It is now of the same order as other terms in the sum and is thus not dominating anymore. As the sum merely contains absolute values, the right inequality in (7.30) can not be satisfied anymore. This does not imply that stability is impossible, but it does imply that it is impossible for the Gershgorin discs to be contained within the unit circle. In turn, this is an indication that stability is difficult to achieve.

The Von Neumann and Gershgorin stability analyses fail give a sufficient result when $D_r = O((\Delta\theta)^m)$, $m \geq 2$. We therefore do simulations with $m < 2$ so that the stability criterium from Property 7.7 can be used.

7.4.6.2 Numerical stability analysis

Aside from the analytical argument we have obtained in the previous section, the stability can also be determined by calculating the largest absolute eigenvalue of the system matrix \mathbf{C} . This can be done efficiently by the use of the power method and inverse power method to determine the largest and smallest eigenvalue respectively.

The power method works as follows. Say we consider a matrix $\mathbf{C} \in \mathbb{C}^{n \times n}$ with unknown eigenpairs $(\lambda_l, \mathbf{e}_l)$, $l \in \{1, 2, \dots, n\}$. The eigenvectors are normalized and span $\mathbb{C}^{n \times n}$. Say we choose an initial vector $\mathbf{z}_0 \in \mathbb{C}^n$. This vector can be written as

$$\mathbf{z}_0 = \sum_{i=1}^n \alpha_i(\mathbf{e}_i)_i$$

as the eigenvectors span the space in question. We have

$$\begin{aligned}\mathbf{z}_j &= \mathbf{C}^j \cdot \mathbf{z}_0 \\ &= \mathbf{C}^j \cdot \sum_{i=1}^n \alpha_i(\mathbf{e}_i)_i \\ &= \sum_{i=1}^n \alpha_i \lambda_i^j (\mathbf{e}_i)_i.\end{aligned}$$

Say $\lambda_1 = \lambda_2 = \dots = \lambda_m, m < n$ are the largest eigenvalues of \mathbf{C} . Then

$$\begin{aligned} \mathbf{z}_j &= \sum_{i=1}^m [\alpha_i \lambda_i^j (\mathbf{e}_l)_i] + \sum_{i=m+1}^n [\alpha_i \lambda_i^j (\mathbf{e}_l)_i] \\ &= \lambda_1^j \left(\sum_{i=1}^m [\alpha_i (\mathbf{e}_l)_i] + \sum_{i=m+1}^n \left[\alpha_i \underbrace{\left(\frac{\lambda_i}{\lambda_1} \right)^j}_{<1} (\mathbf{e}_l)_i \right] \right). \end{aligned}$$

If $j \uparrow \infty$ then $\mathbf{z}_j \rightarrow \lambda_1^j \left(\sum_{i=1}^m [\alpha_i (\mathbf{e}_l)_i] \right)$ and $\mathbf{z}_{j+1} \rightarrow \lambda_1^{j+1} \left(\sum_{i=1}^m [\alpha_i (\mathbf{e}_l)_i] \right)$ so that any component of the quotient $\frac{\mathbf{z}_{j+1}}{\mathbf{z}_j} \rightarrow \lambda_1$. To avoid excessive increases or decreases between two successive iterates, the new vector is normalized each iteration.

The largest eigenvalue is now obtained. The smallest eigenvalue is still unknown. The inverse power method solves this problem. It merely applies the power method to the inverse of \mathbf{C} , denoted by $\mathbf{C}^{-1} \in \mathbb{C}^{n \times n}$. It works as follows. We know that

$$\mathbf{C} = \mathbf{V} \mathbf{D} \mathbf{C}^{-1}$$

where \mathbf{D} is a matrix with the eigenvalues as the only nonzero components on the diagonal. Matrix \mathbf{V} contains the corresponding eigenvectors. Consequently, we have for the inverse

$$\mathbf{C}^{-1} = (\mathbf{V} \mathbf{D} \mathbf{C}^{-1})^{-1} = \mathbf{V} \mathbf{D}^{-1} \mathbf{V}^{-1}$$

wherefrom it follows that the eigenvalues of \mathbf{C}^{-1} are the reciprocals of the eigenvalues of \mathbf{C} . Thus applying the power method to \mathbf{C}^{-1} gives the largest eigenvalue of \mathbf{C}^{-1} which is the smallest eigenvalue of \mathbf{C} . In every iteration, \mathbf{C}^{-1} is applied on a vector. Calculating the LU decomposition of \mathbf{C} , or the Cholesky decomposition when \mathbf{C} is symmetric, and subsequently doing a forward backward substitution increases the efficiency of the process.

The smallest and largest eigenvalues of \mathbf{C} can now be found. If the largest absolute eigenvalue is smaller or equal to one, the numerical scheme is stable.

Chapter 8

The RSC tensor form

8.1 Introduction

In this chapter we analyze the tensor form of the RSC model [13] as constructed in Chapter 5. We analyze both the intact as well as the decomposed form. We consider the different contributions of the equations in Section 8.2. Dimensional analysis gives some information about the characters of the equations in Section 8.3. In a particular case of the RSC model, there is a known analytical solution in Section 8.4. In Section 8.5 we construct the numerical scheme to solve the RSC equation. The scheme is checked for the conservation of the important properties of \mathbf{A} . Consistency is proven and a stability analysis is made to imply convergence under certain conditions.

8.2 Interpretation

We recall the tensor RSC model in intact form (5.13)

$$\dot{\mathbf{A}} = \mathbf{W} \cdot \mathbf{A} - \mathbf{A} \cdot \mathbf{W} + \xi \{ \mathbf{D} \cdot \mathbf{A} + \mathbf{A} \cdot \mathbf{D} - 2[\mathbb{A} + (1 - \kappa)(\mathbb{L} - \mathbb{M} : \mathbb{A})] : \mathbf{D} \} + 2\kappa C_I \dot{\gamma}(\mathbf{I} - 3\mathbf{A}). \quad (8.1)$$

and in decomposed form (5.2), (5.10)

$$\begin{aligned} \dot{\lambda}_i &= 2\xi(\lambda_i \mathbf{D} : \mathbf{e}_i \mathbf{e}_i - \mathbf{e}_i \mathbf{e}_i : \mathbb{A} : \mathbf{D}) + 2C_I \dot{\gamma}(1 - 3\lambda_i) \\ \dot{\mathbf{e}}_i &= \mathbf{W} \cdot \mathbf{e}_i + \xi \frac{\lambda_2 + \lambda_1 - 4\bar{A}_{1212}}{\lambda_2 - \lambda_1} (\mathbf{D} : \mathbf{e}_1 \mathbf{e}_2) (\delta_{2i} \mathbf{e}_1 - \delta_{1i} \mathbf{e}_2) \\ &\quad + \xi \frac{\lambda_3 + \lambda_2 - 4\bar{A}_{2323}}{\lambda_3 - \lambda_2} (\mathbf{D} : \mathbf{e}_2 \mathbf{e}_3) (\delta_{3i} \mathbf{e}_2 - \delta_{2i} \mathbf{e}_3) \\ &\quad + \xi \frac{\lambda_1 + \lambda_3 - 4\bar{A}_{3131}}{\lambda_1 - \lambda_3} (\mathbf{D} : \mathbf{e}_3 \mathbf{e}_1) (\delta_{1i} \mathbf{e}_3 - \delta_{3i} \mathbf{e}_1). \end{aligned} \quad (8.2)$$

In this equation, tensors \mathbf{D} and \mathbf{W} and scalar $\dot{\gamma}$, as defined in Subsections 3.2.2 and 3.3.1 are functions of the velocity field \mathbf{v} , in particular on its gradient $\nabla \mathbf{v}$. In general, the velocity field depends on both space and time. We restrict ourselves to the consideration of flow fields that only depend linearly at most on the space variables and on time in any order. These flows are also referred to as homogeneous flow fields. As a consequence, $\nabla \mathbf{v}$ is constant in space, and thus so are \mathbf{D} , \mathbf{W} and $\dot{\gamma}$. The fourth order tensors \mathbb{L} and \mathbb{M} depend merely on \mathbf{A} by definition. Due to the closure relation, \mathbb{A} also depends only on \mathbf{A} . The ξ , κ and C_I are constants. Equation (8.1) is thus an ordinary differential equation (ODE) for $\mathbf{A}(t)$ when considering homogeneous flow fields. It is not linear in \mathbf{A} though. The fourth order tensor \mathbb{L} depends on the eigenvalues of \mathbf{A} . The eigenvalues λ originate from the cubic characteristic polynomial of \mathbf{A} . Using Cardano's formula gives solutions for λ , which are nonlinear in the components of \mathbf{A} . Moreover, the closure relation for \mathbb{A} does not have to depend linearly on \mathbf{A} . In combination with an initial condition (IC)

$$\mathbf{A}(t_0) = \mathbf{A}_{t_0} \quad (8.3)$$

we have an initial value problem (IVP). In short, we write

$$\dot{\mathbf{A}}(t) = \mathbf{F}(\mathbf{A}(t), t), \quad \mathbf{A}(t_0) = \mathbf{A}_{t_0}. \quad (8.4)$$

The intact form (8.1) can be split up in three different contributions.

- LD: $\mathbf{W} \cdot \mathbf{A} - \mathbf{A} \cdot \mathbf{W} + \xi \{ \mathbf{D} \cdot \mathbf{A} + \mathbf{A} \cdot \mathbf{D} - 2\mathbb{A} : \mathbf{D} \}$.
- FFI: $2C_I \dot{\gamma}(\mathbf{I} - 3\mathbf{A})$.
- RSC: $2(\kappa - 1)(\mathbb{L} - \mathbb{M} : \mathbb{A}) : \mathbf{D} + 2(\kappa - 1)C_I \dot{\gamma}(\mathbf{I} - 3\mathbf{A})$.

Doing this for the eigenvalues of the decomposed form (8.2) gives the following.

- LD: $2\xi(\lambda_i \mathbf{D} : \mathbf{e}_i \mathbf{e}_i - \mathbf{e}_i \mathbf{e}_i : \mathbb{A} : \mathbf{D})$
- FFI: $2C_I \dot{\gamma}(1 - 3\lambda_i)$
- RSC: $2\xi(\kappa - 1)(\lambda_i \mathbf{D} : \mathbf{e}_i \mathbf{e}_i - \mathbf{e}_i \mathbf{e}_i : \mathbb{A} : \mathbf{D}) + 2C_I \dot{\gamma}(\kappa - 1)(1 - 3\lambda_i)$

Considering the LD contribution we see from the intact form that the vorticity and strain has been 'inherited' from Jeffery's equation. The straining is proportional to ξ . With the exception of the last term, it is linear in \mathbf{A} . This is certainly not the case for the LD contribution to the eigenvalues. It depends linearly on the eigenvalue that is considered but also on the tensor product $\mathbf{e}_i \mathbf{e}_i$ which depends nonlinearly on all the eigenvalues. This sets the tendency that solving the intact form will be easier than solving the decomposed form. In addition, it stands out that the vorticity is only present in the eigenvectors. This has an interesting consequence, as we will see in Section 8.4. We see again that the straining is proportional to ξ and \mathbf{D} .

The FFI contribution 'pulls' the tensor component component in question to zero if it is a off diagonal component, and to one third if it is a diagonal component. The $\mathbf{A} \rightarrow \frac{\mathbf{I}}{3}$ represents the random distribution. The strength of the FFI is proportional to $C_I \dot{\gamma}$. A similar effect is observed for the eigenvalues: they are pulled to one third. As a consequence, the eigenvectors are not uniquely defined anymore, as explained in Section 4.4 after Property 4.7.

The RSC contribution reduces the LD and FFI with its first and second term respectively. Thses reductions are proportional to κ . The effect in the eigenvalues is similar.

8.3 Dimensional analysis

For the dimensional analysis of (8.1) we recall the quantities

$$m = \sum_{i,j} |\kappa_{ij}|, \quad \bar{\mathbf{W}} = \frac{\mathbf{W}}{m}, \quad \bar{\mathbf{D}} = \frac{\mathbf{D}}{m}, \quad \bar{\dot{\gamma}} = \frac{\dot{\gamma}}{m}, \quad \bar{t} = m \cdot t$$

from Section 7.3. Substitution gives

$$m \dot{\mathbf{A}} = m \bar{\mathbf{W}} \cdot \mathbf{A} - \mathbf{A} \cdot m \bar{\mathbf{W}} + \xi \{ m \bar{\mathbf{D}} \cdot \mathbf{A} + \mathbf{A} \cdot m \bar{\mathbf{D}} - 2[\mathbb{A} + (1 - \kappa)(\mathbb{L} - \mathbb{M} : \mathbb{A})] : m \bar{\mathbf{D}} \} + 2\kappa C_I \bar{\dot{\gamma}} m (\mathbf{I} - 3\mathbf{A})$$

which after division of m gives

$$\dot{\mathbf{A}} = \bar{\mathbf{W}} \cdot \mathbf{A} - \mathbf{A} \cdot \bar{\mathbf{W}} + \xi \{ \bar{\mathbf{D}} \cdot \mathbf{A} + \mathbf{A} \cdot \bar{\mathbf{D}} - 2[\mathbb{A} + (1 - \kappa)(\mathbb{L} - \mathbb{M} : \mathbb{A})] : \bar{\mathbf{D}} \} + 2\kappa C_I \bar{\dot{\gamma}} (\mathbf{I} - 3\mathbf{A}).$$

From the latter we see that if we consider \mathbf{A} as a function of the scaled time $m \cdot t$ instead of the regular time t , the solution varies less under the strength of the flow field. In particular, if \mathbf{K} contains merely diagonal or off diagonal components, then $m = \dot{\gamma}$ so that $\bar{\dot{\gamma}} = 1$. This makes the solution invariant under the change of the shear or stress rate.

In an analogous way, the decomposed form becomes

$$\begin{aligned} \dot{\lambda}_i &= 2\xi (\lambda_i \bar{\mathbf{D}} : \mathbf{e}_i \mathbf{e}_i - \mathbf{e}_i \mathbf{e}_i : \mathbb{A} : \bar{\mathbf{D}}) + 2C_I \bar{\dot{\gamma}} (1 - 3\lambda_i) \\ \dot{\mathbf{e}}_i &= \bar{\mathbf{W}} \cdot \mathbf{e}_i + \xi \frac{\lambda_2 + \lambda_1 - 4\bar{A}_{1212}}{\lambda_2 - \lambda_1} (\bar{\mathbf{D}} : \mathbf{e}_1 \mathbf{e}_2) (\delta_{2i} \mathbf{e}_1 - \delta_{1i} \mathbf{e}_2) \\ &\quad + \xi \frac{\lambda_3 + \lambda_2 - 4\bar{A}_{2323}}{\lambda_3 - \lambda_2} (\bar{\mathbf{D}} : \mathbf{e}_2 \mathbf{e}_3) (\delta_{3i} \mathbf{e}_2 - \delta_{2i} \mathbf{e}_3) \\ &\quad + \xi \frac{\lambda_1 + \lambda_3 - 4\bar{A}_{3131}}{\lambda_1 - \lambda_3} (\bar{\mathbf{D}} : \mathbf{e}_3 \mathbf{e}_1) (\delta_{1i} \mathbf{e}_3 - \delta_{3i} \mathbf{e}_1). \end{aligned}$$

Similar results hold: setting out the eigenpairs against the scaled time $m \cdot t$ instead of against the regular time t makes the solution less variant under the strength of the flow field and invariant if \mathbf{K} contains only diagonal or off diagonal components.

8.4 Analytically solvable case

In a certain case, the IVP (8.4) is analytically solvable. Such a solution provides insight in the behavior of the ODE and a check for numerical approaches.

Say the length to diameter ratio of the fibers is $r_e = \frac{l}{d} = 1$, then $\xi = \frac{r_e^2 - 1}{r_e^2 + 1} = 0$. Filling this in in (8.2) gives

$$\begin{aligned} \dot{\lambda}_i &= 2C_I \dot{\gamma} \kappa (1 - 3\lambda_i) \\ \dot{\mathbf{e}}_i &= \mathbf{W} \cdot \mathbf{e}_i. \end{aligned}$$

Assuming furthermore that the velocity field \mathbf{v} is stationary makes \mathbf{W} and $\dot{\gamma}$ independent of t and thus constant. Rewriting the rate equation for λ_i we get

$$\begin{aligned}
\dot{\lambda}_i + 6C_I\dot{\gamma}\kappa\lambda_i &= 2C_I\dot{\gamma}\kappa \\
e^{6C_I\dot{\gamma}\kappa t}(\dot{\lambda}_i + 6C_I\dot{\gamma}\kappa\lambda_i) &= e^{6C_I\dot{\gamma}\kappa t}2C_I\dot{\gamma}\kappa \\
\int_{t'=t_0}^t \frac{d}{dt'} \left(e^{6C_I\dot{\gamma}\kappa t'} \lambda_i dt' \right) &= 2C_I\dot{\gamma}\kappa \int_{t'=t_0}^t e^{6C_I\dot{\gamma}\kappa t'} dt' \\
e^{6C_I\dot{\gamma}\kappa t} \lambda_i(t) - e^{6C_I\dot{\gamma}\kappa t_0} \lambda_i(t_0) &= \frac{1}{3} (e^{6C_I\dot{\gamma}\kappa t} - e^{6C_I\dot{\gamma}\kappa t_0}) \\
\lambda_i(t) &= \frac{1}{3} + \left(\lambda_i(t_0) - \frac{1}{3} \right) e^{6C_I\dot{\gamma}\kappa(t_0-t)}. \tag{8.5}
\end{aligned}$$

Note that

$$\lim_{t \rightarrow \infty} \lambda_i(t) = \frac{1}{3}$$

since $C_I, \dot{\gamma}, \kappa > 0$. Also, the eigenvalues never cross each other in this particular case when their initial values differ, since the diminishing factor $e^{6C_I\dot{\gamma}\kappa(t_0-t)}$ is the same for every eigenvalue.

In a similar way, we obtain from the rate equation for the eigenvector \mathbf{e}_i

$$\begin{aligned}
\dot{\mathbf{e}}_i - \mathbf{W} \cdot \mathbf{e}_i &= 0 \\
e^{-\mathbf{W}t} \cdot (\dot{\mathbf{e}}_i - \mathbf{W} \cdot \mathbf{e}_i) &= 0 \\
\mathbf{V} \cdot e^{-\mathbf{D}t} \cdot \mathbf{V}^{-1} \cdot \dot{\mathbf{e}}_i - \mathbf{V} \cdot e^{-\mathbf{D}t} \cdot \mathbf{V}^{-1} \cdot \mathbf{V} \cdot \mathbf{D} \cdot \mathbf{V}^{-1} \cdot \mathbf{e}_i &= 0 \\
e^{-\mathbf{D}t} \cdot \dot{\mathbf{f}}_i - e^{-\mathbf{D}t} \cdot \mathbf{D} \cdot \mathbf{f}_i &= 0 \\
\frac{d}{dt} (e^{-\mathbf{D}t} \cdot \mathbf{f}_i) &= 0 \\
\int_{t'=t_0}^t \frac{d}{dt'} (e^{-\mathbf{D}t'} \cdot \mathbf{f}_i) dt' &= 0 \\
e^{-\mathbf{D}t} \cdot \mathbf{f}_i(t) &= e^{-\mathbf{D}t_0} \cdot \mathbf{f}_i(t_0) \\
\mathbf{V}^{-1} \cdot \mathbf{e}_i(t) &= e^{\mathbf{D}(t-t_0)} \cdot \mathbf{V}^{-1} \cdot \mathbf{e}_i(t_0) \\
\mathbf{e}_i(t) &= \mathbf{V} \cdot e^{\mathbf{D}(t-t_0)} \cdot \mathbf{V}^{-1} \cdot \mathbf{e}_i(t_0) \\
\mathbf{e}_i(t) &= e^{\mathbf{W}(t-t_0)} \cdot \mathbf{e}_i(t_0). \tag{8.6}
\end{aligned}$$

Note that $e^{\mathbf{W}(t-t_0)}$ is an orthogonal tensor, say $\mathbf{Q}(t)$, due to the antisymmetry of \mathbf{W} :

$$(\mathbf{Q}(t))^T = \left(e^{\mathbf{W}(t-t_0)} \right)^T = e^{\mathbf{W}^T(t-t_0)} = e^{-\mathbf{W}(t-t_0)} = \left(e^{\mathbf{W}(t-t_0)} \right)^{-1} = (\mathbf{Q}(t))^{-1}.$$

Tensor $\mathbf{Q}(t)$ is thus a periodic rotation induced by the spin tensor \mathbf{W} , rotating $\mathbf{e}_i(t_0)$ with a constant rate to obtain \mathbf{e}_i .

Taking (8.5) and (8.6) for the eigenpairs we get for \mathbf{A}

$$\begin{aligned}
\mathbf{A}(t) &= \sum_i \lambda_i(t) \mathbf{e}_i(t) \mathbf{e}_i(t) \\
&= \sum_i \left(\frac{1}{3} + \left(\lambda_i(t_0) - \frac{1}{3} \right) e^{6\kappa C_I \dot{\gamma} (t_0-t)} \right) (\mathbf{Q}(t) \cdot \mathbf{e}_i(t_0)) (\mathbf{Q}(t) \cdot \mathbf{e}_i(t_0)).
\end{aligned}$$

Note that

$$\begin{aligned}
\lim_{t \rightarrow \infty} \mathbf{A}(t) &= \lim_{t \rightarrow \infty} \sum_i \left(\frac{1}{3} + \left(\lambda_i(t_0) - \frac{1}{3} \right) e^{6\kappa C_I \dot{\gamma} (t_0-t)} \right) (\mathbf{Q}(t) \cdot \mathbf{e}_i(t_0)) (\mathbf{Q}(t) \cdot \mathbf{e}_i(t_0)) \\
&= \sum_i \left[\lim_{t \rightarrow \infty} \left(\frac{1}{3} + \left(\lambda_i(t_0) - \frac{1}{3} \right) e^{6\kappa C_I \dot{\gamma} (t_0-t)} \right) \lim_{t \rightarrow \infty} ((\mathbf{Q}(t) \cdot \mathbf{e}_i(t_0)) (\mathbf{Q}(t) \cdot \mathbf{e}_i(t_0))) \right] \\
&= \frac{1}{3} \lim_{t \rightarrow \infty} \sum_i [((\mathbf{Q}(t) \cdot \mathbf{e}_i(t_0)) (\mathbf{Q}(t) \cdot \mathbf{e}_i(t_0)))] \\
&= \frac{\mathbf{I}}{3}.
\end{aligned}$$

The limit of the products and product of the limits are equal since they both converge as we just proved. This justifies the third step. Since $\mathbf{Q}(t)$ is orthogonal and $\{\mathbf{e}_i(t_0)\}_{i \in \{1,2,3\}}$ is an orthonormal basis, $\{\mathbf{Q}(t) \cdot \mathbf{e}_i(t_0)\}_{i \in \{1,2,3\}}$ is an orthonormal basis, which justifies the equality

$$\mathbf{I} = \sum_i [(\mathbf{Q}(t) \cdot \mathbf{e}_i(t_0))(\mathbf{Q}(t) \cdot \mathbf{e}_i(t_0))].$$

8.5 Numerical approach

8.5.1 Time discretization

The system (8.2) is, with the exception of FFI term in the rate equation for the eigenvalues and the vorticity term in the rate equation for the eigenvectors, nonlinear. The fourth order tensors \mathbb{L} and \mathbb{M} need not to be calculated for this system. The fourth order tensor \mathbb{A} however, needs to be calculated in both the chosen and principal basis. In particular, these bases can coincide.

The form (8.1) has a larger linear part and needs the tensors \mathbb{L} , \mathbb{M} and \mathbb{A} in the chosen basis. Experience with implementations of both approaches has the tendency that the form (8.1) is more efficient. In accordance, we will only treat the numerical approach of this form.

As the nonlinear part of ODE (8.1) is substantial, our choice for time integration goes to Euler forward,

$$\begin{aligned} \mathbf{A}(t_{k+1}) &= \mathbf{A}(t_k) + \int_{t'=t_k}^{t_{k+1}} \dot{\mathbf{A}}(t') dt' \\ &\approx \mathbf{A}(t_k) + \Delta t \dot{\mathbf{A}}(t_k) \end{aligned} \quad (8.7)$$

for the equidistant partition $\{t_0, t_1, \dots, t_{end}\}$ and $\mathbf{A}(t_0)$ given.

8.5.2 Conservation of properties of second order tensor

Chapter 4 is dedicated to the orientation tensors. It includes many useful properties of the second order orientation tensor \mathbf{A} . To summarize, these properties are

1. domain and target space of tensor $\mathbf{A} : \mathbb{R} \rightarrow [-\frac{1}{2}, 1]$,
2. symmetry $\mathbf{A} = \mathbf{A}^T$,
3. positive semidefiniteness $\mathbf{x} \cdot \mathbf{A} \cdot \mathbf{x} \geq 0$,
4. target space of eigenvalues $\forall i \quad 0 \leq \lambda_i \leq 1$,
5. real eigenvectors $\forall i \quad \mathbf{e}_i \in \mathbb{R}^3$,
6. orthonormality of eigenvectors $\mathbf{e}_i \cdot \mathbf{e}_j = \delta_{ij}$,
7. unit trace $\text{tr}(\mathbf{A}) = 1$.

These properties have to be conserved by the numerical scheme in order to be adequate. Points one, four, five and six follow from the depiction of the solution. We thus omit the treatment of these properties. The remaining properties are symmetry, positive semidefiniteness and the unit trace. These properties will be treated in the following subsections.

8.5.2.1 Symmetry

Property 8.1. *The numerical scheme (8.7) conserves symmetry.*

Proof. Checking the conservation of symmetry by (8.7) is formulated as

$$\forall k \quad (\mathbf{A}(t_{k+1}))^T = \mathbf{A}(t_{k+1}) \quad \text{given} \quad (\mathbf{A}(t_k))^T = \mathbf{A}(t_k).$$

We see that

$$\begin{aligned}
(\mathbf{A}(t_{k+1}))^T &= (\mathbf{A} + \Delta t \dot{\mathbf{A}})^T \\
&= \mathbf{A} + \Delta t (\mathbf{W} \cdot \mathbf{A} - \mathbf{A} \cdot \mathbf{W} + \xi \{ \mathbf{D} \cdot \mathbf{A} + \mathbf{A} \cdot \mathbf{D} - 2[\mathbb{A} + (1 - \kappa)(\mathbb{L} - \mathbb{M} : \mathbb{A})] : \mathbf{D} \} \\
&\quad + 2\kappa C_I \dot{\gamma} (\mathbf{I} - 3\mathbf{A}))^T \\
&= \mathbf{A} + \Delta t (-\mathbf{A} \cdot \mathbf{W} + \mathbf{W} \cdot \mathbf{A} + \xi \{ \mathbf{A} \cdot \mathbf{D} + \mathbf{D} \cdot \mathbf{A} - 2([\mathbb{A} + (1 - \kappa)(\mathbb{L} - \mathbb{M} : \mathbb{A})] : \mathbf{D})^T \} \\
&\quad + 2\kappa C_I \dot{\gamma} (\mathbf{I} - 3\mathbf{A}))
\end{aligned}$$

where we have omitted the indication of time t_k on the RHS. We will treat the term that includes the fourth order terms separately. For \mathbb{A} we have to check if

$$(\mathbb{A} : \mathbf{D})^T = \mathbb{A} : \mathbf{D} \quad \Leftrightarrow \quad \sum_{k,l} A_{jikl} D_{lk} = \sum_{k,l} A_{ijkl} D_{lk}.$$

The latter holds, by construction, for the orthotropic closure as treated in Chapter 6. The proof for the QC is trivial. The symmetry of $\mathbb{L} : \mathbf{D}$ and $\mathbb{M} : \mathbb{A} : \mathbf{D}$ follow immediately from the definitions of \mathbb{L} and \mathbb{M} from Section 5.3.

We conclude that symmetry of \mathbf{A} is conserved by the numerical scheme (8.7). \square

8.5.2.2 Positive semidefiniteness

Property 8.2. *The numerical scheme (8.7) does not conserve positive semidefiniteness.*

Proof. Checking the conservation of positive semidefiniteness by (8.7) is formulated as

$$\forall k \quad \mathbf{x} \cdot \mathbf{A}(t_{k+1}) \cdot \mathbf{x} \geq 0 \quad \text{given} \quad \mathbf{x} \cdot \mathbf{A}(t_k) \cdot \mathbf{x} \geq 0.$$

We see that

$$\mathbf{x} \cdot \mathbf{A}(t_{k+1}) \cdot \mathbf{x} = \underbrace{\mathbf{x} \cdot \mathbf{A}(t_k) \cdot \mathbf{x}}_{\geq 0} + \underbrace{\Delta t \mathbf{x} \cdot \dot{\mathbf{A}}(t_k) \cdot \mathbf{x}}_{> 0}.$$

Furthermore,

$$\mathbf{x} \cdot \int_S \psi \mathbf{p} \mathbf{p} d^2 \mathbf{p} \cdot \mathbf{x} = \int_S \psi \underbrace{(\mathbf{x} \cdot \mathbf{p})^2}_{\geq 0} d^2 \mathbf{p}$$

which can be negative. An example hereof is if $\dot{\psi}$ is such that it is negative somewhere on S where the 'weight' $(\mathbf{x} \cdot \mathbf{p})^2$ is stronger than where $\dot{\psi} \geq 0$ on S . Note that the latter must hold to conserve $\int_S \dot{\psi} d^2 \mathbf{p} = 0$. It can be concluded that Δt must be such that

$$\mathbf{x} \cdot \mathbf{A}(t_k) \cdot \mathbf{x} \geq \Delta t \mathbf{x} \cdot \dot{\mathbf{A}}(t_k) \cdot \mathbf{x} \quad \text{if} \quad \mathbf{x} \cdot \dot{\mathbf{A}}(t_k) \cdot \mathbf{x} < 0.$$

To formulate a condition for Δt herefrom is difficult and perhaps impossible, as it must hold $\forall \mathbf{x} \neq \mathbf{0}$.

If $\mathbf{x} \cdot \dot{\mathbf{A}}(t_k) \cdot \mathbf{x} \geq 0$, the positive semidefiniteness is conserved $\forall \Delta t$.

It is concluded that (8.7) does not necessarily conserve positive semidefiniteness. \square

8.5.2.3 Unit trace

Property 8.3. *The numerical scheme (8.7) conserves the unit trace of \mathbf{A} .*

Proof. Checking the conservation of the unit trace by (8.7) is formulated as

$$\forall k \quad \text{tr}(\mathbf{A}(t_{k+1})) = 1 \quad \text{given} \quad \text{tr}(\mathbf{A}(t_k)) = 1.$$

We see that

$$\begin{aligned}
\text{tr}(\mathbf{A}(t_{k+1})) &= \text{tr}(\mathbf{A}(t_k) + \Delta t \dot{\mathbf{A}}(t_k)) \\
&= 1 + \Delta t \cdot \text{tr}(\dot{\mathbf{A}}(t_k))
\end{aligned}$$

which reduces the question to if

$$\text{tr}(\dot{\mathbf{A}}(t_k)) = 0.$$

Substitution of $\dot{\mathbf{A}}$ gives

$$\text{tr} \left(\dot{\mathbf{A}}(t_k) \right) = \text{tr} \left(\mathbf{W} \cdot \mathbf{A} - \mathbf{A} \cdot \mathbf{W} + \xi \{ \mathbf{D} \cdot \mathbf{A} + \mathbf{A} \cdot \mathbf{D} - 2[\mathbb{A} + (1 - \kappa)(\mathbb{L} - \mathbb{M} : \mathbb{A})] : \mathbf{D} \} + 2\kappa C_I \dot{\gamma}(\mathbf{I} - 3\mathbf{A}) \right).$$

We have that

$$\text{tr}(\mathbf{W} \cdot \mathbf{A}) = \text{tr}(\mathbf{A} \cdot \mathbf{W}) = \text{tr}(\mathbf{I} - 3\mathbf{A}) = 0, \quad \text{tr}(\mathbb{L} : \mathbf{D}) = \text{tr}(\mathbf{D} \cdot \mathbf{A}) = \text{tr}(\mathbf{A} \cdot \mathbf{D}) = \mathbf{A} : \mathbf{D}.$$

If we would have the exact \mathbb{A} , we would also have

$$\text{tr}(\mathbb{A} : \mathbf{D}) = \text{tr}(\mathbb{M} : \mathbb{A} : \mathbf{D}) = \mathbf{A} : \mathbf{D}.$$

Instead we are using closure approximations for \mathbb{A} , which must suffice to the latter. The more explicit conditions stem from the following,

$$\begin{aligned} \text{tr}(\mathbb{A} : \mathbf{D}) &= \sum_{i,j,k} A_{iij k} D_{kj} \\ &= \sum_{j,k} A_{jk} D_{kj} \\ &= \mathbf{A} : \mathbf{D}. \end{aligned}$$

Thus, we must have that $\sum_i A_{iij k} = A_{jk}$. The orthotropic fitted closures and QC satisfy this condition by construction.

For $\text{tr}(\mathbb{M} : \mathbb{A} : \mathbf{D})$ we have

$$\begin{aligned} \text{tr}(\mathbb{M} : \mathbb{A} : \mathbf{D}) &= \sum_{i,j,k,l,m} M_{iij k} A_{kjlm} D_{ml} \\ &= \sum_{j,k,l,m,n} (\mathbf{e}_n)_j (\mathbf{e}_n)_k (\mathbb{A} : \mathbf{D})_{kj} \\ &= \left(\sum_n (\mathbf{e}_n)(\mathbf{e}_n) \right) : \mathbb{A} : \mathbf{D} \\ &= \mathbf{I} : \mathbb{A} : \mathbf{D} \\ &= \sum_{i,j,k,l} \delta_{ij} A_{iij k} D_{lk} \\ &= \mathbf{A} : \mathbf{D}. \end{aligned}$$

In the latter procedure we used

$$\mathbf{I} = \left(\sum_n (\mathbf{e}_n)(\mathbf{e}_n) \right) \quad \wedge \quad \sum_i A_{iij k} = A_{jk}.$$

The former is satisfied up to machine precision and the latter was already discussed. We conclude that the unit trace of \mathbf{A} is conserved. \square

8.5.3 Consistency, stability and convergence

As we used Euler forward it follows that the LTE is $O((\Delta t)^2)$ and is thus consistent. The LTE has an accelerative character.

We rewrite the scheme as

$$\dot{\mathbf{a}} = \mathbf{B} \cdot \mathbf{a} + \mathbf{f} + \mathbf{g}$$

with

$$\mathbf{a} = \begin{bmatrix} A_{11} \\ A_{22} \\ A_{33} \\ A_{12} \\ A_{13} \\ A_{23} \end{bmatrix}$$

and

$$\mathbf{B} = \begin{bmatrix} 2\xi D_{11} - 6C_I \dot{\gamma} \kappa & 0 & 0 \\ 0 & 2\xi D_{22} - 6C_I \dot{\gamma} \kappa & 0 \\ 0 & 0 & 2\xi D_{33} - 6C_I \dot{\gamma} \kappa \\ -W_{12} + \xi D_{12} & W_{12} + \xi D_{12} & 0 \\ -W_{13} + \xi D_{13} & 0 & W_{13} + \xi D_{13} \\ 0 & -W_{23} + \xi D_{23} & W_{23} + \xi D_{23} \\ 2W_{12} + 2\xi D_{12} & 2W_{13} + 2\xi D_{13} & 0 \\ -2W_{12} + 2\xi D_{12} & 0 & 2W_{23} + 2\xi D_{23} \\ 0 & -2W_{13} + 2\xi D_{13} & -2W_{23} + 2\xi D_{23} \\ \xi D_{11} + \xi D_{22} - 6C_I \dot{\gamma} \kappa & W_{23} + \xi D_{23} & W_{13} + \xi D_{13} \\ -W_{23} + \xi D_{23} & \xi D_{11} + \xi D_{33} - 6C_I \dot{\gamma} \kappa & W_{12} + \xi D_{12} \\ -W_{13} + \xi D_{13} & -W_{12} + \xi D_{12} & \xi D_{22} + \xi D_{33} - 6C_I \dot{\gamma} \kappa \end{bmatrix}$$

and

$$\mathbf{f} = 2C_I \dot{\gamma} \kappa \begin{bmatrix} 1 \\ 1 \\ 1 \\ 0 \\ 0 \\ 0 \end{bmatrix}$$

and \mathbf{g} containing the linear terms.

As in Chapter 7, we limit ourselves to the stability analysis of the linear part. Recalling Theorem 7.2 we must have

$$1 + \Delta t \left(B_{mm} + \sum_{n, n \neq m} |B_{mn}| \right) \leq 1 \quad \wedge \quad 1 + \Delta t \left(B_{mm} - \sum_{n, n \neq m} |B_{mn}| \right) \geq -1$$

$$B_{mm} + \sum_{n, n \neq m} |B_{mn}| \leq 0 \quad \wedge \quad B_{mm} - \sum_{n, n \neq m} |B_{mn}| \geq -\frac{2}{\Delta t}.$$

The left condition is satisfied if C_I and κ are large, hence if the diffusion and the strain reduction are strong. The only way to satisfy the right condition is to take Δt sufficiently small, as \mathbf{K} is arbitrary.

Besides the use of Gershgorin's circle theorem to get an indication on the stability, the eigenvalues of $\mathbf{C} := \mathbf{I} + \Delta t \mathbf{B}$ can easily be calculated by a program as it only has size 6×6 . In addition, we emphasize that experience with the program has the tendency that the nonlinear RSC contribution makes the scheme more stable.

Part II

Test models

Chapter 9

Simple shear flow

9.1 Introduction

The simple shear flow field is used widely in the literature to test fiber orientation models. It is important in many processing flows and often indicated to be the most difficult flow to match for closure approximations [15]. We discuss the characteristics of the simple shear flow field and what we expect from the fiber orientation. We check if these expectations are met and (de)motivate them with the results from the different models. Herewith, we start with considering the motion of a single ellipsoidal particle immersed in a viscous fluid. This is done with Jeffery's equation. Afterwards, we extend to the Folgar-Tucker model by adding fiber-fiber interaction. Different parameter sets are considered to study the variation of the fiber orientation. Initiation effects are investigated by varying the initial condition and increasing the shear and stress rates in time. We extend to the Wang-O'Gara-Tucker model by adding the strain reduction term and interpret the results. Comparisons between the 'exact' solutions and the approximations of the orientation tensors are made.

DSM, and DSM only, is provided with the implementations in question. The output in this report, and the output corresponding with any other feasible parameter set, can be reproduced by DSM personnel. The simulations mentioned in this report are therefore limited to merely the most prominent cases.

9.2 The simple shear flow field

The simple shear flow field is characterized by

$$\mathbf{v} = \mathbf{K} \cdot \mathbf{x} = \begin{bmatrix} 0 & G & 0 \\ 0 & 0 & 0 \\ 0 & 0 & 0 \end{bmatrix} \cdot \mathbf{x} \quad (9.1)$$

where $\mathbf{v}[\frac{m}{s}]$ is the velocity, $G[\frac{1}{s}]$ is the shear rate and $\mathbf{x}[m]$ represents the space. As \mathbf{K} is constant in space, it is a homogeneous flow field. Recalling (3.7), the flow is assumed to be incompressible. It is independent of time and thus the stream, path and streak lines are the same. The velocity is depicted in Figures 9.1 and 9.2 by the use of cones. As can be seen from the figures, the velocity field does not differ in the z direction. For every cut parallel to the x - y plane perpendicular to the z axis, the velocity field is the same. Interpreting the curl of the velocity field as a measure for rotation, we see that

$$\nabla \times \mathbf{v} = -G\mathbf{e}_z$$

where \mathbf{e}_z is the unit vector corresponding to the z direction. Simple shear thus induces a counterclockwise rotation proportional to the shear rate G .

Say we consider a batch of fibers in the simple shear flow with, initially, a random distribution in orientation. The lift and drag of the flow on the fiber are clearly not symmetric around the midpoint of the fiber and will induce a rotation. Note that we speak of a midpoint instead of the center of gravity to emphasize that the fibers are modelled as massless ellipsoids. It is expected that the fibers keep rotating as the lift and drag are never symmetric around the midpoint, with the exception of the highly improbable state that a fiber is parallel to the x or z axis.

Aside from the lift and drag induced rotation, there is also FFI. The interaction counteracts the lift and drag induced rotation and will keep the fibers from reaching a smooth rotary state. In the sense of probability density of the orientation, it is expected that this phenomenon expresses itself as a decrease in comparison with the case without FFI. In the sense of the components of the tensor form, it is expected that this phenomenon expresses itself as a tendency to the random distribution $A_{11} = A_{22} = A_{33} = \frac{1}{3}$. This tendency gets stronger as the FFI gets stronger, thus when C_I increases.

When considering long fibers, the length to diameter ratio of the ellipsoid is traditionally set to infinity, so $r_e = \frac{l}{d} = \infty$. This corresponds with $\xi = 1$. This quantitative state can be split into two separate cases. Either the length is finite and the diameter goes to zero or the diameter is finite and the length goes to infinity. In both cases it is expected that the rotation of the fibers is transient. In

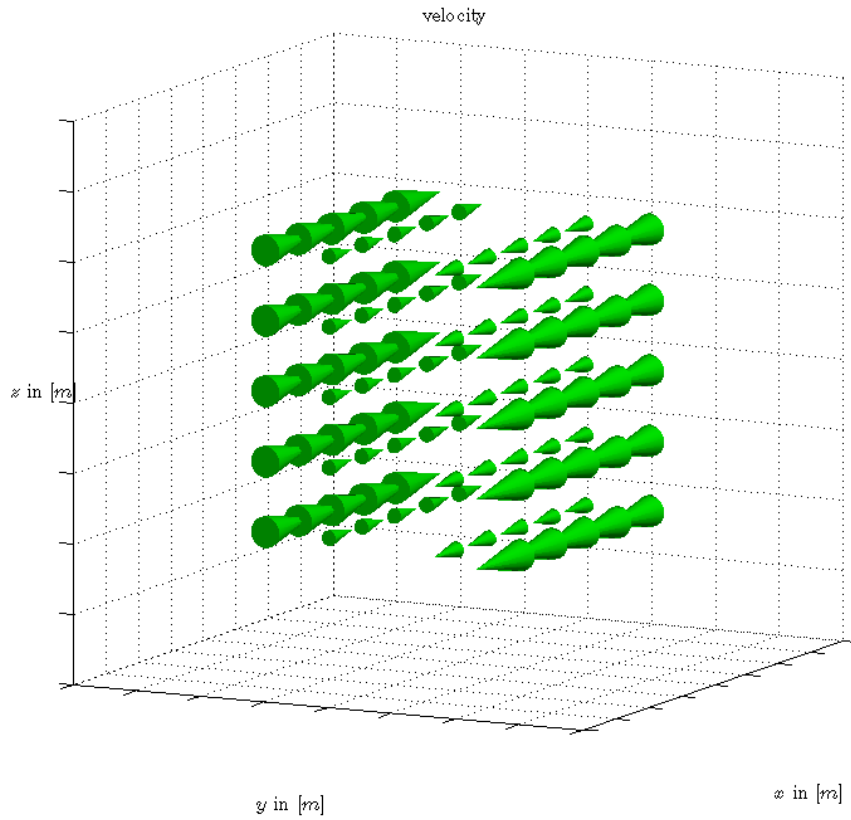


Figure 9.1: simple shear velocity field cones in three dimensional view.

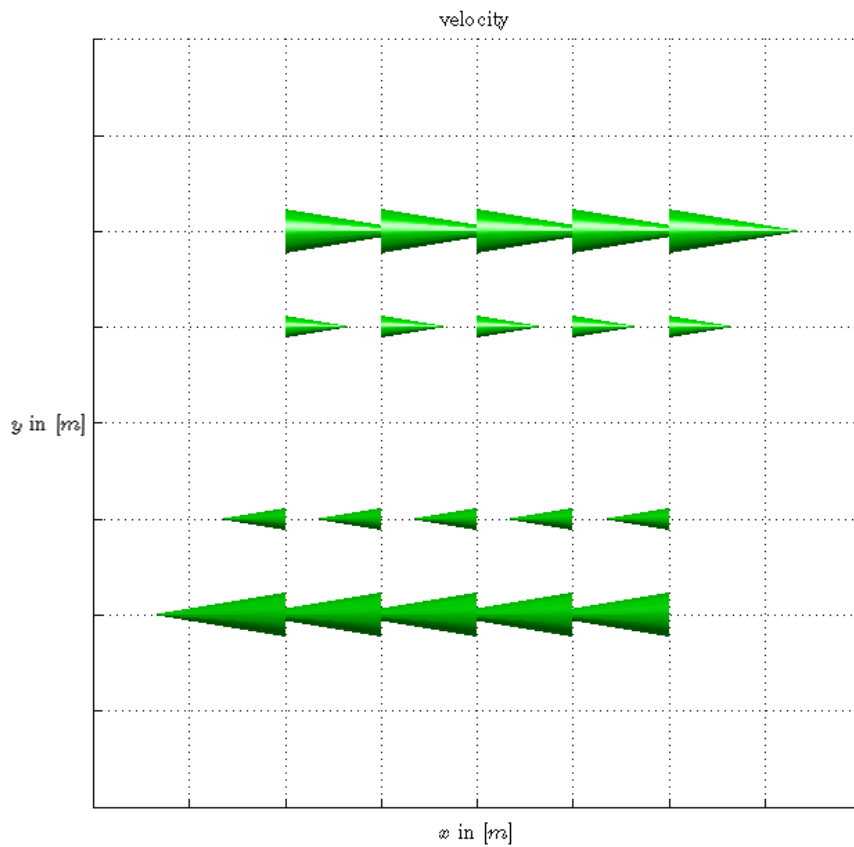


Figure 9.2: simple shear velocity field cones in x - y view.

the former case this expectation is justified as follows. When the length is finite and the diameter goes to zero, the flux inducing rotation goes to zero when the fibers are aligned with the x axis. In other words, the effects of lift and drag vanish when the fiber is infinitely thin. Hence, the flow will not induce a rotation. In the case that the diameter is finite and the length goes to infinity, the expectation is justified in an analogous way.

As we are mainly concerned with the case of plastics filled with long fibers, the emphasize will be on ξ close and equal to one in the report.

9.3 Results Jeffery's equation

The expectations of the orientational distribution in the simple shear flow field have now been discussed, mainly qualitatively. For the sake of quantative results, we start with considering Jeffery's equation (3.3) or (3.4) in combination with (9.1). Note that $(C_I, \kappa) = (0, 1)$ so that the only contribution to the orientation that is left is the LD. The orientation will depend merely on the balance between the LD and the stress within the ellipsoidal fiber. Recall

$$\underbrace{\dot{\mathbf{p}} - \mathbf{W} \cdot \mathbf{p} - \xi \mathbf{D} \cdot \mathbf{p}}_{\text{difference between velocity flow and velocity fiber}} = \underbrace{-\xi \mathbf{D} : \mathbf{p}\mathbf{p}\mathbf{p}}_{\text{stress within fiber}} .$$

Simple shear (9.1) results in

$$\begin{aligned} (\mathbf{W} \cdot \mathbf{p})_i &= \frac{G}{2}(\delta_{i1} \sin(\theta) \sin(\phi) - \delta_{i2} \sin(\theta) \cos(\phi)) \\ (\mathbf{D} \cdot \mathbf{p})_i &= \frac{G}{2}(\delta_{i1} \sin(\theta) \sin(\phi) + \delta_{i2} \sin(\theta) \cos(\phi)) \\ \mathbf{D} : \mathbf{p}\mathbf{p} &= \frac{G}{2} \sin^2(\theta) \sin(2\phi). \end{aligned}$$

The $(\mathbf{W} \cdot \mathbf{p})_1$ and $(\mathbf{D} \cdot \mathbf{p})_1$ are the largest at $(\theta, \phi) \in \{(\frac{\pi}{2}, \frac{\pi}{2}), (\frac{\pi}{2}, \frac{3\pi}{2})\}$, confer Figure 9.3. Physically, this

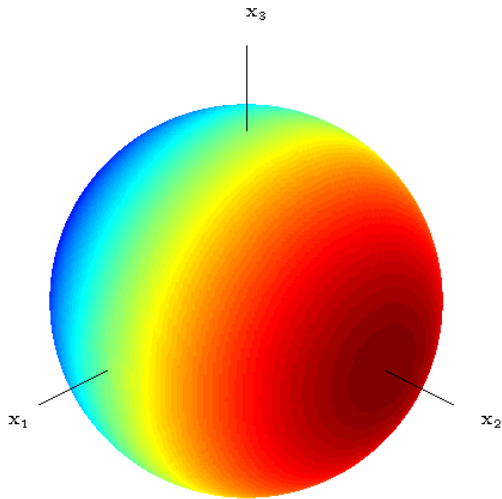


Figure 9.3: $p_2 = \sin(\theta) \sin(\phi)$.

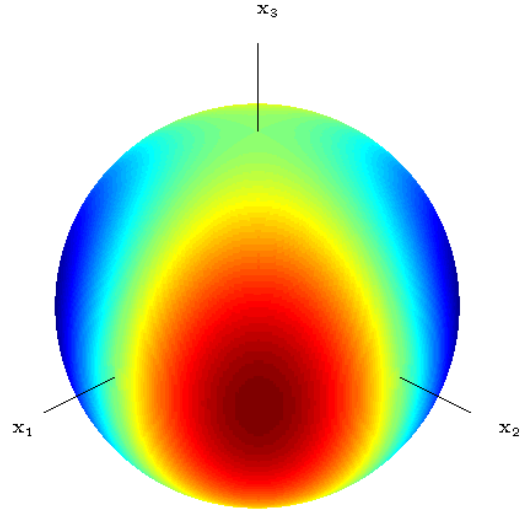


Figure 9.4: $\frac{\sin^2(\theta) \sin(\phi)}{2}$.

means that the spin and strain contributions of the velocity of the flow are the largest when the fiber is aligned with the x_2 axis. This is justifiable as at these angles, the arm of the fiber in the x_2 direction is the largest. The x_2 direction is the direction wherein the velocity in the x_1 direction increases maximally.

When ξ is in the neighborhood or equal to one, the second components of $\mathbf{W} \cdot \mathbf{p} + \xi \mathbf{D} \cdot \mathbf{p}$ are small or vanish for an prolate ellipsoid. For a oblate ellipsoid, the first and second components of $\mathbf{W} \cdot \mathbf{p}$ and $\mathbf{D} \cdot \mathbf{p}$ obviously interswitch. In the case $\xi = 0$ we have a spherical particle wherefore the strain is zero. The spin term $\mathbf{W} \cdot \mathbf{p}$ remains. The third components of $\mathbf{W} \cdot \mathbf{p} + \xi \mathbf{D} \cdot \mathbf{p}$ are zero as the flow field lies in the x_1 - x_2 plane.

The $\mathbf{D} : \mathbf{p}\mathbf{p}$ is the largest at $(\theta, \phi) \in \{(\frac{\pi}{2}, \frac{\pi}{4}), (\frac{\pi}{2}, \frac{5\pi}{4})\}$, confer Figure 9.4. As $\mathbf{D} : \mathbf{p}\mathbf{p}$ is a measure for the internal stress of the fiber, the location of the maxima is justified by considering the principal axes of \mathbf{D} . We have

$$\mathbf{D} = \frac{G}{2} \begin{bmatrix} 0 & 1 & 0 \\ 1 & 0 & 0 \\ 0 & 0 & 0 \end{bmatrix}$$

so that the principal values are $\lambda_i \in \{-\frac{G}{2}, 0, \frac{G}{2}\}$ and the corresponding principal axes

$$\mathbf{e}_i \in \left\{ \begin{bmatrix} 1 \\ -1 \\ 0 \end{bmatrix}, \begin{bmatrix} 0 \\ 0 \\ 1 \end{bmatrix}, \begin{bmatrix} 1 \\ 1 \\ 0 \end{bmatrix} \right\}.$$

Herewith, it is proven that the internal stress is maximal if one considers the direction of the principal axes, which indeed corresponds with $(\theta, \phi) \in \{(\frac{\pi}{2}, \frac{\pi}{4}), (\frac{\pi}{2}, \frac{5\pi}{4})\}$. A simple shear flow field is thus equivalent with a tensile stress under an angle of $\frac{\pi}{4}$ and a compressive stress under an angle $\frac{5\pi}{4}$, both proportional to $\frac{G}{2}$. The former is equivalent with decomposing the velocity vectors in components along the principal axes of the rate of deformation tensor \mathbf{D} , confer Figure 9.5.

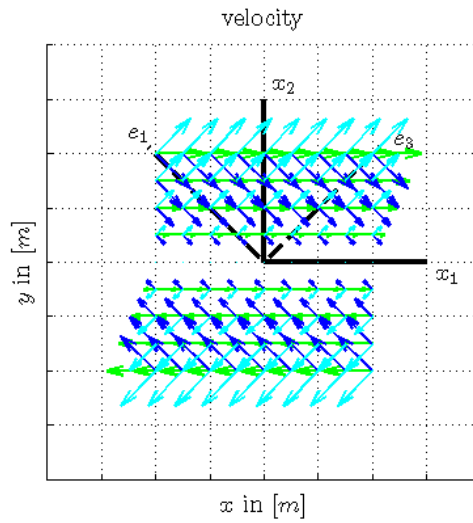


Figure 9.5: velocity vectors decomposed along the eigenvectors of \mathbf{D} .

The stationary points of (3.4) are interesting. We evaluate (3.4) in combination with (9.1) and obtain

$$\begin{aligned} \dot{\theta} &= \frac{\xi G \sin(2\theta) \sin(2\phi)}{4} \\ \dot{\phi} &= \frac{G}{2} (\xi \cos(2\phi) - 1). \end{aligned} \quad (9.2)$$

Setting $\dot{\theta} = 0, \dot{\phi} = 0$ we find

$$\begin{aligned} \sin(2\theta) = 0 \quad \vee \quad \sin(2\phi) = 0 &\Leftrightarrow \theta \in \{0, \frac{\pi}{2}, \pi\} \quad \vee \quad \phi \in \{0, \frac{\pi}{2}, \pi, \frac{3\pi}{2}, 2\pi\} \\ \xi \cos(2\phi) - 1 = 0 &\Leftrightarrow \phi \in \{\frac{\pi}{2}, \frac{3\pi}{2}\} \text{ if } \xi = -1 \quad \vee \quad \phi \in \{0, \pi, 2\pi\} \text{ if } \xi = 1. \end{aligned}$$

It stands out that there are no stationary points when $|\xi| < 1$. The reason for this is that if $|\xi| < 1$, the ellipsoid has a short axis unequal to zero and will thus always be subjected to a rotation, excluding the possibility of stationary points.

Summarizing the stationary points, they are the x_3 and x_2 axes for $\xi = -1$ and the x_3 and x_1 axes for $\xi = 1$. This can be seen from the Jeffery orbits for these particular cases, confer Figures 9.6 and 9.7. If the initial orientation $\mathbf{p}_0 \neq [0 \ 0 \ 1]^T$, the fiber will always align with the x_2 and x_1 axis for $\xi = -1$ and $\xi = 1$ respectively. If we take $\mathbf{p}_0 = [0 \ 0 \ 1]^T$, the fiber stays aligned with the x_3 axis, confer Figure 9.8.

If $|\xi| < 1$, the Jeffery orbit has no stationary points and is periodic. The further ξ is away from

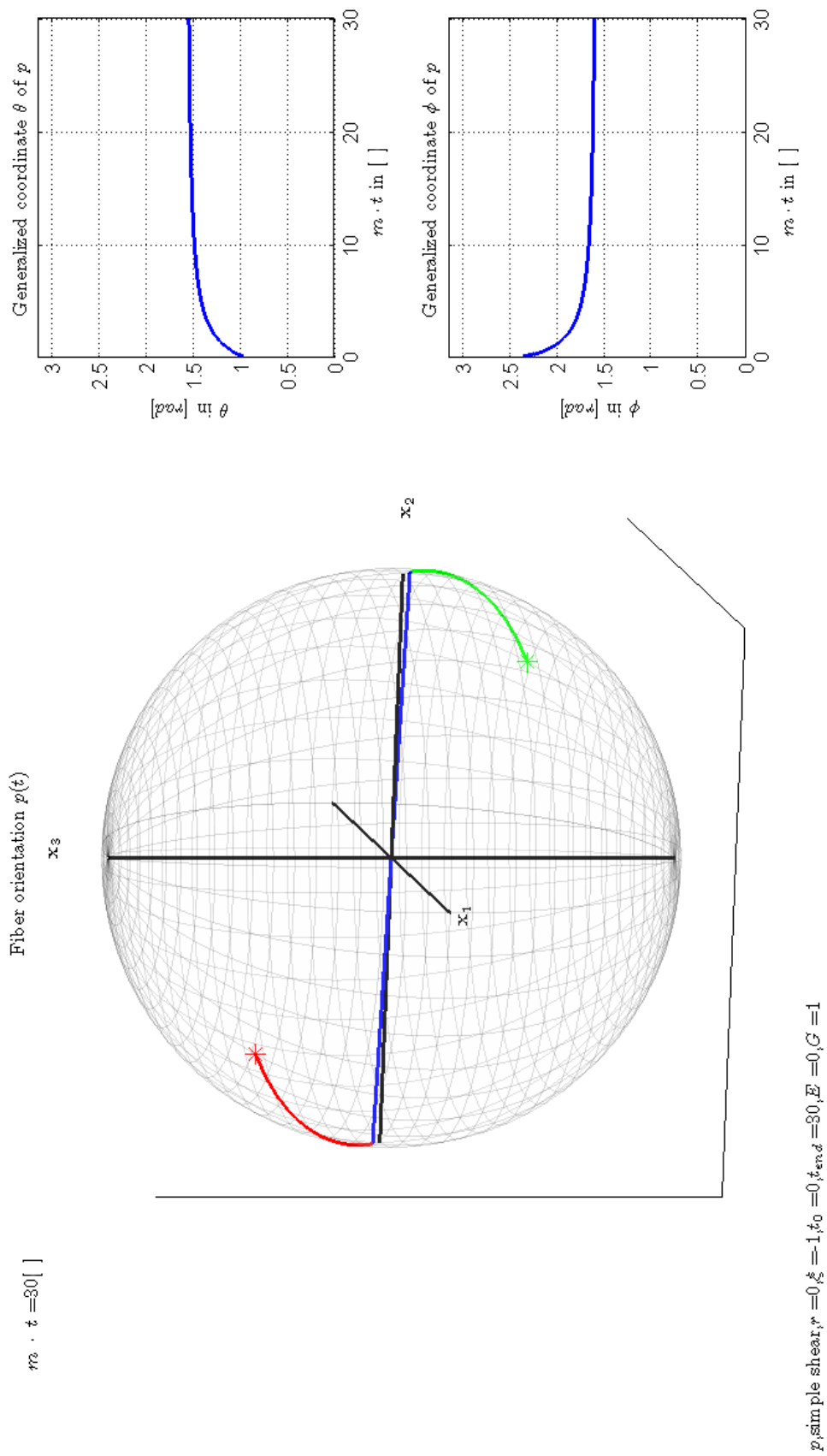


Figure 9.6: stationary point for $\xi = -1, p_0 = \frac{1}{\sqrt{3}}[1 \ -1 \ 1]^T$.

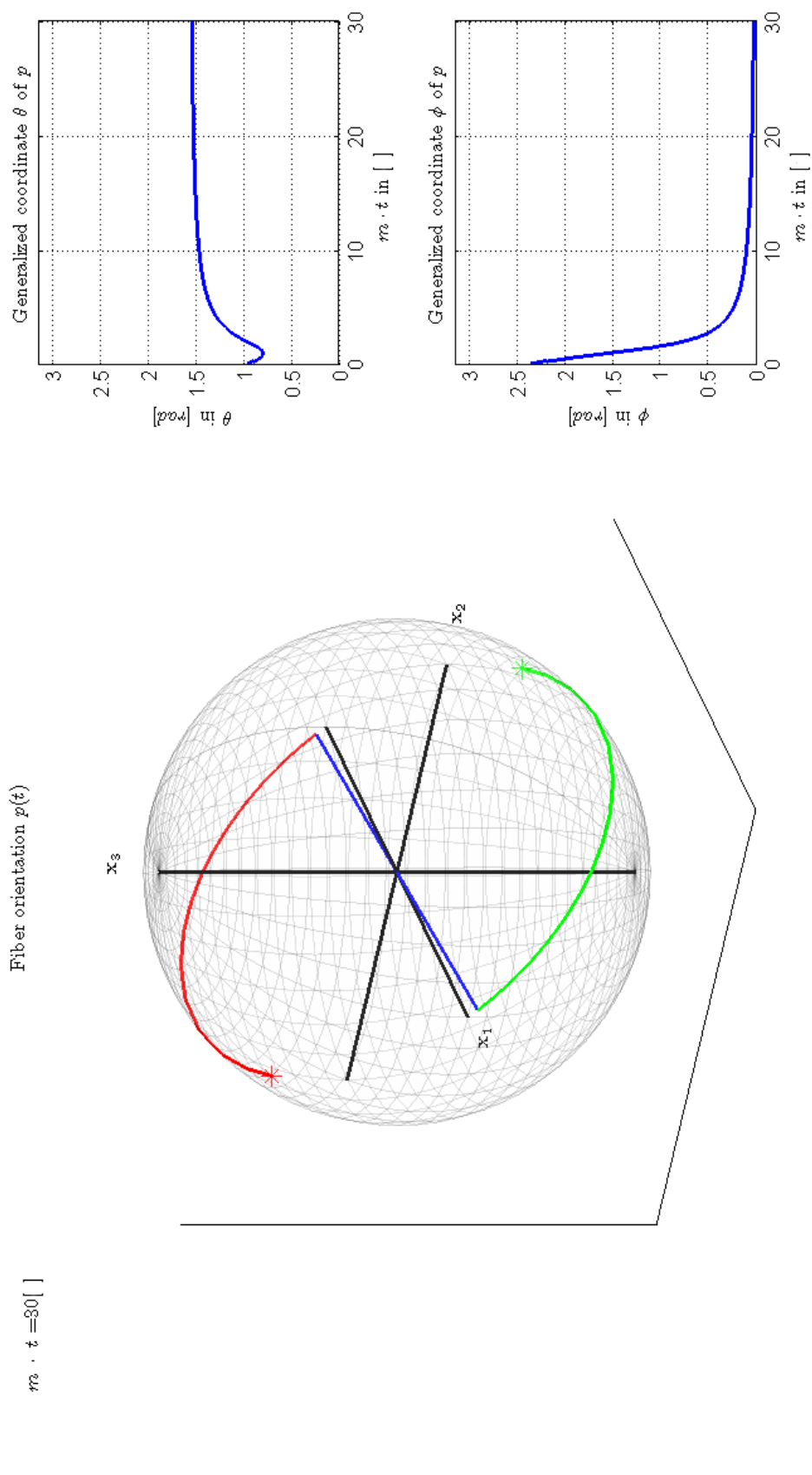


Figure 9.7: stationary point for $\xi = 1, \mathbf{p}_0 = \frac{1}{\sqrt{3}}[1 \ -1 \ 1]^T$.

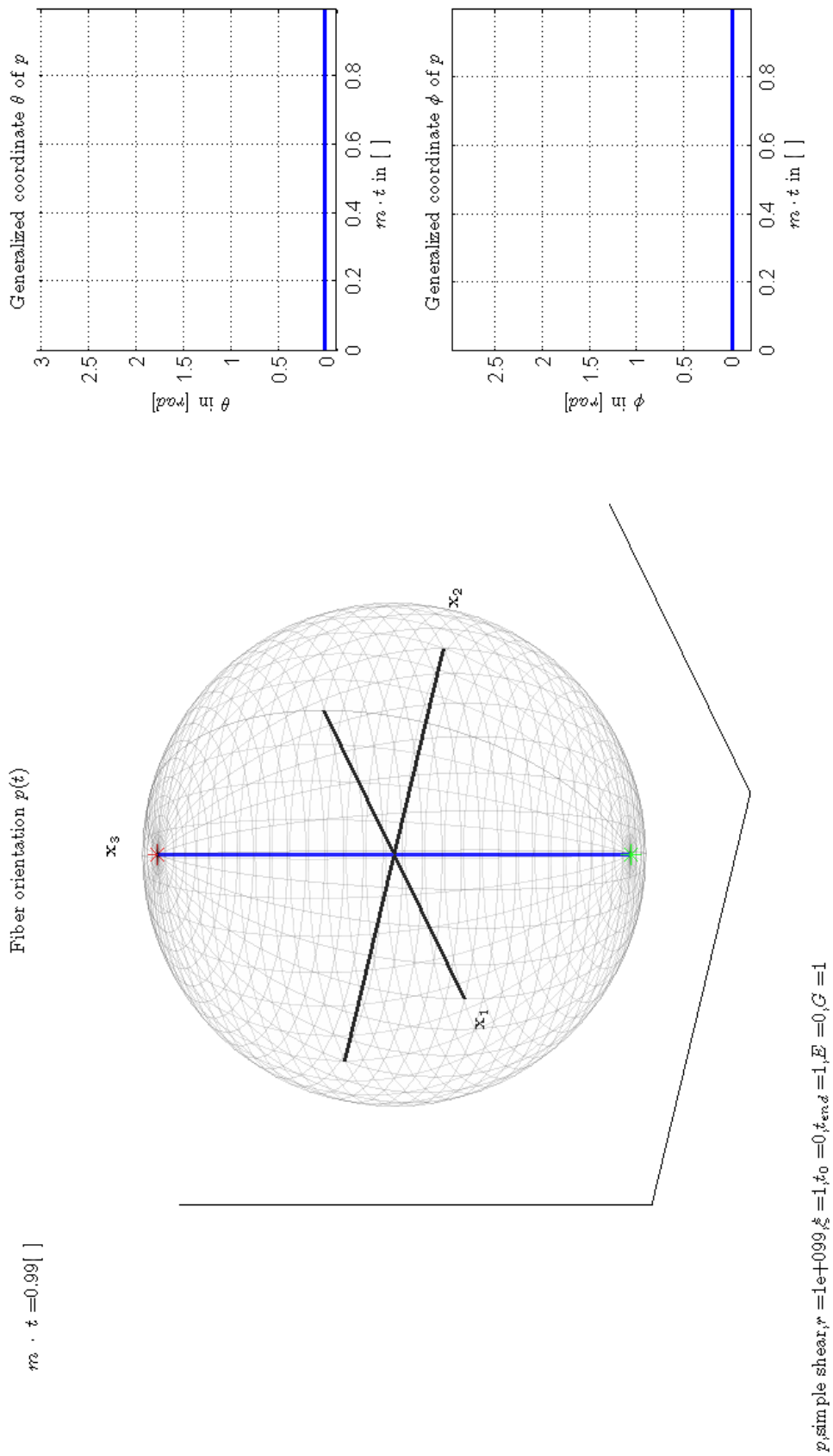


Figure 9.8: stationary point for $\xi = 1, \mathbf{p}_0 = [0 \ 0 \ 1]^T$.

$\xi = -1$ and $\xi = 1$, the larger the distance of the Jeffery orbit to the x_2 or x_1 axis respectively, and the shorter the period, confer Figures 9.9 and 9.10. An exception is the case where $(\mathbf{p}_0)_3 = 0$. In this case, the fiber passes through the x_1 and x_2 axis. The period however, still get shorter when ξ is further away from $\xi = -1$ and $\xi = 1$. This emphasizes the domination of spin if $|\xi| < 1$.

As we consider the results in the dimensionless time \bar{t} , $\psi(\mathbf{p}, \bar{t})$ does not vary under variation of G in the case of simple shear. And since we consider the fibers to be massless, there are no occurrences of initiation effects due to high accelerations by the shear rate G .

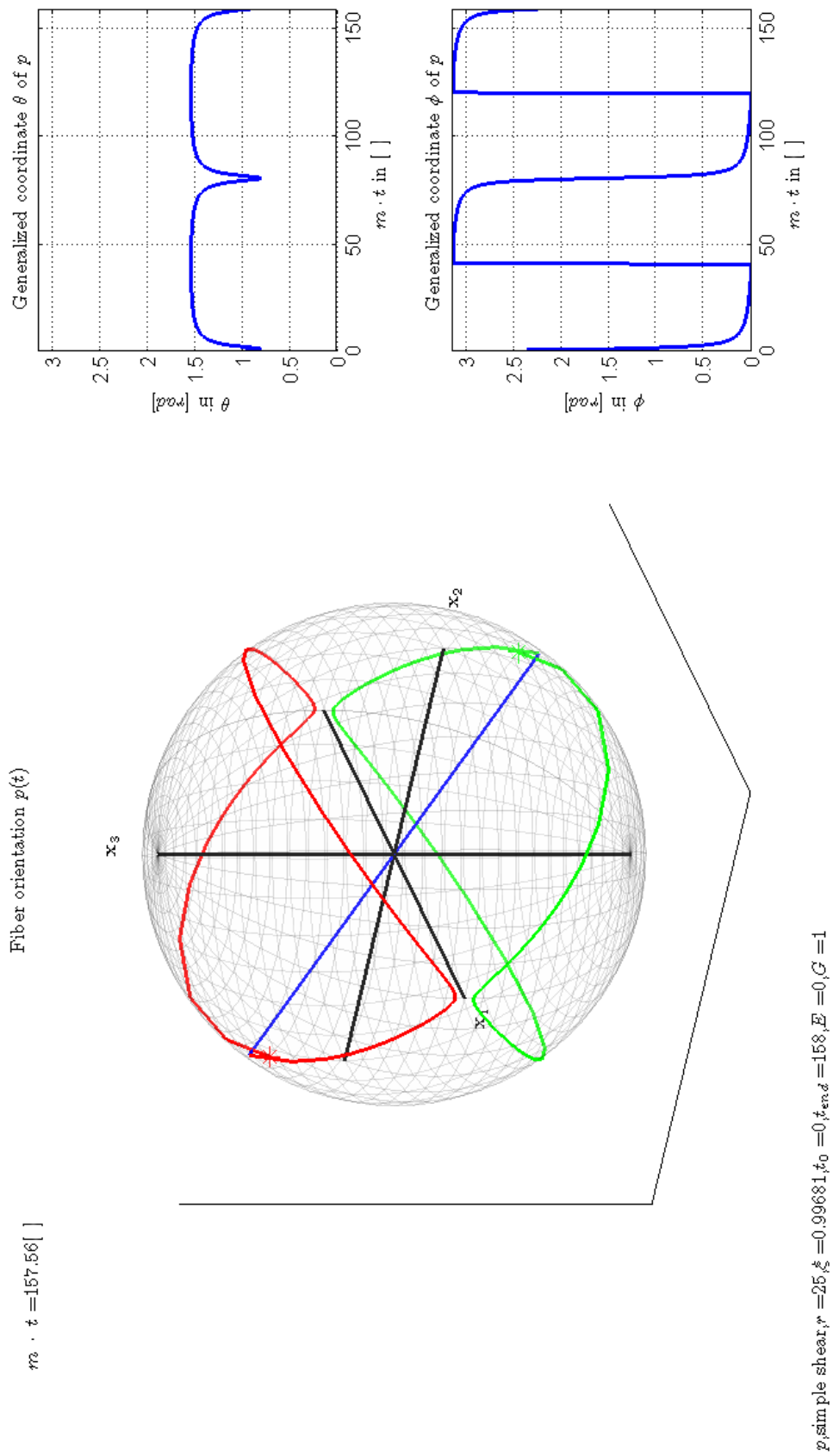


Figure 9.9: Jeffery orbit for $r = 25, \mathbf{p}_0 = \frac{1}{\sqrt{3}}[-1 \ -1 \ 1]^T$.

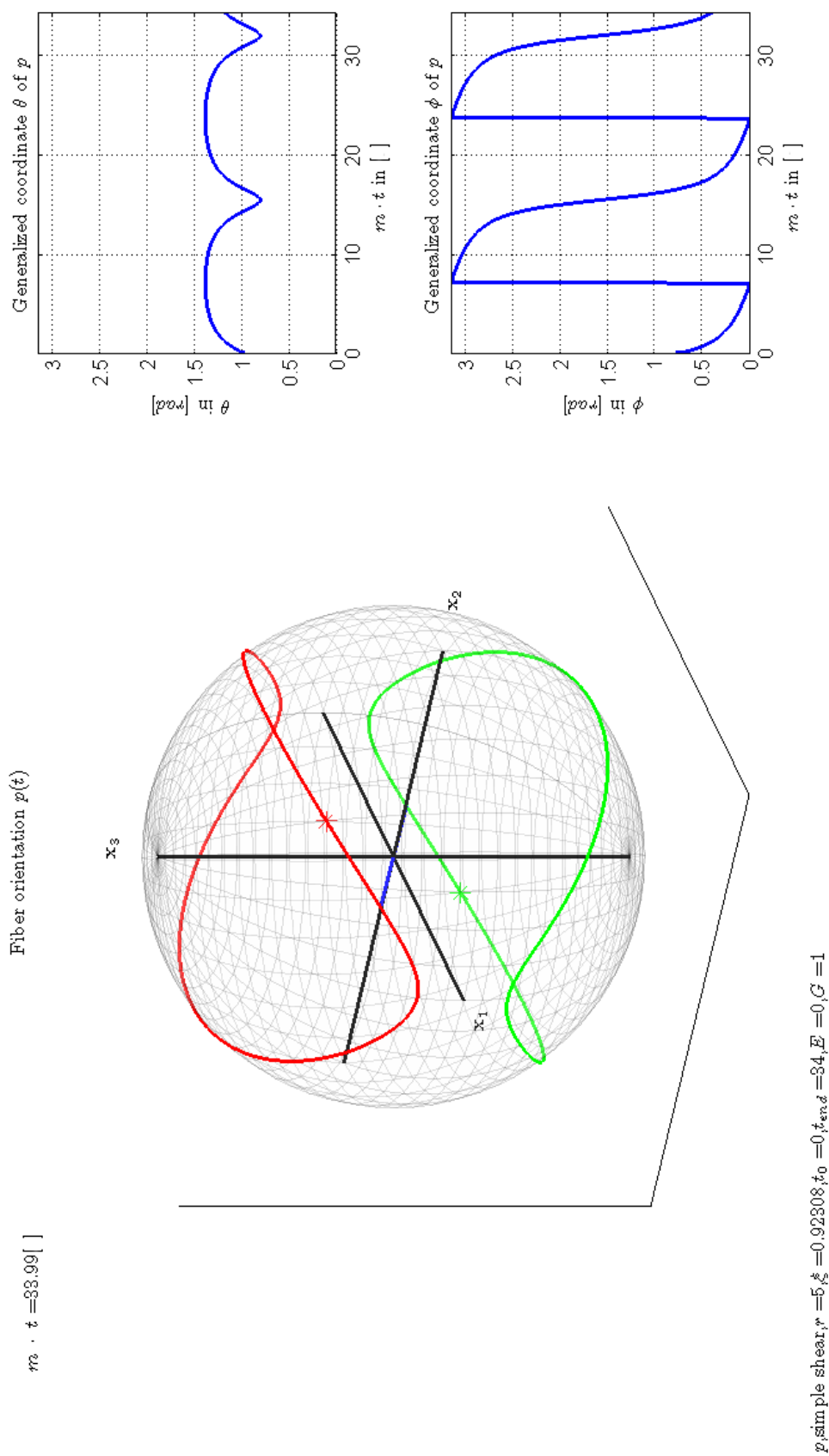


Figure 9.10: Jeffery orbit for $r = 5, \mathbf{p}_0 = \frac{1}{\sqrt{3}}[1 \ 1 \ 1]^T$.

9.4 Results kinetic theory

9.4.1 Relation to Jeffery's equation

By using the approach as explained thoroughly in Chapter 7, we solve the probability density of the fiber orientation for the simple shear flow field.

Having treated the equation of Jeffery for simple shear, we can already say something about the probability density when there is no additional rotary diffusion or decrease of the kinetics, $(C_I, \kappa) = (0, 1)$. From Property 7.3 we obtain

$$\psi(\mathbf{p}(t), t) = \psi(\mathbf{p}_0, t_0) e^{\xi \mathbf{D} : \mathbf{p}(t) \mathbf{p}(t) (t - t_0)} = \psi(\mathbf{p}_0, t_0) e^{\frac{\xi G \sin^2(\theta(t)) \sin(2\phi(t)) (t - t_0)}{2}} \quad (9.3)$$

which states that along a Jeffery orbit, the initial probability density increases or decreases dependent on the internal stress of the fiber.

For the power of the exponential, provided that $G, t - t_0 > 0$, we have

$$\frac{\xi G \sin^2(\theta(t)) \sin(2\phi(t)) (t - t_0)}{2} > 0 \Leftrightarrow \begin{cases} (\theta(t), \phi(t)) \in (0, \pi) \times \left(0, \frac{\pi}{2}\right) \cup \left(\pi, \frac{3\pi}{2}\right) & \text{if } \xi > 0 \\ (\theta(t), \phi(t)) \in (0, \pi) \times \left(\frac{\pi}{2}, \pi\right) \cup \left(\frac{3\pi}{2}, 2\pi\right) & \text{if } \xi < 0 \end{cases} \quad (9.4)$$

Hence, depending on the aspect ratio of the ellipsoidal particles and their Jeffery orbits, the solution is bounded or unbounded for $t \uparrow \infty$. If $|\xi| < 1$, the Jeffery orbits do not have steady states, as mentioned in Section 9.3, and keep passing through the areas mentioned in (9.4). The probability density thus keeps increasing there $\forall t$ and so the solution is unbounded. If $\xi \in \{-1, 1\}$ the Jeffery orbits do have steady states, namely the at the x_2 and x_1 axes respectively. These axes are not in the domains (9.4). However, the Jeffery orbits converge to the x_2 and x_1 axes, but never actually reach them. It follows that the probability density keeps increasing in (9.4) and is also unbounded when $\xi \in \{-1, 1\}$.

It is interesting to ask where the maxima of ψ are. If $|\xi| < 1$, the Jeffery orbits of a set of fibers 'cover' S at all time. The maxima of the power lie at $(\theta, \phi) \in \left\{\left(\frac{\pi}{2}, \frac{\pi}{4}\right), \left(\frac{\pi}{2}, \frac{5\pi}{4}\right)\right\}$. If $\xi \in \{-1, 1\}$, the Jeffery orbits of a set of fibers converge to the x_2 and x_1 axes respectively. The PDF will converge to

$$\psi_s(\mathbf{p}) := \lim_{t \uparrow \infty} \psi(\mathbf{p}, t) = \frac{1}{2} \left(\delta\left(\mathbf{p} - \begin{bmatrix} 0 \\ -1 \\ 0 \end{bmatrix}\right) + \delta\left(\mathbf{p} - \begin{bmatrix} 0 \\ 1 \\ 0 \end{bmatrix}\right) \right)$$

and

$$\psi_s(\mathbf{p}) = \frac{1}{2} \left(\delta\left(\mathbf{p} - \begin{bmatrix} -1 \\ 0 \\ 0 \end{bmatrix}\right) + \delta\left(\mathbf{p} - \begin{bmatrix} 1 \\ 0 \\ 0 \end{bmatrix}\right) \right)$$

respectively. Note that the factor $\frac{1}{2}$ stems from the constraint $\int_S \psi d^2\mathbf{p} = 1$.

The unboundedness of ψ confirms the difficulty of constructing a solution on a finite partition as particular cells will keep increasing in value whereas surrounding cells may converge to zero. This results in an infinite gradient which needs an infinitely fine grid. In contrast, rotary diffusion bounds the solution, making a finite partition sufficient. Nonetheless, as $C_I \downarrow 0$, the grid needs to be refined drastically as the upper bound for the solution increases. In addition, stability criteria demand that Δt decreases along with the space partition. This increases the computation times to unacceptable large levels.

In this section, we will exploit our interest in the Wang-O'Gara-Tucker model wherefore $(C_I, \kappa) \neq (0, 1)$. In addition, an analysis of the case $(C_I, \kappa) = (0, 1)$ would be futile as we already have the deterministic result from Jeffery's equation and inefficient due to the stability criteria as treated in Subsection 7.4.6. Results of the case $(C_I, \kappa) = (0, 1)$ will therefore be omitted.

9.4.2 Adding fiber-fiber interaction

9.4.2.1 Probability density

Taking FFI into account, we expect the LD contribution to the orientation to be counteracted, since FFI 'pulls' ψ to the random fiber orientation $\psi = \frac{1}{4\pi}$. Due to this FFI being modeled as rotary diffusion, we expect the gradients in space $\frac{\partial \psi}{\partial \theta}, \frac{\partial \psi}{\partial \phi}$ to decrease and thus also

$$\psi_{min}(t) := \min_{\theta, \phi} \psi(\theta, \phi, t), \quad \psi_{max}(t) := \max_{\theta, \phi} \psi(\theta, \phi, t)$$

are expected to decrease and increase respectively.

We consider the case $(\xi, C_I, \kappa) = (1, 0.001, 1)$. This means that the ratio of the long axis to the short axis of the ellipsoidal particle is infinite, that there is a marginal amount of rotary diffusion and that the additional flux from the Wang-O'Gara-Tucker model is not yet being used. The results are depicted in Figures 9.11, 9.12 and 9.13. After about $3[s]$ a tendency becomes clear. The probability density increases in the neighborhood of the x_1 axis. The maxima stop moving when they are almost lying on the x_1 axis. The reason that the maxima are now slightly off, in contrast with the outcome of Jeffery's equation where the solution converges to the x_1 axis, is the rotary diffusion. The diffusion pulls the density to $\psi = \frac{1}{4\pi}$. Density from dense areas is diffused to the sparser environment. The balance between the convection and diffusion does not only induce smaller maxima and larger minima in comparison with the diffusionless case, it also causes a change in location of the extrema. Physically, this means that a collection of fibers in the simple shear flow field are not probable to be oriented the most purely in the x_1 direction. It has an inclination that is slightly off the x_1 axis, which is a result from FFI avoiding the fibers to align in the x_1 direction. This inclination becomes stronger as C_I increases, as can be seen in Figure 9.14. Hence, the tendency to a random orientation in the x_1 - x_2 plane becomes stronger. It also stands out from the color bar that indeed ψ_{min} increases and ψ_{max} decreases.

The progression of the locations of the extrema of the PDF in time is depicted in Figure 9.15. From the value of the maximum in time, it becomes clear that the convection and diffusion are not immediately in balance. After $30[s]$ the maximum is within one percent of its equilibrium. We call this the transient time. This transient time decreases if C_I increases. Starting with a uniform distribution, the stationary location of the maximum is reached after $13.1[s]$. This is depicted in the two lower graphs. Because the θ corresponding to the maximum of ψ is at about $\theta = \frac{\pi}{2}$, it is hard for the numerical scheme to stay accurate. This is why the angular locations of the minimum and maximum appear to be alternating between $\phi = \frac{\pi}{2}$ and $\phi = \frac{3\pi}{2}$, and $\phi = 0$ and $\phi = \pi$ respectively. Plotting the graphs with a modulo π modification clarifies the graph.

Recalling (7.1) we conclude that there is a C_I wherefore $\dot{\psi}$ becomes diffusion dominated so that the balance between convection and diffusion is immediate and not after an 'overshoot'. Indeed, the diffusion has an oppsite sign in (7.1) and can vary with C_I independently of the LD contribution.

From the latter alinea one could suspect that the overshoot is an initiation effect, which indeed turns out to be the case. Consider the convection term and write

$$\tilde{\nabla} \cdot (\psi \dot{\mathbf{p}}) = (\tilde{\nabla} \psi) \cdot \dot{\mathbf{p}} + \psi \tilde{\nabla} \cdot \dot{\mathbf{p}} = (\tilde{\nabla} \psi) \cdot \dot{\mathbf{p}} - \xi \mathbf{D} : \mathbf{p} \mathbf{p} \psi.$$

The left term on the RHS 'builds up' in time, as $\tilde{\nabla} \psi = 0$ when taking an IC uniform in space. The right term however, is immediately of a substantial strength as $\psi, \tilde{\nabla} \cdot \dot{\mathbf{p}} \neq 0$. To explain it physically, a set of fibers is subjected to an internal stress by the flow field, resulting in a convection of orientation if the IC is unequal to the steady state orientation. This internal stress is immediate as the fibers are assumed to be massless. To complete the argument, we note that the diffusion

$$C_I G \tilde{\nabla} \cdot \tilde{\nabla} \psi$$

also has to initiate, as it depends on the second derivative in space of ψ , which is zero at initiation when using a uniform IC. The overshoot is thus the result of the balance between

$$(\tilde{\nabla} \psi) \cdot \dot{\mathbf{p}} \quad \wedge \quad C_I G \tilde{\nabla} \cdot \tilde{\nabla} \psi$$

and

$$\psi \tilde{\nabla} \cdot \dot{\mathbf{p}}.$$

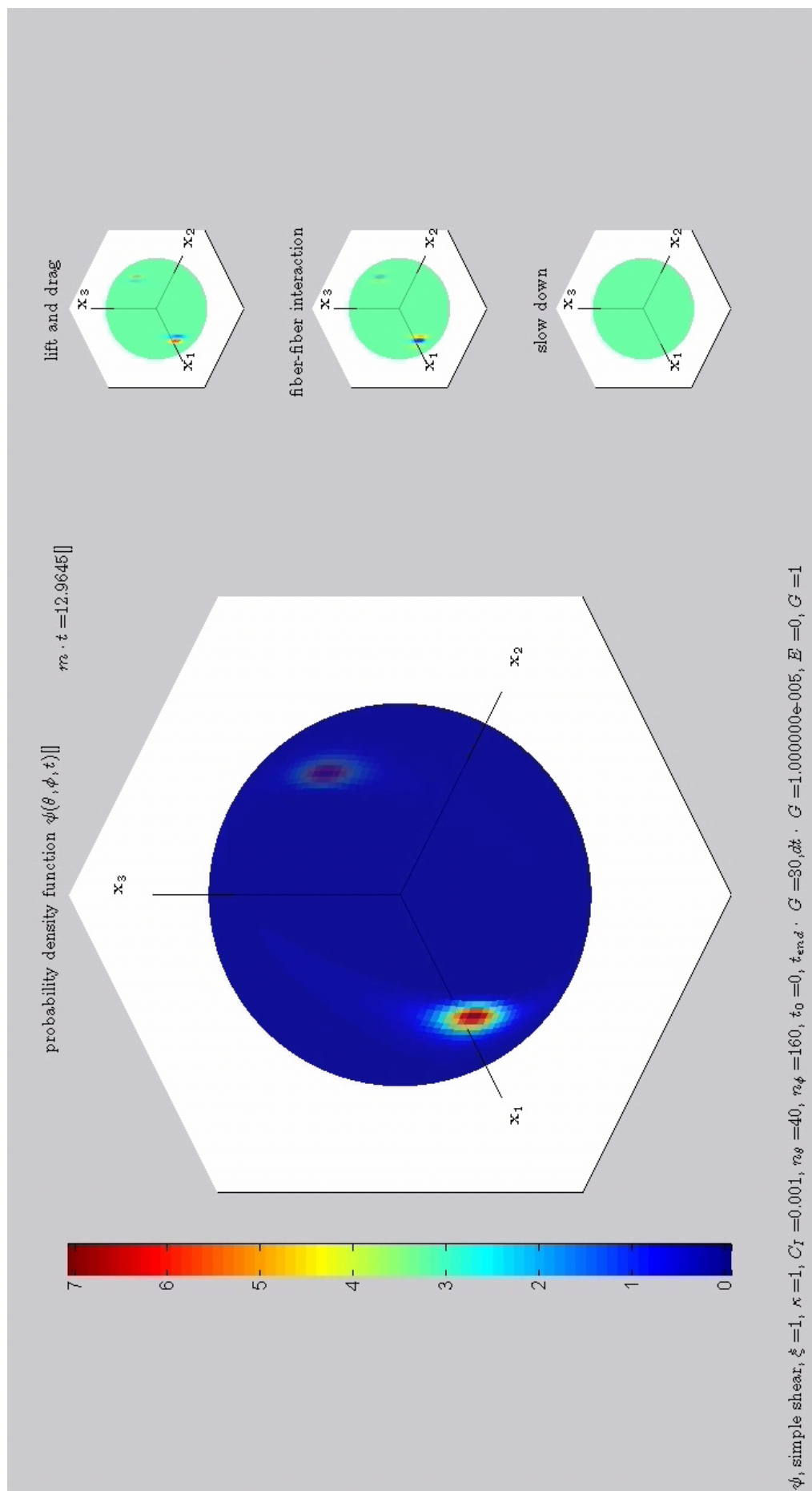
It is interesting to investigate if the initiation effects can be changed by varying certain parameters. Such a consideration also gives insight in how much the probability density depends on its history, in how much it has 'memory'. To this end we study the influence of the IC and a time dependent shear rate on the PDF.

We recall the nonuniform IC (7.23)

$$\psi_{i,j}^0 = a \cdot (\sin(\theta_i - b))^{2d} (\cos(\phi_j - c))^{2e} + f, \quad a > 0, b \in \left[0, \frac{\pi}{2}\right], c \in [0, 2\pi), d, e \in \mathbb{Z}^+, f \geq 0.$$

The terms

$$(\tilde{\nabla} \psi) \cdot \dot{\mathbf{p}} \quad \wedge \quad C_I G \tilde{\nabla} \cdot \tilde{\nabla} \psi$$

Figure 9.12: development of ψ for the simple shear flow field.

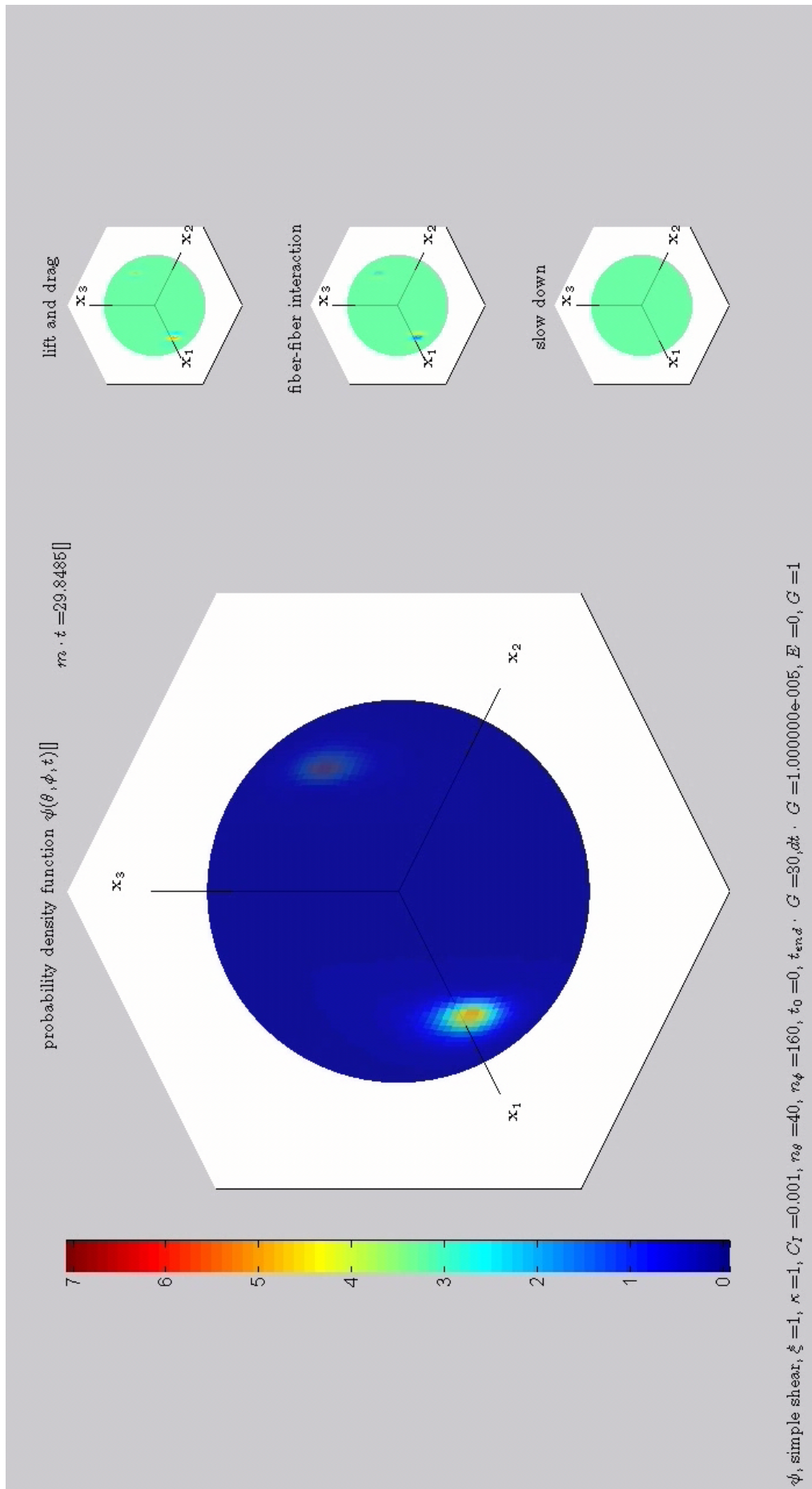


Figure 9.13: development of ψ for the simple shear flow field.

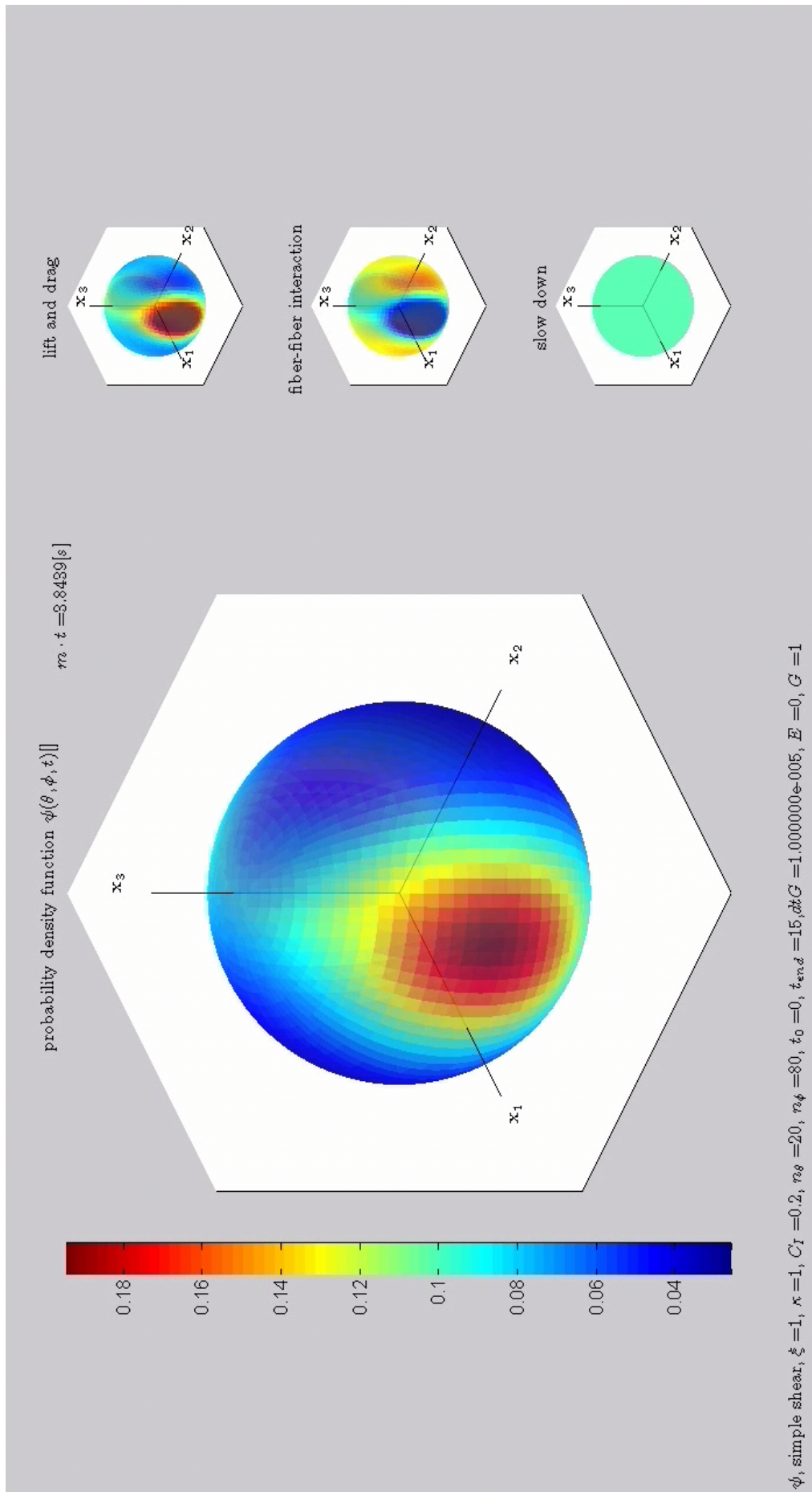


Figure 9.14: deviation of the x_1 axis increases when the diffusion becomes stronger.

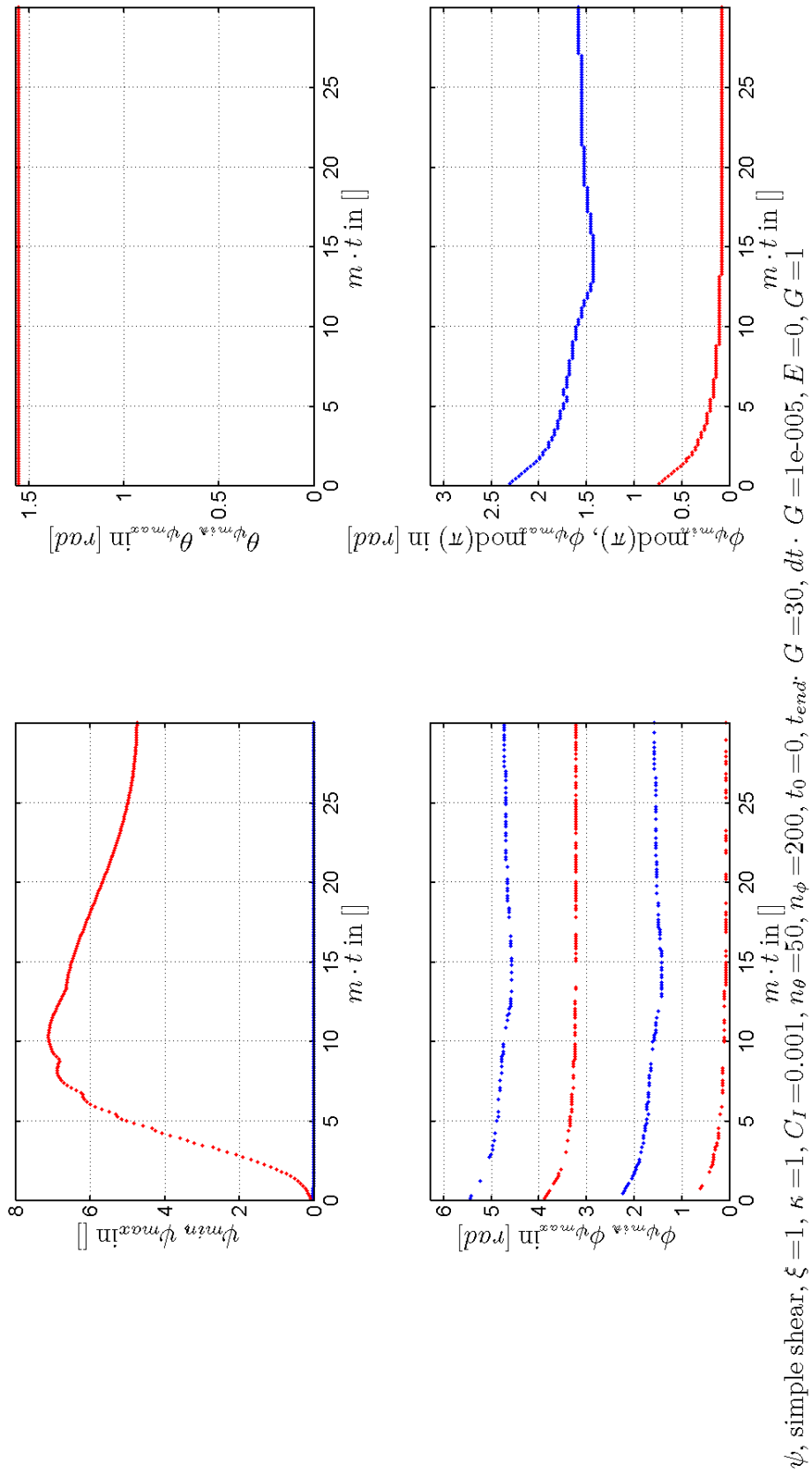


Figure 9.15: location and values of the extrema of the probability density. The maximum is red, the minimum is blue.

do not start at zero for this IC. This changes the balance between the convective and diffusive terms. We take $b = c = f = 0$ so that we get

$$\psi_{i,j}^k = a \cdot (\sin \theta_i)^{2d} (\cos \phi_j)^{2e}.$$

Taking $a = 3.2627$ and $d = e = 20$, we get the progression of the extrema of ψ as depicted in Figure 9.16. The progression differs a lot from the progression depicted in Figure 9.15. As the emphasis in this thesis is on the results for the second order tensor \mathbf{A} , we will consider the influence of the IC more extensive in Subsubsection 9.4.2.2.

In the former cases, the shear rate G was immediately at its 'final' value. It was not progressively built up in time. Although the accelerations in the flow in the process of injection molding are large, a certain dependence of the shear rate on time seems plausible. In accordance, we introduce a logistic function which we use as a time dependent factor to smoothly build up the shear rate in time. It has the form

$$g(t) = \frac{1}{1 + \frac{1}{e^{h(t-j)}}} = \frac{e^{h(t-j)}}{e^{h(t-j)} + 1}. \quad (9.5)$$

In this way, the LD contribution to the fiber orientation is smoothly built up. In particular, the convection as a result of the internal stress in the fiber, $\psi \nabla \cdot \dot{\mathbf{p}}$, is now smoothly built up. The rotary diffusion remains unchanged. Taking $(h, j) = (0.1, 40)$ gives the logistic function as depicted in Figure 9.17 and the progression of the extrema of ψ as depicted in Figure 9.18.

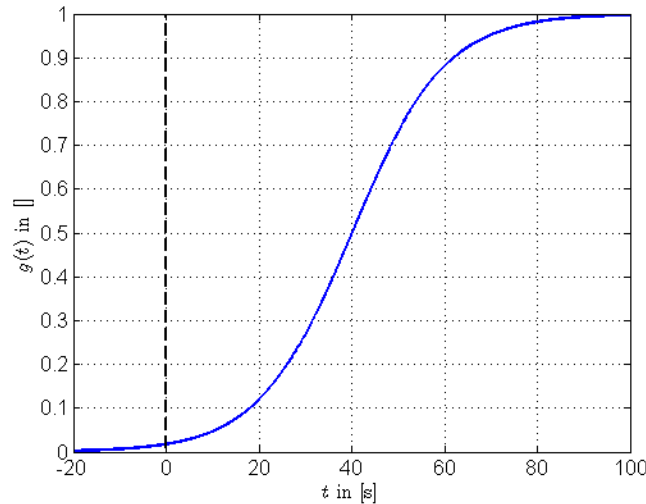


Figure 9.17: logistic function to smoothly build up the shear rate in time.

For the time dependent shear rate in question, the balance between the convection and diffusion is immediate, and not after an overshoot. As the shear rate is almost zero at initiation, and slowly increases, the convective and diffusive contributions to the orientation have a different ratio in comparison with the former cases. Where the LD dominated the FFI in the former cases, the FFI now 'gets more time' to counteract the slowly increasing LD. As before, the emphasis will be on the second order orientation, and thus the consequences of using a time dependent shear rate are treated more thorough in Subsection 9.4.2.2.

Aside from the particular case that the ellipsoidal fibers have an infinite ratio for the long to short axis, or $\xi = 1$, it is also interesting to consider cases where $\xi \neq 1$ but close to one. As discussed in 9.3, the fibers do not have stationary points in this case. From (9.3), it follows that the probability density will not have a steady state. When rotary diffusion is added, ψ does have a steady state. It is reached when the convection and diffusion are in balance. This balance is expected to be at a lower values of ψ compared to the $\xi = 1$ case. This is justified by the fact that we are considering a probability density for a set of fibers. When $\xi = 1$, every fiber of this set will align the same way, creating extrema of ψ that are concentrated in a small area $\in S$. When $\xi \neq 1$, all the fibers of the set keep rotating and so the probability density is smeared out over the area that the fibers 'pass'. As the initial positions of the fibers in the set are arbitrary, this area is S . Extrema of ψ will therefore be less concentrated, confer Figures 9.19 and 9.20. In effect, also the steady state values will be lower.

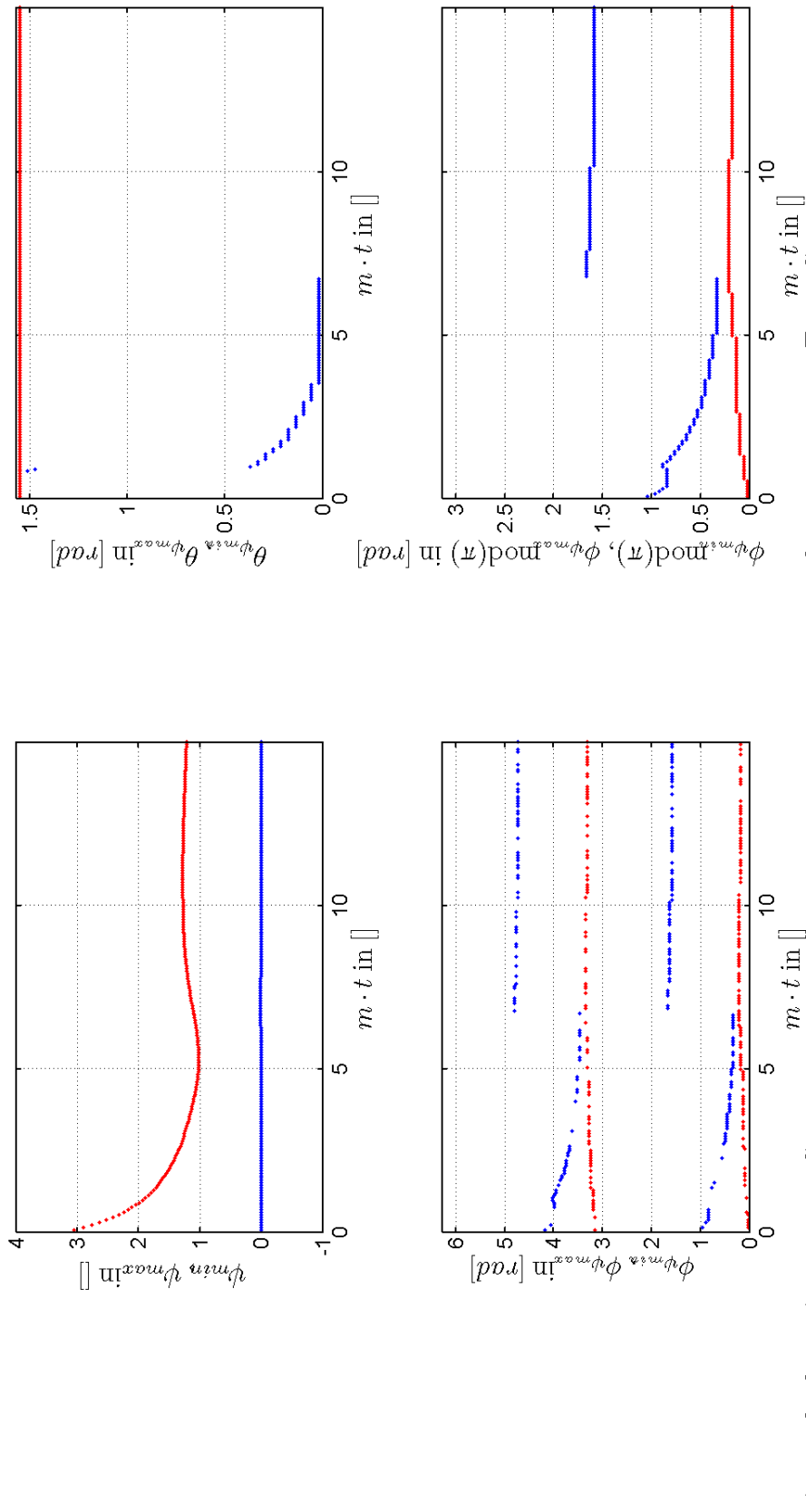


Figure 9.16: location and values of the extrema of the probability density for the nonuniform IC (7.23).

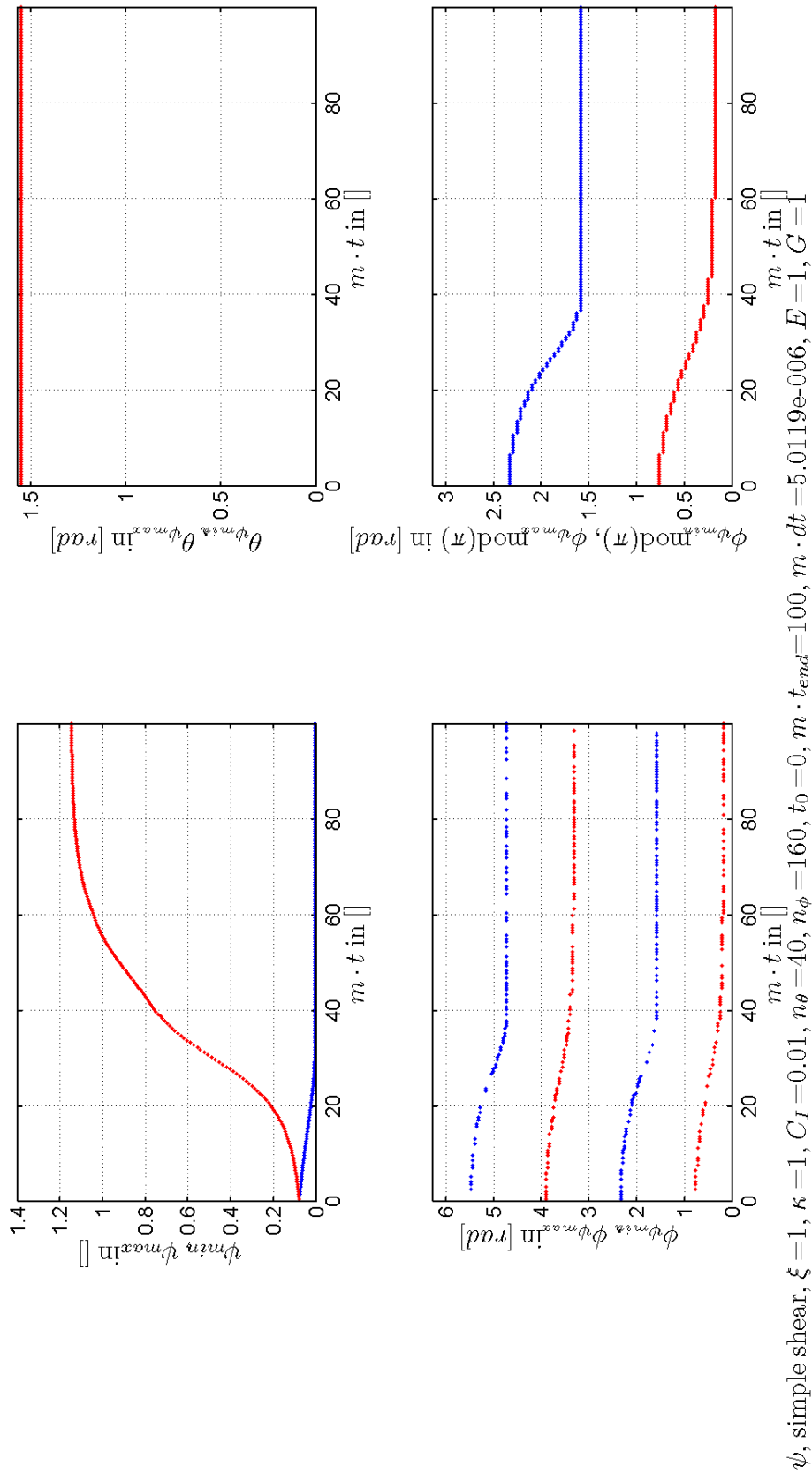


Figure 9.18: location and values of the extrema of the probability density for a time dependent shear rate.

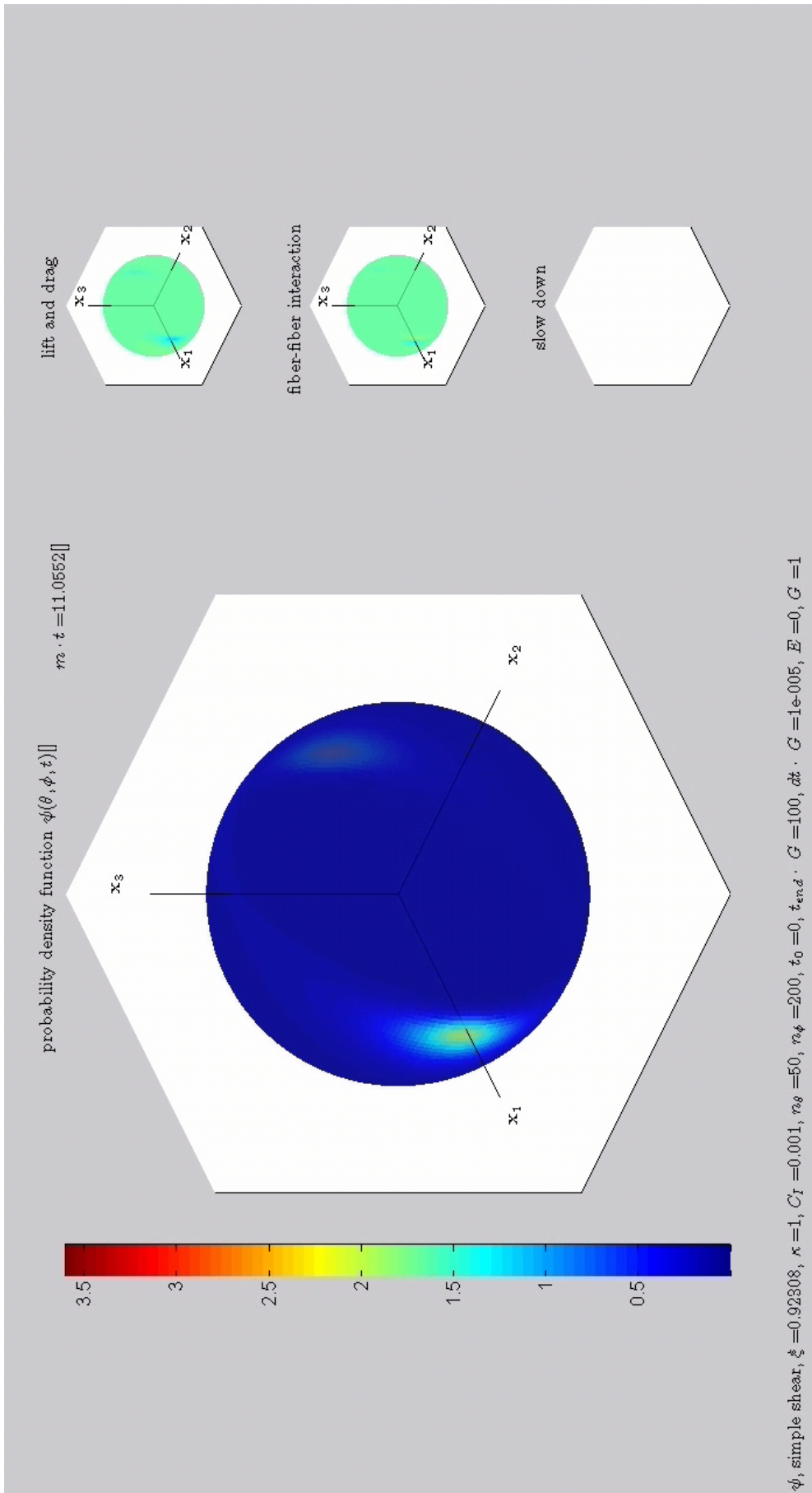


Figure 9.19: the extrema are less concentrated in space when $\xi \neq 1$.

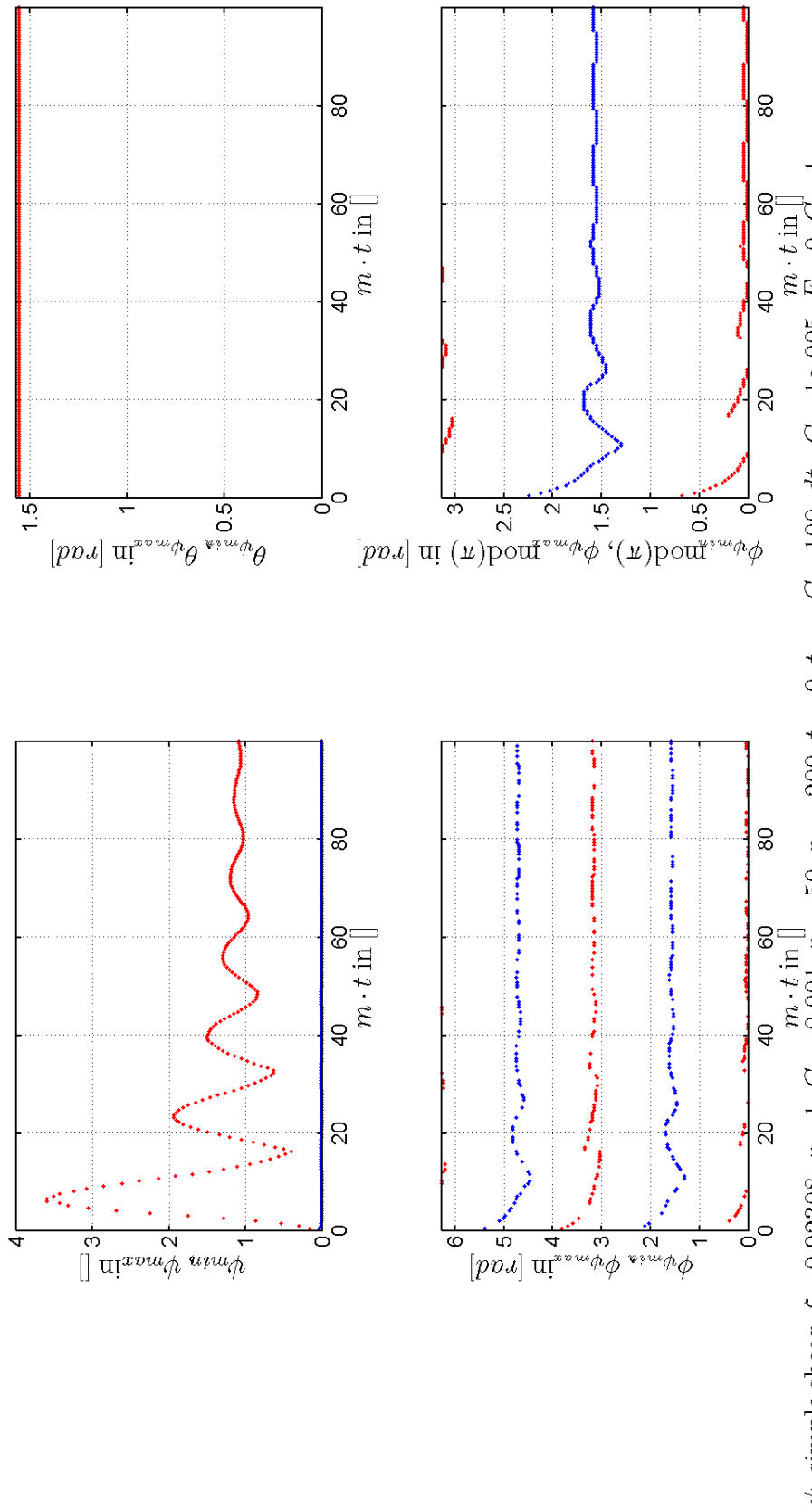


Figure 9.20: the minima are larger and the maxima are lower when $\xi \neq 1$.

The remaining parameter that can be varied is the shear rate $G[\frac{1}{s}]$. However, recalling Section 7.3 it follows that in the case of the simple shear flow field, it merely scales the time. The process time decreases inversely proportional to G . The other quantities remain the same. It follows that the consideration of the shear rate is redundant.

9.4.2.2 Second order orientation tensor

We have constructed the numerical solution of ψ from the Folgar-Tucker model. It contains all the information on the fiber orientation. Nonetheless, it is still important to consider the orientation tensors as these are the quantities that we want to use eventually to obtain data from practical injection molding processes. We can relate the observations we make from the orientation tensors to the observations we made from the PDF.

We recall Definition 4.1

$$\mathbf{A}(t) = \oint_S \psi(\mathbf{p}, t) \mathbf{p} \mathbf{p} d^2 \mathbf{p}.$$

and in particular Property 4.9

$$\mathbf{A}(t) = 2 \int_{S^{up}} \psi(\mathbf{p}, t) \mathbf{p} \mathbf{p} d^2 \mathbf{p}$$

where S^{up} is the surface of the upper hemisphere. Using generalized coordinates the tensor becomes the matrix

$$\mathbf{A}(t) = 2 \int_{\phi=0}^{2\pi} \int_{\theta=0}^{\frac{\pi}{2}} \psi(\theta, \phi, t) \mathbf{p}(\theta, \phi) \mathbf{p}(\theta, \phi) \sin(\theta) d\theta d\phi.$$

From this identity, \mathbf{A} can be seen as a sum of ψ times a weight $\mathbf{p} \mathbf{p} \sin \theta$, both varying in space. Depending on the position on the upper hemisphere, the probability density is represented with a certain strength in \mathbf{A} . We depicted the weights in Figures 4.1-4.6 to indicate where the PDF is represented stronger or weaker, per component of \mathbf{A} .

For the case $(\xi, C_I, \kappa, G) = (1, 0.001, 1, 1)$ the components of \mathbf{A} and $\dot{\mathbf{A}}$ are depicted in Figure 9.21. The A_{13} and A_{23} components are zero to machine precision, as the flow field does not vary in the x_3 direction. It stands out that A_{11} is the strongest component. The reason for this is that both ψ and $p_1^2 \sin \theta$ are the strongest in the neighborhood of the x_1 axis. The contribution of ψ to A_{11} is smaller away from the x_1 axis. As we are still considering the Folgar-Tucker model and not the Wang-O'Garra-Tucker model with additional RSC term, $\dot{\mathbf{A}}^{RSC} = 0$. As the preferred direction is the x_1 axis, A_{22} and A_{33} are much smaller than A_{11} . This also holds for the fluxes. Because the probability density is not all at the ends of the x_1 axis, but rather with a slightly increased ϕ away from the x_1 axis, the A_{12} component is nonzero. The principal axes are thus not aligned with the axes of the velocity flow field, confer Figures 9.22, 9.23 and 9.24. The color of the axes represents the strength of the direction, which stems from the corresponding eigenvalues. The discontinuities in the ϕ graph stem from the eigenvector that is aligned with the x_3 axis. As in this case we have that $\theta = 0$, it does not matter what ϕ is. Its values are scattered due to

$$\phi = \arctan \frac{(\mathbf{e}_i)_2}{(\mathbf{e}_i)_1}$$

with $(\mathbf{e}_i)_1$ zero or zero to machine precision.

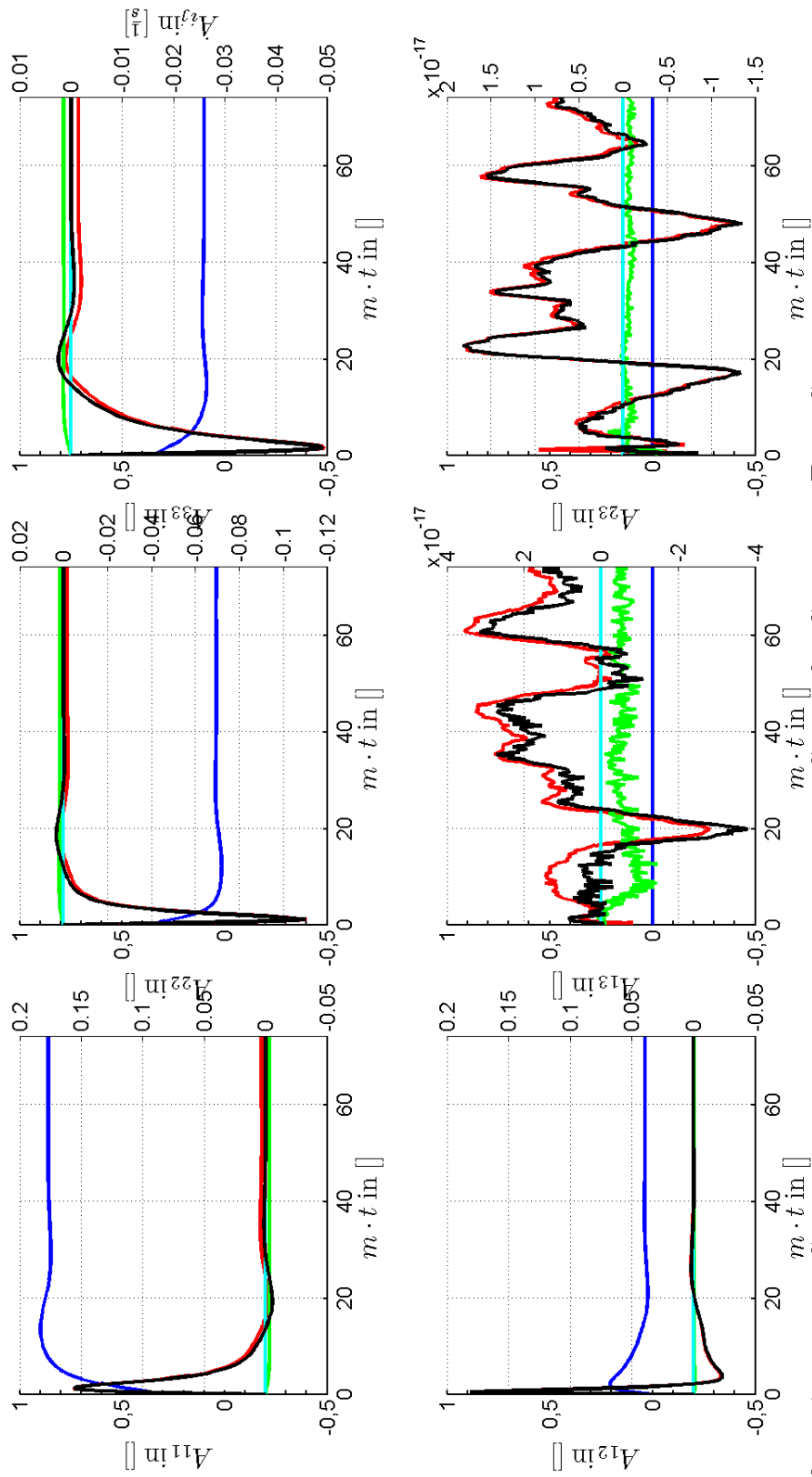
We see that all the nonzero components of \mathbf{A} show an overshoot before they reach their equilibrium. The origin hereof has already been discussed in Subsubsection 9.4.2.1. It was found that the IC and time dependence of the shear rate were of importance for the balance between the convection and the diffusion. We will discuss both variations.

We recall the nonuniform IC (7.23)

$$\psi_{i,j}^0 = a \cdot (\sin(\theta_i - b))^{2d} (\cos(\phi_j - c))^{2e} + f, \quad a > 0, b \in \left[0, \frac{\pi}{2}\right], c \in [0, 2\pi), d, e \in \mathbb{Z}^+, f \geq 0.$$

In particular, we set $b = c = f = 0$ so that the maxima of the IC lie at $(\theta, \phi) \in \{(\frac{\pi}{2}, 0), (\frac{\pi}{2}, \pi)\}$. In this way, the probability density is already somewhat set to the preferred direction of the simple shear flow field. Because the IC is nonuniform, the rotary diffusion

$$\tilde{\nabla} \cdot \tilde{\nabla} \psi$$



ψ , simple shear, $\xi = 1$, $\kappa = 1$, $C_I = 0.001$, $n_\theta = 50$, $n_\phi = 200$, $t_0 = 0$, $t_{end} = 74$, $dt \cdot G = 1e-005$, $E = 0$, $G = 1$

Figure 9.21: the components of \mathbf{A} and $\dot{\mathbf{A}}$. The blue lines represent the components of \mathbf{A} , the black lines the components of $\dot{\mathbf{A}}$, and the red, green and turquoise lines the LD, FFI and RSC contributions hereof respectively.

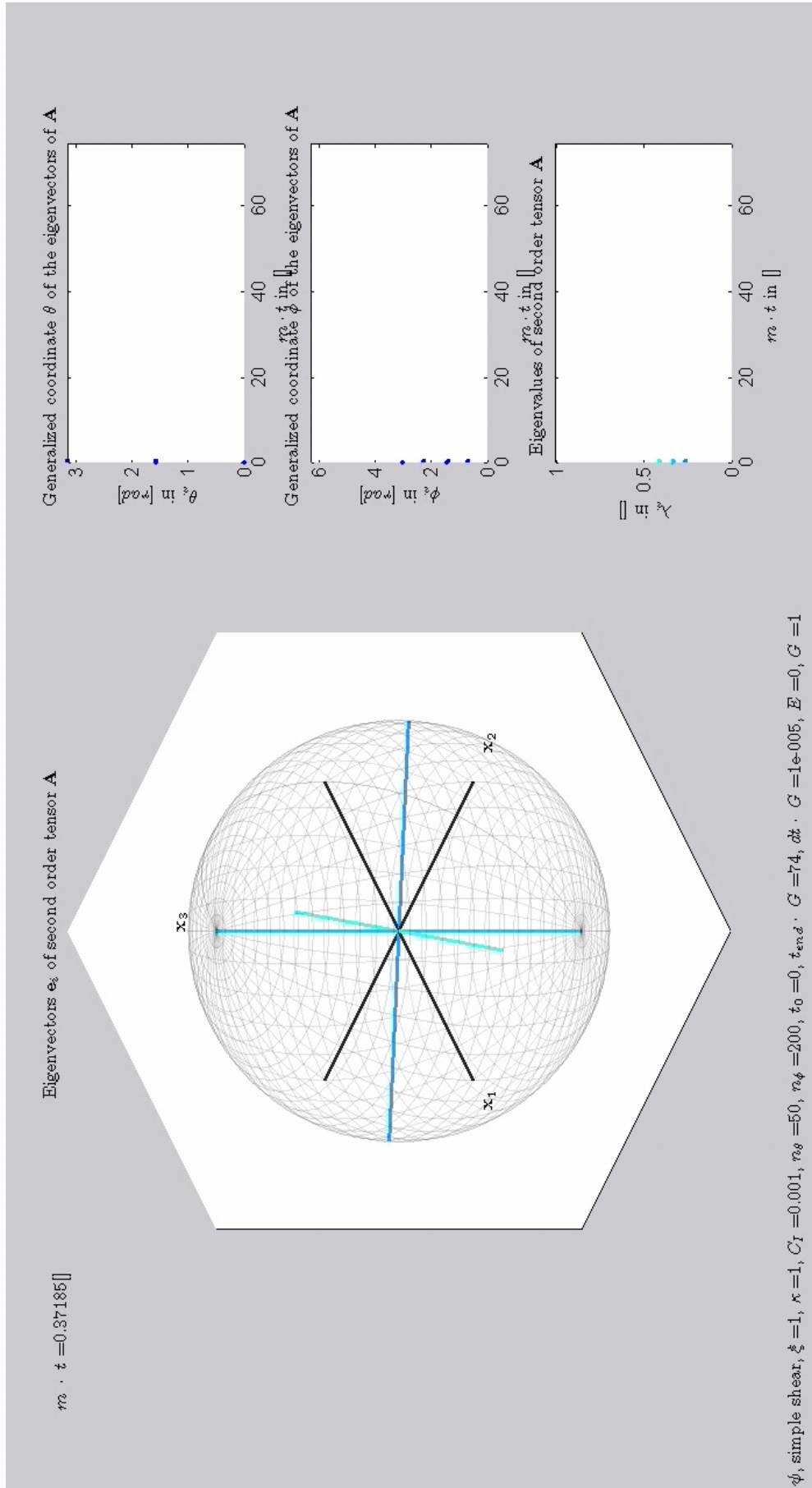


Figure 9.22: initial state of the eigenpairs.

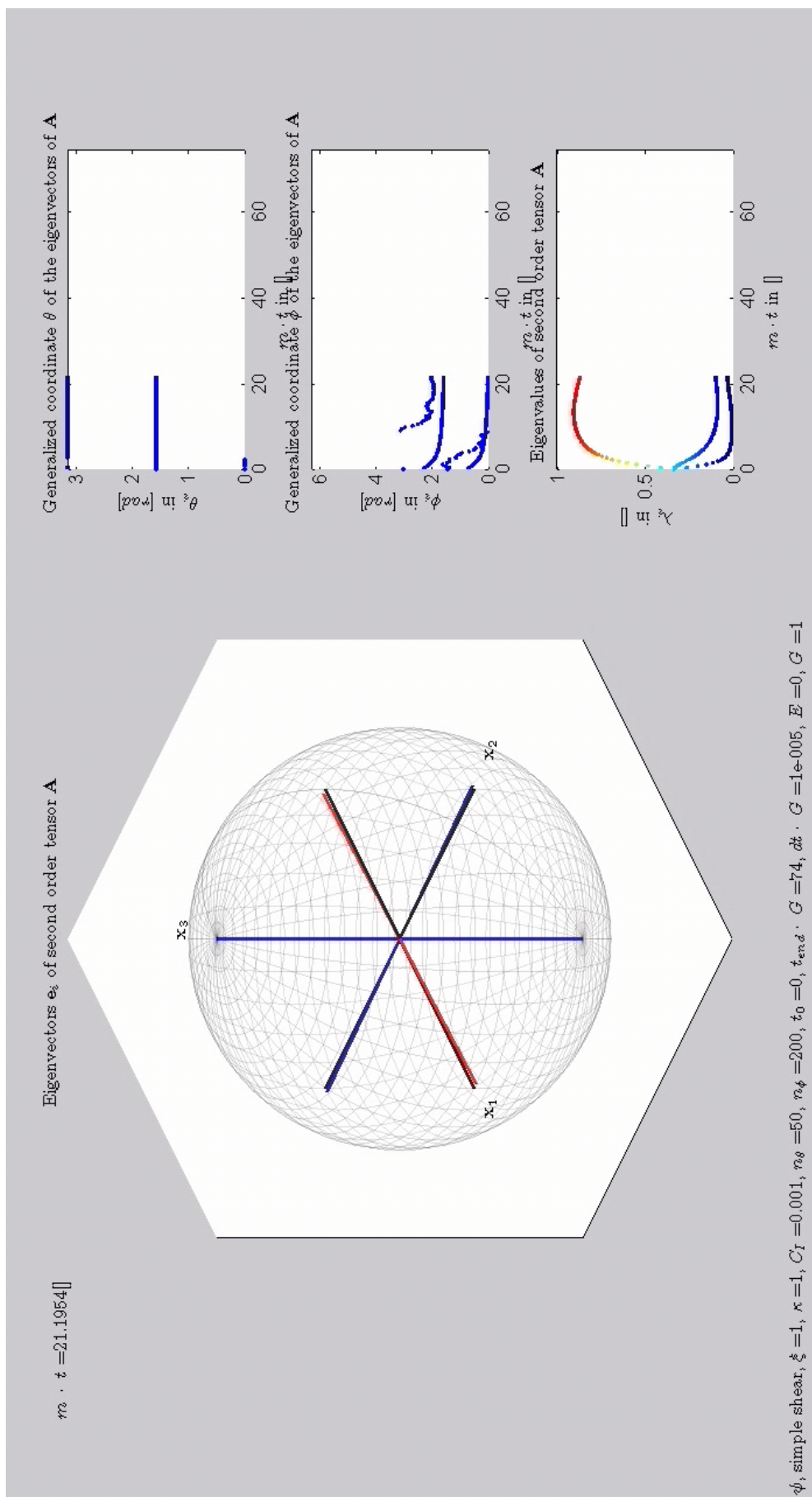


Figure 9.23: the principal axes almost align with the flow field axes.

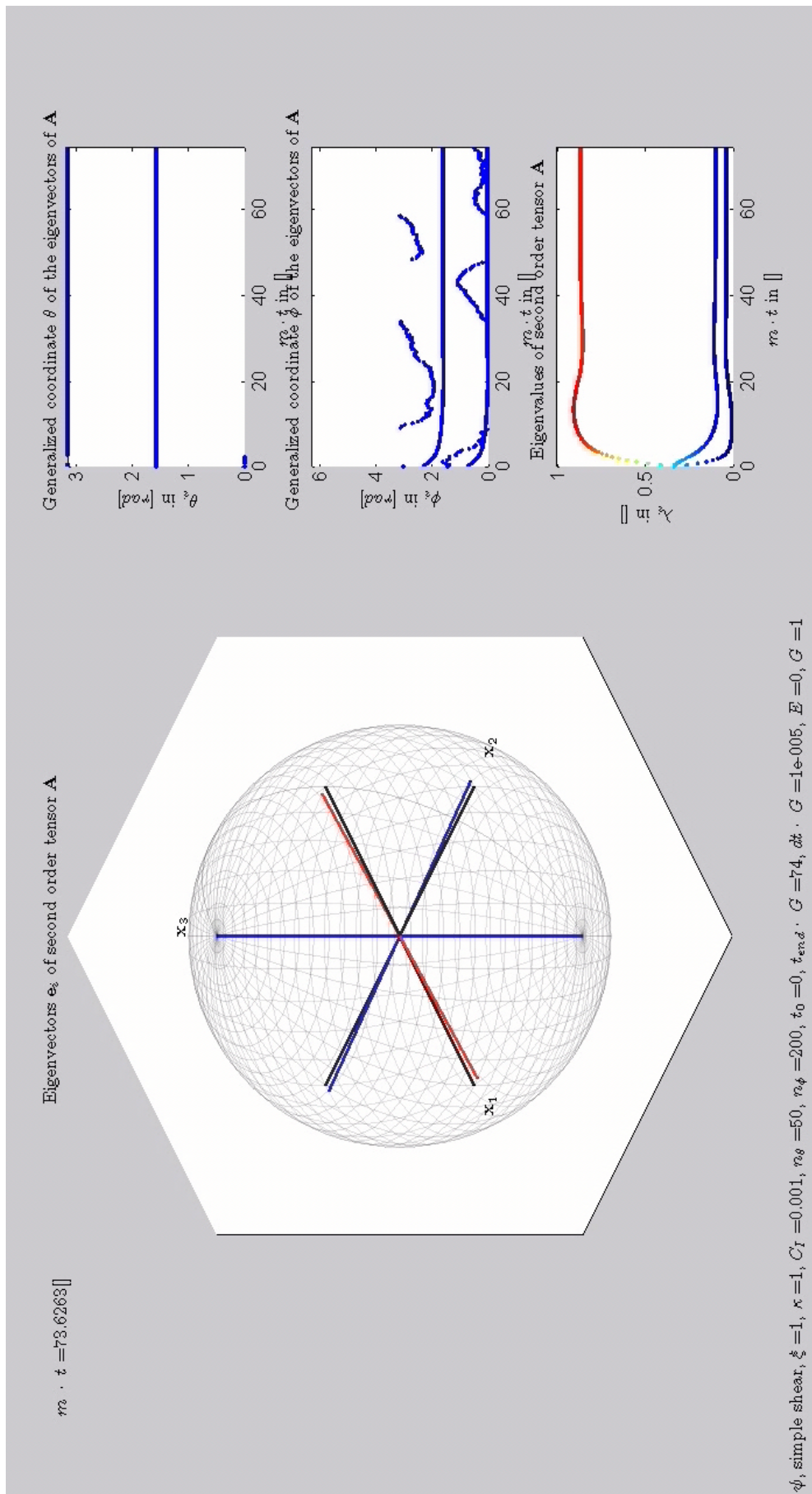


Figure 9.24: diffusion pulls the principal axes away from the flow field axes, to a random orientation state.

is not zero everywhere and thus also the FFI contribution $\dot{\mathbf{A}}^{FFI}(t_0) \neq 0$. This results in a different ratio between the convection and diffusion. Increasing the powers of the sinusoids and taking a such that $\int_S \psi d^2\mathbf{p} = 1$, we have that $A_{11} \uparrow 1$, $A_{22}, A_{33} \downarrow 0$, as depicted in Figure 9.25. The extrema are clearly displaced in time per case of the powers. Nevertheless, the components maintain the same steady state and thus the solutions calculated with different ICs will eventually converge, as we observe. The variation of the IC indicates how 'strong' the memory of the tensor is. In other words, to what extent in time the variation of the IC results in a different value of the components of \mathbf{A} .

For varying the shear rate we recall the logistic function (9.5)

$$g(t) = \frac{1}{1 + \frac{1}{e^{h(t-j)}}} = \frac{e^{h(t-j)}}{e^{h(t-j)} + 1}$$

and set $h = 0.1$, $j = 40$, confer Figure 9.18. We use the latter as a factor for G to make the shear rate time dependent. The result is depicted in Figure 9.26. As mentioned in Subsubsection 9.4.2.1, the shear rate is not immediate anymore, so that the orientation is not convection dominated at initiation. The convection and diffusion are of the same order of magnitude. The balance is now also immediate, instead of first overshooting.

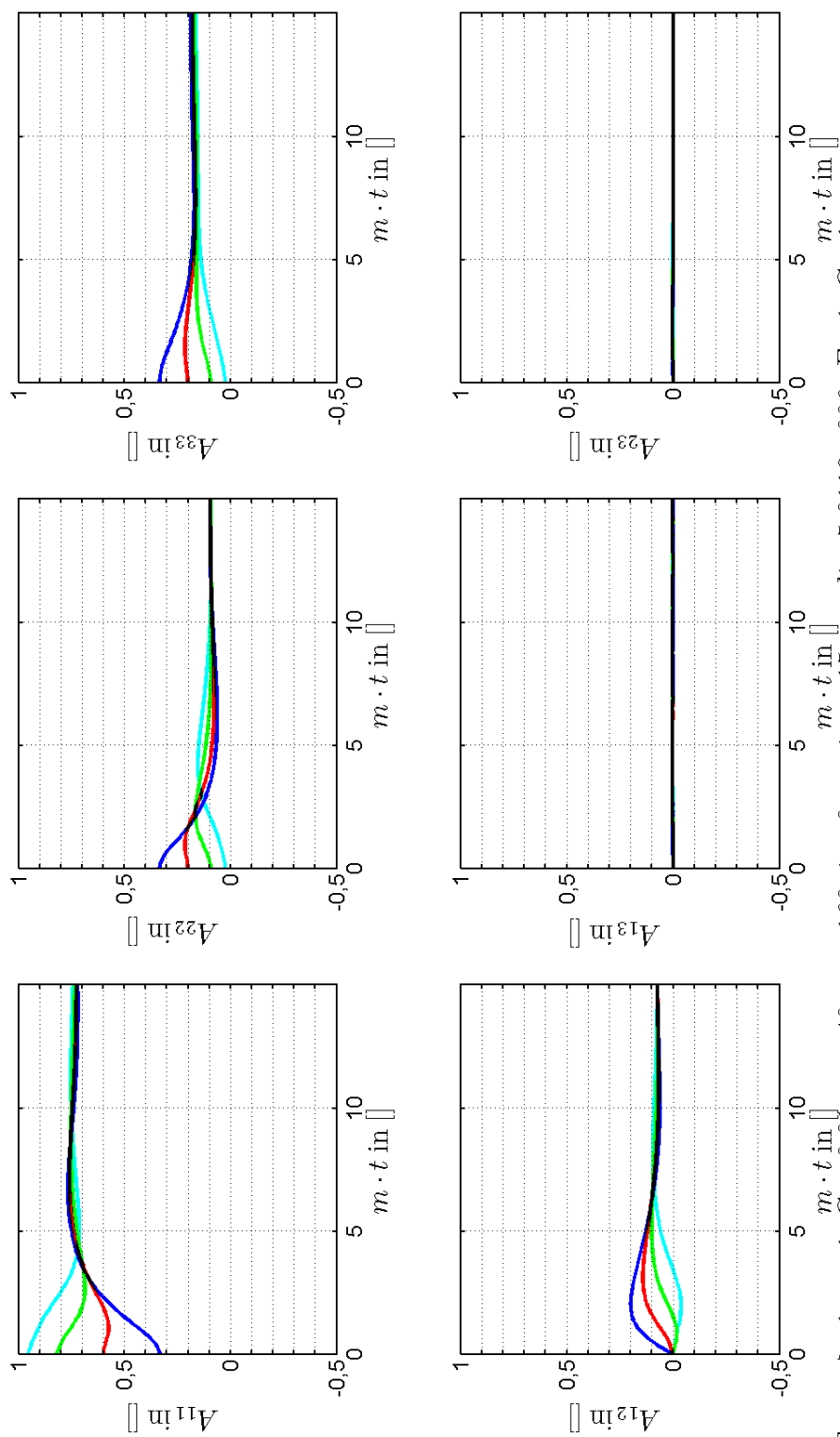
For the cases $(\xi, \kappa, C_I, G) \in \{(1, 1, 0.01, 1), (1, 1, 0.1, 1)\}$ similar behavior is observed. The corresponding Figures are 9.27 and 9.28, and 9.29 and 9.30 respectively. Increasing the strength of the rotary diffusion, C_I , makes the FFI contribution $\dot{\mathbf{A}}^{FFI}$ stronger. The counteraction to the LD contribution increases and the total change $\dot{\mathbf{A}}$ decreases, leaving \mathbf{A} closer to its uniform initial condition, the random orientation state. This implies that the diagonal components have a tendency towards the value $\frac{1}{3}$. Indeed, the diagonal components show this tendency, as do the eigenvalues of \mathbf{A} . As the flow field does not vary in the x_3 direction, the inclination to a random orientation state takes place in the x_1 - x_2 plane. This implies that

$$\psi \rightarrow \frac{\delta(\theta - \frac{\pi}{2})}{4\pi} \quad \Rightarrow \quad \mathbf{A} \rightarrow \begin{bmatrix} \frac{1}{2} & 0 & 0 \\ 0 & \frac{1}{2} & 0 \\ 0 & 0 & 0 \end{bmatrix}.$$

The factor $\frac{1}{4\pi}$ in ψ again stems from the conservation of the total probability, $\int_S \psi d^2\mathbf{p} = 1$. A possible set of eigenpairs of the latter is

$$(\lambda_i, \mathbf{e}_i) \in \left\{ \left(\frac{1}{2}, \begin{bmatrix} 1 \\ 1 \\ 0 \end{bmatrix} \right), \left(\frac{1}{2}, \begin{bmatrix} 1 \\ -1 \\ 0 \end{bmatrix} \right), \left(0, \begin{bmatrix} 0 \\ 0 \\ 0 \end{bmatrix} \right) \right\}.$$

The inclination to this state is depicted in Figure 9.30. As the difference between the principal axes and flow field basis becomes larger, also the A_{12} component increases.



ψ , simple shear, $\xi = 1$, $\kappa = 1$, $C_I = 0.01$, $n_\theta = 40$, $n_\phi = 160$, $t_0 = 0$, $m \cdot t_{end} = 15$, $m \cdot dt = 5.0119e-006$, $E = 1$, $G = 1$

Figure 9.25: making the IC nonuniform changes the balance between convection and diffusion.

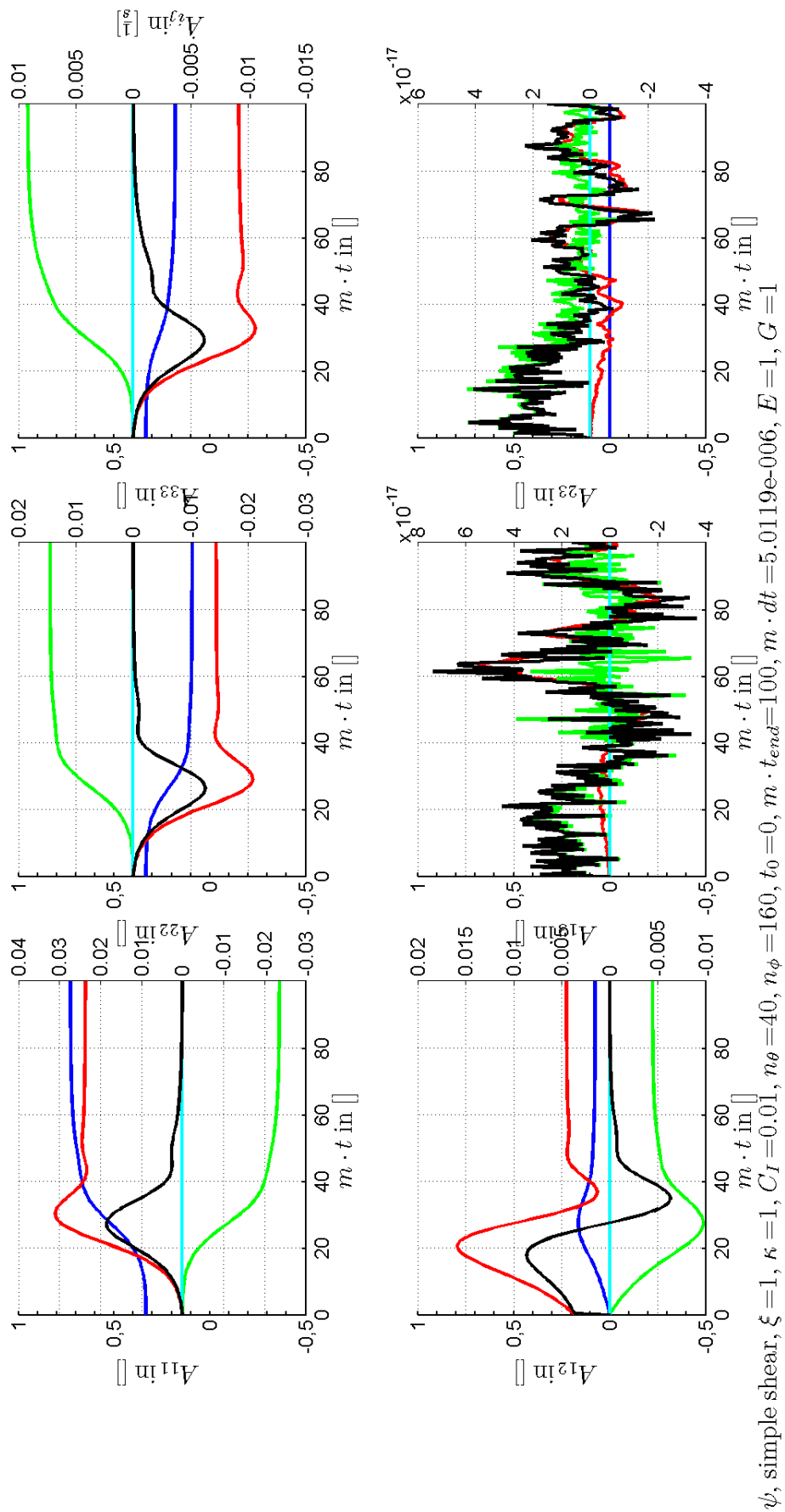


Figure 9.26: building up the shear rate changes the balance between convection and diffusion.

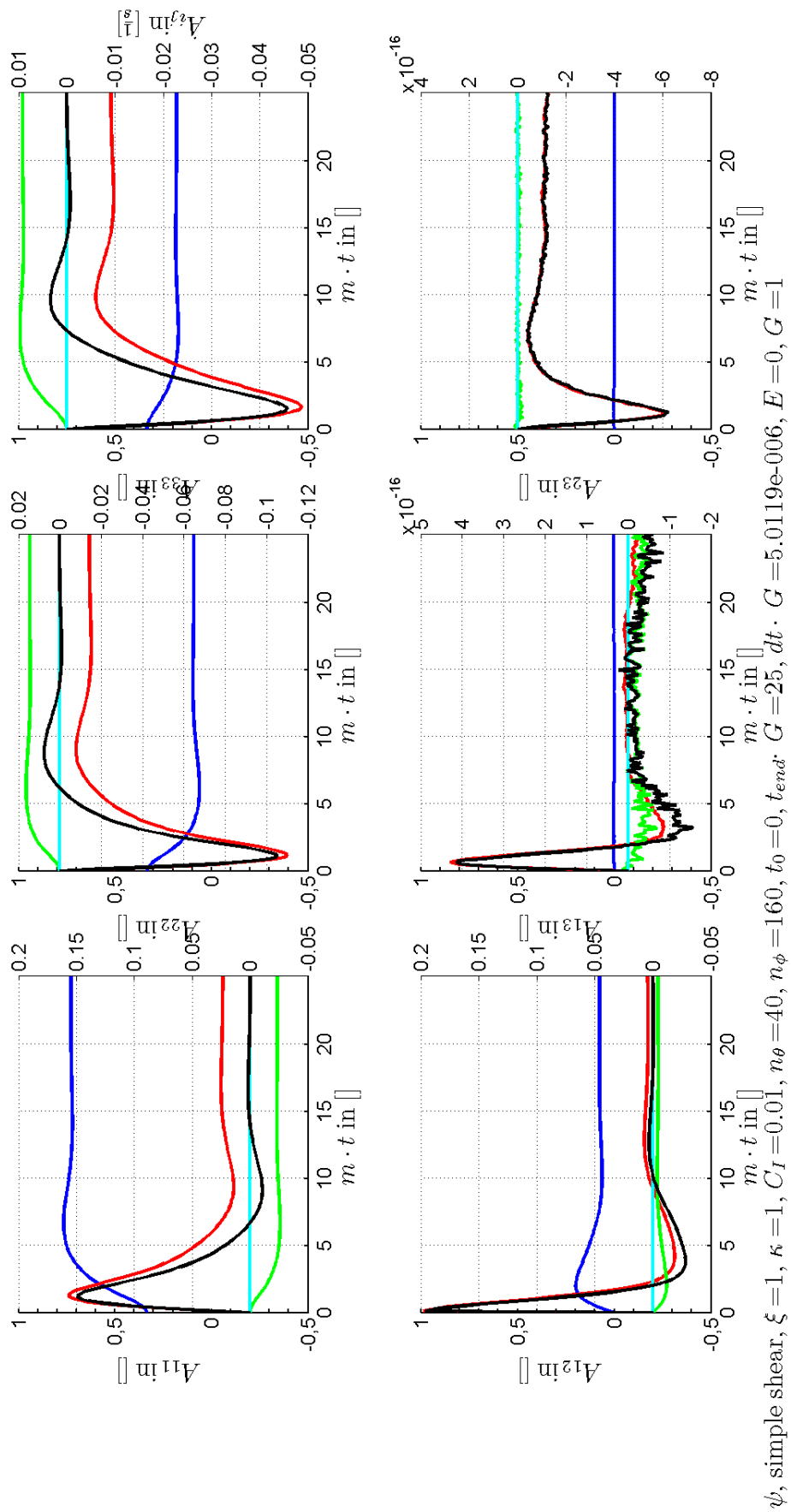


Figure 9.27: the components of \mathbf{A} and $\tilde{\mathbf{A}}$.

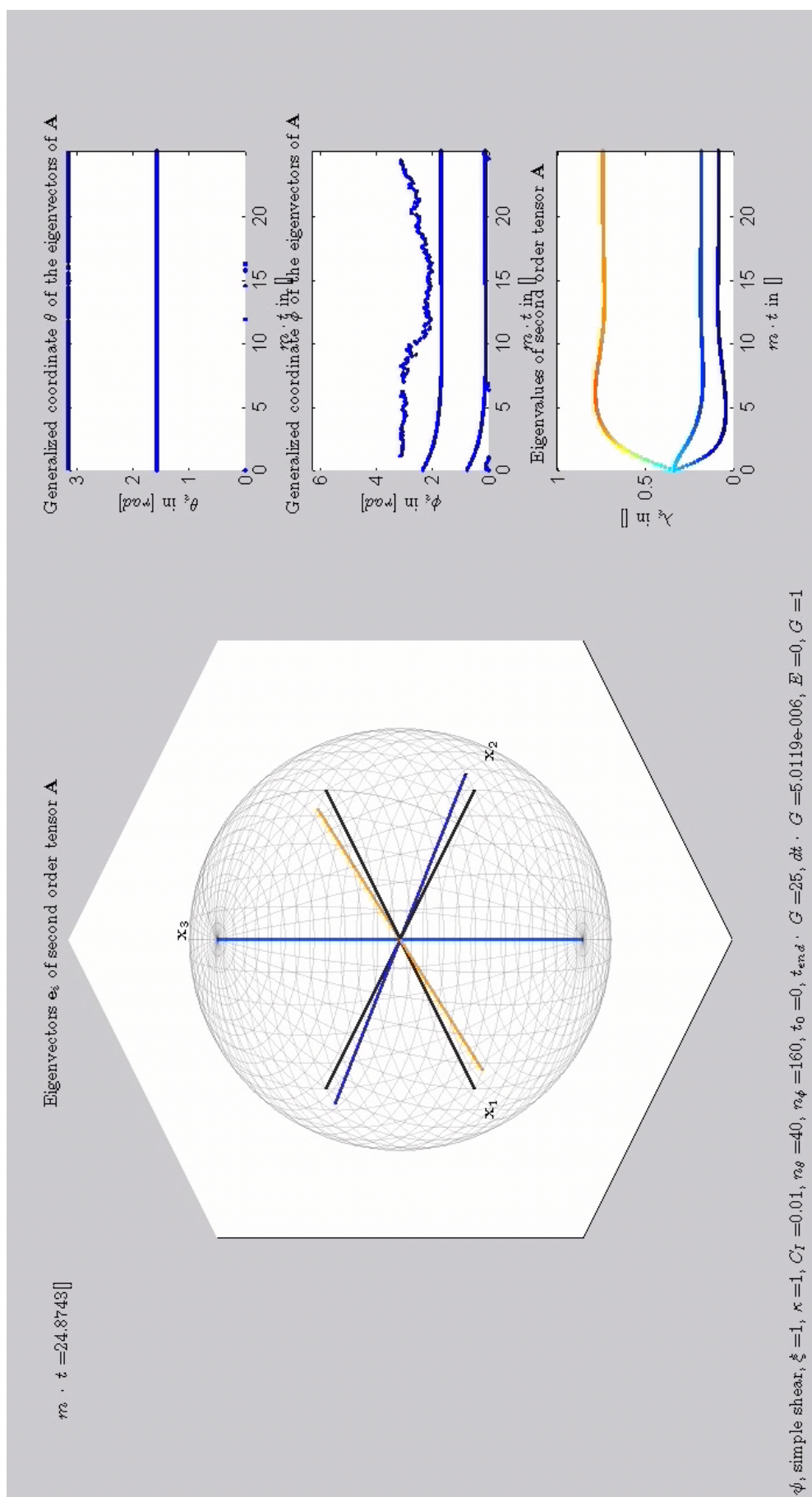


Figure 9.28: diffusion pulls the principal axes away from the flow field axes, to a random orientation state.

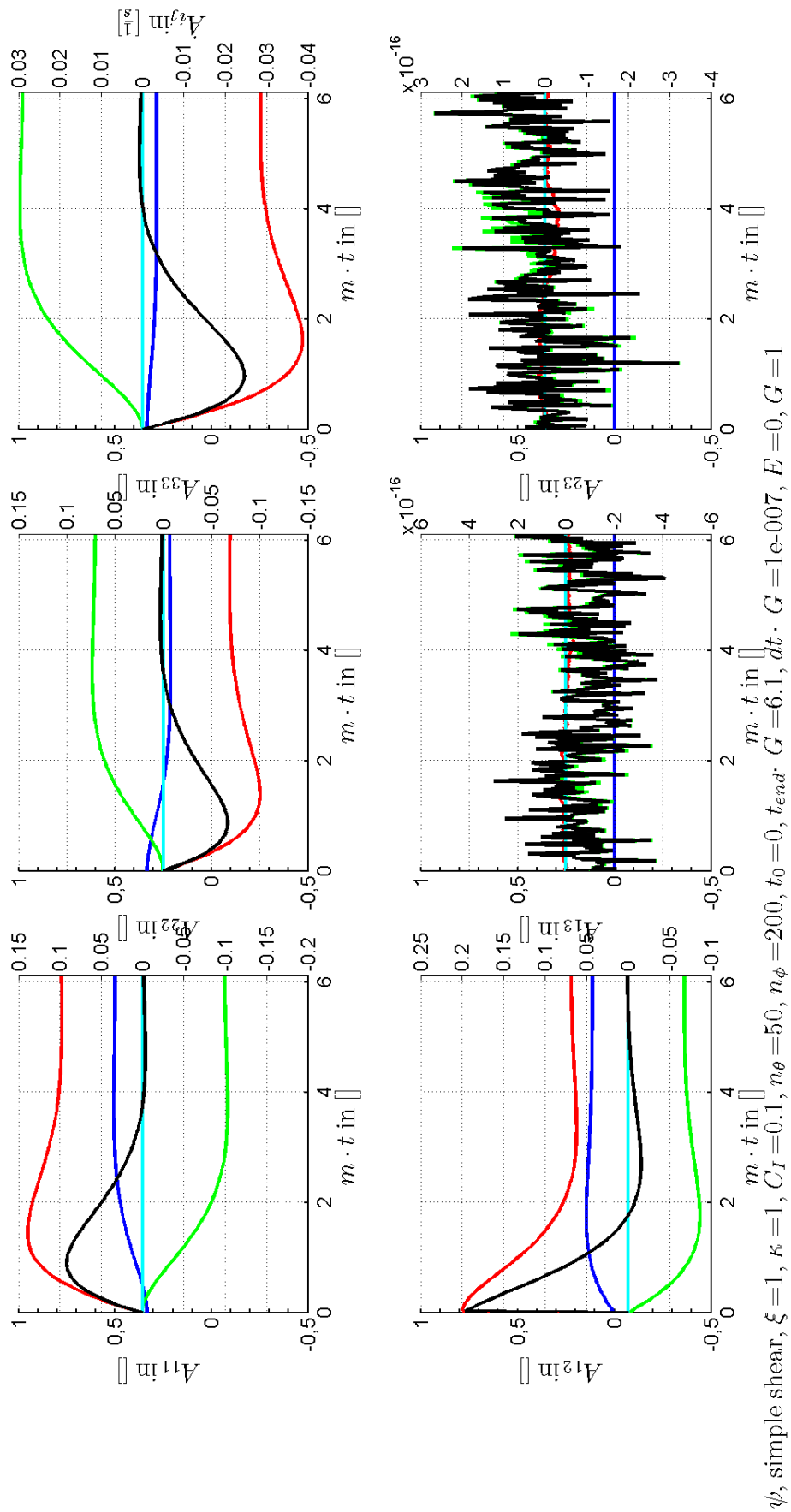


Figure 9.29: the components of \mathbf{A} and $\bar{\mathbf{A}}$.

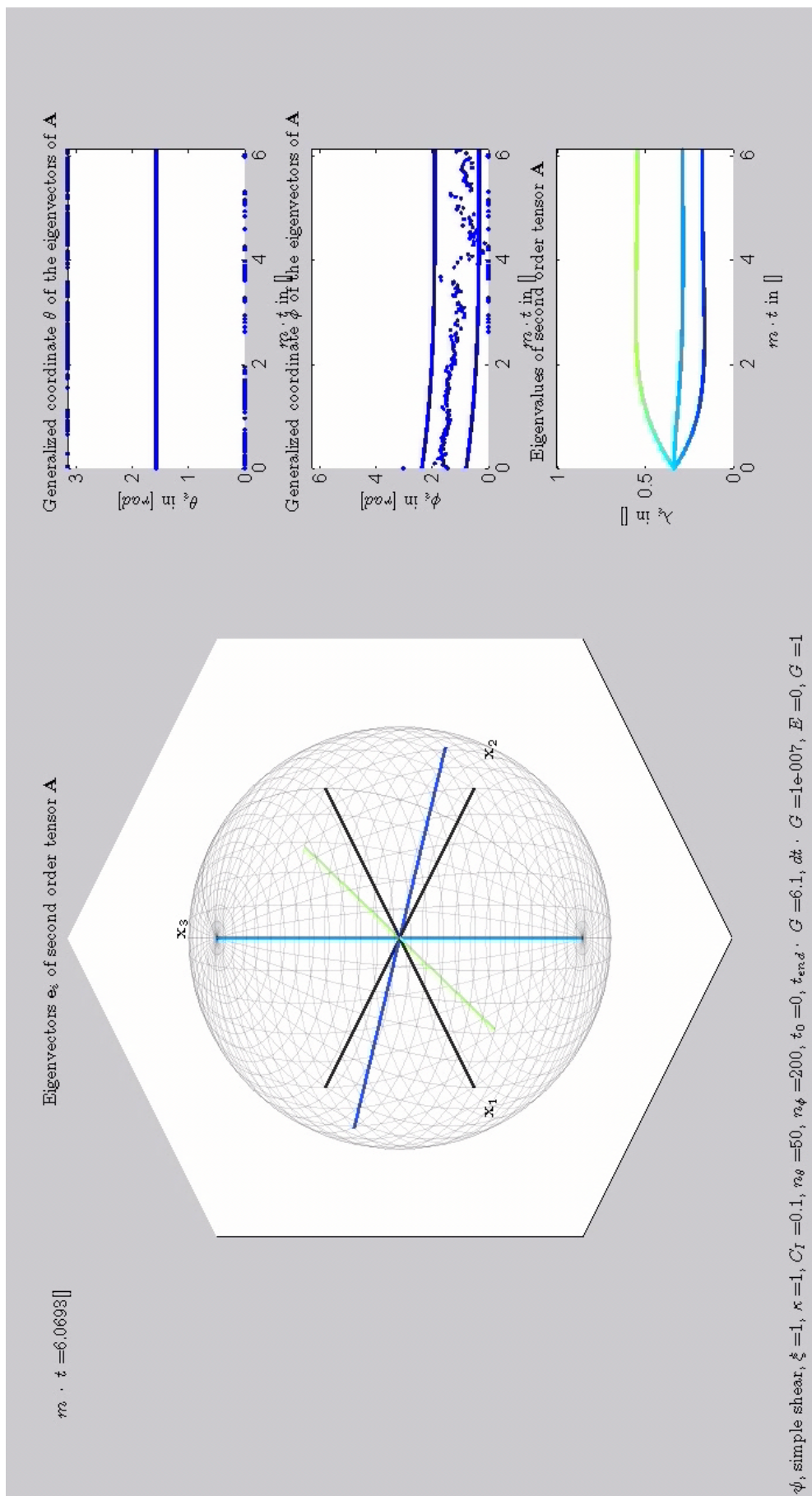


Figure 9.30: diffusion pulls the principal axes away from the flow field axes, to a random orientation state.

9.4.3 The RSC extension

Adding the RSC term to the original Folgar-Tucker model, we obtain the kinetic theory of the Wang-O'Gara-Tucker model

$$\begin{aligned}\dot{\psi} &= -\tilde{\nabla} \cdot (\psi \dot{\mathbf{p}} + \mathbf{q}) \\ \dot{\mathbf{p}} &= \mathbf{W} \cdot \mathbf{p} + \xi(\mathbf{D} \cdot \mathbf{p} - \mathbf{D} : \mathbf{p}\mathbf{p}\mathbf{p}) - C_I \dot{\gamma} \tilde{\nabla} \ln \psi \\ \mathbf{q} &= \sum_l \beta_l (\mathbf{e}_l \mathbf{e}_l \cdot \mathbf{p} - \mathbf{e}_l \mathbf{e}_l : \mathbf{p}\mathbf{p}\mathbf{p}) \\ \beta_l &= -\frac{5(1-\kappa)}{4\pi} [\xi(\lambda_l \mathbf{D} : \mathbf{e}_l \mathbf{e}_l - \mathbf{e}_l \mathbf{e}_l : \mathbb{A} : \mathbf{D}) + C_I \dot{\gamma} (1 - 3\lambda_l)].\end{aligned}$$

As discussed in Section 5.5, the additional RSC term 'draws' fibers toward, or 'pushes' them away from, the eigenvectors of \mathbf{A} . This is done in a way that the strain is reduced, so that the transient time is prolonged. The steady state values should remain the same. The strain reduction changes both the convection and the diffusion, altering the balance between them. As a result, the extrema are displaced, as depicted in Figure 9.31.

We consider the rate equation for the second order orientation tensor

$$\dot{\mathbf{A}} = \mathbf{W} \cdot \mathbf{A} - \mathbf{A} \cdot \mathbf{W} + \xi\{\mathbf{D} \cdot \mathbf{A} + \mathbf{A} \cdot \mathbf{D} - 2[\mathbb{A} + (1 - \kappa)(\mathbb{L} - \mathbb{M} : \mathbb{A})] : \mathbf{D}\} + 2\kappa C_I \dot{\gamma} (\mathbf{I} - 3\mathbf{A}).$$

As discussed in Chapter 8, both the LD and FFI contribution are decreased by the RSC term. This slows down the orientation, as depicted in Figure 9.32. The transient time is prolonged and the steady state values remain the same. The extrema are displaced. The overshoots have the tendency to disappear, meaning that the balance between the convection and diffusion has the tendency to be immediate.

Varying the parameters ξ , G , C_I and the IC does not offer any new perspectives. The results are analogous to the $\kappa = 1$ case.

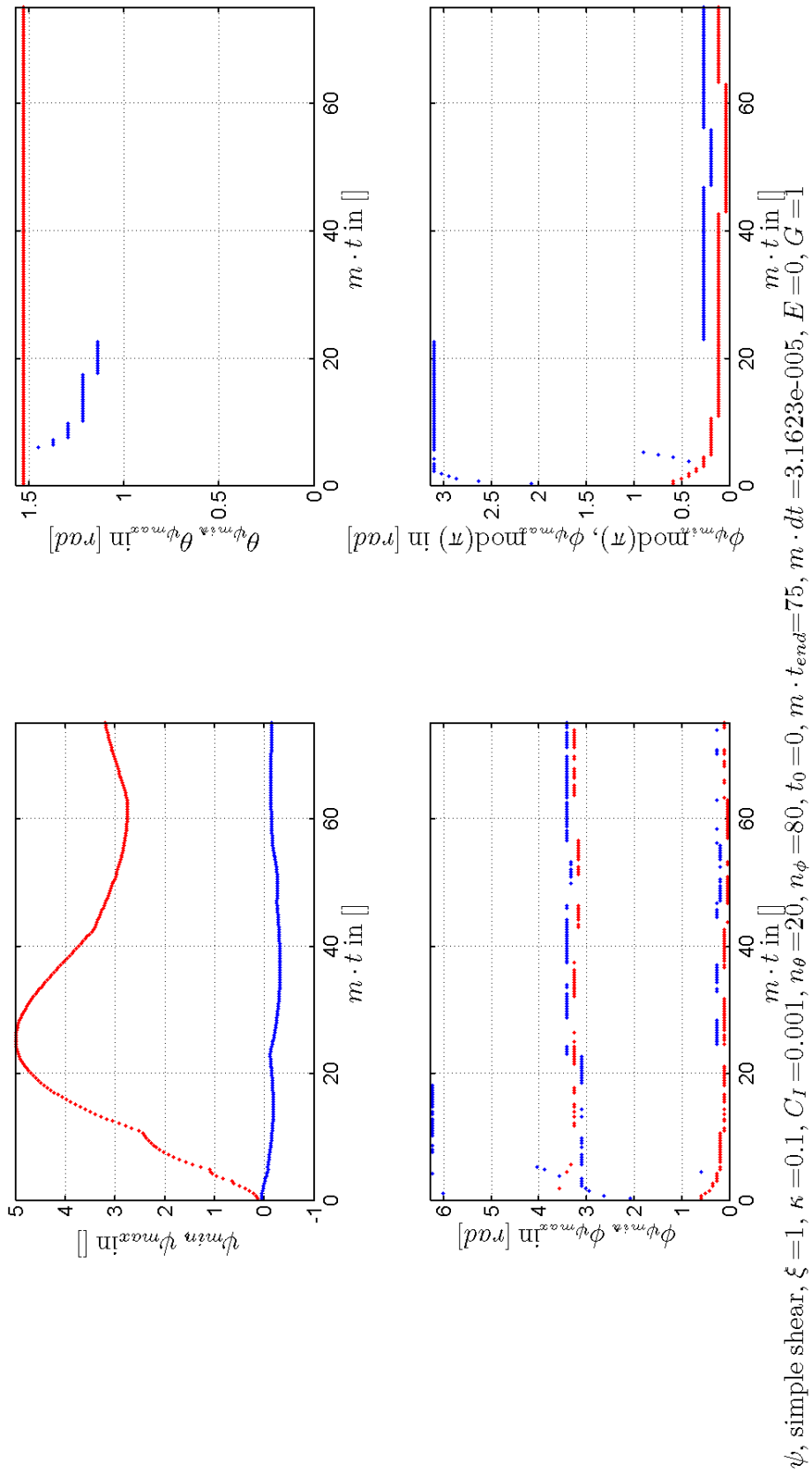


Figure 9.31: the extrema are displaced as the strain is reduced by taking $\kappa = 0.1$.

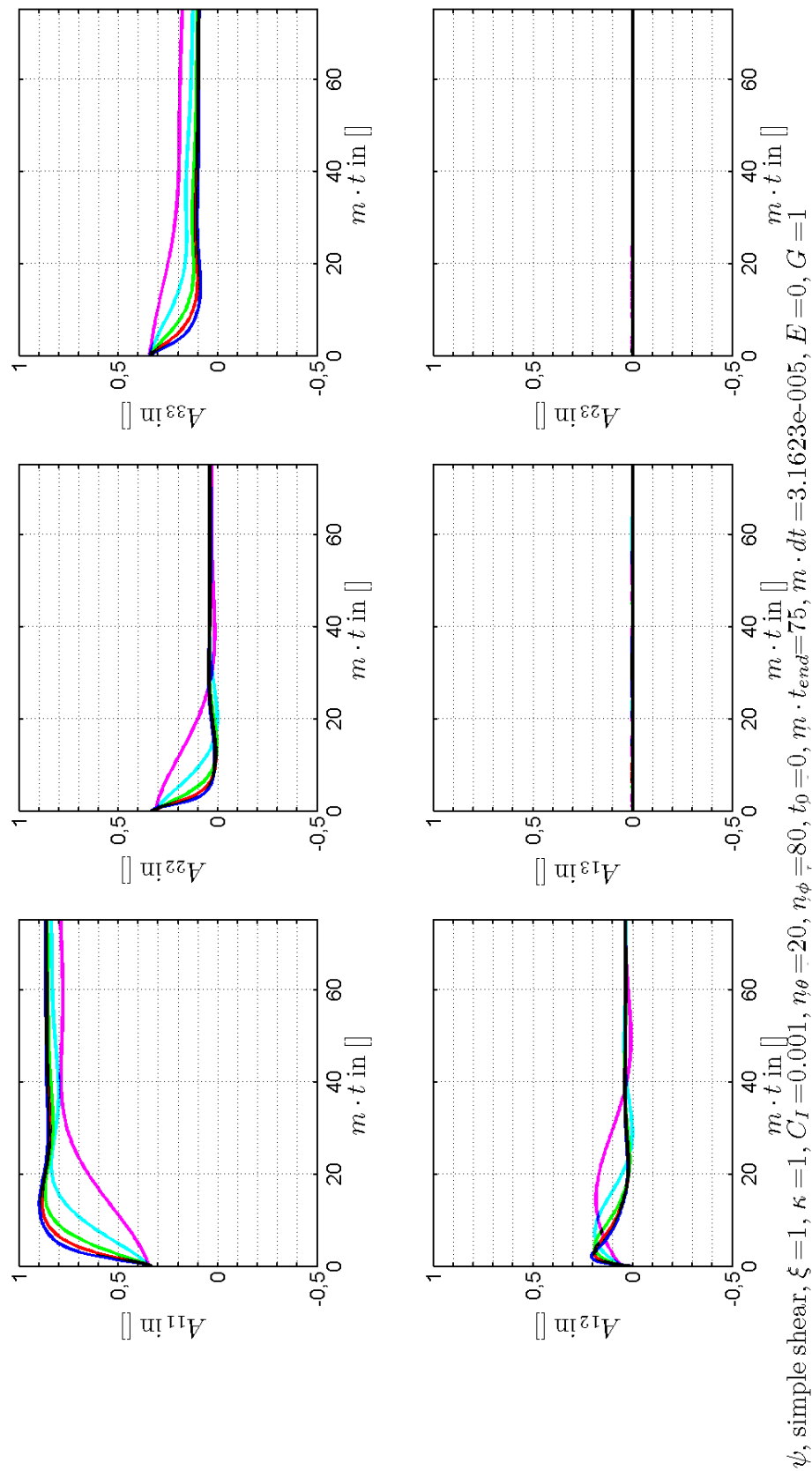


Figure 9.32: the strain is reduced, prolonging the transient time. The used factors are $\kappa \in \{1, 0.75, 0.5, 0.25, 0.1\}$ in blue, red, green, cyan and purple respectively.

9.5 Results tensor approximation

In this section we use the approach as described in Chapters 6 and 8 to obtain solutions for the orientation tensors. We will consider the quadratic, orthotropic smooth and orthotropic fitted closures (QC, OSC and OFC) as constructed in [15]. The coefficients for the OFC were constructed with five different flow fields with the parameters set to $\xi = 1$ and $C_I = 0.01$:

- simple shear, $v_1 = Gx_2, v_2 = v_3 = 0$,
- shearing/stretching flow, $v_1 = -Ex_1 + Gx_2, v_2 = -Ex_2, v_3 = 2Ex_3, \frac{G}{E} = 10$,
- shearing/stretching flow, $v_1 = -Ex_1 + Gx_2, v_2 = -Ex_2, v_3 = 2Ex_3, \frac{G}{E} = 1$,
- uniaxial elongation, $v_1 = 2Ex_1, v_2 = -Ex_2, v_3 = -Ex_3$,
- biaxial elongation, $v_1 = Ex_1, v_2 = Ex_2, v_3 = -2Ex_3$.

The time range for the flows is taken such that the steady state is reached, but not overemphasized. Subsequently, we can compare these approximate solutions with the kinetic theory solutions (KTS) from Section 9.4.

We recall the RSC equation in intact form (5.13)

$$\dot{\mathbf{A}} = \mathbf{W} \cdot \mathbf{A} - \mathbf{A} \cdot \mathbf{W} + \xi \{ \mathbf{D} \cdot \mathbf{A} + \mathbf{A} \cdot \mathbf{D} - 2[\mathbb{A} + (1 - \kappa)(\mathbb{L} - \mathbb{M} : \mathbb{A})] : \mathbf{D} \} + 2\kappa C_I \dot{\gamma} (\mathbf{I} - 3\mathbf{A}) \quad (9.6)$$

and in eigenpair decomposed form (5.2), (5.10)

$$\begin{aligned} \dot{\lambda}_i &= 2\xi (\lambda_i \mathbf{D} : \mathbf{e}_i \mathbf{e}_i - \mathbf{e}_i \mathbf{e}_i : \mathbb{A} : \mathbf{D}) + 2C_I \dot{\gamma} (1 - 3\lambda_i) \\ \dot{\mathbf{e}}_i &= \mathbf{W} \cdot \mathbf{e}_i + \xi \frac{\lambda_2 + \lambda_1 - 4\bar{A}_{1212}}{\lambda_2 - \lambda_1} (\mathbf{D} : \mathbf{e}_1 \mathbf{e}_2) (\delta_{2i} \mathbf{e}_1 - \delta_{1i} \mathbf{e}_2) \\ &\quad + \xi \frac{\lambda_3 + \lambda_2 - 4\bar{A}_{2323}}{\lambda_3 - \lambda_2} (\mathbf{D} : \mathbf{e}_2 \mathbf{e}_3) (\delta_{3i} \mathbf{e}_2 - \delta_{2i} \mathbf{e}_3) \\ &\quad + \xi \frac{\lambda_1 + \lambda_3 - 4\bar{A}_{3131}}{\lambda_1 - \lambda_3} (\mathbf{D} : \mathbf{e}_3 \mathbf{e}_1) (\delta_{1i} \mathbf{e}_3 - \delta_{3i} \mathbf{e}_1). \end{aligned} \quad (9.7)$$

Combining (9.6) and (9.7) with

$$\mathbf{K} = \begin{bmatrix} 0 & G & 0 \\ 0 & 0 & 0 \\ 0 & 0 & 0 \end{bmatrix} \Leftrightarrow \mathbf{D} = \frac{G}{2} \begin{bmatrix} 0 & 1 & 0 \\ 1 & 0 & 0 \\ 0 & 0 & 0 \end{bmatrix} \wedge \mathbf{W} = \frac{G}{2} \begin{bmatrix} 0 & 1 & 0 \\ -1 & 0 & 0 \\ 0 & 0 & 0 \end{bmatrix}$$

simplifies the terms containing \mathbf{D} or \mathbf{W} . It shows that the dependence between the components of \mathbf{A} is marginal in comparison with the case that \mathbf{K} has only nonzero components. Unfortunately, this is hardly as illuminating as the simplifications we found for the Jeffery and Fokker-Planck equations in Section 9.3.

We first compare the tensors for the case $(\xi, C_I, \kappa, G) = (1, 0.01, 1, 1)$, wherefore the coefficients of the OFC were constructed in [15]. The results are depicted in Figure 9.33. The OFC is clearly the best closure in this case. It follows the tensor solution of ψ properly for all components at almost all times. The largest error is made in the A_{11} component for $t \in [7, 18]$. The OSC performs reasonably for the A_{22} and A_{33} components, but fails for the A_{11} and A_{12} components. The QC fails completely. Indeed, it is not constructed with any physical argument in contrast with the OSC and OFC.

It is also interesting to consider the approximations for cases other than where the coefficients of the OFC have been constructed for. We therefore consider both a case with a smaller and a larger interaction coefficient C_I . In addition, we consider a case wherefore $\xi \neq 1$. For $C_I = 0.001$ the results are depicted in Figure 9.34. In this case, the results of the OFC are poor. It contains nonphysical oscillations. The OSC performs better. For the second and third diagonal components, it follows the same trend as the KTS. For the A_{11} and A_{12} components, it also fails. The QC performs almost as bad as the OFC. It can be concluded that decreasing the C_I has disastrous consequences for the OFC. In response to this, the authors of [15] constructed coefficients for the $C_I = 0.001$ case. Herewith the approximation from the OFC followed the KTS properly again.

Decreasing the C_I had a negative response. We consider the case $C_I = 0.1$ to see if increasing the rotary diffusion has the same effect. The results are depicted in Figure 9.35. The results are surprising.

All three closures have improved approximations, wherein OFC is the best, OSC follows and the QC is the worst. Apparently, the C_I can be increased with a factor ten without resulting in negative responses. The reason hereof is that the contribution of the closure decreases when C_I increases, as it makes the diffusion stronger and the convection, which contains the closure, weaker.

Most of the cases where $\xi < 1$ do not offer any new perspectives. In combination with C_I in the neighborhood of 0.01, the differences with the $\xi = 1$ case are minimal. If C_I is in the neighborhood of 0.001, the quality of the results decay. The QC and OSC give bad results and the OFC even worse, as it shows unphysical oscillations. An example is depicted in Figure 9.36. It can be seen that the results are disastrous. The closures have difficulties following the exact solution. The oscillations are the origin of this problem. The amplitude, frequency and phase are not adapted in a proper way. We do however, see a tendency that the OFC has about the same guide line as the exact solution. In this sense, the OFC gives better results than the OSC and QC.

Another question that arises is if the RSC addition effects the results of the closures. Testing the simple shear with the same closures for $\kappa \in \{0.1, 0.25, 0.5, 0.75\}$ shows some differences. For $\kappa \geq 0.5$, the results do not change excessively. The QC still has poor results. The OSC is, due to its moderate results for all cases, the best in overall sense. The OFC is excellent in the case that the interaction is equal to the case wherefore the coefficients were constructed, namely for $C_I = 0.01$. Increasing the interaction to $C_I = 0.1$ does not introduce any decay and decreasing to $C_I = 0.001$ is disastrous. Taking $\kappa < 0.5$ shows an improvement in the results. When using the OFC, the components of the tensor approximation improve in the sense that they do not show any nonphysical oscillations anymore for $C_I = 0.001$. Nonetheless, the errors are still substantial and thus the quality of the OFC solution is not good. In addition, the QC is still the worst and the OSC gives again moderate results. Three examples are depicted in Figures 9.37, 9.38 and 9.39.

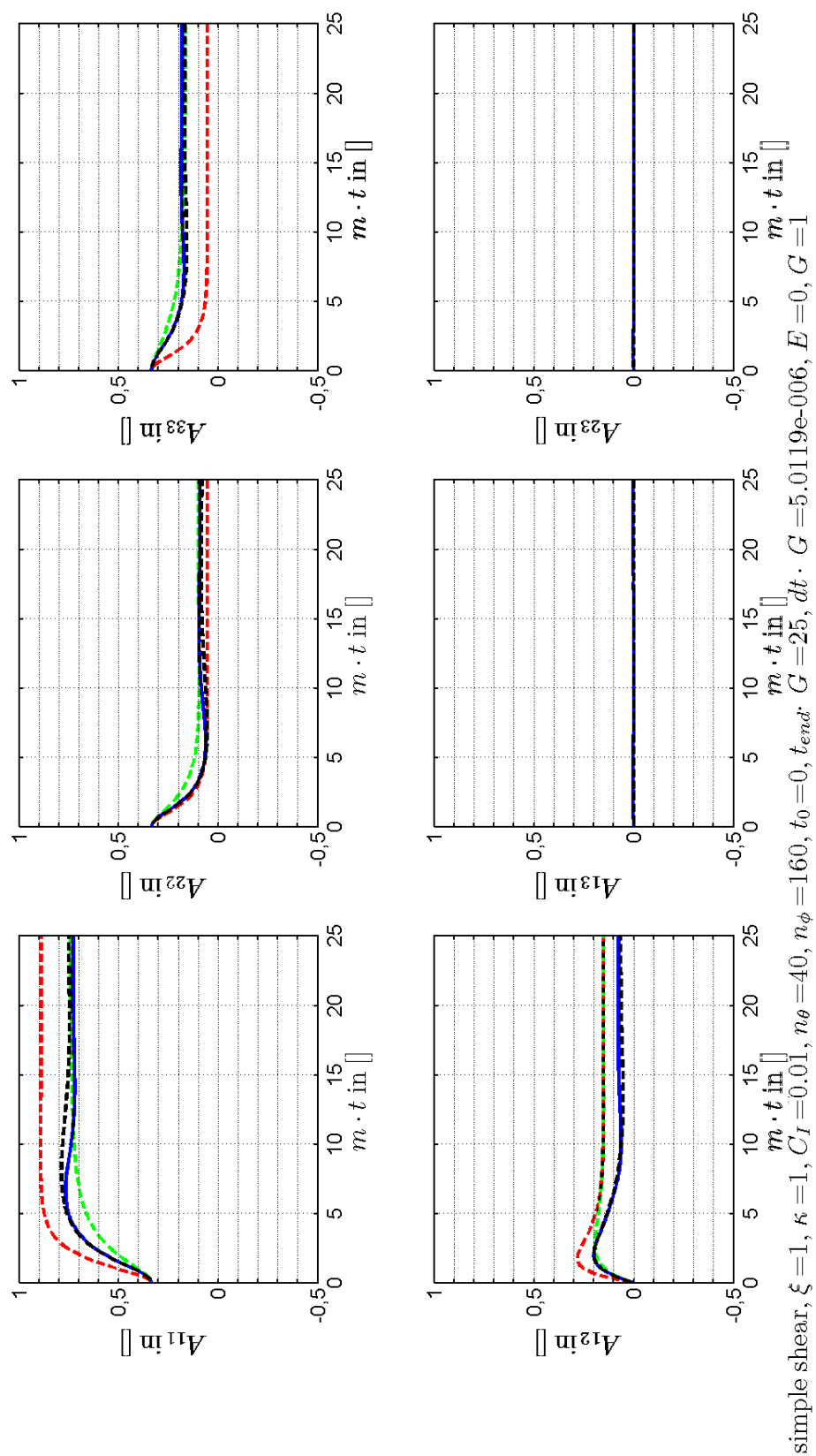
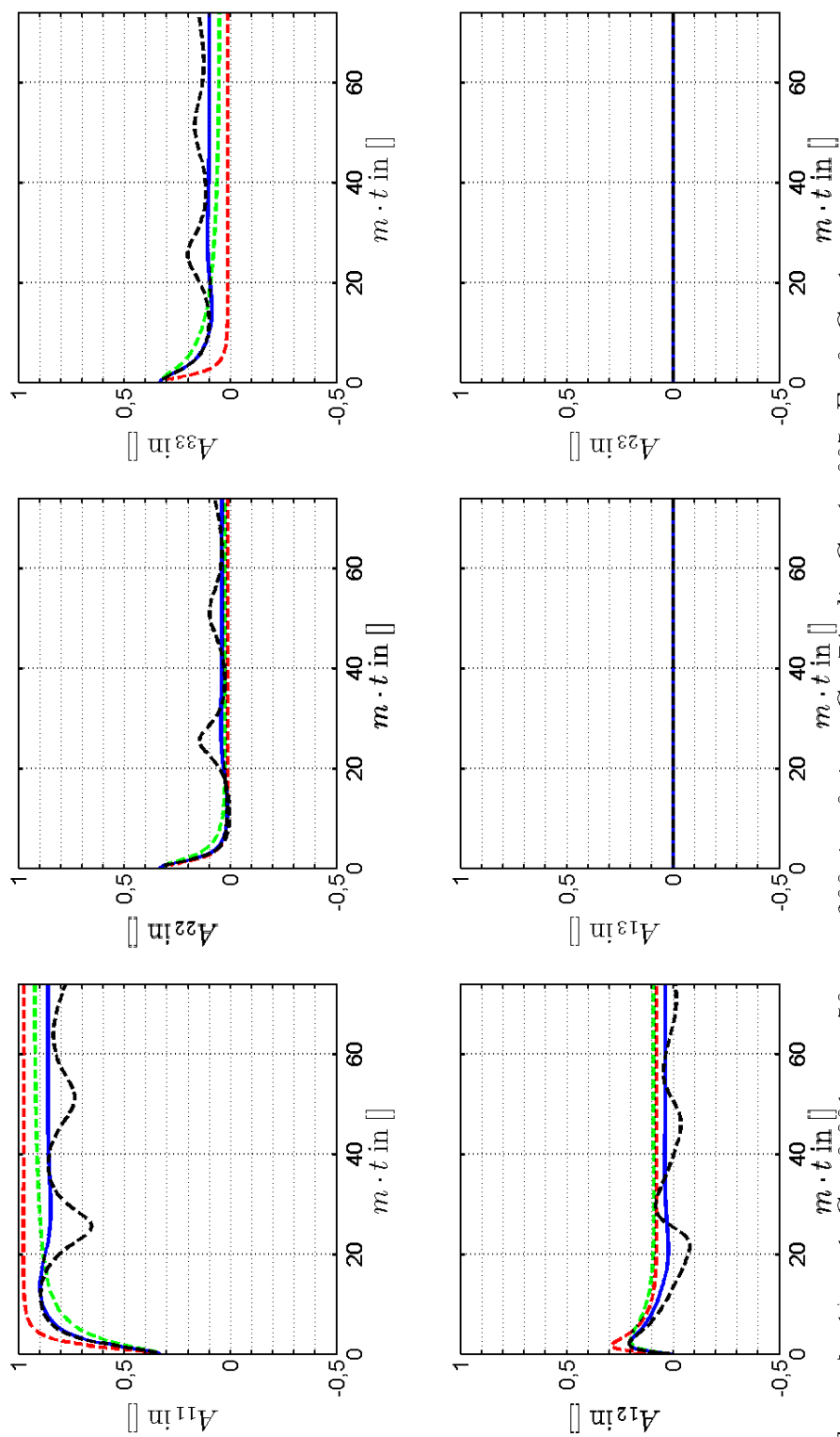
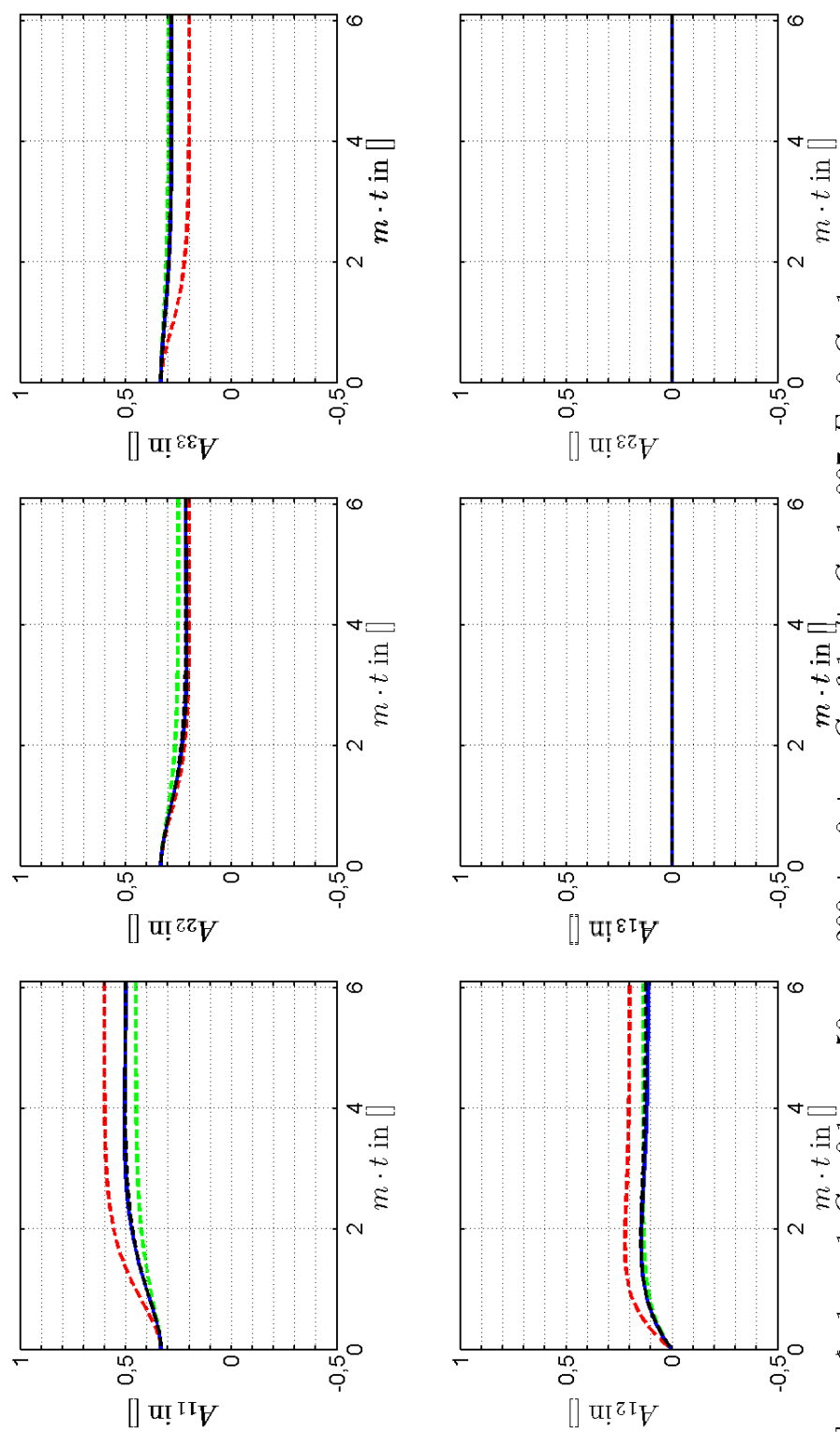


Figure 9.33: comparison of \mathbf{A} from ψ , in blue, and the QC, OSC and OFC in red, green and black respectively.



simple shear, $\xi = 1$, $\kappa = 1$, $C_I = 0.001$, $n_\theta = 50$, $n_\phi = 200$, $t_0 = 0$, $t_{end} = 74$, $dt \cdot G = 1e-005$, $E = 0$, $G = 1$

Figure 9.34: comparison of \mathbf{A} from ψ and the QC, OSC and OFC.



simple shear, $\xi = 1$, $\kappa = 1$, $C_I = 0.1$, $n_\theta = 50$, $n_\phi = 200$, $t_0 = 0$, $t_{end} = 6.1$, $dt = 1e-007$, $E = 0$, $G = 1$

Figure 9.35: comparison of \mathbf{A} from ψ and the QC, OSC and OFC.

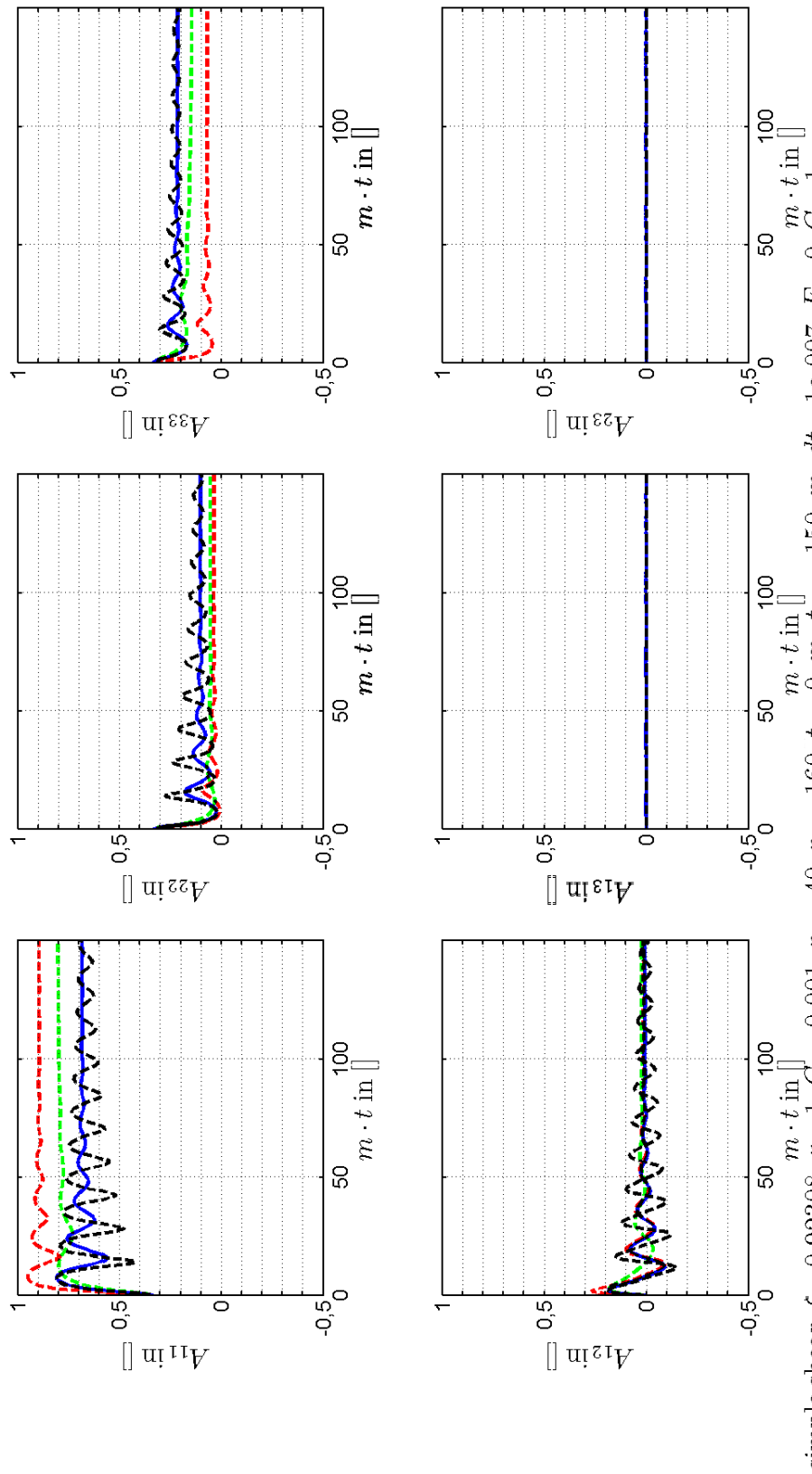
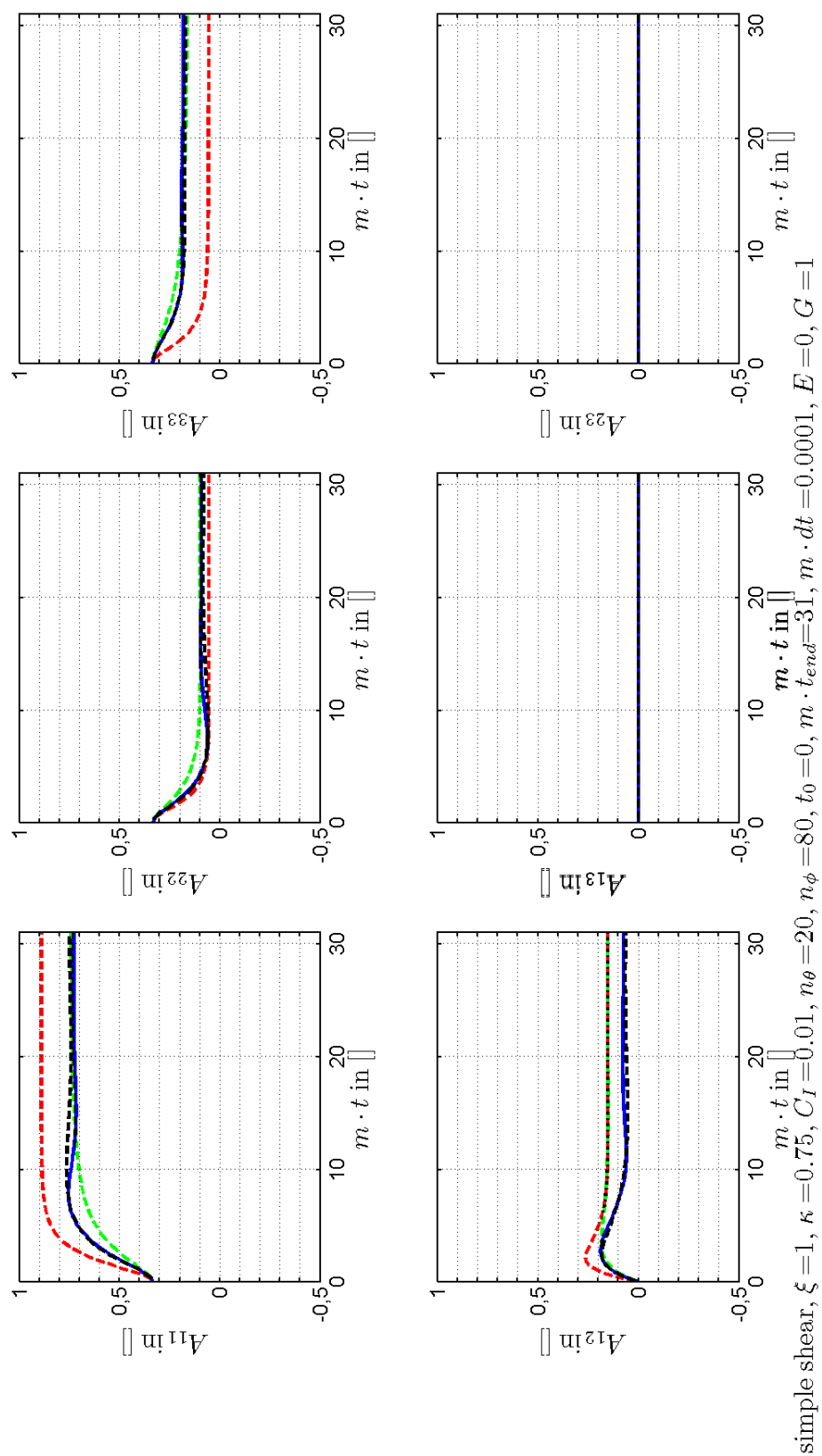


Figure 9.36: comparison of \mathbf{A} from ψ and the QC, OSC and OFC for $(r, C_I) = (5, 0.001)$.

Figure 9.37: comparison of \mathbf{A} from ψ and the QC, OSC and OFC for $\kappa = 0.75$.

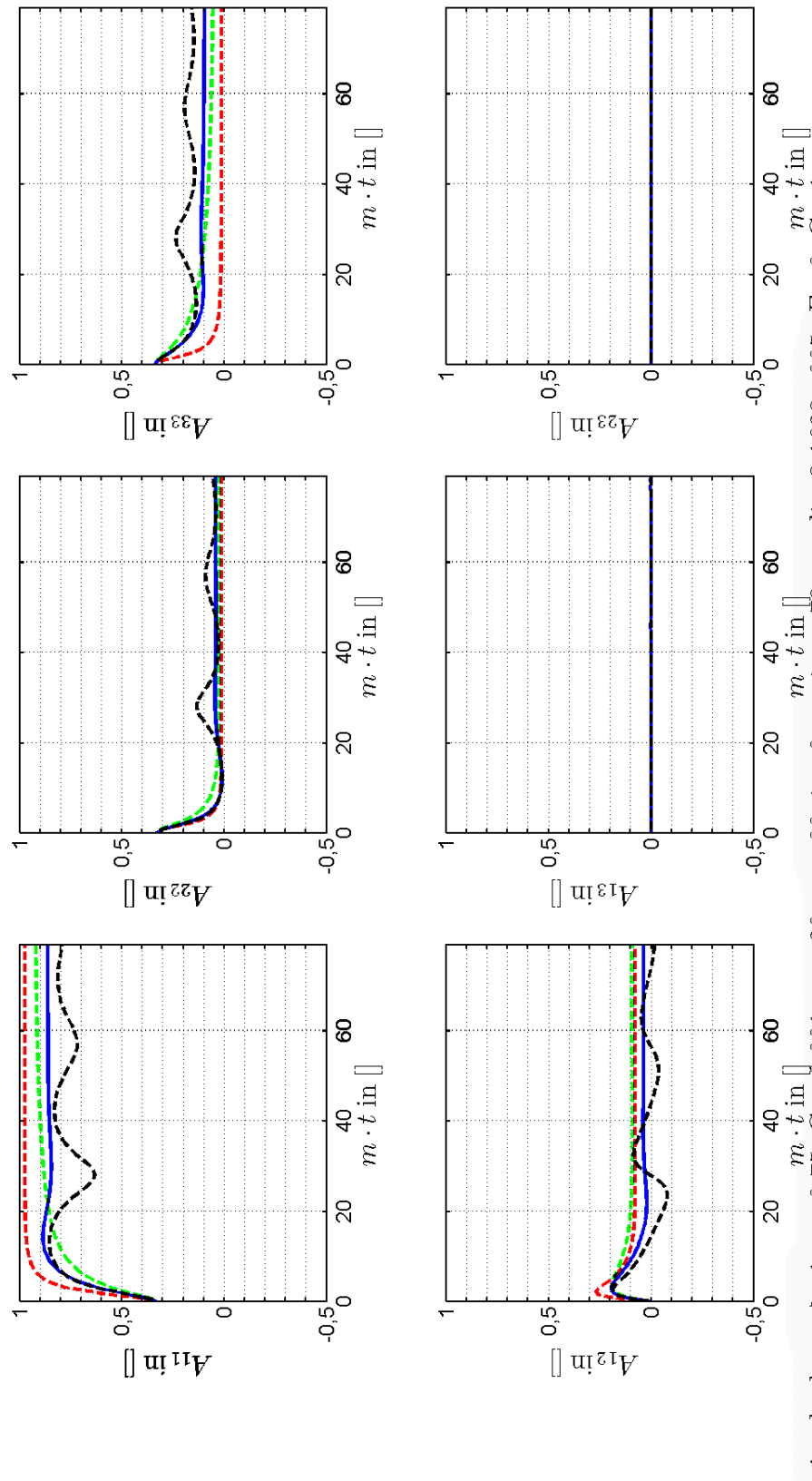
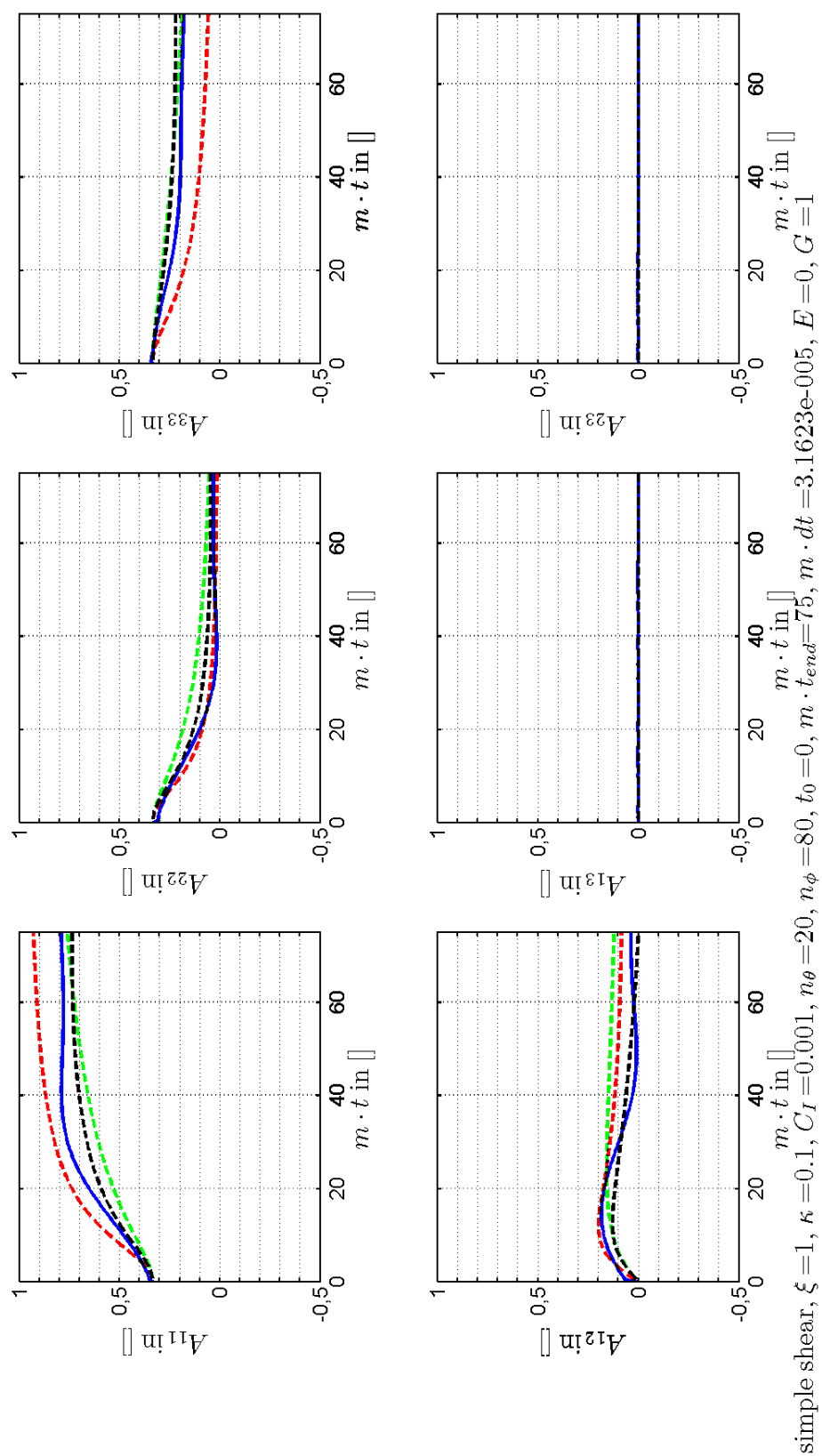


Figure 9.38: comparison of \mathbf{A} from ψ and the QC, OSC and OFC for $\kappa = 0.75$.

Figure 9.39: comparison of \mathbf{A} from ψ and the QC, OSC and OFC for $\kappa = 0.1$.

9.6 Conclusion

Varying the shear rate of the simple shear flow field scales the transient time linearly. Increasing the shear rate with, for instance, a factor two, decreases the transient time with a factor two.

The balance between convection and diffusion is sensitive for the initial condition for the probability distribution and the (initial) progression of the shear rate. The influence hereof, decays with time and the steady state values remain the same. Such results can be used to give an indication on whether the IC and/or progression of the shear rate influence the fiber orientation in a practical injection molding process. In accordance, the transient time corresponding to a certain IC and progression of the shear rate should be compared with the injection time of a product.

The OFC performs good for the cases wherefore the coefficients were generated. Increasing the FFI contribution by increasing C_I , decreases the LD contribution relatively. The LD contribution contains the closure term, and thus the results remain good. In contrast, decreasing the C_I increases the influence of the closure and leads to poor results. Similar results are obtained for most of the cases where $\kappa < 1$. Taking κ in the neighborhood of 0.1 shows an improvement for the OFC in the weak diffusion cases in the sense that nonphysical oscillations are no longer present. Taking $\xi \neq 1$ also leads to similar results, with the exception of the cases where C_I is in the neighborhood of 0.001. In the latter case, the components of \mathbf{A} keep oscillating and the closures fail to have the same phase, amplitude, frequency and guide line. Only the OFC manages to approximately have the same guide line as the exact solution.

Chapter 10

Uniaxial elongational flow

10.1 Introduction

The second homogeneous flow field we consider is uniaxial elongation. We discuss the characteristics of the uniaxial elongation flow field and what we expect from the fiber orientation. We check if these expectations are met and (de)motivate them with the results from the different models. An approach similar to the approach in Chapter 9 is maintained: the simplest form, Jeffery's equation, is treated first, continuing with the more difficult Folgar-Tucker and Wang-O'Gara-Tucker models. Comparisons between the 'exact' solutions and the approximations of the orientation tensors are made.

10.2 The uniaxial elongational flow field

The uniaxial elongational flow field is characterized by

$$\mathbf{v} = \mathbf{K} \cdot \mathbf{x} = \begin{bmatrix} 2E & 0 & 0 \\ 0 & -E & 0 \\ 0 & 0 & -E \end{bmatrix} \cdot \mathbf{x} \quad (10.1)$$

where $E[\frac{1}{s}]$ is the strain rate. Tensor \mathbf{K} is diagonal resulting in $\mathbf{D} = \mathbf{K}$, $\mathbf{W} = \mathbf{O}$. Hence, there is no spin, but merely strain. We have that

$$\nabla \cdot \mathbf{v} = 0 \quad \wedge \quad \nabla \times \mathbf{v} = \mathbf{0}.$$

The homogeneous flow field is thus both solenoidal or incompressible and irrotational. The flow field is depicted in Figures 10.1 and 10.2. From both the figure and the name it is clear that a prolate ellipsoid in such a flow is expected to align with the x_1 axis. The x_1 axis should represent a steady state. Considering the x_2 - x_3 plane, it is also expected that an ellipsoidal particle has a stationary orientation in this plane when $x_1 = 0$ as the streamlines are axisymmetric in this case. This stationary equilibrium however, is expected to be unstable as a small perturbation in the x_1 direction results in a stable alignment with the x_1 axis.

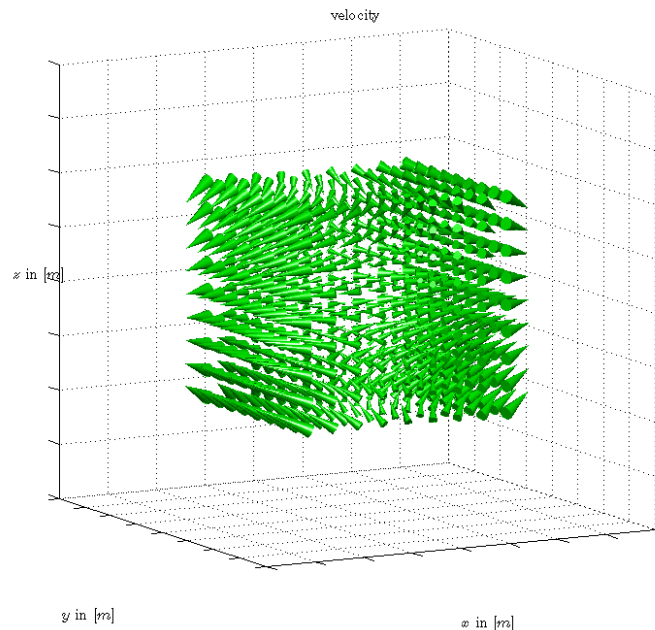


Figure 10.1: the uniaxial elongational flow field.

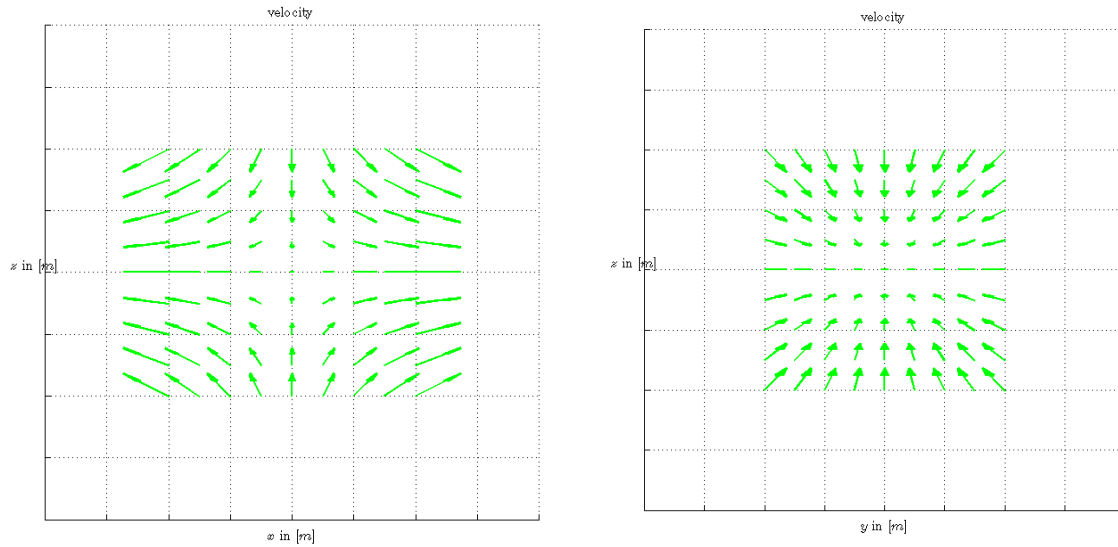


Figure 10.2: the uniaxial elongational flow field, x_1 - x_3 and x_2 - x_3 views.

10.3 Results Jeffery's equation

Recall

$$\underbrace{\dot{\mathbf{p}} - \xi \mathbf{D} \cdot \mathbf{p}}_{\text{difference between velocity flow and velocity fiber}} = \underbrace{-\xi \mathbf{D} : \mathbf{p}\mathbf{p}\mathbf{p}}_{\text{stress within fiber}}.$$

Uniaxial elongational flow (10.1) results in

$$\begin{aligned} \mathbf{W} \cdot \mathbf{p} &= \mathbf{0} \\ \mathbf{D} \cdot \mathbf{p} &= E \begin{bmatrix} 2 \sin(\theta) \cos(\phi) \\ -\sin(\theta) \sin(\phi) \\ -\cos(\theta) \end{bmatrix} \\ \mathbf{D} : \mathbf{p}\mathbf{p} &= 3 \sin^2(\theta) \cos^2(\phi) - 1. \end{aligned}$$

The distribution of the $\mathbf{D} : \mathbf{p}\mathbf{p}$ is depicted in Figure 10.3. The internal stress in the ellipsoidal particle is the largest in the x_1 axis. This is justifiable as the strain rate there is $2E$ in contrast with $-E$ along the other axes.

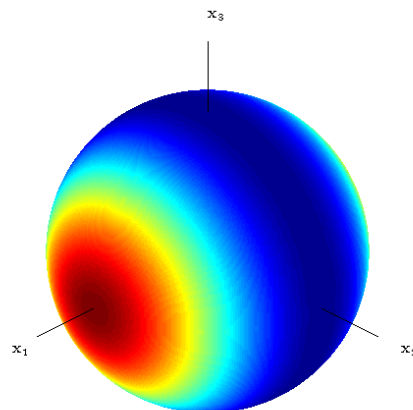


Figure 10.3: $\sin^2(\theta) \cos^2(\phi)$.

We omit a further interpretation of the general form of Jeffery's equation as considering it in combination with its generalized coordinates is more clear. In accordance, we determine the rate equations for the

azimuth and elevation to be

$$\dot{\theta} = \frac{3\xi E \sin(2\theta) \cos^2(\phi)}{2} \quad (10.2)$$

$$\dot{\phi} = \frac{-3\xi E \sin(2\phi)}{2}. \quad (10.3)$$

The stationary point of $\dot{\theta}$ are

$$\theta \in \left\{0, \frac{\pi}{2}, \pi\right\} \quad \vee \quad \phi \in \left\{\frac{\pi}{2}, \frac{3\pi}{2}\right\}$$

and for $\dot{\phi}$

$$\phi \in \left\{0, \frac{\pi}{2}, \pi, \frac{3\pi}{2}, 2\pi\right\}.$$

Omitting identical stationary points we get

$$(\theta, \phi) \in \left\{\left(\frac{\pi}{2}, 0\right), \left(\theta, \frac{\pi}{2}\right), \left(\theta, \frac{3\pi}{2}\right)\right\}$$

which correspond to the x_1 axis and x_2 - x_3 plane. Note that, in contrast with the steady states for the simple shear flow field, steady states now also exist when $|\xi| < 1$. The stability of these steady states is determined by considering the signs of both $\dot{\theta}$ and $\dot{\phi}$. We note that

$$\sin(2\alpha) \begin{cases} > 0 & \text{if } \alpha \in \left(0, \frac{\pi}{2}\right) \cup \left(\pi, \frac{3\pi}{2}\right) \\ < 0 & \text{if } \alpha \in \left(\frac{\pi}{2}, \pi\right) \cup \left(\frac{3\pi}{2}, 2\pi\right) \end{cases}.$$

It follows that for $\xi > 0$ the x_1 axis is a stable equilibrium and the x_2 - x_3 plane an unstable equilibrium. For $\xi < 0$, it is the other way around. If $\xi = 0$, the particle remains at its initial state. Examples of Jeffery orbits are depicted in Figures 10.4 and 10.5.

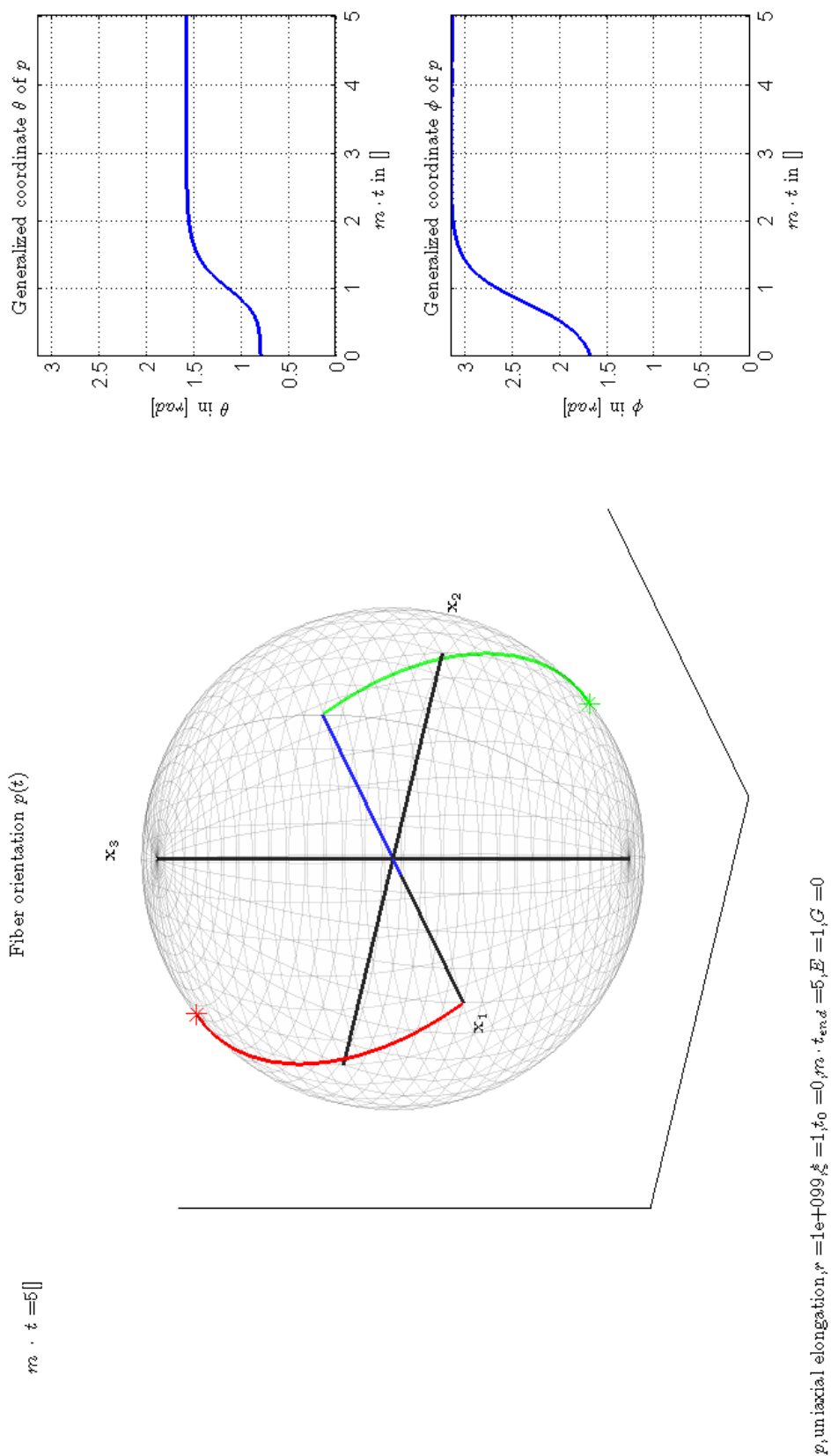


Figure 10.4: Jeffery's orbit for uniaxial elongation with $p_0 = \frac{1}{\sqrt{201}}[1 \ -10 \ 10]^T$.

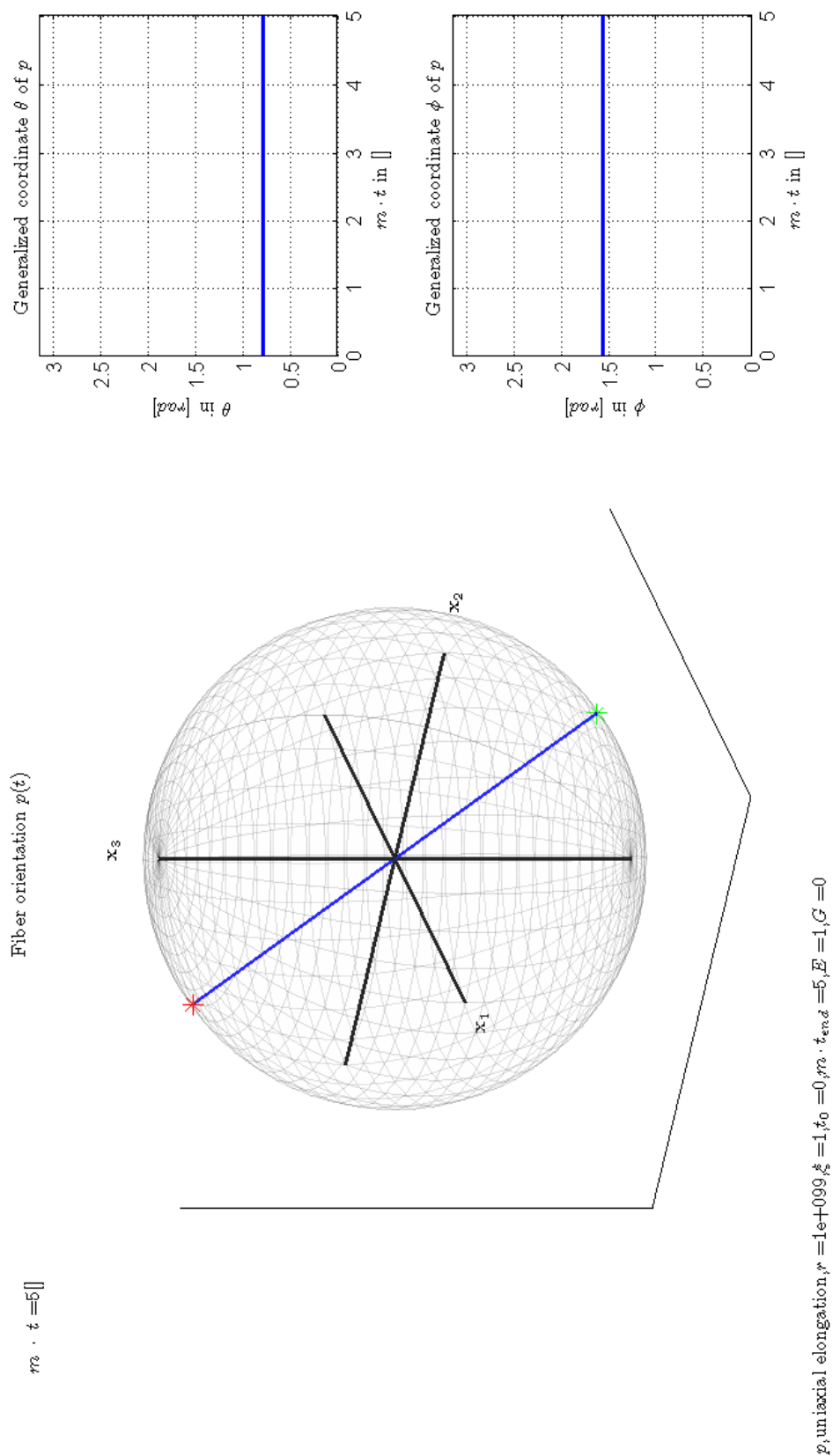


Figure 10.5: Jeffery's orbit for uniaxial elongation with $p_0 = \frac{1}{\sqrt{200}}[0 \ -10 \ 10]^T$.

10.4 Results kinetic theory

Recalling Property 7.3, it follows that

$$\psi(\mathbf{p}(t), t) = \psi(\mathbf{p}_0, t_0) e^{\xi \mathbf{D}:\mathbf{p}\mathbf{p}(t-t_0)} = \psi(\mathbf{p}_0, t_0) e^{\xi(3\sin^2(\theta(t))\cos^2(\phi(t))-1)(t-t_0)}$$

when $(C_I, \kappa) = (0, 1)$. If $\xi = 0$, the solution remains at its initial state. If $\xi > 0$, the Jeffery orbits converge to the x_1 axis and thus the power of the exponential goes to $2\xi(t - t_0)$. If $\xi < 0$, the Jeffery orbits converge to the x_2 - x_3 plane and the power of the exponential converges to $-\xi(t - t_0)$. It follows that in both cases the solution is unbounded as $t \uparrow \infty$ and 'needs' rotary diffusion, or $C_I \neq 0$, for obtaining an upper bound. In particular, we take $C_I \geq 0.01$ to avoid the necessity of very small space and time steps.

The power of the exponential is proportional to ξ . It thus controls the progression of ψ along an arbitrary Jeffery orbit. It also controls the convergence rate of the Jeffery orbits as $\dot{\theta}, \dot{\phi} \propto \xi$. In contrast with the simple shear flow, the Jeffery orbits for uniaxial elongation also have steady states if $|\xi| < 1$. Hence, taking $1 < |\xi|$ only slows the progression of ψ down. If FFI is added, this deceleration in progression is still noticeable. A similar reasoning holds for the variation of the strain rate E as also $\dot{\theta}, \dot{\phi} \propto E$. In addition, we know from the dimensional analysis that E does not change the quantities when using the scaled time $E \cdot t$.

In the case $(\xi, C_I, \kappa, E) = (1, 0.1, 1, 1)$, the solution is depicted in Figure 10.6. The variation of the parameters ξ , E and C_I does not offer illuminating perspectives. The variation of ξ and E induces the same changes as in the diffusionless case, and the FFI coefficient C_I merely determines the lower and upper bounds of ψ .

The variation of the initial condition does give a new perspective. It gives an indication in how strong the 'memory' of the probability density is. We recall the nonuniform IC (7.23)

$$\psi_{i,j}^0 = a \cdot (\sin(\theta_i - b))^{2d} (\cos(\phi_j - c))^{2e} + f, \quad a > 0, b \in \left[0, \frac{\pi}{2}\right], c \in [0, 2\pi), d, e \in \mathbb{Z}^+, f \geq 0.$$

and set $d = e = 1$ and $b = f = 0$. Furthermore, we take $c \in \left\{\frac{\pi}{8}, \frac{2\pi}{8}, \frac{3\pi}{8}\right\}$ so that the maxima initially lie at $(\theta, \phi) \in \left\{\left(\frac{\pi}{2}, \frac{\pi}{8} + l\pi\right), \left(\frac{\pi}{2}, \frac{2\pi}{8} + l\pi\right), \left(\frac{\pi}{2}, \frac{3\pi}{8} + l\pi\right)\right\}$, with $l \in \{0, 1\}$. The results are depicted in Figure 10.7. We make some interesting observations. It stands out that when considering A_{22} , there is a crossing of two graphs. The origin hereof is that for the uniform IC, the probability density 'comes from all sides' of the x_1 axis, and for the nonuniform IC only from the x_2 axis. In this way, the weight $p_2^2 \sin \theta$ is 'applied' differently to ψ in each of the latter cases. In addition, ψ_{max} lies at $(\theta, \phi) = \left(\frac{\pi}{2}, 0 + l\pi\right)$ in the case of the uniform IC, whereas in the case of the nonuniform IC it progresses from $(\theta, \phi) = \left(\frac{\pi}{2}, \frac{\pi}{4} + l\pi\right)$ to $(\theta, \phi) = \left(\frac{\pi}{2}, 0 + l\pi\right)$.

When considering A_{33} , we see that in case of the nonuniform IC, the component is nonzero for a moment. This is justified by the decay of ψ_{max} at the beginning, and subsequent increase when it comes near the x_1 axis. In effect, the density increases slightly in the direction of the x_3 axis, to subsequently decrease again.

The crossing of the A_{12} components stems from the weight $p_1 p_2 \sin \theta$. The maximum is initially at $(\theta, \phi) = \left(\frac{\pi}{2}, \frac{3\pi}{8}\right)$, moves toward the x_1 axis and so passes the maxima of the weight $p_1 p_2 \sin \theta$.

As in the case of the simple shear flow field, the balance between the convection and diffusion can be altered by varying the IC. Varying the strain rate in time also alters this balance.

As discussed in Section 5.5, the additional RSC term 'draws' fibers toward, or 'pushes' them away from, the eigenvectors of \mathbf{A} . This is done in a way that the strain is reduced, so that the transient time is prolonged. The steady state values should remain the same. The strain reduction changes both the convection and the diffusion, altering the balance between them. As a result, the extrema are displaced, as depicted in Figure 10.8.

10.5 Results tensor approximation

In this section we use the approach as described in Chapters 6 and 8 to obtain solutions for the orientation tensors. We will consider the quadratic, orthotropic smooth and orthotropic fitted closures (QC,

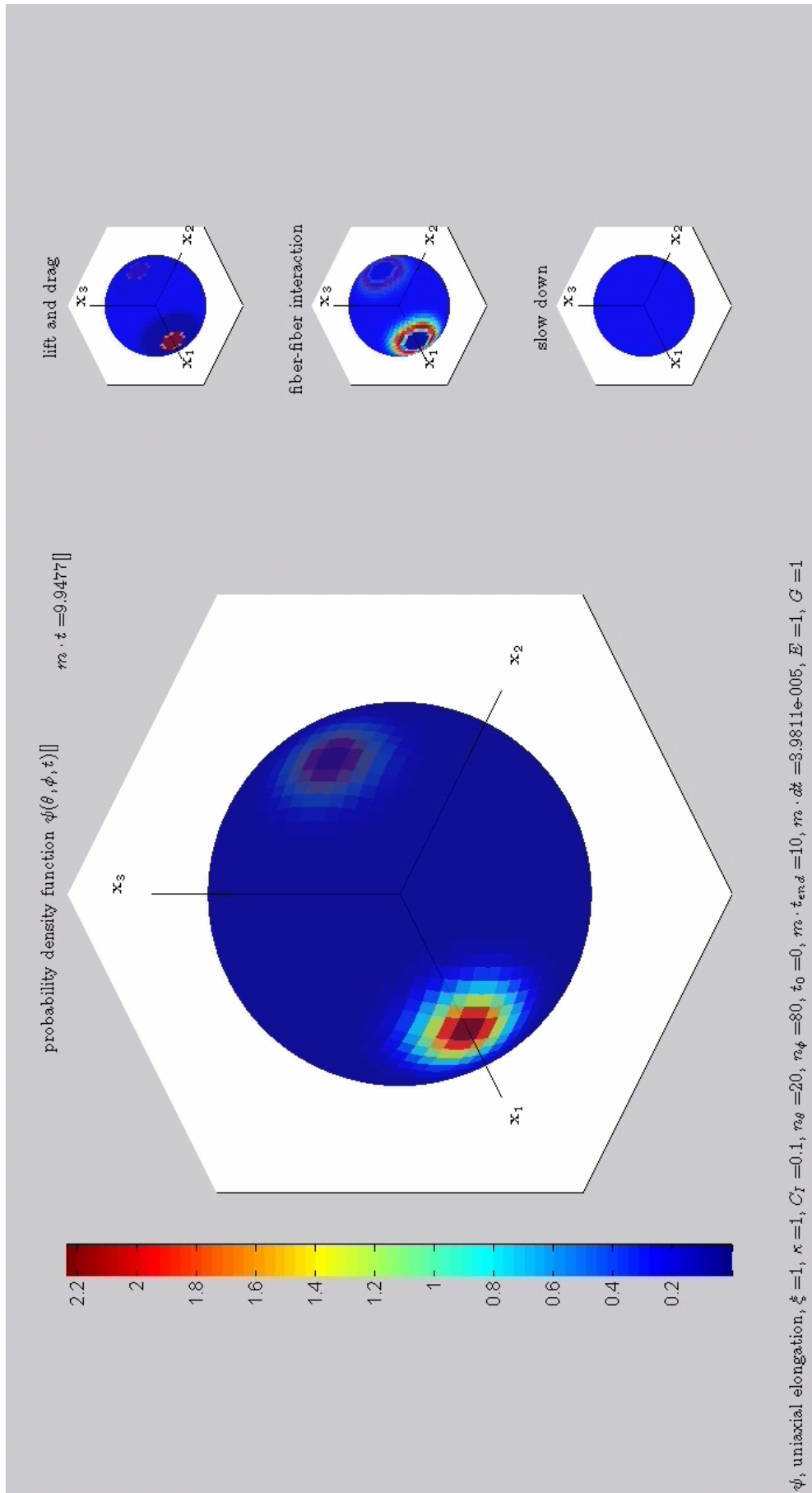


Figure 10.6: solution for uniaxial elongation with $(\xi, C_I, \kappa, E) = (1, 0.1, 1, 1)$.

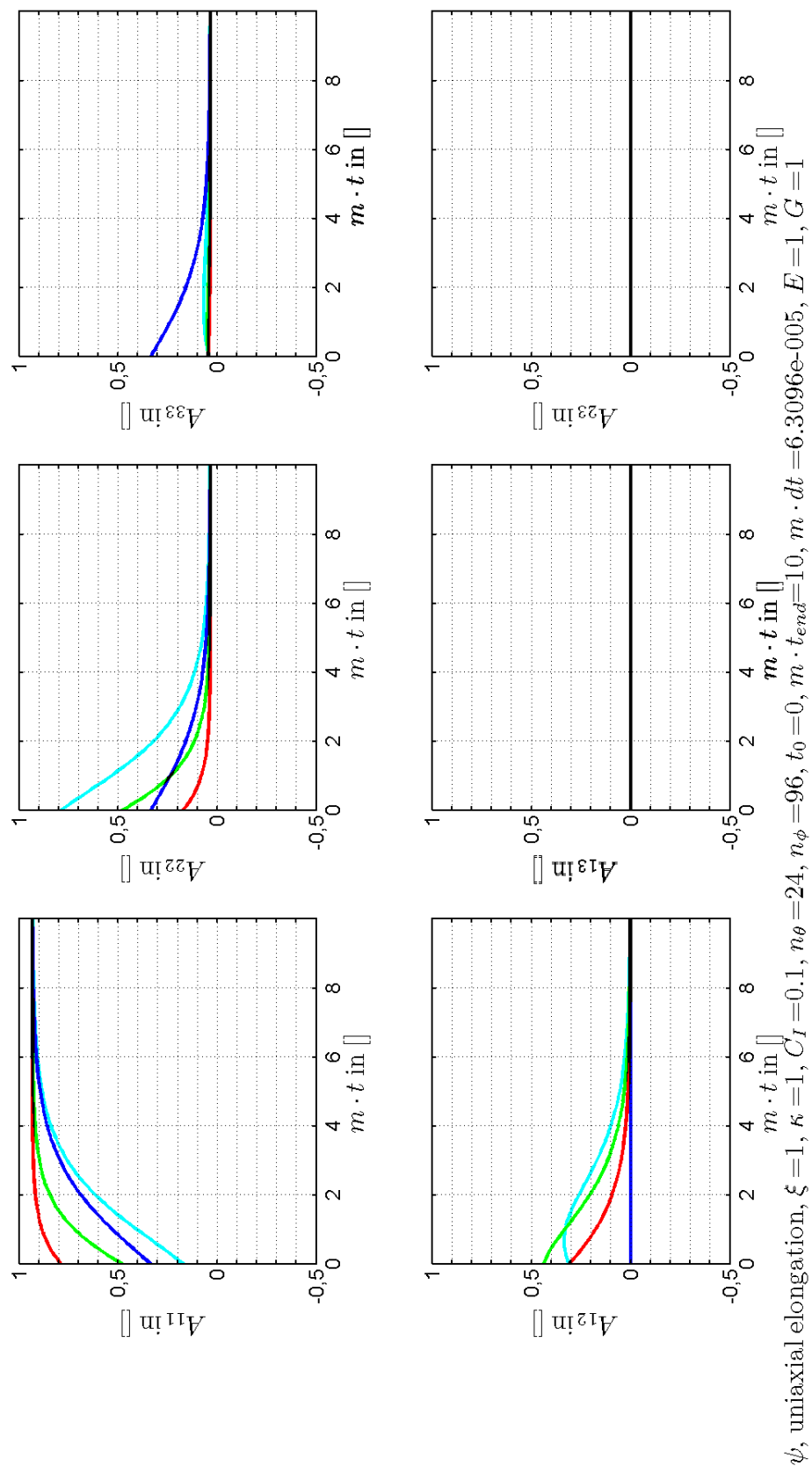
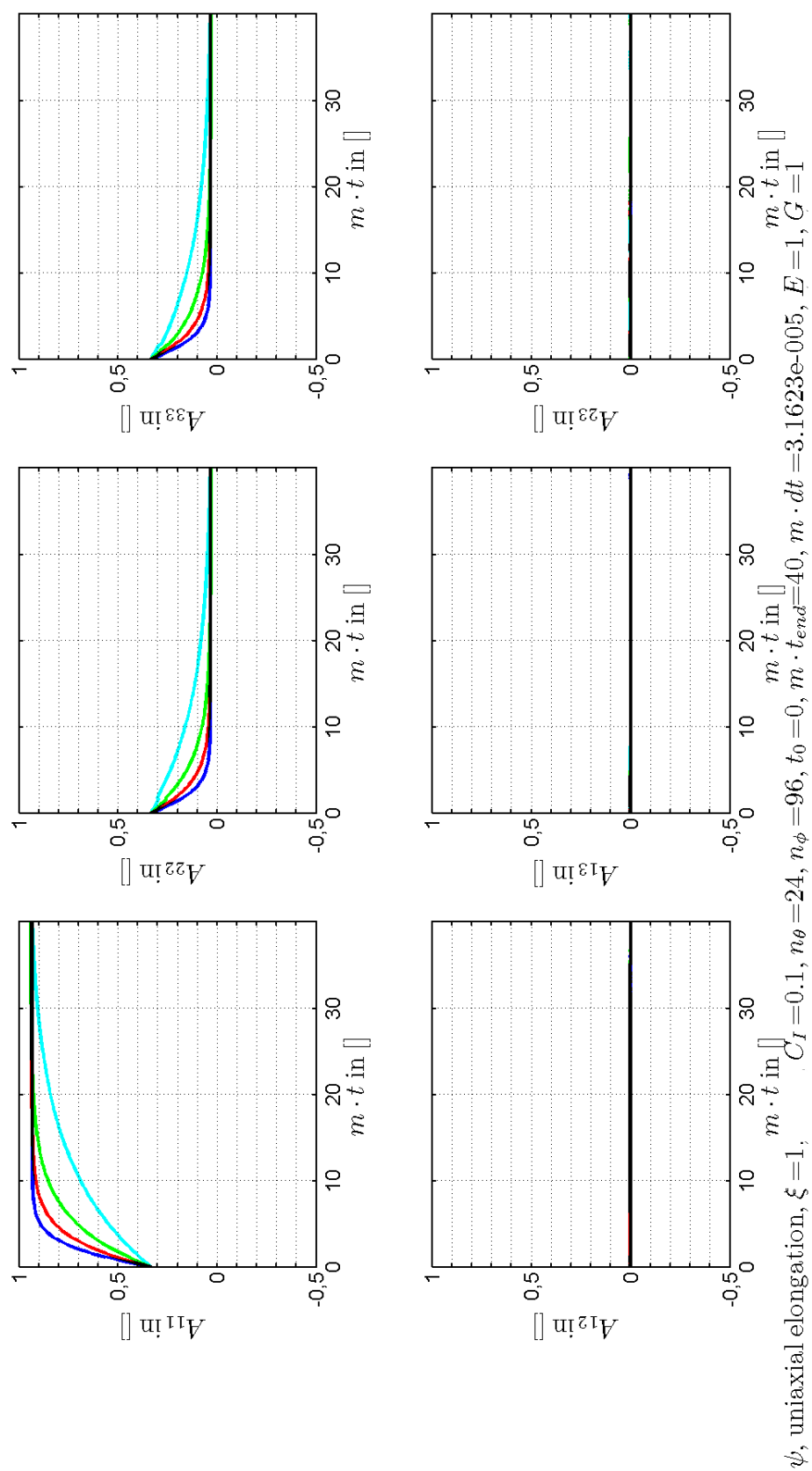


Figure 10.7: nonuniform IC with $c \in \{\frac{\pi}{8}, \frac{2\pi}{8}, \frac{3\pi}{8}\}$ in red, green and cyan respectively. The results for a uniform IC are depicted in blue.

Figure 10.8: influence of strain reduction, $\kappa \in \{0.25, 0.5, 0.75, 1\}$.

OSC and OFC) as constructed in [15]. The coefficients for the OFC were constructed with five different flow fields with the parameters set to $\xi = 1$ and $C_I = 0.01$, as mentioned in Section 9.5. The time range for the flows is taken such that the steady state is reached, but not overemphasized. We can compare these approximate solutions with the kinetic theory solutions (KTS) from Section 10.4.

The results of the case $(\xi, C_I, \kappa, E) = (1, 0.01, 1, 1)$ are depicted in Figure 10.9. The approximation using the OFC is good. It follows the KTS even better than for the simple shear flow field. The QC results in a poor approximation. The OSC gives moderate results. Its transient period is too short.

Increasing the C_I for the simple shear flow field did not result in bad approximations. This was motivated by the increasing ratio of the LD to FFI contributions. The closure only influences the LD contribution, thus, stronger diffusion obviously leads to weaker contributions of the closure and in effect better approximations. The results of the $(\xi, C_I, \kappa, E) = (1, 0.1, 1, 1)$ case for uniaxial elongational flow are therefore surprising, confer Figure 10.10. The approximations all give bad results, even the OSC which consistently gave moderate results. The origin of these bad approximations lies largely in the error in the A_{1111} component. The increase of C_I causes a too large decay in the A_{1111} component of the closures. It can be concluded that the interpolation causes a large error in the case of uniaxial elongational flow, even though the LD contribution gets weaker. It is interesting to check how the approximations behave when 'new' coefficients are generated for the OFC, namely for the $C_I = 0.1$ case. Such a generation is not part this project, and thus a comparison is omitted.

Taking $\kappa \neq 1$ gives some interesting results. Setting $(\xi, C_I, \kappa, E) = (1, 0.01, 0.75, 1)$, the quality of the approximations does not suffer, confer Figure 10.11. The quality of the approximations do, however, suffer when κ is changed to 0.25. The approximations of the latter are depicted in Figure 10.12. The OFC converges too fast to the steady state. The decrease of κ weakens the LD contribution and thus the contribution of the fourth order tensor, but this reduction differs from the one that is induced by the usage of the OFC. It can be concluded that these reductions are alike when κ is in the neighborhood of 0.75, but differ when κ decreases further. In the latter case, coefficients for the OFC should be generated for similar values of κ .

Taking ξ not equal to one, but in the neighborhood of one, does result in large differences with the $\xi = 1$ solution. In effect, the approximations also do not suffer from such a variation of ξ .

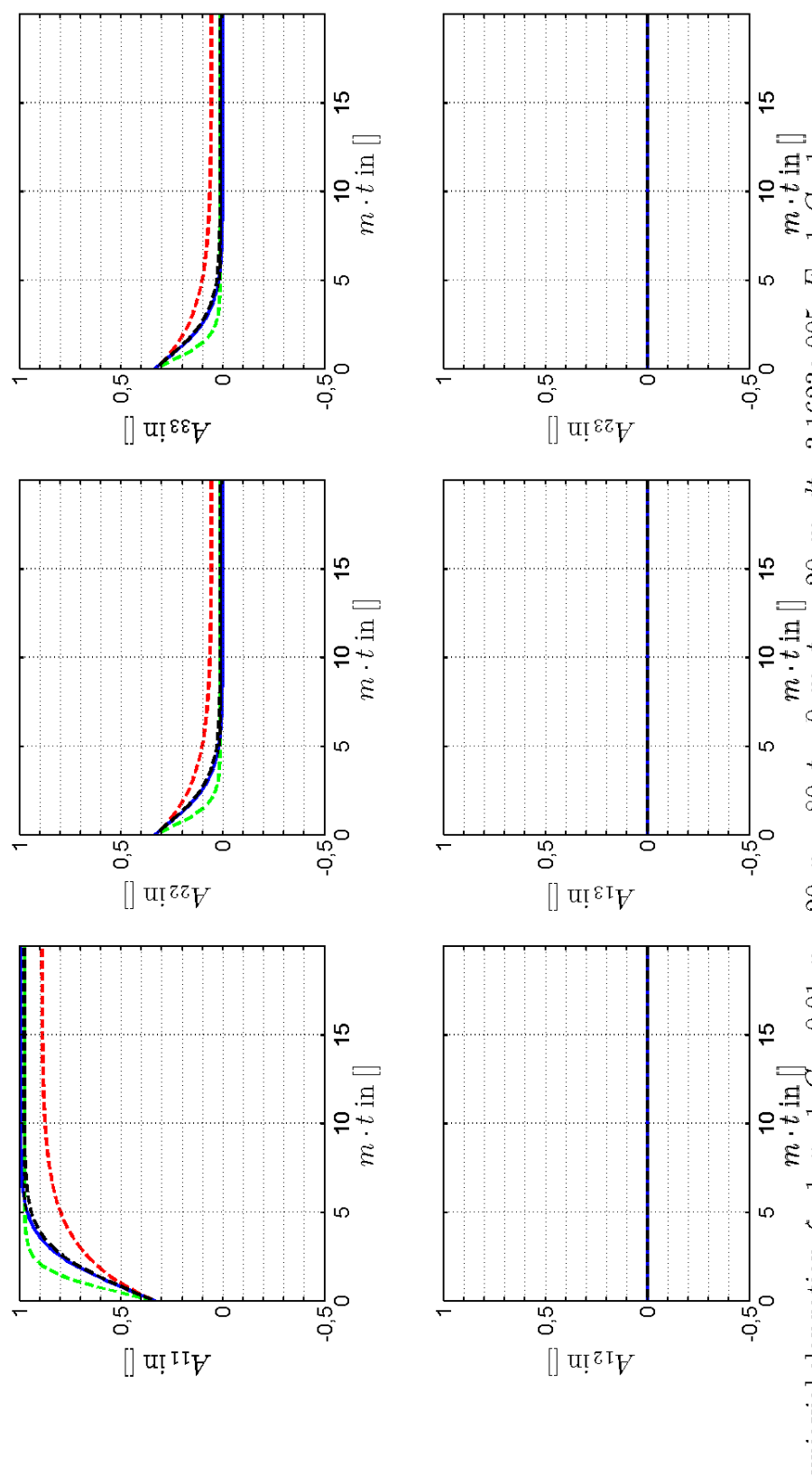


Figure 10.9: comparison of KTS and the approximations.

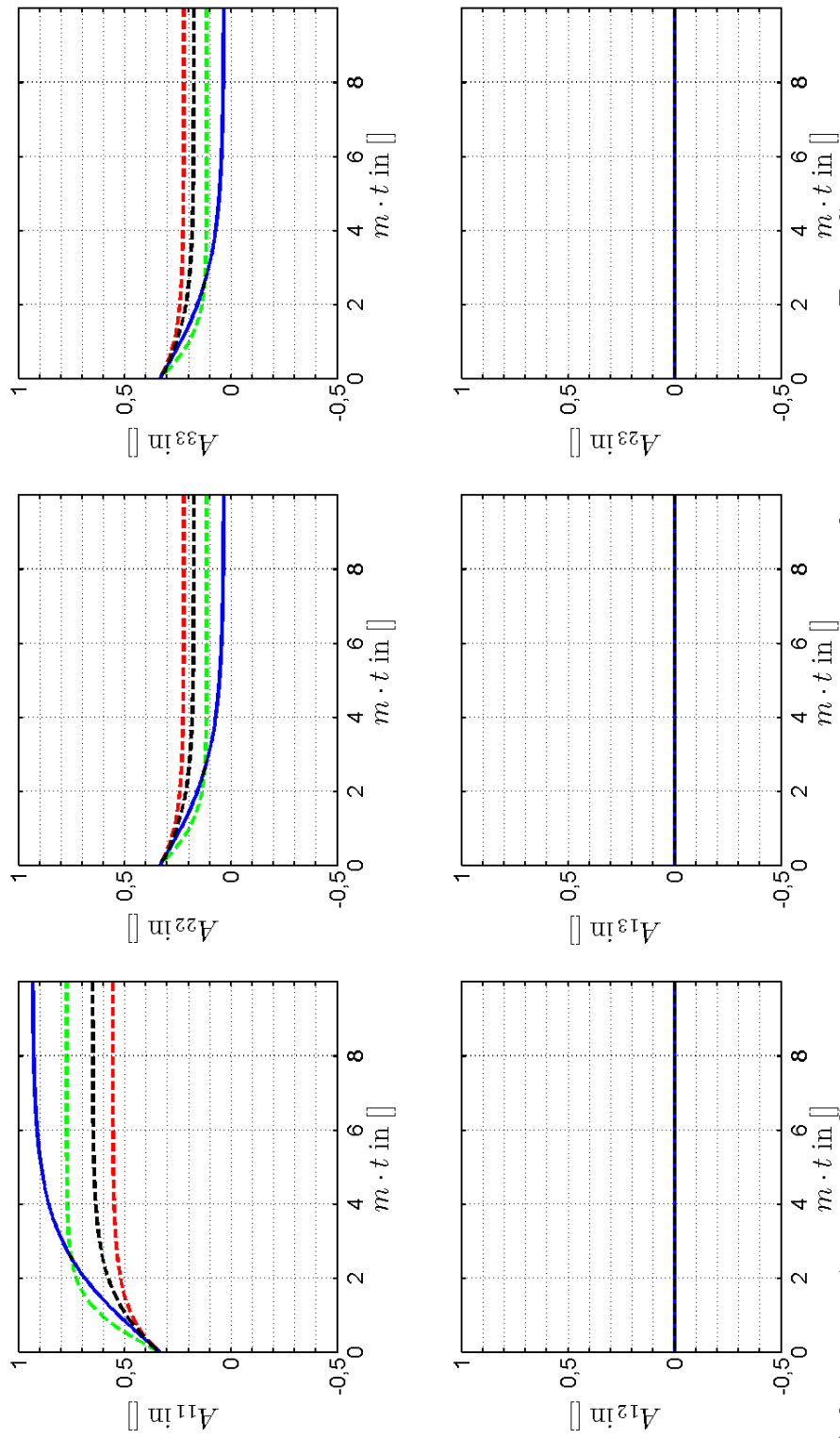


Figure 10.10: comparison of KTS and the approximations for a larger FFI contribution.

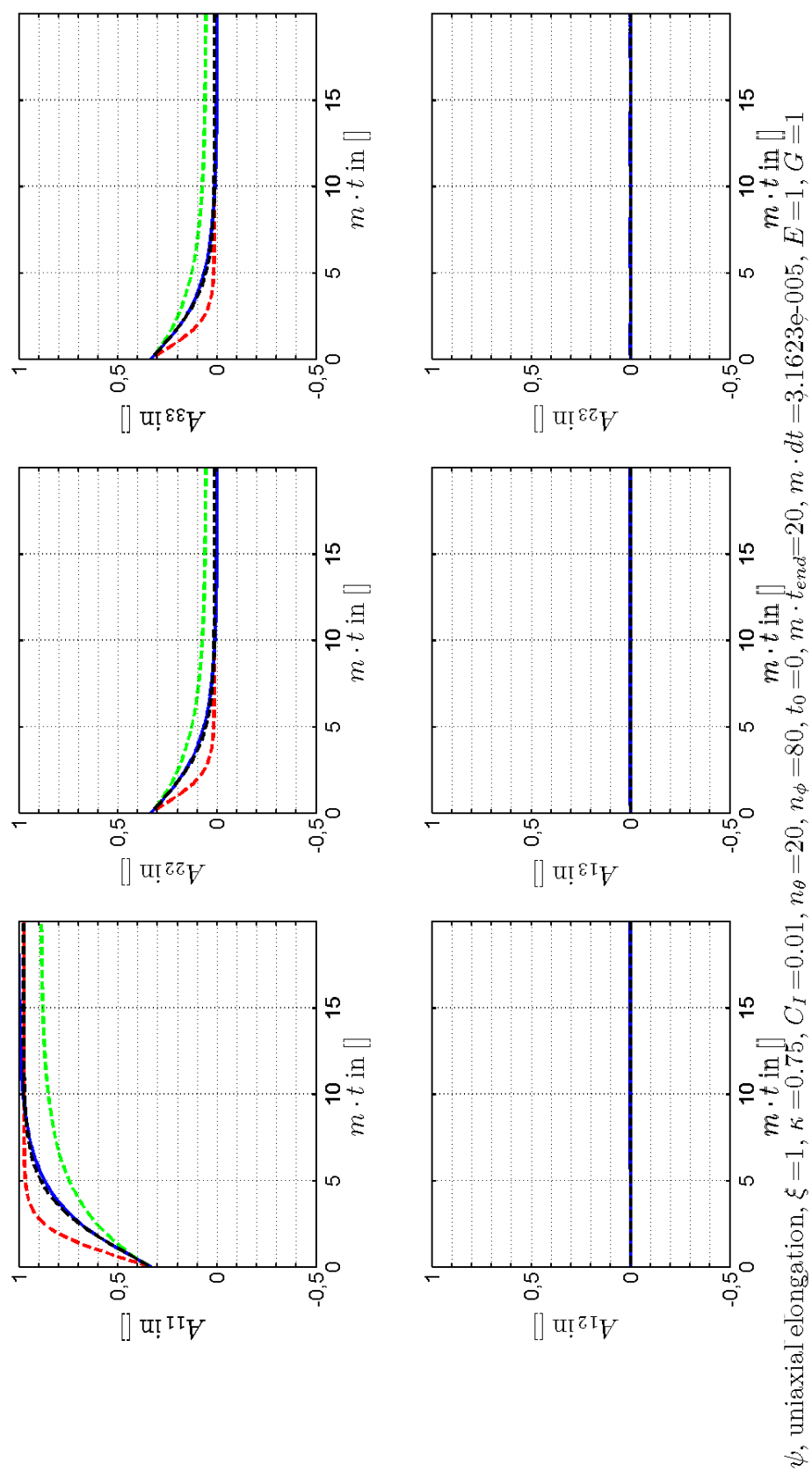


Figure 10.11: comparison of KTS and the approximations for a larger RSC contribution.

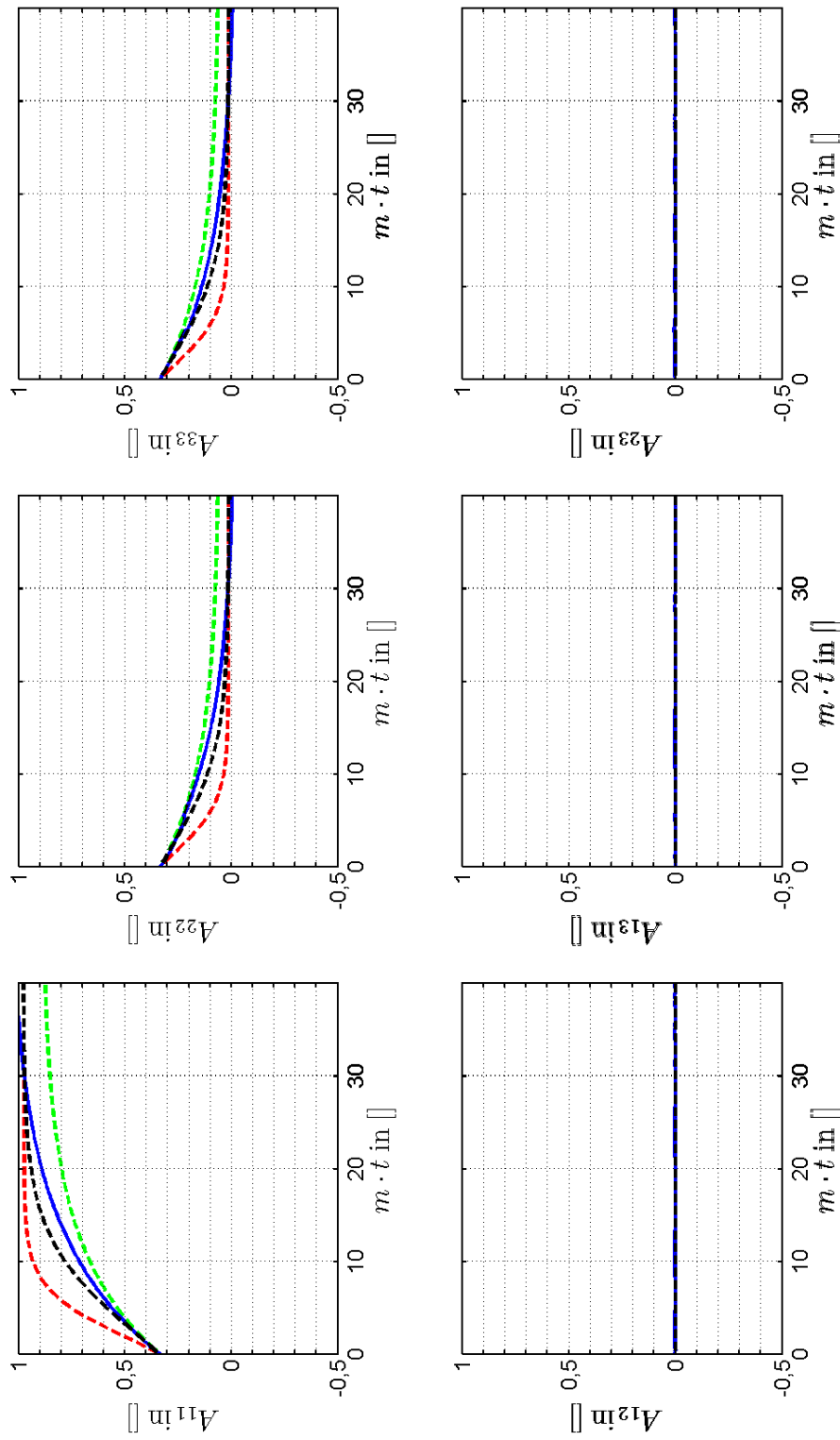


Figure 10.12: comparison of KTS and the approximations for a larger RSC contribution.

10.6 Conclusion

Varying the strain rate of the uniaxial elongational flow field scales the transient time linearly. Increasing the strain rate with, for instance, a factor two, decreases the transient time with a factor two.

The balance between convection and diffusion is sensitive for the initial condition for the probability distribution. The influence hereof, decays with time and the steady state values remain the same. Such results can be used to give an indication on whether the IC and/or progression of the shear rate influence the fiber orientation in a practical injection molding process. In accordance, the transient time corresponding to a certain IC should be compared with the injection time of a product.

The OFC performs good for the cases wherefore the coefficients were generated. In contrast with the simple shear test model, the quality of the approximations suffer from an increase of C_I . This indicates that even though the contribution of the closure is expected to be weaker, the loss of quality due to a change of the parameters can still be substantial. It would be illuminating to generate coefficients for the $C_I = 0.1$ case. Such a generation is, however, beyond the scope of this project and was thus omitted.

The quality of the approximations is unaffected if κ is in the neighborhood of one. The quality is still good if $\kappa = 0.75$. If $\kappa = 0.25$, the quality has already decayed substantially. Varying ξ does little when ξ stays in the neighborhood of one.

Part III

Conclusions and recommendations

Chapter 11

Conclusions and recommendations

11.1 Introduction

Based on the evaluations made throughout this project, conclusions can be drawn and recommendations can be made concerning the modeling of the fiber orientation. Conclusions are drawn with respect to the numerical approaches used. The results from the test models are reconsidered. The quality of the closure approximations are discussed. References to recent publications are made.

11.2 Conclusions

The numerical approach as described in Chapter 7 is sufficient for the modeling of the fiber orientation in homogeneous flow fields with the Wang-O’Gara-Tucker model. The spherical partition in space and explicit time integration conserve the intrinsic properties of a probability density function. Although the time increments need to be small for stability, the computation times are still modest, especially when considering the linear Folgar-Tucker model. A noticeable property is that the local truncation error has a nature of four different types, namely acceleration, production or vanishing, convection and diffusion of probability density. The stability criterium for the model is rather strict, involving the ratio between the space and time partition, diffusion and strain reduction. The latter extension, has the tendency to weaken the stability criterium, even though it induces a nonlinear term.

Explicit time integration is also sufficient for the tensor form of the Wang-O’Gara-Tucker model, as shown in Chapter 8. The intrinsic properties of the second order tensor are conserved, with the exception of positive semidefiniteness. The stability criterium is not demanding.

The simple shear and uniaxial elongational flow field are sensitive to the variation of the initial condition and the progression of the shear and strain rate, respectively, in time. They are inherent to the balance of the convection and diffusion of the fiber orientation. The strain reduction induces longer transient times but does not alter the steady state values. It is therefore a useful phenomenological parameter that enables theoretic results to be fitted to experimental results.

The quality of the closure approximations varies with the parameters and the flow fields. The quality is good for the cases where the parameter set is the same as the set wherefore the orthotropic fitted closure was originally fitted. Varying the aspect ratio of the fibers does not seem to have a large impact. Varying the strength of the fiber-fiber interaction leads to inconsistent results. In most cases it is disastrous. The exception lies in the increase of the strength of the fiber-fiber interaction for the simple shear flow field. The latter seems to conserve the good quality of the approximations, which they have when the parameter set matches the set wherefore the orthotropic fitted closure was originally fitted. Varying the strain reduction somewhat does not reduce the quality of the approximations. A substantial strain reduction, however, leads to poor results. Varying the strain or shear rate merely scales the transient time linearly with the rate, conserving the quality of the approximations. Due to the somewhat inconsistent results when varying the parameters, it can be concluded that is wise to generate coefficients for the interpolation function of the orthotropic fitted closure, per parameter set. This ensures a good quality of the approximations.

11.3 Recommendations

The research in the modeling of fiber orientation in fiber filled injection molded thermoplastics is far from complete. Papers have been published that either motivate a different approach, or extend the existing models. In [14], the Wang-O’gara-Tucker model is extended with anisotropic rotary diffusion to replace the isotropic rotary diffusion by J.H. Phelps and C.L. Tucker. D.A. Jack and D.E. Smith have published various papers, e.g. [3], wherein they motivate the use of the exact fourth order tensor and approximate the sixth order tensor. Such approaches should be taken into account when attempting to model the fiber orientation.

The closure approximations should be fitted to the correct parameter set. The $\lambda_1-\lambda_2$ curve should cover a substantial part of the green shaded area in Figure 6.1. This can be achieved by choosing appropriate types of flow. Such fits ensure a good quality of the approximations.

The possibilities for the numerical approaches for both the kinetic theory and tensor form of the Wang-O'Gara-Tucker model should be investigated. Indeed Euler forward is simple to implement and conserves the intrinsic properties of the quantities, but perhaps more stable approaches can be constructed. Finding such an approach is complexified by the definition of a probability density, as it makes many demands, but it is not necessarily impossible. Perhaps it is possible to conserve the positive semidefiniteness of the second order tensor with a certain scheme. Also a stability analysis should be made for the full model, not just the linear part.

The orthotropic fitted closures can be investigated further. There are many adequate interpolation functions possible and many different flows to choose when generating the coefficients for the closure. Their influence on the quality of the tensor approximations should be investigated extensively to ensure a proper approximation for practical injection molding simulations.

Part IV

Appendices, bibliography and nomenclature

Appendix A

Proofs

A.1 Introduction

Throughout this thesis, various proofs are given to motivate theorems and properties. Some of them are 'classical' and do not fit the main construction line of the thesis. In accordance, these proofs are denoted in this chapter.

A.2 Nonnegative real eigenvalues

Proof. Denoting the eigenpairs of \mathbf{A} with $(\lambda_j, \mathbf{e}_j)_{j \in \{1,2,3\}}$ with $\mathbf{e}_j \cdot \mathbf{e}_k = \delta_{jk}$ we have

$$(\mathbf{A} \cdot \mathbf{e}_j, \mathbf{e}_j) = (\lambda_j \mathbf{e}_j, \mathbf{e}_j) = \lambda_j^*$$

and

$$(\mathbf{A} \cdot \mathbf{e}_j, \mathbf{e}_j) = (\mathbf{e}_j, \mathbf{A} \cdot \mathbf{e}_j) = (\mathbf{e}_j, \lambda_j \mathbf{e}_j) = \lambda_j$$

and so $\forall j \lambda_j = \lambda_j^* \Rightarrow \lambda_j \in \mathbb{R}$.

For proving the positivity of the eigenvalues we use the property positive definiteness

$$\mathbf{x} \cdot \mathbf{A} \cdot \mathbf{x} \geq 0 \quad \forall \mathbf{x} \in \mathbb{R} \setminus \{\mathbf{0}\}$$

and Property 4.1. The positive semidefiniteness can be extended to the more general, complex form

$$\bar{\mathbf{x}} \cdot \mathbf{A} \cdot \mathbf{x} \geq 0 \quad \forall \mathbf{x} \in \mathbb{C} \setminus \{\mathbf{0}\}.$$

Take for $\mathbf{x} = \mathbf{e}_i$ an eigenvector. Then

$$\begin{aligned} \bar{\mathbf{e}}_i \cdot \mathbf{A} \cdot \mathbf{e}_i &\geq 0 \\ \bar{\mathbf{e}}_i \cdot \lambda_i \mathbf{e}_i &\geq 0 \\ \lambda_i \bar{\mathbf{e}}_i \cdot \mathbf{e}_i &\geq 0 \\ \lambda_i \|\mathbf{e}_i\|_2^2 &\geq 0. \end{aligned}$$

Due to $\|\mathbf{e}_i\|_2^2 \geq 0$ it follows that $\lambda_i \geq 0$, which concludes the proof. \square

A.3 Real eigenvectors

Proof. By Property 4.3, we already know that $\lambda_j \in \mathbb{R}$ and so

$$\underbrace{(\mathbf{A} - \lambda_j \mathbf{I})}_{\in \mathbb{R}} \cdot \mathbf{e}_j = \underbrace{\mathbf{0}}_{\in \mathbb{R}}.$$

The eigenvectors are determined by Gaussian elimination in combination with $\|\mathbf{e}_j\|_2 = 1$. As $\mathbf{A} - \lambda_j \mathbf{I}$ contains merely real elements, Gaussian elimination will result in elements with $\text{Im}((\mathbf{e}_j)_k) = 0$. The normalization merely stems from the multiplication of \mathbf{e}_j with a constant $\in \mathbb{R}$. In effect, the $\forall j \mathbf{e}_j \in \mathbb{R}^3$. \square

A.4 Orthonormal eigenvectors

Proof. Consider two eigenpairs $(\lambda_1, \mathbf{e}_1), (\lambda_2, \mathbf{e}_2), \lambda_1 \neq \lambda_2, (\lambda_1, \lambda_2) \in \mathbb{R}$. Then

$$\begin{aligned} \mathbf{A} \cdot \mathbf{e}_1 = \lambda_1 \mathbf{e}_1 \quad \wedge \quad \mathbf{A} \cdot \mathbf{e}_2 = \lambda_2 \mathbf{e}_2 &\Rightarrow (\mathbf{A} \cdot \mathbf{e}_1, \mathbf{e}_2) = (\lambda_1 \mathbf{e}_1, \mathbf{e}_2) \quad \wedge \quad (\mathbf{e}_1, \mathbf{A} \cdot \mathbf{e}_2) = (\mathbf{e}_1, \lambda_2 \mathbf{e}_2) \\ &\Rightarrow (\mathbf{A} \cdot \mathbf{e}_1, \mathbf{e}_2) = \lambda_1 (\mathbf{e}_1, \mathbf{e}_2) \quad \wedge \quad (\mathbf{A} \cdot \mathbf{e}_1, \mathbf{e}_2) = \lambda_2 (\mathbf{e}_1, \mathbf{e}_2) \\ &\Rightarrow \lambda_1 (\mathbf{e}_1, \mathbf{e}_2) = \lambda_2 (\mathbf{e}_1, \mathbf{e}_2) \\ &\Rightarrow (\mathbf{e}_1, \mathbf{e}_2) = 0 \end{aligned}$$

where we used, in order, $\lambda_2 \in \mathbb{R}$, symmetry of \mathbf{A} and $\lambda_1 \neq \lambda_2$. \square

A.5 Genuine eigenvectors

Proof. Consider tensor \mathbf{A} with eigenpairs $(\lambda_i, \mathbf{e}_i)_{i \in \{1,2,3\}}$. Then we have

$$\forall i \in \{1, 2, 3\} \quad \exists d \in \mathbb{Z}^+ \quad (\mathbf{A} - \lambda_i \mathbf{I})^d \cdot \mathbf{e}_i = \mathbf{0}.$$

Recall that \mathbf{e}_i is a genuine eigenvector if $d = 1$ and a generalized one if $d \neq 1$.

Say $d = 2$, then

$$\begin{aligned} \forall i \quad (\mathbf{A} - \lambda_i \mathbf{I})^2 \cdot \mathbf{e}_i = \mathbf{0} &\Rightarrow ((\mathbf{A} - \lambda_i \mathbf{I})^2 \cdot \mathbf{e}_i, \mathbf{e}_i) = (\mathbf{0}, \mathbf{e}_i) \\ &\Leftrightarrow ((\mathbf{A} - \lambda_i \mathbf{I}) \cdot \mathbf{e}_i, (\mathbf{A} - \lambda_i \mathbf{I}) \cdot \mathbf{e}_i) = 0 \\ &\Leftrightarrow \|(\mathbf{A} - \lambda_i \mathbf{I}) \cdot \mathbf{e}_i\|_2^2 = 0 \\ &\Leftrightarrow (\mathbf{A} - \lambda_i \mathbf{I}) \cdot \mathbf{e}_i = \mathbf{0} \end{aligned}$$

and so \mathbf{e}_i is a genuine eigenvector.

Say we consider the common case for d , then

$$\begin{aligned} \forall i \quad (\mathbf{A} - \lambda_i \mathbf{I})^d \cdot \mathbf{e}_i = \mathbf{0} &\Leftrightarrow (\mathbf{A} - \lambda_i \mathbf{I})^2 \cdot (\mathbf{A} - \lambda_i \mathbf{I})^{d-2} \cdot \mathbf{e}_i = \mathbf{0} \\ &\Leftrightarrow (\mathbf{A} - \lambda_i \mathbf{I})^2 \cdot \mathbf{f}_i = \mathbf{0} \\ &\Rightarrow (\mathbf{A} - \lambda_i \mathbf{I}) \cdot \mathbf{f}_i = \mathbf{0} \\ &\Leftrightarrow (\mathbf{A} - \lambda_i \mathbf{I})^{d-1} \cdot \mathbf{e}_i = \mathbf{0} \\ &\Leftrightarrow (\mathbf{A} - \lambda_i \mathbf{I})^2 \cdot (\mathbf{A} - \lambda_i \mathbf{I})^{d-3} \cdot \mathbf{e}_i = \mathbf{0} \\ &\Leftrightarrow (\mathbf{A} - \lambda_i \mathbf{I})^2 \cdot \mathbf{g}_i = \mathbf{0} \\ &\Leftrightarrow \dots \\ &\Leftrightarrow (\mathbf{A} - \lambda_i \mathbf{I}) \cdot \mathbf{e}_i = \mathbf{0} \end{aligned}$$

which concludes the induction proof. □

A.6 Spectral decomposition

Proof. Due to Property 4.5 we have

$$E = \{\mathbf{e}_i\}_{i \in \{1,2,3\}} = \text{span}(\mathbb{R}^3).$$

The second order unit tensor \mathbf{I} can be expressed as a dyadic, a combination of dyads, as

$$\mathbf{I} = \sum_{i,j} \delta_{ij} \mathbf{e}_i \mathbf{e}_j = \sum_j \left(\sum_i \delta_{ij} \mathbf{e}_i \right) \mathbf{e}_j = \sum_j \mathbf{e}_j \mathbf{e}_j$$

where we used the independence of i and j to interchange the sums, linearity and association of the tensor product. It follows that

$$\mathbf{A} = \mathbf{A} \cdot \mathbf{I} = \mathbf{A} \cdot \left(\sum_i \mathbf{e}_i \mathbf{e}_i \right) = \sum_i (\mathbf{A} \cdot \mathbf{e}_i) \mathbf{e}_i = \sum_i (\lambda_i \mathbf{e}_i) \mathbf{e}_i = \sum_i \lambda_i \mathbf{e}_i \mathbf{e}_i$$

which represents the spectral decomposition of \mathbf{A} . We used linearity and association of the tensor product, and the eigenvalues of \mathbf{A} . □

Appendix B

Instruction programming codes

B.1 Introduction

The most important contribution of this master project is that the DSM personnel has programming codes to their disposal to model fiber orientation for homogeneous flows. This chapter focusses on the explanation of these codes to facilitate their usage. In other words, this chapter is a manual for the codes. We explain the code on the user level. In accordance, we do not explain all the called functions thoroughly, but rather refer to the sections in the thesis wherein the details are described.

The implementations are done in Matlab R2008b. It is assumed that the reader is sufficiently acquainted with Matlab R2008b. We will omit explanations of commonly used commands.

There are three main programs: the implementation of Jeffery's equation and the kinetic theory and tensor form of the Wang-O'Gara-Tucker model. A schematic of the implementations is depicted in Figure B.1. Of each step in the schematic, we give a description. In effect, we analyze the codes line by line so that the user can understand them fully.

The notation in the programming codes is analogous to the notation used in the thesis. Explanations of the used notation are therefore omitted. One can refer to last page of the thesis for the nomenclature.

We motivate the instruction of the program by treating an example. In this example, we consider the kinetic theory of the Wang-O'Gara-Tucker model for the simple shear flow field. The treatment of the other two programs are omitted, as their structure and the used functions are analogous to the treated program.

B.2 Example: simple shear flow

B.2.1 Preamble

Every program starts with the piece of code

```
clc, close all, clear global, clear all
format compact;
format long e;
set(0,'defaulttextinterpreter','latex');
set(0,'defaulttextfontsize',12);
set(0,'defaultaxesfontsize',12);
tic
```

. The first line clears the command window, regular and global variables and closes all figure windows. The lines after set the format to a 16 digit exponential compact notation. The command `set(0,'option',option_value)` sets the default option 'option' to the given value `option_value`. We increase some font sizes for the sake of clarity. In addition, we set the interpreter of the text to 'latex'. The latter is known to be somewhat buggy. If it gives any problems, it can be switched to 'none'. The command `tic` starts the stopwatch so that the computation time can be measured.

B.2.2 Physical and numerical parameters

All three programs need a set of physical and numerical parameters as input. The physical parameters are inherent to the process that is considered. The numerical parameters are inherent to the numerical approach.

A basis E_b has to be chosen. The program is written for bases fixed in time. In our case, we choose a basis wherein the flow field is described as

$$\mathbf{v} = \mathbf{K} \cdot \mathbf{x}, \quad \mathbf{K} = \begin{bmatrix} 0 & G & 0 \\ 0 & 0 & 0 \\ 0 & 0 & 0 \end{bmatrix}.$$

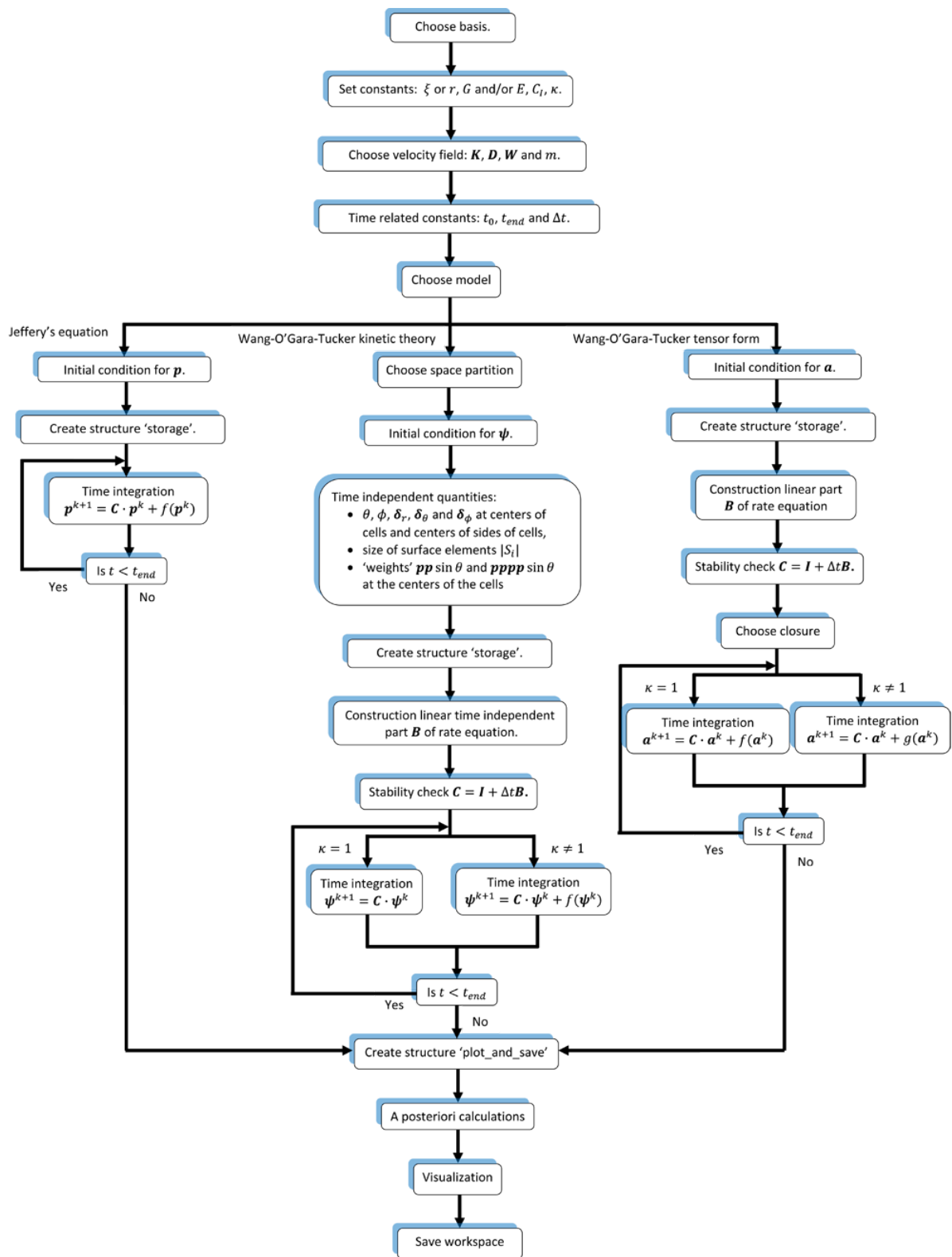


Figure B.1: schematic of implementations.

There are certain parameters that are used not only by the main program, but also by a set of functions. If a parameter is used often outside the main program, one can consider declaring this parameter as a global variable. In this way, it does not have to be given to the function as an argument. The global variables we use are denoted in

```
%% Define global variables.

global n
global theta dtheta n_theta
global phi dphi n_phi
global n_DOF
global lambda_min lambda_plus
global G Kappa D_r m
global dt
global S
global xi C_I
```

. The used notation is in accordance with the report, as mentioned in the nomenclature. When declaring a variable as global, an empty variable is created in the workspace of global variables. We still have to assign values to them. We implement

```
%% Defining the constants.

% Fixed parameters.
n=3; %Number of dimensions.
% r_e=10; %Ratio of long axis and short axis of ellipsoid.
% xi=(r_e^2-1)/(r_e^2+1); %Aspect ratio of fibers, xi=(r_e^2-1)/(r_e^2+1), r_e=L/D.
xi=1;
lambda_min=(xi-1)/2;
lambda_plus=(xi+1)/2;
kappa=1; %To slow down the kinetics, 0<kappa<=1
C_I=0.01; %Fiber-fiber interaction coefficient.

% Rates.
E=10^0; %Strain rate in [1/s].
G=10^0; %Shear rate in [1/s].
```

. It stands out that two command lines are considered as comments. This is done because we chose $\xi = 1$. The latter corresponds with $r_e = \infty$ and can thus not be expressed in the program. Nonetheless, one can take r_e large so that $\xi = 1$ to machine precision. For $|\xi| < 1$, the user might find it more clear to express the physics by assigning a value to r_e . In this case, the two lines should not be considered as comments and the line after should.

The next step is to define the homogeneous flow field by

```
%% Definition of the homogeneous flow field.

vfield='simple shear'; %Later used in file and directory names.
[Kappa,D,W,gamma_dot]=simple_shear(G);
D_r=C_I*gamma_dot;
storage.m=sum(sum(abs(Kappa)));
m=storage.m;

if D_r==0
    fprintf(1,['The coefficient D_r=0. It is recommended to use '...
        'the p_dot program to calculate p instead of psi.\n\n']);
end
```

. The specification of the name of the flow field is used later to define the name of the directory wherein the output is stored. The program `simple_shear` needs the shear rate as an argument and returns \mathbf{K} , its symmetric and antisymmetric parts \mathbf{D} and \mathbf{W} respectively, and m , the measure for the strength of the velocity field. The latter is used to scale certain variables, as described in Sections 7.3 and 8.3. The

parameter m is stored in the structure `storage`, which is meant for the storage of all the important quantities. The situation $D_r = 0$ implies that $C_I = 0$ so that there is no rotary diffusion. If in addition $\kappa = 1$, the program suggests to use Jeffery's equation to obtain the requested information, as it is much more efficient. The Folgar-Tucker model is not meant for diffusionless cases, as motivated in Chapter 3.

Now that m is known from the velocity field, the scaling of the time is known and the time related constants can be defined. This is done in

```

%% Time related constants.

dt=10^-5/m; %Time step size.
t_0=0; %Initial time.
t_end=10/m; %End time.
t=t_0:dt:t_end;
t_length=length(t);

```

. It stands out that both the time step and end time are taken inversely proportional to $m = G$. We continue with the choice of the partition in space

```

% Space related constants.
n_theta=50; %Partition number of theta domain. Must be even.
theta_begin=0;
theta_end=pi/2;
dtheta=(theta_end-theta_begin)/n_theta; %Step size theta.
theta=theta_begin:dtheta:theta_end; %Vector containing possible values of theta.
theta_mid=theta_begin+dtheta/2:dtheta:theta_end-dtheta/2;

n_phi=4*n_theta; %Partition number of phi domain.
n_DOF=n_theta*n_phi; %(N)umber of (d)egrees (o)f (f)reedom.
if mod(n_phi,2)==1
    fprintf(1,['WARNING: n_phi is odd, which makes it impossible for the '...
              'program to run properly. Ending program.\n\n']);
    return
end
phi_begin=0;
phi_end=2*pi;
dphi=(phi_end-phi_begin)/n_phi; %Step size phi.
phi=phi_begin:dphi:phi_end; %Vector containing possible values of phi.
phi_mid=phi_begin+dphi/2:dphi:phi_end-dphi/2;

[Phi_mid,Theta_mid]=meshgrid(phi_mid,theta_mid); %Construct a meshed grid.

```

. The partition of the θ and ϕ directions are made. The coordinates of the centers of the resulting cells are constructed with the `meshgrid` command. The θ does not end at π but at $\frac{\pi}{2}$ as ψ is an even function. The $\phi \in [0, 2\pi]$ so we take the partition number in the ϕ direction, n_ϕ , four times as large as n_θ . A warning is given when n_ϕ is odd. As explained in Subsection 7.4.3, n_ϕ has to be even for the sake of the conservation of the properties of ψ .

B.2.3 Preliminary calculations

Now that the space S has been partitioned, the IC can be constructed. The IC must suffice to the conservation of probability (7.22)

$$2 \sum_{i,j} \psi_{i,j}^0 |S_i| = 1 \quad \wedge \quad \forall i,j \quad \psi_{i,j}^0 \geq 0.$$

In addition, the IC should be constructed with the space partition in mind in the sense of gradients. Large gradients between cells may lead to large errors. This can result in divergence of the solution, or that it takes a long time for the errors to decrease to an acceptable level. In the literature, the random fiber orientation IC is often used, so $\forall i,j \quad \psi_{i,j}^0 = \frac{1}{4\pi}$. As an alternative, the IC can also be nonuniform. An example hereof is (7.23).

The values of θ , ϕ , δ_r , δ_θ and δ_ϕ at the centers of the cells and centers of the sides of the cells are used in the calculation of the nonlinear RSC term. This term has to be calculated each time increment and it is thus important for it to be efficient. As the former set of variables is merely dependent on space and not on time, we calculate them before the time integration process. Also their products occur in (3.14) are determined before the time integration process:

```
% Determine the basis vectors at the sides of each cell. Will be used later
% for the calculations of the nonlinear RSC part.
[bdrW,bdtW,bdpW,bdrN,bdtN,bdpN,bdrS,bdtS,bdpS,bdrE,bdtE,bdpE,...
 dphisinthetaN,dphisinthetaS,...
 bdrbdpW,bdrbdtN,bdrbdtS,bdrbdpE,...
 theta_N,theta_S]=bvaWNSE;
```

. Other quantities that are used often and that do not depend on time are $|S_i|$, $pp \sin \theta$ and $pppp \sin \theta$. They are calculated by

```
% Determine surface elements.
S=dphi*dtheta*sin(theta(1:end-1)+dtheta/2).';
S_full=S*ones(1,n_phi);

% Determine (pp)_ij|S_i| and (pppp)_ij|S_i| in advance for efficiency.
[PPS,PPPS]=PPSnPPPS;
```

. For the storage of important quantities, we construct the structure `storage`. We store the quantities with commands like

```
storage.psi=zeros([size(psi_0) length(t_storage)]);
```

, where `t_storage` contains the time values whereon the data is stored and has the size that the user chooses by defining `n_storage`.

With the piece of code

```
%% Construction of linear part of Fokker-Planck equation.

B_ld=lpFPeqn(0); %Convection only, D_r=0.
if D_r~=0
    B=lpFPeqn(D_r); %Convection and diffusion.
else
    B=B_ld;
end
B_ffl=B-B_ld; %Diffusion only.

% Storage of matrices.
storage.matrices.B_ld=B_ld;
storage.matrices.B_ffl=B_ffl;
storage.matrices.B=B;
```

we call the function `lpFPeqn(D_r)` to construct the linear parts of the Fokker-Planck equation. We are not only interested in the 'total' linear part, but also in the LD and FFI contributions. To this end, we call `lpFPeqn(0)` to determine the coefficients for the LD contribution and `lpFPeqn(D_r)` to determine the coefficients for the total contribution. Subsequently, the FFI contribution is determined by subtracting the former from the latter. These quantities are stored in the structure `storage`.

From Euler forward it follows that the system matrix is $\mathbf{C} = \mathbf{I} + \Delta t \mathbf{B}$. In accordance, we construct the sparse matrix with

```

%% Construction of the matrix C.
C=speye(n_DOF,n_DOF)+dt*B;
storage.matrices.C=C;

%% Stability check for linear part.
plot_and_save.stability_check=0;
stability_check(plot_and_save,C);

```

and check the stability of the linear part of the scheme by determining the largest absolute eigenvalue with the function `stability_check(plot_and_save,C)`. For more details on stability analyses, we refer to Subsections 7.4.6 and 8.5.3. Note that we have also constructed the structure `plot_and_save` wherein we store certain settings. In this case, the setting concerns whether the stability check should be done or skipped.

Table B.1 contains various tested settings for the time and space partition that are stable. The tested settings give an indication on how the space and time partition should be chosen. Note that these settings do, however, not guarantee that $\forall t \psi \geq 0$. It is guaranteed that the errors will decay as $t \uparrow \infty$ so that $\forall t \psi \geq 0$ will hold if $t \uparrow \infty$.

flow field	ξ	C_I	κ	n_θ	n_ϕ	$m\Delta t$
simple shear	1	0.01	1	40	160	$10^{-5.3}$
simple shear	1	0.001	1	40	160	10^{-5}
simple shear	1	0.005	1	40	160	10^{-5}
simple shear	1	0.05	1	40	160	$10^{-6.2}$
simple shear	1	0.1	1	40	160	10^{-7}
simple shear	0.99501	0.001	1	50	200	$10^{-5.5}$
simple shear	0.9230769	0.001	1	50	200	10^{-7}
simple shear	0.99681	0.01	1	40	160	$10^{-5.1}$
uniaxial elongation	1	0.01	1	24	96	$10^{-4.3}$
uniaxial elongation	1	0.1	1	24	96	$10^{-4.2}$

Table B.1: tested stable settings.

B.2.4 Time integration

The time integration loop starts as

```

%% Time integration.

% In case kappa=1 we set Q to zero.
Q=spalloc(n_theta,n_phi,0);
for t_step=2:t_length %Time step.
%   Determine nonlinear RSC part of Fokker-Planck equation.
if kappa~=1
    Q=nlpFPeqn(bdrW,bdpW,bdrN,bdtN,bdrS,bdtS,bdrE,bdpE,...
        dphisinthetaN,dphisinthetaS,PPS,PPPS,...
        D,kappa,xi,D_r,n,dtheta,psi,n_theta,n_phi);
    Q=-dt./S_full.*Q;
    Q=Q(:);
    psi_l=C*psi_l+Q;
else
    psi_l=C*psi_l;
end

```

. The first command line is to create an empty sparse matrix that uses a minimal amount of memory. This is merely done to set to set the RSC contribution to zero if $\kappa = 1$. This `Q` is replaced if $\kappa \neq 1$. The function `nlpFPeqn` constructs the nonlinear RSC part of the kinetic theory. The command `Q=Q(:)` constructs a column vector from the two dimensional matrix. The reason herefore becomes obvious in the line after: the system of equations can be written in the form

$$\psi_l^{k+1} = C \cdot \psi_l^k + q(\psi_l^k).$$

If $\kappa = 1$, the construction of \mathbf{Q} is redundant and the system of equations is merely

$$\psi_l^{k+1} = \mathbf{C} \cdot \psi_l^k.$$

In addition, there are interesting cases of $\mathbf{K}(t)$, so where the matrix of the homogeneous flow field is dependent on time. In that case, one could add the piece of code

```
% The time;
t=t_0+(t_step-1)*dt;

% Determine time dependent linear part.
a=1;
b=5;
dtB_ld_td=dtB_ld/(1+1/(exp(a*(t-b))));
C=C_unity_ffl+dtB_ld_td;
```

to the time integration loop, so that the LD contribution is multiplied with a time dependent function. E.g. a logistic function as described by (9.5).

The time integration loop also contains

```
% Storage of variables.
if mod(t_step+1,n_storage_step)==1
    storage_step=ceil((t_step+1)/n_storage_step);
    fprintf(1,['Process at time ' num2str(m*t_storage(storage_step)) ...
        '[] of total time ' num2str(m*t_storage(end)) '[].\n']);

% Reshape psi vector to psi matrix.
psi=reshape(psi_l,n_theta,n_phi);

% Storage of flux contributions.
f_ld=reshape(B_ld*psi_l,n_theta,n_phi);
f_ffl=reshape(B_ffl*psi_l,n_theta,n_phi);
f_RSC=reshape(Q/dt,n_theta,n_phi);
psi_dot=f_ld+f_ffl+f_RSC;

% Storage.
storage.psi(:,:,storage_step)=psi;
end
```

to store the requested quantities in `storage`. In addition, it prints a line in the command window to give an indication of the progress of the program. The commands for the storage are trivial. The command `reshape` is used to reshape the one dimensional vectors 'back' to their original two dimensional matrix form.

B.2.5 Output

The code

```
%% Stop stopwatch.
t_CPU=toc;
storage.t_CPU=t_CPU;
```

stops the stopwatch to determine the calculation time. It is stored in `storage`. The code

```

%% Save data in question.

% In this cell, all the data that is of importance is saved to a mat file.
% Herewith, all output can be constructed.
string_parameters=['psi,' vfield ',xi=' num2str(xi) ',kappa=' num2str(kappa) ...
    ',C_I=' num2str(C_I) ',n_theta=' num2str(n_theta) ',n_phi=' num2str(n_phi) ...
    ',t_0=' num2str(t_0) ',mt_end=' num2str(m*t_end) ',mdt=' num2str(m*dt,'%6.6e') ...
    ',E=' num2str(E) ',G=' num2str(G)];
curdir=pwd; %Save current path.

% Check if a directory 'Results' exists. If not, create it and change
% directory to it, if it does, just change directory to it.
erd=exist([pwd '\Results'],'dir'); %Stands for (e)xistence (r)esults (d)irectory.
if erd==7
    cd([pwd '\Results']);
else mkdir('Results');cd([pwd '\Results']);
end

[status,message,messageid]=mkdir(string_parameters);
if status==1
    cd(string_parameters);
    outputdir=pwd;
else fprintf(1,'Output not created due to error from mkdir command.\n\n')
end
cd(curdir) %Change back to original working path.

```

creates a string that is used to name the directory wherein the output is saved. It first checks if the directory `Results` exists. If it does not, it created and subsequently the directory wherein the data will be saved is created. If it does, the directory is changed to `Results` and subsequently the directory wherein the data will be saved is created. An error is given when the make directory command `mkdir` fails to create the output directory. At the end of the code, the directory is changed back to the original working directory. The user should keep in mind that the string for the directory name is rather large. This can give problems if the maximum amount of characters for a pathname is exceeded. This can be solved by shortening the string or to put the directory in the lower levels of a directory structure. Such problems can differ per operating system.

The main calculation process has finished. What follows are the a posteriori calculations, visualization and saving the workspace to the hard disk. To determine which data should be visualized and/or saved, settings are stored in the structure `plot_and_save`. As an example, we treat the call of the function that visualizes the probability density,

```

%% Visualization of output.

% Necessary for multiple visualizations.
plot_and_save.output_directory=outputdir;
plot_and_save.string_parameters_latex=['$\psi$, ' vfield ', $\xi=$' ...
    num2str(xi) ', $\kappa=$' num2str(kappa) ', $C_I=$' num2str(C_I) ...
    ', $n_{\theta}=$' num2str(n_theta) ', $n_{\phi}=$' num2str(n_phi) ...
    ', $t_0=$' num2str(t_0) ', $m \cdot t_{end}=$' num2str(m*t_end) ...
    ', $m \cdot dt=$' num2str(dt*m) ', $E=$' num2str(E) ', $G=$' ...
    num2str(G)];

% Plotting the probability density.
plot_and_save.psi_pd.relative_or_absolute_colors='abs';
plot_and_save.psi_pd.avioutput=1;
plot_and_save.psi_pd.filename='probability_density';
plot_and_save.psi_pd.fps=10;

vis_psi_pd(storage,plot_and_save);

```

. The first line saves the output directory. The second line creates a $\text{L}^{\text{A}}\text{T}_{\text{E}}\text{X}$ string that is denoted in the

lower left corner of each plot. There are some settings that are needed for the function `vis_psi_pd`. The first is if the limits of the colorbar for the probability density are taken for all time or absolute, or at each time increment or relative. An animation is created when `plot_and_save.psi_pd.avioutput` is equal to one. This is skipped if the value is zero. The filename and frames per second (FPS) for the animation are also set. When all the parameters are set, the visualization function is called. The settings and output requests differ per visualization program. Information on the latter can be recovered by considering the first lines of the visualization function in question. The following visualization programs are available.

- Function `vis_psi_pd`, for depicting the probability density and its LD, FFI and RSC contributions on the sphere. An example is Figure 9.11.
- Function `vis_psi_checks`. This is a function wherewith the adequacy of the solution can be checked. It depicts the occurrences of negative elements of ψ , and calculates the integrals of ψ and $\dot{\psi}$ over the sphere at each time. Obviously, a proper solution does not have any negative ψ elements, and integrals with values one and zero respectively. An example is depicted in Figure B.2.
- Function `vis_A_2`. This function visualizes the components of \mathbf{A} , $\dot{\mathbf{A}}$ and its LD, FFI and RSC contributions, and the eigenpairs of \mathbf{A} . Examples are the Figures 9.21 and 9.22.
- Function `vis_A_4`, which visualizes the fifteen independent components of \mathbf{A} . An example is Figure B.3.
- Function `vis_psi_extr`, which visualizes the extrema of ψ and their corresponding generalized coordinates θ and ϕ . An example is Figure 9.15.
- Function `steady_state_info`. It calculates the steady states times and values for all quantities.

The program is concluded with

```

%% Save all data in workspace to hard disk.

save([outputdir '\workspace.mat']);

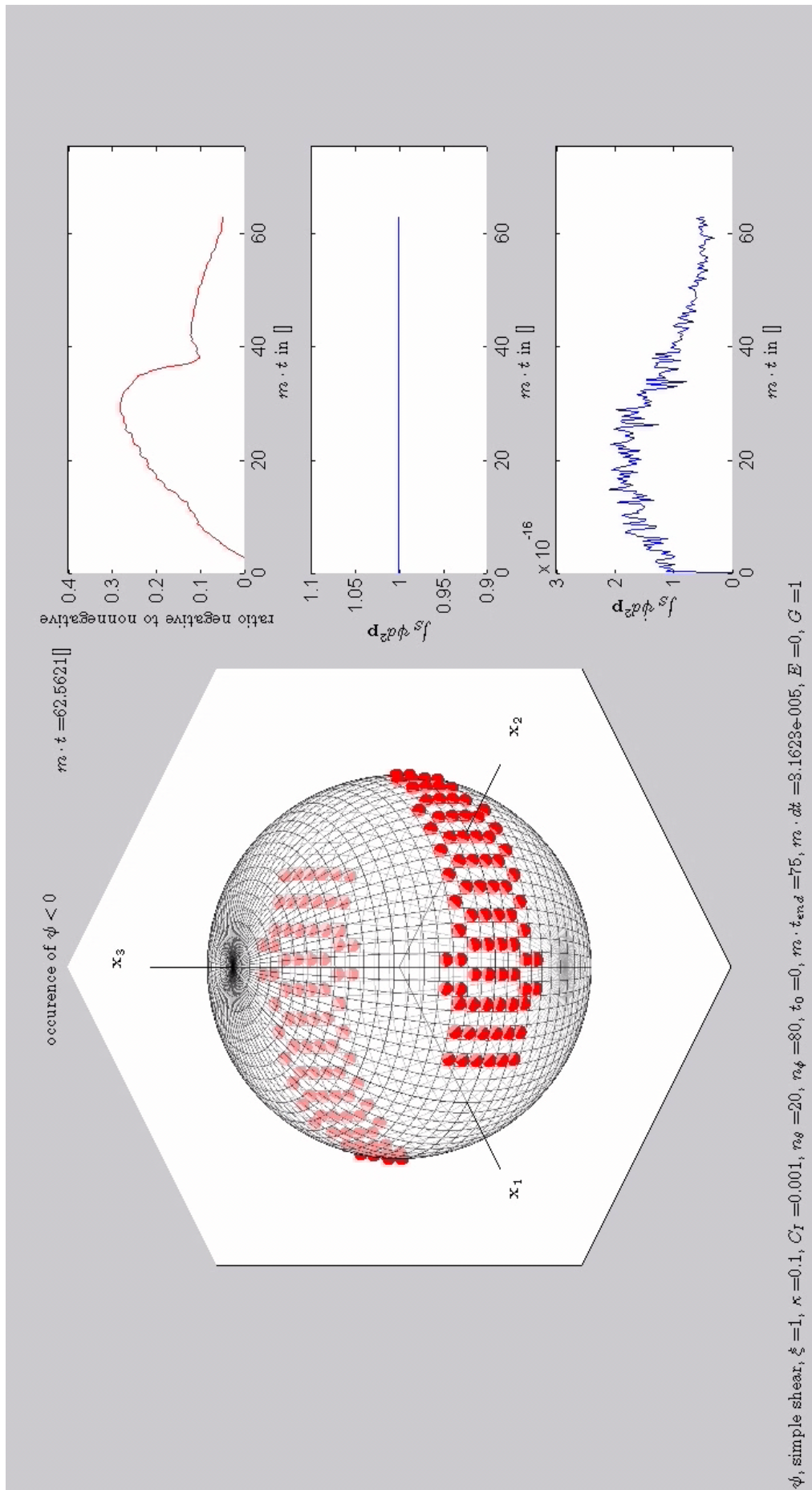
%% Put settings back to factory settings.

set(0,'defaulttextinterpreter','factory');
set(0,'defaulttextfontsize','factory');

%% Ending program. Back to console.

fprintf(1,'\nEnd of program.\n\n')
```

, which saves the workspace to the hard disk, sets the settings that were changed in the preamble back to the factory defaults, and prints the line `End of program.` in the command window. The former is important in particular, as it can be used to construct coefficients for the an OFC.

Figure B.2: example of the output of the function `vis_psi_checks`.

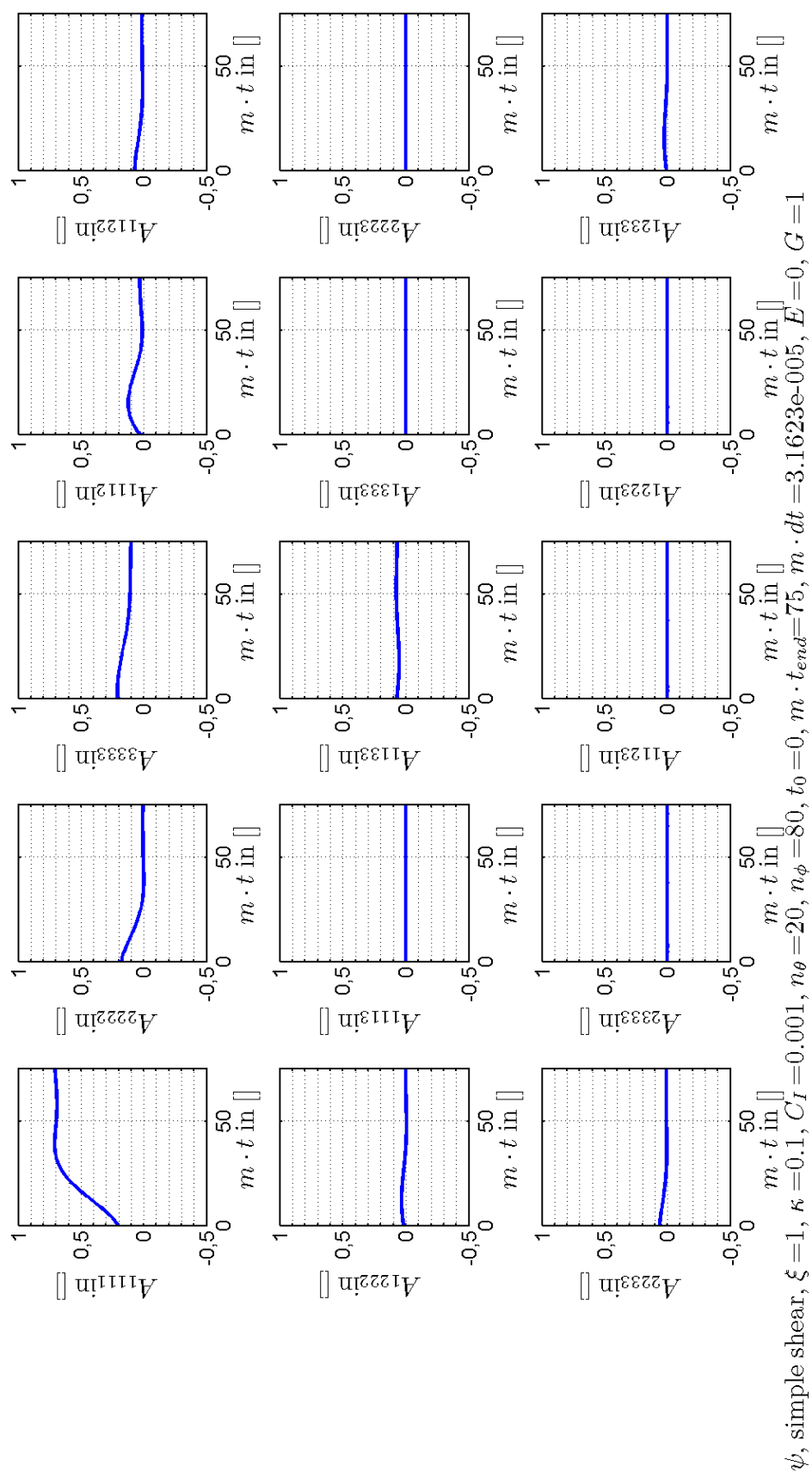


Figure B.3: example of the output of the function vis_A.4.

B.2.6 Input

For the sake of completeness, we summarize the input parameters that arised during the walkthrough of the code, in this section. The input parameters are denoted in Tables B.2 and B.3, each with their possible values and description. The order corresponds with the order in the code.

Input	Values	Description
r_e	\mathbb{R}^+	Aspect ratio of ellipsoidal particle, $\frac{l}{d}$. An alternative is to specify ξ .
ξ	$[-1, 1]$	Function of the aspect ratio $\frac{r_e^2-1}{r_e^2+1}$. An alternative is to specify r_e and calculate ξ .
C_I	\mathbb{R}^+	Strength of the fiber-fiber interaction.
κ	$(0, 1]$	Strength of the strain reduction to prolong the transient times.
E	\mathbb{R}	Strain rate.
G	\mathbb{R}	Shear rate.
n_θ	\mathbb{Z}^+	Partition number in θ direction.
n_ϕ	$\{2, 4, \dots\}$	Partition number in ϕ direction.
vfield	string	String that is used in the name of the output directory.
K	$\mathbb{R}^{3 \times 3}$	Homogeneous flow field matrix.
Δt	\mathbb{R}^+	Step size for time integration loop.
t_0	\mathbb{R}	Starting time.
t_{end}	\mathbb{R}	End time, $t_{end} > t_0$.
$\psi_{i,j}^0$	\mathbb{R}^+	Initial probability density at the mesh element with its center at $(\theta_i - \frac{\Delta\theta}{2}, \phi_i - \frac{\Delta\phi}{2})$. The condition that $2 \sum_{i,j} \psi_{i,j}^0 S_i = 1$ must be satisfied.
$n_{storage}$	\mathbb{N}	Number of storage times. At these time, requested data is stored in the structure storage . Note that $n_{storage}$ must be smaller than the total number of time increments.

Table B.2: needed input for program.

Input	Values	Description
<code>stability_check</code>	$\{0, 1\}$	If value is one, the largest absolute eigenvalue of the linear system matrix will be determined. If the value is zero, this check is skipped.
<code>psi_pd.relative_or_absolute_colors</code>	'abs' 'rel'	Determines if the limits of the color bar are set per time increment or one time for all time increments.
<code>psi_pd.avioutput</code>	$\{0, 1\}$	One for creation of an animation in an AVI container, zero if not.
<code>psi_pd.filename</code>	string	Filename of animation.
<code>psi_pd.fps</code>	\mathbb{Z}^+	Frame rate of animation.
<code>psi_checks.save</code>	$\{0, 1\}$	One if animation of the checks of the PDF should be saved.
<code>psi_checks.name</code>	string	Filename of the animation.
<code>psi_checks.fps</code>	\mathbb{Z}^+	Frame rate of animation.
<code>A.six_graphs.plot</code>	$\{0, 1\}$	Plots the six components of \mathbf{A} in six graphs if one.
<code>A.six_graphs.save</code>	$\{0, 1\}$	Save the former if one.
<code>A.six_graphs.name</code>	string	Filename of the former.
<code>A.six_graphs_with_fluxes.plot</code>	$\{0, 1\}$	Plots the six components of \mathbf{A} and its fluxes in six graphs if one.
<code>A.six_graphs_with_fluxes.save</code>	$\{0, 1\}$	Save the former if one.
<code>A.six_graphs_with_fluxes.name</code>	string	Filename of the former.
<code>A.one_graph.plot</code>	$\{0, 1\}$	Plots the six components of \mathbf{A} in one graph if one.
<code>A.one_graph.save</code>	$\{0, 1\}$	Save the former if one.
<code>A.one_graph.name</code>	string	Filename of the former.
<code>A.symmetry.plot</code>	$\{0, 1\}$	Plots the six components of $\mathbf{A} - \mathbf{A}^T$ to check the conservation of symmetry if one.
<code>A.symmetry.save</code>	$\{0, 1\}$	Save the former if one.
<code>A.symmetry.name</code>	string	Filename of the former.
<code>A.trace.plot</code>	$\{0, 1\}$	Plots the trace of \mathbf{A} if one.
<code>A.trace.save</code>	$\{0, 1\}$	Save the former if one.
<code>A.trace.name</code>	string	Filename of the former.
<code>A.eigenpairs.plot</code>	$\{0, 1\}$	Plots the eigenpairs of \mathbf{A} if one.
<code>A.eigenpairs.save</code>	$\{0, 1\}$	Save the former if one.
<code>A.eigenpairs.name</code>	string	Filename of the former.
<code>A.eigenpairs.fps</code>	\mathbb{Z}^+	Frame rate of animation.
<code>A_4.fifteen_graphs.plot</code>	$\{0, 1\}$	Plots the fifteen independent components of \mathbb{A} if one.
<code>A_4.fifteen_graphs.save</code>	$\{0, 1\}$	Save the former if one.
<code>A_4.fifteen_graphs.name</code>	string	Filename of the former.
<code>psi_extrema.plot</code>	$\{0, 1\}$	Plot the extrema of ψ if one.
<code>psi_extrema.save</code>	$\{0, 1\}$	Save the former if one.
<code>psi_extrema.filename</code>	string	Filename of the former.

Table B.3: needed input for program in the structure `plot_and_save`.

Bibliography

- [1] AUTODESK INC., *Fiber orientation (3d) solver validation*. Autodesk Inc., San Rafael, 2009.
- [2] R. BAY, *FIBER ORIENTATION IN INJECTION MOLDED COMPOSITES: A COMPARISON OF THEORY AND EXPERIMENT*, PhD thesis, University of Illinois, Urbana, 1991.
- [3] D.A. JACK AND D.E. SMITH, *Elastic Properties of Short-fiber Polymer Composites, Derivation and Demonstration of Analytical Forms of Expectation and Variance from Orientation Tensors*, Journal of Composite Materials, 42 (2008), pp. 277–308.
- [4] D.J. RIXEN, *Engineering dynamics*. Delft University of Technology, Delft, 2006.
- [5] ———, *Numerical methods in engineering dynamics*. Delft University of Technology, Delft, 2007.
- [6] E.T. ONAT AND F.A. LECKIE, *Representation of Mechanical Behavior in the Presence of Changing Internal Structure*, Journal of Applied Mechanics, 55 (1988), pp. 1–10.
- [7] F. FOLGAR AND C.L. TUCKER III, *Orientation Behavior of Fibers in Concentrated Suspensions*, Journal of Reinforced Plastics and Composites, 3 (1984), pp. 98–109.
- [8] G.A. HOLZAPFEL, *Nonlinear Solid Mechanics, A Continuum Approach for Engineering*, John Wiley & Sons Ltd, West Sussex, 2007.
- [9] G.B. JEFFERY, *The motion of ellipsoidal particles immersed in a viscous fluid*, Ser. A, 102 (1922), pp. 161–179.
- [10] G.E. ANDREWS, R. ASKEY AND R. ROY, *Special Functions*, Cambridge University Press, Cambridge, 2001.
- [11] H. BIJL, A.H. VAN ZUIJLEN, A. DE BOER, AND D.J. RIXEN, *Fluid-structure interaction*. Delft institutes of aerospace and mechanical engineering, Delft, 2007.
- [12] H. RISKEN, *The Fokker-Planck Equation*, Springer, Berlin, 1996.
- [13] J. WANG, J.F. O’GARA AND C.L. TUCKER III, *An objective model for slow orientation kinetics in concentrated fiber suspensions: Theory and rheological evidence*, Journal of Rheology, 52(5) (2008), pp. 1179–1200.
- [14] J.H. PHELPS AND C.L. TUCKER III, *An anisotropic rotary diffusion model for fiber orientation in short- and long-fiber thermoplastics*, Journal of Non-Newtonian Fluid Mechanics, 156 (2009), pp. 165–176.
- [15] J.S. CINTRA AND C.L. TUCKER III, *Orthotropic closure approximations for flow-induced fiber orientation*, Journal of Rheology, 39 (1995), pp. 1095–1122.
- [16] P.K. KENNEDY, *Practical and scientific aspects of injection molding simulation*, PhD thesis, TU Eindhoven, Eindhoven, 2008.
- [17] R.J. LEVEQUE, *Finite volume methods for hyperbolic problems*, Cambridge University Press, Cambridge, 2002.
- [18] S.G. ADVANI AND C.L. TUCKER III, *The Use of Tensors to Describe and Predict Fiber Orientation in Short Fiber Composites*, Journal of Rheology, 31 (1987), pp. 751–784.
- [19] ———, *Closure approximations for three-dimensional structure tensors*, Journal of Rheology, 34 (1990), pp. 367–386.
- [20] T.D. PAPATHANASIOU AND D.C. GUELL, *Flow-induced alignment in composite materials*, Woodhead Publishing Limited, Cambridge, 1997.
- [21] C. VUIK, P. VAN BEEK, F. VERMOLEN, AND J. VAN KAN, *Numerieke methoden voor differentiaalvergelijkingen*. Delft institute of applied mathematics, Delft, 2004.

Nomenclature

Symbol	Dimension	Description
ϕ	rad	Azimuth. Spherical coordinate.
$\dot{\gamma}$	$\frac{1}{s}$	Shear rate, see also E .
κ	1	RSC or strain reduction factor.
λ	1	Function of r_e , $\frac{r_e^2-1}{r_e^2+1}$, see also ξ .
λ_i	1	The i^{th} eigenvalue of \mathbf{A} .
λ^-	1	Function of λ , $\frac{\lambda-1}{2}$.
λ^+	1	Function of λ , $\frac{\lambda+1}{2}$.
θ	rad	Elevation. Spherical coordinate.
ξ	1	Function of r_e , $\frac{r_e^2-1}{r_e^2+1}$, see also λ .
ψ	1	Probability density.
δ_r	1	Unit basis vector for the radius, see also \mathbf{p} .
δ_θ	1	Unit basis vector for the elevation, see also \mathbf{q} .
δ_ϕ	1	Unit basis vector for the azimuth, see also \mathbf{s} .
f	$\frac{1}{s}$	Flux of probability density.
m	$\frac{1}{s}$	Measure of the strength of \mathbf{K} , defined as $\sum_{i,j} \kappa_{ij} $.
r	m	Radial length of vector.
r_e	1	Aspect ratio of ellipsoid, $\frac{l}{d}$.
t	s	Time.
\mathbf{e}_i	1	The i^{th} eigenvector of \mathbf{A} .
\mathbf{p}	1	Unit basis vector for the radius, see also δ_r .
\mathbf{q}	1	Unit basis vector for the elevation, see also δ_θ . Nonlinear RSC or strain reduction term in kinetic theory.
\mathbf{s}	1	Unit basis vector for the azimuth, see also δ_ϕ .
\mathbf{x}	m	Space vector, $(x\ y\ z)^T$ or $(x_1\ x_2\ x_3)^T$.
C_i	1	Boundary of S_i .
C_I	1	Fiber-fiber interaction coefficient.
D_r	$\frac{1}{s}$	Defined as $C_I m$.
E	$\frac{1}{s}$	Strain rate.
G	$\frac{1}{s}$	Shear rate, see also $\dot{\gamma}$.
S	1	The set $\mathbf{p} \in \mathbb{R}^3 : \ \mathbf{p}\ _2 = 1$.
S_i	1	Mesh element of S .
$ S_i $	1	Size of mesh element S_i .
\mathbf{A}	1	Tensor $\int_S \psi \mathbf{p} \mathbf{p} d^2 \mathbf{p}$, second order moment or orientation tensor.
\mathbf{D}	$\frac{1}{s}$	The symmetric part of \mathbf{K} , rate of deformation tensor.
\mathbf{I}	1	Unit tensor.
\mathbf{K}	1	Homogenous flow field tensor.
\mathbf{Q}	1	Proper orthogonal tensor or rotation with $\det(\mathbf{Q}) = 1$ and $\mathbf{Q}^{-1} = \mathbf{Q}^T$.
\mathbf{W}	$\frac{1}{s}$	The antisymmetric part of \mathbf{K} , spin rate tensor.
\mathbb{A}	1	Voigt index version of \mathbb{A} , second order tensor.
\mathbb{A}	1	Tensor $\int_S \psi \mathbf{p} \mathbf{p} \mathbf{p} \mathbf{p} d^2 \mathbf{p}$, fourth order moment or orientation tensor.
\mathbb{C}	1	The set of complex numbers.
\mathbb{L}	1	Auxiliary fourth order tensor, defined as $\sum_i \lambda_i \mathbf{e}_i \mathbf{e}_i \mathbf{e}_i \mathbf{e}_i$.
\mathbb{M}	1	Auxiliary fourth order tensor, defined as $\sum_i \mathbf{e}_i \mathbf{e}_i \mathbf{e}_i \mathbf{e}_i$.
\mathbb{N}	1	The set of natural numbers.
\mathbb{P}	1	Probability.
\mathbb{R}	1	The set of real numbers.
\mathbb{Z}	1	The set of integers.
∇	1	The $\frac{\partial}{\partial \mathbf{p}}$ operator or gradient.
$\tilde{\nabla}$	1	The $\frac{\partial}{\partial \mathbf{p}}$ operator or constrained gradient.



DSM in Geleen.